/

Magnetosome-specific expression of chimeric proteins in *Magnetospirillum gryphiswaldense* for applications in cell biology and biotechnology

Dissertation

der Fakultät für Biologie

der Ludwig-Maximilians-Universität München

vorgelegt von

Claus Lang

aus Bergisch Gladbach

München

am 19. März 2009

1. Gutachter: Prof. Dr. Dirk Schüler, LMU München

2. Gutachter: Prof. Dr. Kirsten Jung, LMU München

Tag des Promotionskolloquiums: 09.07.2009

Publications originating from this thesis

Original research papers

Manuscript 1

<u>**Lang, C.**</u>**, and D. Schüler.** 2008. Expression of green fluorescent protein fused to magnetosome proteins in microaerophilic magnetotactic bacteria. Appl. Environ. Microbiol. **74:**4944-4953.

Manuscript 2

<u>**Lang, C.**</u>**, R. Uebe, and D. Schüler.** Analysis of promoters for efficient and inducible gene expression in *M. gryphiswaldense*. in revision

Manuscript 3

Ceyhan, B., P. Alhorn, <u>C. Lang</u>, D. Schüler, and C. M. Niemeyer. 2006. Semi-synthetic biogenic magnetosome nanoparticles for the detection of proteins and nucleic acids. Small **2:**1251-1255.

Manuscript 4

Wacker, R., B. Ceyhan, P. Alhorn, D. Schüler, <u>C. Lang</u>, and C. M. Niemeyer. 2007. Magneto-Immuno PCR: A homogeneous immunoassay based on biogenic magnetosome nanoparticles. Biochem. Biophys. Res. Commun. **357:**391-396.

Manuscript 5

Hartung, A., M. R. Lisy, K.-H. Herrmann, I. Hilger, D. Schüler, <u>C. Lang</u>, M. E. Bellemann, W. A. Kaiser, and J. R. Reichenbach. 2007. Labelling of macrophages using bacterial magnetosomes and their characterization by magnetic resonance imaging. J. Magn. Magn. Mater. **311:**454–459.

Manuscript 6

Lisy, M.-R., A. Hartung, <u>C. Lang</u>, D. Schüler, W. Richter, J. R. Reichenbach, W. A. Kaiser, and I. Hilger. 2007. Fluorescent bacterial magnetic nanoparticles as bimodal contrast agents. Invest. Radiol. **42:**235-241.

Manuscript 7

Schwarz, S., F. Fernandes, L. Sanroman, M. Hodenius, <u>C. Lang</u>, U. Himmelreich, M. Gamac, T. Schmitz-Rode, D. Schüler, M. Hoehn, M. Zenke, and T. Hieronymus.

Synthetic and biogenic magnetite nanoparticles for tracking of stem cells and dendritic cells. J. Magn. Magn. Mater. in press

Review articles and book chapters

Manuscript 8

Lang, C., and D. Schüler. 2006. Biomineralization of magnetosomes in bacteria: Nanoparticles with potential applications, p. 107-124. *In* B. Rehm (ed.), Microbial Bionanotechnology: Biological Self-assembly Systems and Biopolymer-based Nanostructures. Horizon bioscience, Wymondham.

Manuscript 9

Lang, C., and D. Schüler. 2006. Biogenic nanoparticles: Production, characterization, and application of bacterial magnetosome. J. Phys.: - Condens. Matter **18:**S2815-S2828.

Manuscript 10

Lang, C., D. Schüler, and D. Faivre. 2007. Synthesis of magnetite nanoparticles for bio- and nanotechnology: Genetic engineering and biomimetics of bacterial magnetosomes. Macromol. Biosci. **7:**144-151.

Additional publication

Manuscript 11

Coker, V. S., I. P. Pearce, C. Lang, G. Van der Laan, R. A. D. Pattrick, N. Telling, D. Schüler, E. Arenholz, and J. R. Lloyd. 2007. Cation site occupancy of biogenic magnetite compared to polygenic ferrite spinels determined by X-ray magnetic circular dichroism. Eur. J. Min. **19:**707-716.

Contributions

Manuscript 1

C. Lang carried out all experiments and wrote the manuscript together with D. Schüler.

Manucscript 2

C. Lang developed the concept of the study and wrote the manuscript together with D. Schüler. Except for two vectors (pGEMdc163, pGEMdc262) that were made by R. Uebe, C. Lang constructed all plasmids, with support from A. Pollithy and I. Kostadinov. All other experiments were conducted by C. Lang.

Manuscript 3-7 and Manuscript 11

C. Lang cultivated different strains of *M. gryphiswaldense* in an oxystat fermenter for the large scale production of bacterial biomass. He optimized procedures for the purification of magnetosome particles and produced highly pure magnetosome particles with intact magnetosome membranes. C. Lang controlled the purity and integrity of isolated magnetosomes by transmission electron microscopy (TEM) and quantified the amount of magnetosomes by iron assays. In addition, C. Lang conducted TEM analysis of magnetosome-nanogold conjugates together with B. Ceyhan for manuscript 3.

Manuscript 8 and 9

Both authors contributed equally to the manuscripts.

Manuscript 10

All three authors contributed equally to the summary, introduction and the "properties of magentosomes" section, whereas the "biomimetics" part was written principally by D. Faivre, and the part on "biotechnological applications and functionalization of magnetosomes" was principally written by C. Lang. D. Schüler contributed to all sections of the manuscript with many comments and suggestions on structure, content and wording.

I hereby confirm the above statements:

Claus Lang   Prof. Dr. Dirk Schüler

Table of Contents

Abbreviations

CET	Cryo-electron tomography
CL	Cell lysate
DC	Dendritic cell(s)
ELISA	Enzyme-linked immunosorbent assay
HBsAg	Hepatitis B surface antigen
MAI	Magnetosome island
MM	Magnetosome membrane
MMP	Magnetosome membrane protein(s)
MP	Membrane protein
MRI	Magnetic resonance imaging
MTB	Magnetotactic bacteria
NF	Non-magnetic fraction
NIRF	Near-infrared fluorescence
PDZ	A protein domain also found in the proteins, <u>P</u>SD95, <u>D</u>lgA and <u>Z</u>o-1
SAV	Streptavidin
SDS-PAGE	Sodium dodecyl sulphate – polyacrylamide gel electrophoresis
SP	Soluble protein
TEM	Transmission electron microscopy
TPR	Tetra trico-peptid
XMCD	X-ray magnetic circular dichroism

Summary

Magnetosomes are magnetic nanoparticles that are formed by magnetotactic bacteria (MTB) by a complex, genetically controlled biomineralization process. Magnetosomes from the model organism *Magnetospirillum gryphiswaldense* consist of single-magnetic-domain sized nanocrystals of chemically pure magnetite, which are formed intracellularly within specialized membranous compartments. The natural coating by the biological membrane and the defined physico-chemical properties designate magnetosomes as a biogenic material with high bio- and nanotechnological potential. In addition, there is a great interest in the cell biology of magnetosome formation in MTB. The development of these true bacterial organelles involves the invagination of distinctly sized membrane vesicles and the assembly of magnetosome vesicles in chain-like arrangements along novel cytoskeletal structures.

The first part of this thesis focussed on the development of genetic tools for the functionalization and expression of modified magnetosome proteins. The identification of proteins that are specifically and efficiently inserted into the magnetosome membrane (MM) was facilitated by analysis of green fluorescent protein (GFP) fusions of different magnetosome membrane proteins (MMP). After optimization of cultivation conditions for the utilization of GFP in MTB, it has been demonstrated that fusions of the proteins MamC, MamF and MamG are specifically targeted to the MM. In particular, the MamC-GFP fusion protein was stably integrated and highly abundant in the MM. Therefore, MamC represents an ideal anchor protein for the immobilization of functional proteins in the MM.

To address the question, if a specific signal sequence determines the magnetosome specific targeting of MamC-GFP, the localization of truncated MamC derivatives was studied. These experiments have shown that, except for the last nine C-terminal amino acids, the entire sequence is required for the correct targeting and membrane insertion of MamC. Stability of MamC-GFP is greatly reduced if larger parts are missing or if the N-terminus is deleted.

MamC-GFP localized at the expected position of the magnetosome chain irrespective of cultivation conditions that impeded magnetite formation. This shows that MMP targeting, magnetosome vesicle formation and magnetosome chain assembly are not dependent on the prevalence of magnetite inducing conditions or the presence of magnetite crystals. In contrast, the localization of MamC-GFP was altered in the magnetic *ΔmamK* as well as in the non-magnetic MSR-1B, *ΔmamB*, *ΔmamM*, *ΔmamJKL* mutants in comparison to the wild type. This indicates that the interaction with specific proteins in the magnetosome vesicle is

required for the correct localization of MamC. The spotted MamC-GFP signals in the *ΔmamJ* mutant, which are congruent with the position of magnetosomes in this strain, indicate that MamJ is not required for the magnetosome-specific targeting of MamC-GFP. It has also been demonstrated that the native MamC protein and other proteins encoded by the *mamGFDC* operon are not required for the magnetosome-directed targeting of MamC, as the localization patterns of MamC-GFP in the *ΔmamC* and *ΔmamGFDC* mutants were similar to the localization of MamC-GFP in the wild type and congruent with the position of the magnetosomes.

The comparison of different promoters from *E. coli* and *M. gryphiswaldense* by fluorometry and flow cytometry with a GFP-reporter system revealed that the magnetosomal promoter, P_{mamDC}, is highly efficient in *M. gryphiswaldense*. The applicability of this promoter for the functionalization of magnetosomes has been demonstrated by expression of a fusion protein of MamC and the antibody binding 'ZZ' protein in the MM to generate antibody-binding magnetosomes. In addition, the *E. coli* P_{tet} promoter has been identified as the first inducible promoter for regulated gene expression in MTB. The expression was tightly regulated in the absence of an inducer and a ten-fold increase of the proportion of fluorescent cells was observed in the presence of the inducer anhydrotetracycline. Therefore, the P_{tet} promoter is an important addition to the *M. gryphiswaldense* genetic toolbox.

In the second part of this thesis, magnetosomes were tested for their use in biomedical and biotechnological applications. To this end, large scale procedures for the purification of intact magnetosomes were developed. In collaboration with the groups of Prof. Dr. C. M. Niemeyer (Universität Dortmund) and Dr. R. Wacker (Chimera Biotec), streptavidin-biotin chemistry was employed to develop a modular system for the production of DNA- and antibody-coated magnetosomes. The modified magnetosomes were used in DNA- and protein detection systems, and an automatable magnetosome-based Magneto-Immuno-PCR procedure was developed for the sensitive detection of antigens.

With collaborators from the groups of Dr. T. Hieronymus (RWTH Aachen) and Dr. I. Hilger (Universität Jena), it has been shown that magnetosomes can be used as specific magnetic resonance imaging (MRI) contrast agents for phagocytotic cells such as macrophages and dendritic cells to study cell migration. Fluorescently labelled magnetosomes were successfully used as bimodal contrast agents for the visualization of labelled cells by MRI and fluorescence imaging.

Introduction

The formation of magnetosomes in magnetotactic bacteria (MTB) is of great interdisciplinary interest in fields of microbial cell biology, biotechnology and nanotechnology. Magnetosomes, which serve as navigational tools for geomagnetic orientation, are formed by a complex synthesis process. This process is of particular cell biological interest as it involves the formation of a unique microbial organelle, the magnetosome vesicle, which represents a third membranous compartment in addition to the cytoplasmic and the periplasmic membrane. It has been shown that a novel cytoskeletal element, the magnetosome filament, is essential for the assembly of magnetosome chains. However, due to the limited availability of genetic tools, many aspects of magnetosome formation are still elusive.

Magnetosomes may also represent a superior alternative to chemically synthesized magnetic nanoparticles for a broad range of disciplines including nanosciences, material sciences and biotechnology. Despite of the development of various elaborate chemical procedures, the production of magnetite nanoparticles with uniform magnetic properties, sizes and shapes as well as a stable, biocompatible surface that prevents particle aggregation, has remained a challenge (Gupta *et al.* 2005; Wu *et al.* 2008). The strict biological control of the biomineralization process of bacterial magnetosomes results in nearly monodisperse, membrane-bounded magnetic nanoparticles with unique magnetic properties, which could be useful for many applications.

In this thesis biotechnological applications of magnetosomes were investigated, and novel genetic tools for *M. gryphiswaldense* were developed. These tools have not only been useful for the genetic engineering of magnetosomes but also provided new insights into the cell biology of magnetosome formation.

Magnetotactic bacteria and the natural function of magnetosomes

While analyzing bacterial enrichments from mud samples of a salt marsh close to Woods Hole, Massachussets, the american microbiologist Richard Blakemore made the serendipitous discovery of a novel group of bacteria, which swam along geomagnetic field lines (Blakemore 1975). MTB are a phylogenetically and morphologically heterogeneous group of microorganisms, which are found in the oxic-anoxic transition zone of fresh water and marine habitats (Bazylinski *et al.* 2007b; Flies *et al.* 2005). The outstanding feature of this group is the presence of membrane-bounded magnetic organelles called magnetosomes

(Balkwill *et al.* 1980; Gorby *et al.* 1988). Magnetosomes consist of membrane-bounded nanocrystals of a magnetic iron mineral and are assembled in chain-like structures within the cell. The presence of magnetosome chains cause the cells to align passively along magnetic field lines and to behave like self-propelled compass needles. MTB combine aerotaxis, magnetic orientation in the earth magnetic field and possibly chemotaxis, to efficiently find optimal growth conditions in chemically stratified habitats (Frankel *et al.* 2007). Magnetotactic orientation was found among various Gram-negative organisms of the α-, β- and δ-proteobacteria as well as members of the *Nitrospira*-Phylum, and many different cell morphologies were observed such as cocci, vibrio, rods, spirilla and even multicellular aggregates (Amann *et al.* 2006; DeLong *et al.* 1993; Flies *et al.* 2005; Schüler 2008; Spring *et al.* 1993). As MTB are difficult to cultivate, until now only few strains are available as axenic cultures. The best characterized MTB are the three α-proteobacteria *Magnetospirillum magnetotacticum* MS-1, *Magnetospirillum magneticum* AMB-1 and *Magnetospirillum gryphiswaldense* MSR-1 (Bazylinski *et al.* 2007a).

Magnetospirillum gryphiswaldense

M. gryphiswaldense was isolated 1990 from the sediment of a small river near Greifswald (Schleifer *et al.* 1991; Schüler *et al.* 1992). The helically shaped cells, which are motile by a single flagellum at each cell pole, are 2-3 μm long and 0.5-0.8 μm in diameter. The microaerophilic organism grows chemorganoheterotrophically with different organic acids as energy and carbon source and with oxygen or nitrate as terminal electron acceptors (Schleifer *et al.* 1991). In comparison to other MTB, *M. gryphiswaldense* is characterized by a slightly higher oxygen tolerance (Heyen *et al.* 2003). The availability of a genetic system and the nearly completed draft genome sequence designate *M. gryphiswaldense* as a model organism for molecular biological studies on magnetite biomineralization and for the development of biotechnological applications of magnetosomes (Richter *et al.* 2007; Schüler 2008; Schultheiss *et al.* 2003).

Properties of the magnetic crystal

The properties of the inorganic magnetosome core are critical not only for their natural function in magnetotaxis but also for their application in biotechnology. In contrast to some environmental organisms, which form greigite (Fe_3S_4) magnetosomes (Farina *et al.* 1990; Mann *et al.* 1990), *M. gryphiswaldense* and other cultivated MTB exclusively form magnetite (Fe_3O_4) crystals even under reducing conditions, which have been considered to promote

greigite formation (Faivre *et al.* 2008b; Frankel *et al.* 1979; Schleifer *et al.* 1991). This indicates that MTB exert a high degree of control over the composition of magnetosome crystals. Cultivation experiments of *M. gryphiswaldense* with increased copper, zinc, nickel and manganese concentrations also yielded magnetosomes consisting of pure magnetite, free of contaminations from other metals (Faivre *et al.* 2008b). However, the incorporation of cobalt might be an exception, since the formation of cobalt-doped magnetosomes with modified magnetic properties has been reported recently (Staniland *et al.* 2008). Magnetosome crystals also display a high degree of structural perfection. Recently, the highly sensitive XMCD (X-ray magnetic circular dichroism) method has been employed to analyze magnetite crystals from *M. gryphiswaldense*, extracellularly produced magnetite by *Geobacter sulfurreducens*, *Shewanella oneidensis*, *Geothrix fermentans* as well as geological and chemical magnetite. This study has shown that the structure of magnetosomal magnetite crystals is almost identical to the calculated structure of stoichiometric magnetite. In comparison to stoichiometric magnetite only a slightly higher ratio of Fe^{2+} to Fe^{3+} and a slightly lower ratio of tetrahedral to octahedral iron was observed for magnetosomal magnetite (Coker *et al.* 2007; see Manuscript 11). The high chemical purity and structural perfection of the magnetite crystals is a result from the biomineralization pathway in MTB, which, in contrast to earlier presumptions (Frankel *et al.* 1983), does not proceed via intermediates such as ferrihydrate. Instead, the current model is that Fe^{2+} and Fe^{3+} are first accumulated and then rapidly precipitate in magnetosome vesicles under chemically defined conditions (Faivre *et al.* 2007). For their natural function, it is important to control the chemical composition of magnetosomes, as the slightest changes of the crystal structure could have a great influence on the magnetic properties of the magnetosomes (Staniland *et al.* 2008; Thomas-Keprta *et al.* 2000). From a biotechnological perspective, the chemical purity of magnetosomal magnetite crystals is not only a great advantage, because of the defined magnetic properties of the material, but also because magnetite particles are considered biocompatible (Gupta *et al.* 2005; Schwertmann *et al.* 1991).

The magnetic properties of magnetosomes also largely depend on the crystal morphology (Kopp *et al.* 2006). The crystal morphologies are under species-specific control and almost identical among a single species (Arató *et al.* 2005; Bazylinski 1994; Sparks *et al.* 1986). While many different crystal morphologies such as bullet-shaped, pseudo-hexagonal prismatic and cubooctahedral magnetosomes have been observed in different bacteria, *M. gryphiswaldense* forms cubo-octahedral magnetosomes (Schüler *et al.* 1999).

Similar to the morphology, the magnetosome size can vary greatly between different species. Generally, sizes from 35 nm to around 120 nm in diameter are observed (Arató *et al.* 2005; Devouard *et al.* 1998; Lins *et al.* 1998; Moskowitz *et al.* 1988). Mature magnetosomes of *M. gryphiswaldense* usually have a diameter of 37-42 nm in average (Faivre *et al.* 2008a; Scheffel *et al.* 2008; Schüler *et al.* 1998). The size of magnetite nanoparticles largely determines their magnetic properties. Magnetite particles with sizes from approximately 30 nm to about 150 nm, like magnetosomes, have the maximum magnetization for magnetite (Faivre *et al.* 2008b; Kopp *et al.* 2008). These particles are in a single-magnetic-domain state, which means that all elementary magnetic dipoles are aligned parallel (Faivre *et al.* 2008b; Kopp *et al.* 2008). Smaller magnetite particles (< 35 nm) also consist of a single magnetic domain, but they possess superparamagnetic characteristics and do not retain a temporally stable magnetization at room temperature because of thermal fluctuations. Larger multi-domain particles (> 150 nm) generally consist of several magnetic domains with magnetic moments oriented in different directions. Thus, multidomain particles have a reduced remanent magnetization in comparison to single-domain particles (Faivre *et al.* 2008b).

In summary, their high chemical purity, homogeneous sizes and morphologies as well as their extraordinary magnetic properties designate magnetosomes from MTB as a novel biomaterial for bio- and nanotechnological applications.

Applications of magnetosomes

Magnetic nanoparticles are of interest for a broad range of disciplines including nanosciences, material sciences and biotechnology. Synthetic magnetic nanoparticles are used in commercial applications such as data storage devices and in form of magnetic fluids in liquid sealings, as magnetic inks, dampers and shock absorbers (Wu *et al.* 2008; Zahn 2001). In nanotechnology, magnetic nanoparticles are considered as components of nanomotors, nanogenerators, nanopumps and other similar nanometer-scale devices (Zahn 2001). Magnetic iron oxide nanoparticles are also of interest for various bioapplications, such as magnetic drug targeting, magnetic resonance imaging (MRI), magnetic fluid hyperthermia, magnetofection and procedures for the separation of biological entities such as cells, proteins and nucleic acids (Barry 2008; Gupta *et al.* 2005; Ito *et al.* 2005; Laurent *et al.* 2008; Lu *et al.* 2007; Osaka *et al.* 2006; Schwertmann *et al.* 1991).

Purified magnetosomes represent a distinct class of biogenic magnetic nanomaterials that display uniform sizes and shapes, high magnetic susceptibilities, low toxicity, good dispersibility, and a biocompatible surface in form of the MM. Consequently, magnetosomes

have been suggested in numerous biotechnological and biomedical applications. For instance, magnetosomes have been investigated as carriers in magnetic drug targeting (Guo *et al.* 2008; Sun *et al.* 2008b). Another potential application is the hyperthermal treatment of tumors, which involves magnetic nanoparticles to generate heat in specifically targeted tissues and induce cell necrosis (Thiesen *et al.* 2008). Magnetosomes could be used to increase the efficiency of tumor treatment by hyperthermia, because they have extremely high specific loss powers (960W/g at 10 kA/m and 410 kHz) and generate more heat than chemically synthesized magnetic nanoparticles upon exposure to alternating magnetic fields (Eberbeck *et al.* 2005; Hergt *et al.* 2005). Iron oxide nanoparticles with extraordinary magnetic properties are also needed as contrast agents for the discrimination of tissues by MRI (Sun *et al.* 2008a). For instance, tumor cells can be detected, because they do not possess an effective reticuloendothelial system and do not accumulate resonance enhancing particles (Pankhurst *et al.* 2003). The potential of magnetosomes in MRI applications has been demonstrated by the detection of microtumors in rats (Baeuerlein *et al.* 1998; Reszka 2000).

In addition, a number of biotechnological applications have been reported such as procedures for the extraction of DNA and mRNA from different biological samples such as bacterial cells, blood and tissues (Sode *et al.* 1993; Yoza *et al.* 2003a; Yoza *et al.* 2003b). A number of magnetosome-based immunoassays were developed to detect antigens, environmental pollutants, hormones and toxic substances (Tanaka *et al.* 2000; Tanaka *et al.* 2004; Yoshino *et al.* 2005a; Yoshino *et al.* 2006). Many of these biotechnological applications depend on interactions of surface-modified magnetosomes that interact with certain target molecules. Therefore, a detailed knowledge of the composition and function of the MM is crucial for the development of functional magnetosomes and magnetosome-based biotechnogical applications.

The magnetosome membrane

The biomineralization of magnetite crystals takes place in specialized subcellular compartments, the magnetosome vesicles. Empty and partially filled magnetosome vesicles were observed in iron-starved cells by thin-section transmission electron microscopy (TEM) and cryo-electron tomography (CET) (Gorby *et al.* 1988; Komeili *et al.* 2004; Scheffel *et al.* 2006a). Using CET Komeili *et al.* have recently observed immature magnetite crystals in invaginations of the cytoplasmic membrane (Komeili *et al.* 2006). These findings demonstrate (i) that the MM is formed by invagination of the cytoplasmic membrane, and (ii) that magnetosome vesicles do not necessarily detach from the cytoplasmic membrane prior to

magnetite precipitation (Komeili *et al.* 2006; Schüler 2008). The CET results also suggest that the periplasm and the magnetosome lumen are connected (Komeili *et al.* 2006). However, since magnetosome mineralization relies on controlled redox and pH conditions as well as on supersaturating iron concentrations, the magnetosome vesicles are considered to serve as "nanoreactors" that provide controlled conditions for magnetite biomineralization. Therefore, it has been suggested that chemical exchange between the periplasm and the magnetosome lumen is impeded by a barrier in form of a transport protein (Schüler 2008)

After maturation of the magnetite crystal, the MM provides a "natural coating", which remains attached to the magnetosome crystal even after cell lysis. Biochemical analysis of whole cell lipids and purified magnetosomes from *M. gryphiswaldense* has shown that the most abundant polar lipids in the MM and in whole cell extracts are phosphatidylethanolamine and phosphatidylglycerol (Grünberg *et al.* 2004). Analyses of the fatty acid compositions revealed that the MM contains most of the fatty acids that are found in the whole cell lipid, except for fatty acids that are typically present in the outer membrane of gram-negative bacteria (Grünberg *et al.* 2004; Schüler 2004). These findings are in agreement with the formation of magnetosome vesicles by invagination of the cytoplasmic membrane. Using proteomic approaches, a distinct set of more than 20 proteins that are specifically associated with the MM was found (Gorby *et al.* 1988; Grünberg *et al.* 2004; Grünberg *et al.* 2001; Tanaka *et al.* 2006). Sequence analysis revealed that many proteins identified in the MM of *M. gryphiswaldense* display similarities to proteins identified in the MM of *M. magneticum* and *M. magnetotacticum*. This suggests that different MTB express a conserved set of magnetosome membrane proteins (MMP) (Richter *et al.* 2007; Schüler 2008). In *M. gryphiswaldense,* most of the MMP are encoded within the *mamGFDC*, *mms* and *mamAB* operons (Grünberg *et al.* 2004; Schübbe 2006). These operons are located on a genomic magnetosome island with a size of 130 kb (Ullrich *et al.* 2005). A similar organization of magnetosome genes was later also found in other MTB including *M. magneticum* (Fukuda *et al.* 2006), *M. magnetotacticum*, the magnetic coccus MC-1 and the magnetic vibrio MV-1 (Jogler *et al.* 2008).

The sequences of some MMP display similarities to experimentally analyzed proteins of other organisms. For instance, MamM and MamB belong to the cation diffusion facilitator family (Grünberg *et al.* 2004; Grünberg *et al.* 2001) and have been shown to be involved in the magnetosome-directed iron transport (Junge 2008). Other MMP contain domains with similarities to serine proteases (e.g. MamE, MamO), PDZ domains (MamE), and tetra trico-peptide (TPR) proteins (MamA) (Grünberg *et al.* 2004; Grünberg *et al.* 2001). The serine

proteases might be involved in the processing of MMP, and proteins with PDZ- and TPR-motifs possibly interact with other proteins in the MM (Schüler 2008). Analysis of the MamA protein in *M. magneticum* has indicated that this protein is involved in the activation of magnetosome vesicles prior to magnetite precipitation. A putative heme-binding protein (MamT), an MreB-like protein (MamK) and a putative ion transporter (MamN) were also found in association with the MM (Grünberg *et al.* 2004; Tanaka *et al.* 2006; B. Voigt, T. Schweder, personal communication). In addition, several proteins that contain highly repetitive sequence motifs reminiscent of motifs in proteins involved in other biomineralization systems (Mms6, MamG, MamD and MamJ) (Grünberg *et al.* 2004; Schüler 2008), and many proteins with no homologies to previously characterized proteins were identified.

Even though a specific set of MMP and their genetic determinants were identified, the function of most MMP is still unknown. It is also unclear by which mechanisms the MMP are targeted and assembled in the magnetosome compartment. To understand the biomineralization process on a molecular level, genetic and biochemical analyses of MMP are required. In addition to the aforementioned MamM, MamB and MamA proteins, MamJ, MamK, Mms6 and proteins encoded by the *mamGFDC* operon were analyzed experimentally. The results of these studies are summarized in the following sections.

The *mamGFDC* operon

The proteins encoded by the *mamGFDC* operon contain several putative transmembrane domains and are the most abundant proteins in the MM of *M. gryphiswaldense* (Figure 1). The proteins, which are expressed from a single promoter upstream of *mamG* (P_{mamDC}) (Schübbe 2006), constitute 35% of the proteins in the MM (Grünberg *et al.* 2004). There are no known homologues in organisms other than MTB, and thus the proteins represent unique, MTB-specific protein families (Grünberg *et al.* 2004). The presence of conspicuous LG-rich repetitive motifs, which are reminiscent of proteins that have a tendency for self-aggregation of other biomineralization systems, in MamG and MamD indicate a potential role in biomineralization (Figure 1, C) (Schüler 2008). A similar LG rich repeat was also found in Mms6, which has been suggested to be involved in magnetite nucleation (Amemiya *et al.* 2007). Deletions of *mamC* or of the entire *mamGFDC* operon have shown that the proteins are not essential for magnetite biomineralization, even though the crystals of both mutants displayed slightly decreased sizes. Complementation

9

experiments indicated that MamG, MamF, MamD and MamC have redundant functions and act cumulatively to control the magnetosome crystal size (Scheffel *et al.* 2008).

High abundance in the MM and functional redundancy of MamG, MamF, MamD and MamC is of high relevance for biotechnological applications. Especially the small MamG, MamF and MamC proteins (Figure 1, C) could be useful as anchor proteins for the display of polypeptides and functional proteins in the MM, without changing the properties of the magnetite crystals.
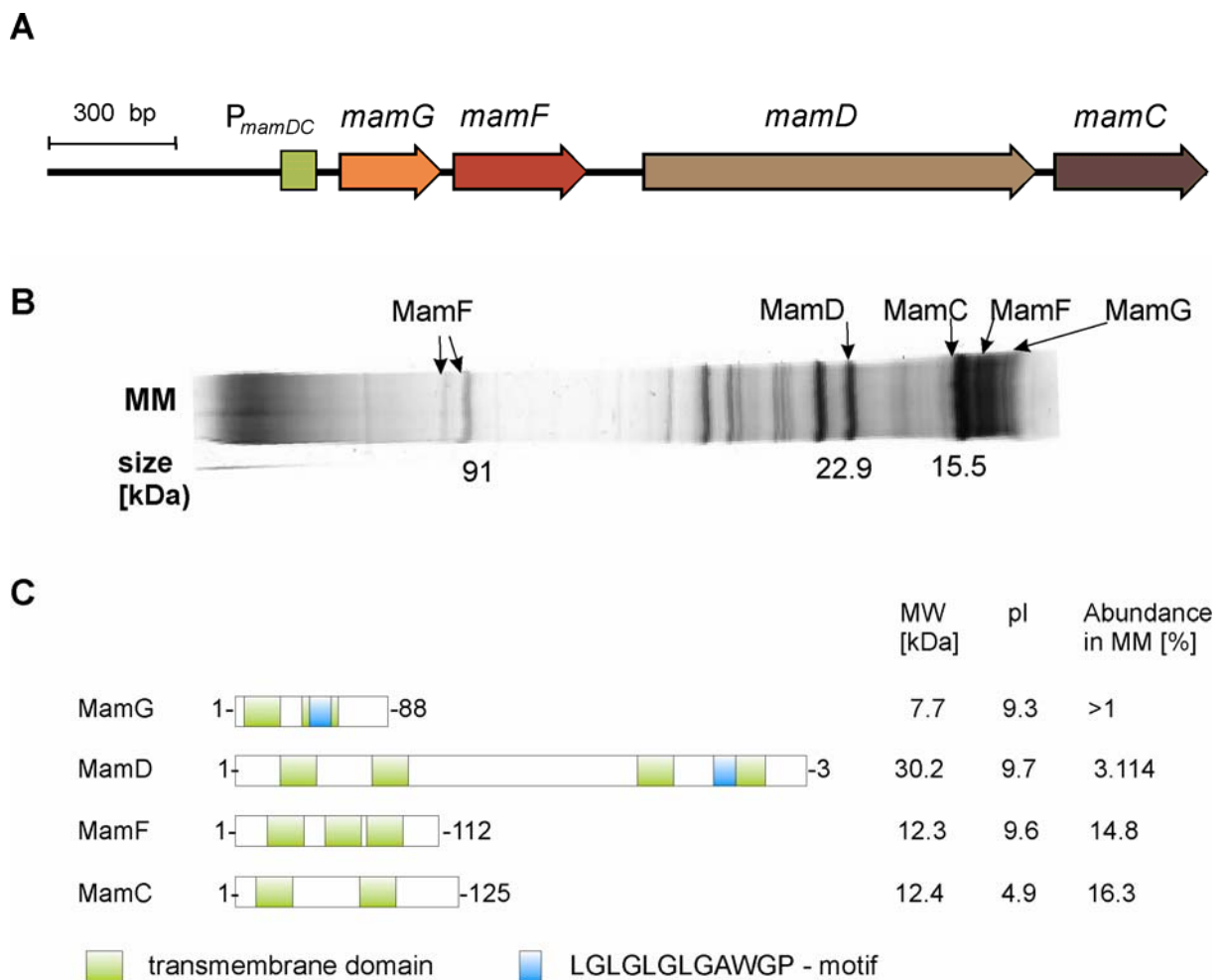
Figure 1: Characteristics of the MMP MamG, MamD, MamF, and MamC. (A) Genetic organization of the *mamGFDC* operon; (B) Separation of MMP by sodium dodecylsulfate polyacrylamide gel electrophoresis (SDS-PAGE) (Grünberg *et al.* 2001). The positions and sizes of MamG, MamD, MamF and MamC are indicated; (C) Bioinformatic prediction of transmembrane domains (TopPred:http://bioweb.pasteur.fr/seqanal/interfaces/toppred.html, *last accessed 20.01.09*) and selected characteristics of MamG, MamD, MamF and MamC. (Modified after (Scheffel 2007; Schüler 2008)

The assembly of magnetosome chains

In independent studies of *M. gryphiswaldense* and *M. magneticum,* intriguing filamentous structures were observed close to the magnetosome vesicles by CET. The so-called magnetosome filament consists of many 3-4 nm thick filaments, which extend from cell pole to cell pole (Komeili *et al.* 2006; Scheffel *et al.* 2006a). Presumably, the magnetosome filaments stabilize magnetosome chains in the cell. This is required as strings of magnetic dipoles easily collapse (Kirschvink 1982), and calculations show that a magnetic moment of a chain of at least eleven magnetosomes is needed to align a bacterial cell in the geomagnetic field (Faivre *et al.* 2008b). In addition, the magnetosome filament might play a role for the transmission of the magnetic torque to the cell.

By analysis of GFP fusions in *M. magneticum* and *M. gryphiswaldense* it was observed that three proteins, MamA, MamJ and MamK, localize as thin lines reminiscent of the magnetosome filament (Komeili *et al.* 2006; Komeili *et al.* 2004; Scheffel *et al.* 2006a; Scheffel *et al.* 2007). As a deletion of MamA in *M. magneticum* did not affect the localization of magnetosomes but resulted in a reduced number of magnetosome crystals per cell, the protein is probably not involved in magnetosome chain assembly (Komeili *et al.* 2004). A deletion of the MreB-like MamK protein in *M. magneticum* resulted in cells with magnetosomes dispersed throughout the cell (Komeili *et al.* 2006). In *M. gryphiswaldense,* cells lacking MamK still contained magnetosome chains, but the chains were shorter and often several short chains were observed in the same cell (Katzmann, personal communication). In addition, *in vitro* data and the expression of MamK-Mcherry in *E. coli* demonstrated that MamK polymerizes to filamentous structures (Pradel *et al.* 2006; Taoka *et al.* 2007). All these studies indicate that MamK is involved in the formation of the magnetosome filament.

A deletion of *mamJ,* which encodes for an acidic protein with a high content of repetitive sequence motifs, does not affect biomineralization but resulted in the formation of three dimensional magnetosome clusters instead of magnetosome chains (Scheffel *et al.* 2006a). Bacterial two-hybrid studies have shown that MamJ interacts with MamK (Scheffel *et al.* 2007). Therefore, it has been hypothesized that the integral MMP MamJ links magnetosome particles to the magnetosome filaments by interaction with MamK (Scheffel *et al.* 2007).

Based on genetic analyses of magnetosome proteins and on ultrastructural data it has been possible to propose a hypothetical model for the molecular mechanisms of magnetite biomineralization and magnetosome chain assembly (Figure 2) (Scheffel *et al.* 2006b).

However, the recent genetic advances and the identification of the magnetosome filament of a novel cytoskeletal structure have clearly demonstrated that magnetosome biomineralization is a highly complex process, which poses many new questions. How is the targeting of magnetosome proteins to the vesicles facilitated? Which factors mediate vesicle invagination? Why are magnetosome chains most often observed at midcell, even though the magnetosome filament bundles extend from cell pole to cell pole? Do magnetosome proteins interact with other cytoskeletal protein or with the cell division machinery? Are interactions with the cell division machinery involved in magnetosome partitioning during cell division? To answer these and other cell biological questions the genetic analysis of additional magnetosome genes and the development of novel genetic tools will be required.
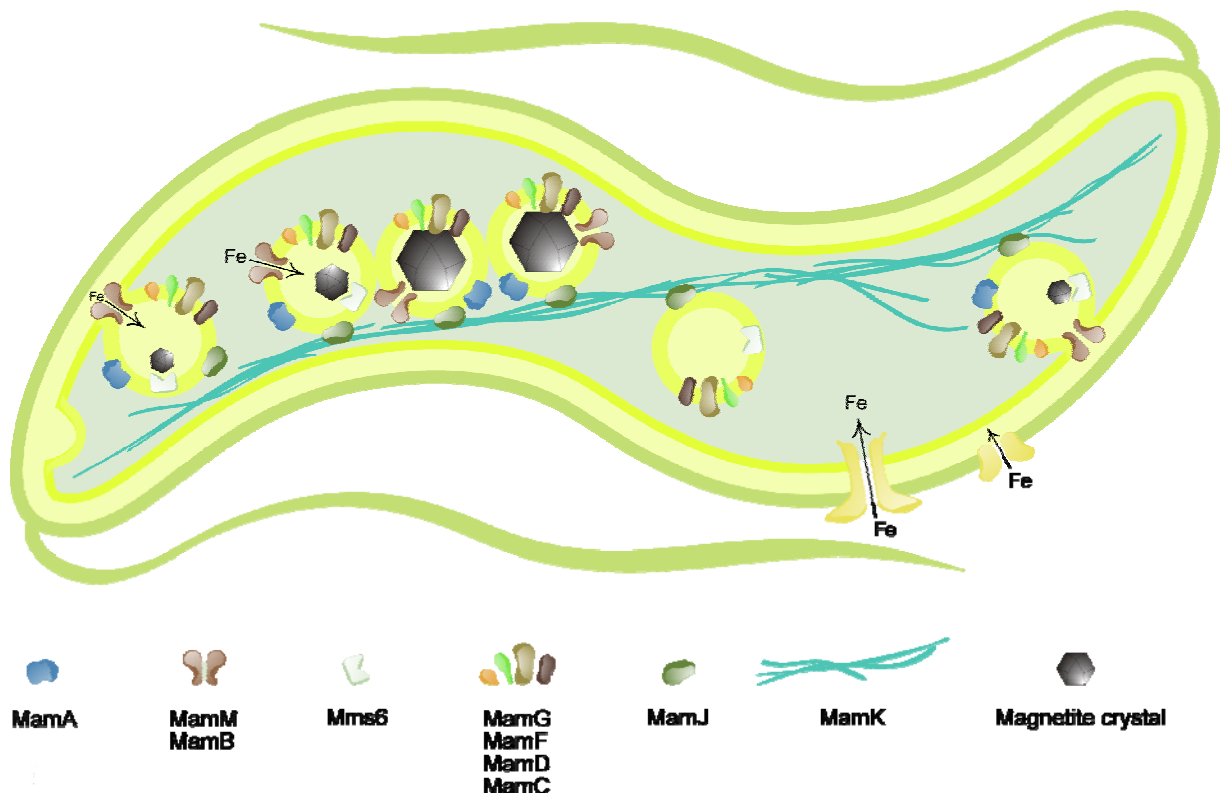
Figure 2: Schematic illustration of the current model for magnetite biomineralization in MTB based on ultrastructural and genetic data. Magnetosome vesicles are formed by invaginations of the cytoplasmic membrane. A number of proteins are incorporated into the MM. After activation by the MamA protein iron might be transported into the magnetosome vesicles either from the periplasm or from the cytoplasm by the MamM and MamB proteins. After iron supersaturation, magnetite nucleation is mediated by the Mms6 protein. Crystal growth is supported by the proteins MamG, MamF, MamD and MamC. The magnetosome vesicles are arranged in a chain-like manner along the longitudinal axis of the cell by interaction of the MMP MamJ and the MamK protein, which is probably part of the magnetosome filament. The possible pathways for iron transport are indicated by black arrows. (Adapted from (Scheffel *et al.* 2006b)).

Tools for the genetic analysis of magnetosome formation and for genetic engineering of magnetosomes

General genetic tools for MTB

Despite considerable efforts by many researchers, the genetic analysis of magnetosome biomineralization in MTB is still cumbersome. This is mainly attributed to their slow growth and their fastidious growth requirements (Jogler *et al.* 2006). Another difficulty of the genetic analysis of MTB is that genomic rearrangements occur frequently (Schübbe *et al.* 2003; Ullrich *et al.* 2005). This is probably caused by mobile genetic elements that are highly abundant in genomes of MTB (Matsunaga *et al.* 2005; Richter *et al.* 2007). Only recently a limited number of procedures for the genetic analysis of MTB has been established.

Transfer of plasmid DNA into MTB is generally achieved by conjugation from *E. coli* (Matsunaga *et al.* 1992; Schultheiss *et al.* 2003). Several attempts to develop an electroporation procedure were made, but, due to adverse effects of the magnetosome chain in strong electric fields, the efficiency is not satisfying (Okamura *et al.* 2003; Schultheiss *et al.* 2003). A number of replicative plasmids with different antibiotic resistance markers are available for MTB. These include broad host range vectors of the IncQ, IncP, and pBBR1 incompatibility groups and an endogenous plasmid from *M. magneticum* (Matsunaga *et al.* 1992; Okamura *et al.* 2003; Schultheiss *et al.* 2003). In addition, procedures for transposon- and site-specific deletions were developed (Matsunaga *et al.* 1992; Schultheiss *et al.* 2004). Systems for the generation of non-marked mutants were developed to minimize pleiotropic effects of deletions of genes located within an operon (Komeili *et al.* 2006; Komeili *et al.* 2004; Scheffel *et al.* 2008; Scheffel *et al.* 2006a). A *cre-lox* based system has also been used recently to generate non-polar, in frame deletions in *M. gryphiswaldense* (Junge 2008; Scheffel *et al.* 2008). For instance, in *M. gryphiswaldense* deletions of the cation diffusion facilitator proteins MamM and MamB, which are encoded in the *mamAB* operon and are part of the magnetosome subproteome (Grünberg *et al.* 2004), indicate, that these proteins are essential for magnetosome formation (Junge 2008).

GFP as a reporter for gene expression and protein localization in MTB

The *green fluorescent protein* (GFP) and its derivatives are reporters that can be used to study gene expression and protein localization in many different bacteria. In *Escherichia coli,* the hierarchically and temporally ordered localization of many different cell division proteins was visualized during cell cycle with fluorescent proteins. Other cell biological model organisms are *Bacillus subtilis* and *Caulobacter crescentus,* in which GFP assisted

studies have led to a better understanding of the determinants of cell shape, sporulation, DNA segregation, cell division and membrane protein targeting (Southward *et al.* 2002; Valdivia *et al.* 1996). Until now, in *M. gryphiswaldense* and other MTB, mostly reporters like β-glucuronidase, encoded by *gusA*, which can be used for blue/white screening (Schultheiss *et al.* 2004) and luciferase (Nakamura et al. 1995b; Matsunaga et al. 2000) have been used for the analysis of gene expression. Only recently, GFP and derivatives have been employed as tools for protein localization studies in MTB (Komeili *et al.* 2006; Komeili *et al.* 2004; Scheffel *et al.* 2006a; Scheffel *et al.* 2007; Schultheiss *et al.* 2005). Even though the utilization of GFP has provided amazing insights especially into the cell biology of MTB, the utilization of GFP in MTB poses some difficulties and pitfalls, which have not been addressed systematically yet. One problem in previous studies was that only a low proportion of cells displayed fluorescence (Komeili *et al.* 2006; Komeili *et al.* 2004). In addition, the use of GFP under micro- and anaerobic growth conditions is limited, since oxygen is required for the maturation of the fluorophore (Heim *et al.* 1994; Reid *et al.* 1997). This is problematic in MTB as magnetite formation only occurs under microaerobic and anaerobic conditions.

Genetic engineering of the magnetosome surface

Most applications of magnetosomes require the presence of specific functional moieties, such as antibodies, oligonucleotides, fluorophores or enzymes, on the particle surface. Generally, the functionalization of magnetosomes with various functions may be facilitated by a number of chemical or genetic approaches (Figure 3). The genetic engineering of MMP holds several advantages compared to chemical procedures for magnetosome functionalization: (i) harsh conditions, which can cause protein denaturation and loss of activity during chemical modification, can be omitted; (ii) integral parts of the MM can be specifically modified in a controlled manner; (iii) it is not necessary to use expensive reagents such as crosslinking agents; (iv) modified magnetosomes can be purified directly from the cells without further need for modification and loss of material. Several studies have been undertaken to generate functionalized magnetosomes by expression of genetically engineered proteins in *M. magneticum*. For instance, the expression of translational fusions of functional proteins such as protein A, which binds antibodies, G-protein coupled receptors or luciferase with *M. magneticum* MagA and Mms16 was demonstrated (Matsunaga *et al.* 2002; Matsunaga *et al.* 1999; Tanaka *et al.* 2000; Yoshino *et al.* 2004). However, by comparison with Mms13, it has recently been shown that MagA and Mms16 are inefficient MM anchors (Yoshino *et al.* 2006). The efficiency of the Mms13 protein in respect to anchoring functional moieties to the magnetosome surface in *M. magneticum* was also demonstrated by expression

of Mms13 fusions with biotin accepting peptides and biotin carboxyl carrier protein to generate biotinylated magnetosomes *in vivo* (Maeda *et al.* 2008). Altogether, previous investigations of procedures for magnetosome functionalization by genetic engineering in *M. magneticum* indicated that the efficiency is largely dependent on a suitable anchor protein. Ideally, this anchor protein should be integrated stably into the MM in high amounts. In addition, the anchor protein should not interfere with biomineralization or with the function of the added moiety. In addition, it has been highlighted that the efficiency of magnetosome functionalization in *M. magneticum* is largely dependent on the promoter that is used for expression of heterologous proteins (Yoshino *et al.* 2005b). Until now, in *M. gryphiswaldense* the *E. coli* P*lac* promoter has been used exclusively, and it was not yet assessed whether this promoter is as active as native promoters in *M. gryphiswaldense.* Even though an inducible expression system would be very useful for the expression of toxic genes and to control the number of functional moieties on the magnetosome surface, such a system is still lacking for MTB.
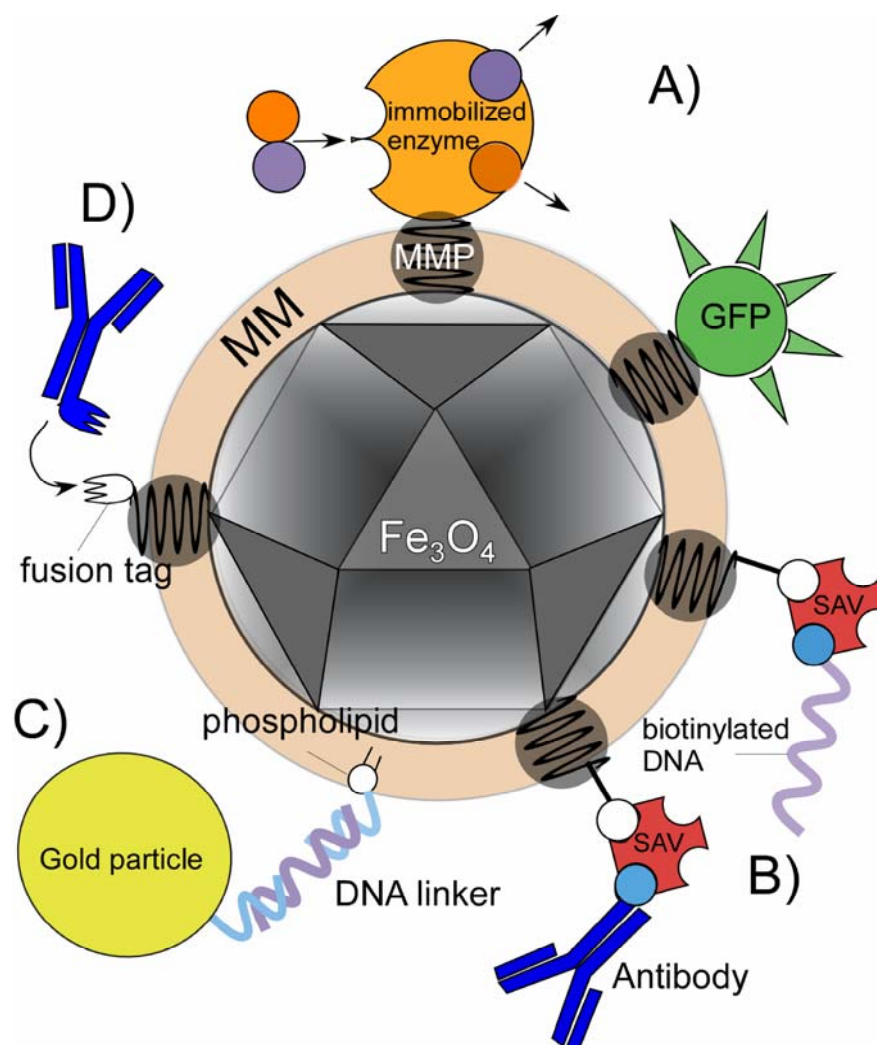

Figure 3: Potential modifications of magnetosome particles by the introduction of different functional moieties resulting in hybrid magnetic nanoparticles. (A) expression of enzyme and fluorophore proteins (e. g.

GFP); (B) biotinylation of membrane lipids and proteins to facilitate subsequent streptavidin-mediated conjugation of antibodies and DNA; (C) conjugates with gold particles or quantum dots via a DNA linker; (D) expression of fusion tags such as intein- or strep-tags as anchor groups for subsequent conjugate formation with various biomolecules. MM magnetosome membrane, MMP magnetosome protein, SAV streptavidin (Adapted from Manuscript 8, Figure 6)

Aims

The central objectives of this thesis have been the development of novel tools for the genetic engineering of magnetosomes in *M. gryphiswaldense* and other MTB, as well as the production of magnetosomes to investigate the usability of bacterial magnetosomes in biomedical, bio- and nanotechnological applications.

The first part of this thesis has been devoted to the development of novel techniques for the expression of genetically engineered proteins in the MM. This approach requires the identification of a suitable membrane anchor protein that is specifically and efficiently targeted to the magnetosome compartment. Translational fusions of this protein should be tightly attached to magnetosomes, withstand mechanical and chemical stresses, and not interfere with biomineralization or with the function of the added moiety. As GFP is a very robust and versatile reporter, it was of interest to optimize the expression conditions for utilization of GFP in MTB. Subsequently, GFP fusions of different MMP should be analyzed to identify a MM anchor and to provide new insights into the localization and targeting of MMP in living cells. Especially, for future functionalization experiments it was of interest to identify a signal sequence or protein domain that facilitates magnetosome-directed protein targeting.

Another prerequisite for the *in vivo* functionalization of magnetosomes is a highly efficient expression system for MTB. At the onset of this investigation in *M. gryphiswaldense* the *E. coli* P_{lac} promoter was used exclusively. As the performance of this promoter had not been assessed systematically, one aim of this thesis was to compare the performance of different promoters in *M. gryphiswaldense* and to develop an efficient expression system for *M. gryphiswaldense*.

The second part of this thesis has been devoted to the production of purified magnetosomes to investigate magnetosome-based applications. It was of particular interest to develop magnetosome-based immunoassays and nucleic acid detection systems, and to investigate if magnetosomes can be used to label specific cell types for MRI.

Results and Discussion

Part I: Development of tools for *in vivo* functionalization of magnetosomes and protein localization in magnetotactic bacteria

The expression of heterologous peptides or proteins on the magnetosome surface by genetic engineering of MMP offers several advantages compared to chemical functionalization approaches. Therefore, the development of suitable genetic tools for *M. gryphiswaldense* is of bio- and nanotechnological significance. Several methods for the genetic analysis of *M. gryphiswaldense* such as the conjugative transfer of plasmids, electroporation, site-directed mutagenesis, expression and intracellular localization of fluorescently labelled proteins have been established recently (Scheffel *et al.* 2008; Scheffel *et al.* 2006a; Scheffel *et al.* 2007; Schultheiss *et al.* 2005; Schultheiss *et al.* 2004; Schultheiss *et al.* 2003). However, studies on magnetosome functionalization by genetic engineering of MMP have been limited to *M. magneticum*. For *M. gryphiswaldense,* specific tools such as efficient MM anchor proteins and protein expression systems are still lacking. In advantage to *M. magneticum,* several mutants of *M. gryphiswaldense* that produce magnetosomes with altered sizes and modified magnetic (e.g. superparamagnetic) properties, are available (Hoell *et al.* 2004; Scheffel *et al.* 2008; Ullrich *et al.* 2005). Magnetosomes from these strains could be used to produce a wide range of magnetic nanoparticles with specifically adapted biochemical and physicochemical characteristics for different applications.

Construction and analysis of GFP-labelled magnetosome membrane proteins

Expression of GFP in microaerophilic bacteria

A variant of the *green fluorescent protein* (GFP) was selected as a tool to study gene expression and protein localization in microaerophilic bacteria. GFP is a highly stable protein, which can be fused to many different proteins without loss of function (Phillips 2001) and which has been used in many different organisms including *M. gryphiswaldense* and *M. magneticum* (Komeili *et al.* 2006; Komeili *et al.* 2004; Scheffel *et al.* 2006a; Scheffel *et al.* 2007; Schultheiss *et al.* 2005). Upon cultivation of a GFP expressing *M. gryphiswaldense* strain under microaerobic growth conditions (1% oxygen; 1:1 ratio of headspace:culture volume), which are usually used during cell cultivation for magnetosome purification, it was

noticed that the overall fluorescence intensity and the proportion of fluorescent to non-fluorescent cells were very low. Since the inefficient maturation of the GFP fluorophore due to lack of oxygen had been reported in other organisms (Hansen *et al.* 2001; Heim *et al.* 1994; Reid *et al.* 1997; Wadhams *et al.* 2002; Zhang *et al.* 2005), GFP fluorescence of cells cultivated under different aeration regimes was investigated. Measurements of the magnetic orientation (C_{mag}) (Schüler *et al.* 1995), fluorescence intensity and the proportion of fluorescent cells after variation of the oxygen concentration and the headspace-to-liquid ratio were conducted. The results showed the highest fluorescence values for aerobically cultivated cells, whereas magnetite formation was maximal under microaerobic conditions. Utilization of air in the headspace and of a headspace-to-liquid ratio of 1:4 resulted in substantial magnetite formation (C_{mag}: 1.7) and a expedient proportion of fluorescent cells (19.7%) (Manuscript 1, Table 4). Under these conditions oxygen decreased gradually during cultivation. Therefore, sufficient oxygen was present to facilitate GFP maturation at the onset of cultivation, while microaerobic conditions prevailed at later growth stages and facilitated magnetite formation.

Even though the utilization of GFP in microaerophilic bacteria requires the accurate control of specific cultivation conditions, there is no equivalent alternative at the moment. Other commonly used enzymatic reporter proteins such as β-glucuronidase, β-galactosidase and luciferase may be suitable to study gene expression in bulk cultures but are inappropriate to study gene expression on a single-cell level. In addition, these reporters are larger and less stable than GFP and cannot be easily fused to other proteins to analyze protein localization *in vivo*. Most of the new commercially available coral reef proteins (Clontech, Mountain View, CA U.S.A) as well as the popular "mFruits" fluorescent proteins are also expected to require oxygen for maturation, as the fluorophores of these proteins are chemically identical to the classical *Aequorea victoria* GFP or to *Discosoma* dsRed, which requires additional reactions during fluorophore formation (Shu *et al.* 2006; Wall *et al.* 2000). In future, flavin-derived fluorescent proteins that fluoresce under anaerobic conditions (Drepper *et al.* 2007) could be used as reporters for gene expression and protein localization in MTB. However, those proteins have not been used as fusion partners for protein localization studies yet and initial attempts to express these proteins in *M. gryphiswaldense* from an *E. coli* P*lac* promoter failed (data not shown).

MamC is an efficient anchor for the display of fusion proteins on magnetosome particles

In *M. magneticum* MagA, Mms16 and Mms13, which is an ortholog of the *M. gryphiswaldense* MamC, were used as MM anchors for the magnetosome specific display

of fusion protein (Matsunaga *et al.* 2002; Matsunaga *et al.* 1999; Tanaka *et al.* 2000; Yoshino *et al.* 2006; Yoshino *et al.* 2004). However, consecutive studies have shown that MagA and Mms16 (renamed as ApdA in *M. gryphiswaldense*) are not part of the magnetosome subproteome of *M. gryphiswaldense* but represent contaminations that non-specifically associated with the magnetosome particles upon cell disruption (Handrick *et al.* 2004; Schultheiss *et al.* 2005).

For the identification of a potential MM anchor protein in *M. gryphiswaldense* GFP was used as a reporter. From a range of C- and N-terminal GFP fusion constructs of different MMP, i.e. MamE, MamO, MamP, MamT, MamC, MamF and MamG, only C-terminal fusions of the highly abundant MMP MamC, MamF and MamG generated fluorescence intensities sufficient for detection by fluorescence microscopy in *M. gryphiswaldense*. Fluorescence of the three fusion proteins was typically observed as linear signals along the cell axis at midcell, where the magnetosome chain is located in most cells. Thus, all three proteins seemed to be targeted specifically and exclusively to the MM (Manuscript 1, Figure 2). This hypothesis was confirmed by immunoblot analysis of different cell fractions for the presence of GFP fusion proteins (Manuscript 1, Figure 3). In addition, quantification of the fluorescence of purified magnetosomes from *M. gryphiswaldense* strains expressing MamC-, MamF- and MamG-GFP demonstrated that the fluorescence is retained *in vitro* (Manuscript 1, Figure 4, Figure 5). The highest level of magnetosome-bound fluorescence was observed with MamC-GFP modified magnetosomes (Manuscript 1, Figure 5). Previous studies have shown that all genes of the *mamGFDC* operon are not essential for magnetosome formation, but that deletions of these protein result in magnetosomes with slightly decreased magnetosome crystal sizes (Scheffel *et al.* 2008). Therefore, the expression of modified versions of these proteins is not expected to inhibit biomineralization, and the three proteins might be well suited as MM anchors.

MamC-GFP modified magnetosomes retained functionality under a variety of storage and incubation conditions *in vitro*. Detection of degradation products of MamF- and MamG-GFP by immunoblot analysis of purified magnetosomes indicated that the fusion proteins are less stable than MamC-GFP (Manuscript 1, Figure 6). Even though expression of native MamC is co-regulated with the other proteins encoded by the *mamGFDC* operon (Schübbe 2006), MamC is the most abundant single protein in the MM (Grünberg *et al.* 2001). This and the fact that the protein withstands tryptic digestion (Grünberg *et al.* 2001) point out that MamC is a highly stable protein. Therefore, from the tested proteins, MamC is the most appropriate MM anchor for magnetosome functionalization in *M. gryphiswaldense*.

In vivo localization of GFP-labelled magnetosome proteins in M. gryphiswaldense

GFP fusion proteins are useful reporters for protein localization in cell biology. Until now, very little is known about magnetosome protein sorting and the assembly of magnetosome vesicles. Therefore, it was of interest to compare the localization patterns of all available GFP-magnetosome protein fusions, to identify different targeting mechanisms and to gain information about the assembly of magnetosome vesicles and chains.

MamC-, MamF- and MamG-GFP predominantly localized at midcell in 0.5-2 µm long linear signals, which were extended along the longitudinal cell axis. In all cases no significant fluorescence was associated with the cytoplasmic membrane (Manuscript 1, Figure 2). The brightest and most compelling signals were observed with MamC-GFP, although the signal was occasionally observed as a single bright fluorescent spot at midcell (Figure 4A). This localization pattern is slightly different from the previously reported localizations of other proteins involved in magnetosome formation.

In collaboration with Katja Junge (AG Schüler), GFP fusions of the presumed magnetosome-specific iron transporter MamM were constructed and analyzed by deconvolution microscopy. The yet unpublished results have shown that MamM-GFP localizes in the cytoplasmic membrane as well as at the position expected for the magnetosome chain (Figure 4A). This could mean that either MamM is non-specifically inserted both into cytoplasmic and magnetosome membranes, or that MamM is integrated into the cytoplasmic membrane prior to magnetosome vesicle invagination and is targeted by a "diffusion-and-capture"-like mechanism, similar as described for the targeting of spore-forming proteins previously (Rudner *et al.* 2002). It is also conceivable that MamM-GFP is far more abundant in the cell than native MamM, due to the artificial *in trans* expression. In this case MamM-GFP might only be inserted into the cytoplasmic membrane after the capacity of the magnetosome vesicles is exceeded. In future, the effect of the expression level of MamM-GFP on its localization could be adressed by localization studies of MamM-GFP expressed from different promoters and by immunoblot quantification of MamM-GFP and native MamM.

In contrast to MamC, MamF and MamG, previously studied GFP fusions of the magnetosome proteins MamK (Komeili *et al.* 2006; Scheffel 2007; Scheffel *et al.* 2007; Schübbe 2005), MamJ (Scheffel *et al.* 2006a) and MamA (Komeili *et al.* 2004) are not specifically and exclusively targeted to the MM. The results of localization studies of MamK are difficult to interpret as until now six different GFP fusions of *M. magneticum* and *M. gryphiswaldense* MamK have been constructed and different localization patterns have been

observed (Komeili *et al.* 2006; Scheffel 2007; Scheffel *et al.* 2007; Schübbe 2005). However, several studies on MamK have indicated that it is involved in magnetosome filament formation and not exclusively targeted to the MM like MamC-, MamF- and MamG-GFP (Komeili *et al.* 2006; Pradel *et al.* 2006; Scheffel *et al.* 2007; Taoka *et al.* 2007; E. Katzmann, personal communication). In exponentially growing *M. magneticum* cells MamA localizes in filamentous structures, which reach from pole to pole. In stationary cells punctuate signals are observed at midcell (Komeili *et al.* 2004). In *M. gryphiswaldense* a MamJ-GFP fusion showed a linear signal extending through most of the cell reminiscent of the MamA-GFP localization in *M. magneticum* (Scheffel *et al.* 2006a). Since the signals of MamA- and MamJ-GFP fusions are much longer than the length of the magnetosome chain, the proteins seem to interact with other parts of the cell and cannot be used to visualize the position of the magnetosome chain *in vivo*.

In summary, the comparison of GFP fusion proteins of different magnetosome proteins shows that MamC-, MamF- and MamG-GFP are targeted specifically and exclusively to the position of the magnetosome chain, whereas other GFP-labelled magnetosome proteins may also localize in different cellular structures such as the cytoplasmic membrane or the magnetosome filament. Due to its strong fluorescence and high abundance in the MM, MamC-GFP is the most appropriate tool to track the position of the magnetosome chain *in vivo*. For instance, MamC-GFP could be used in future experiments to monitor the positioning and partitioning of the magnetosome chain during cell division. In addition, the targeting mechanism of MamC is of great interest to identify the determinants of magnetosome-specific protein sorting.
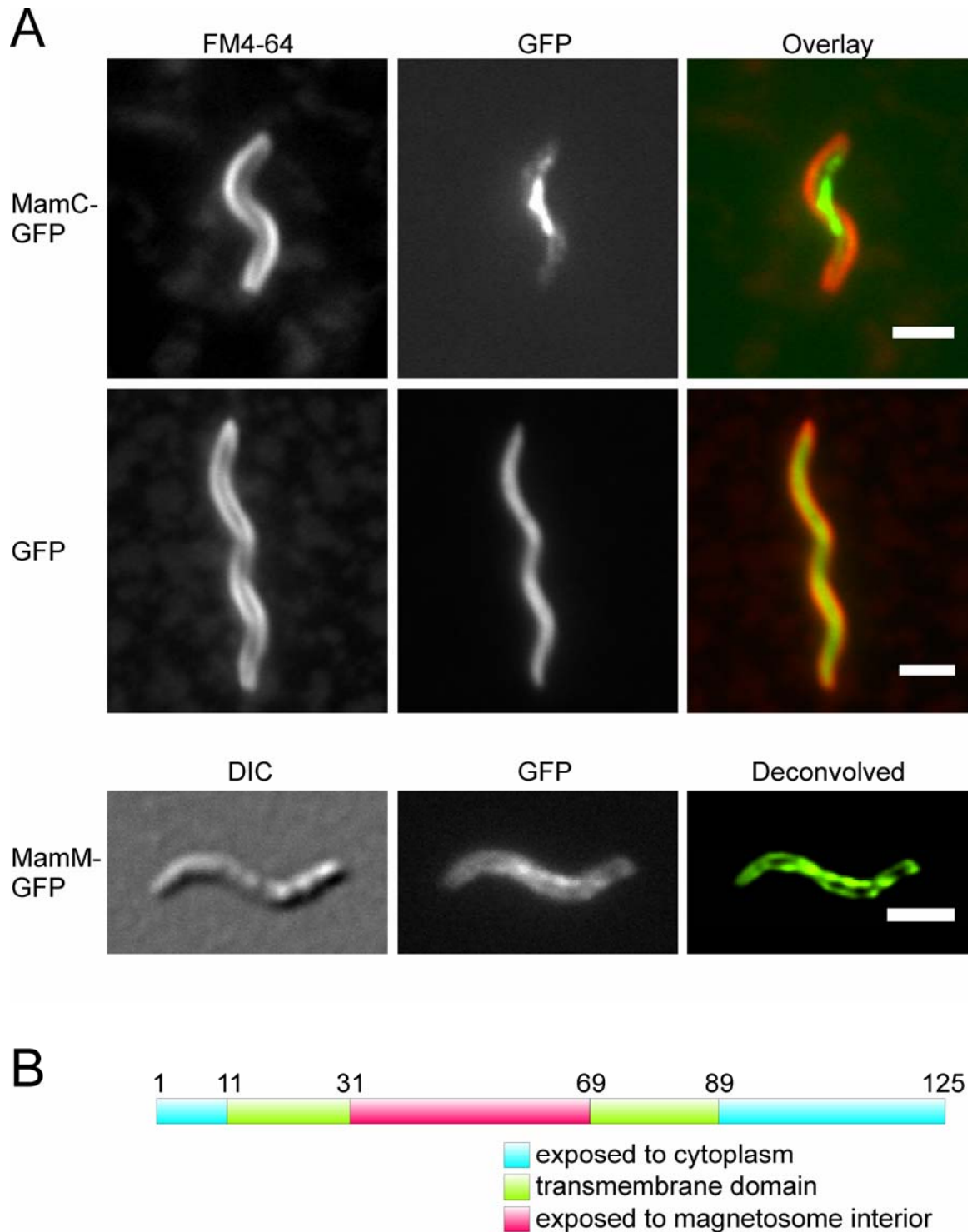
Figure 4: MamC-GFP is specifically targeted to the magnetosome membrane. (A) *In vivo* localization of MamC-GFP and MamM-GFP in wild type cells of *M. gryphiswaldense*. As a control the localization of unfused GFP is shown. The cell membranes were stained with FM4-64 as described in Manuscript 1. In addition, constructs and cultivation conditions for the expression of MamC-GFP and GFP and microscopy procedures are described in Manuscript 1. The construct for the expression of MamM-GFP was cloned in cooperation with Katja Junge (Junge 2008). For better visualisation and to avoid artefacts, the localization of MamM-GFP was studied by deconvolution analysis of image-Z-stacks with the Olympus 3D-Blind algorithm. In addition, the cell shape and position was visualized by differential interference contrast (DIC) microscopy. Scale bars are 2 μm.

(B) Topology of the MamC protein as predicted by the TopPred topology prediction tool (http://bioweb.pasteur.fr/seqanal/interfaces/toppred.html, *last accessed 20.01.09*).

Analysis of GFP fusions of truncated MamC variants

In a further set of unpublished experiments, the MamC protein was investigated more closely to gain more information on the highly specific sorting mechanism of this protein. The identification of signal sequence for magnetosome specific protein targeting would greatly improve the understanding of protein assembly in the MM. In addition, the identification of a signal sequence could be useful for the biotechnological functionalization of magnetosomes.

MamC has two predicted transmembrane domains, and the region between these transmembrane domains is probably located inside the magnetosome vesicle. The short N-terminus (11 amino acids) and the long C-terminal tail (36 amino acids) are exposed to the cytoplasm (Figure 4B). To identify potential targeting signals of MamG, MamF, and MamC the sequences were analyzed with different software tools (TatP (http://www.cbs.dtu.dk/services/TatP/, *last accessed* 05.03.09); TatFind (http://signalfind.org/tatfind.html, *last accessed* 05.03.09); SignalP http://www.cbs.dtu.dk/services/SignalP/, *last accessed* 05.03.09)). In the case of MamC, a potential Sec-dependent translocation signal (probability: 0.577) was predicted by the Hidden Markov Model analysis of the SignalP program but not by any other tool. For MamF no signal sequence was predicted by any of the programs. In contrast, for MamG a putative signal sequence was predicted by the SignalP (probability: 0.997) and the TatP programs. Interestingly, the predicted translocation signals of MamC and MamG overlap with the transmembrane helices predicted by TopPred. This indicates that the proteins are inserted into the membrane but not cleaved and translocated.

As the bioinformatic investigation of the MamC sequence only gave a vague hint for a Sec-dependent membrane insertion mechanism, and as no potential signal sequences were identified by comparison with other MMP, an experimental approach was taken to investigate the targeting of MamC. To test if different protein domains contain a signal sequence for magnetosome-directed targeting, GFP was fused to truncated versions of MamC. These constructs either lacked the N-terminal region (MamC$_{\Delta 1-9}$), the N-terminus and the first transmembrane domain (MamC$_{\Delta 1-31}$), or the region from the N-terminus to the second transmembrane domain (MamC$_{\Delta 1-52}$). In addition, GFP fusions of different C-terminal deletions were constructed including (i) a version that lacks the second transmembrane domain and the whole C-terminal tail (MamC$_{1-53}$), (ii) a version which only lacks the C-terminal tail (MamC$_{1-99}$), and (iii) a version that lacks only the last nine C-terminal amino acids (MamC$_{1-116}$). Using fluorescence microscopy, weak signals for all fusion proteins

except MamC$_{1-116}$-GFP were observed in the cytoplasm (Figure 5). In contrast, the fluorescence intensity of MamC$_{1-116}$-GFP was higher, and the protein localized in a similar pattern as full-length MamC-GFP (Figure 5). Analysis of different cell fractions by anti-GFP-immunoblot showed a strong signal for MamC$_{1-116}$-GFP in the MM fraction and therefore confirmed the results from the fluorescence microscopy (Figure 6). A signal of the expected molecular weight (38 kDa) was also detected in the MMP fraction of cells with the MamC$_{\Delta 1-9}$-GFP fusion. This signal was rather weak, and it is possible that only a small fraction of MamC$_{\Delta 1-9}$-GFP that could not be detected by fluorescence microscopy was inserted into the MM. Even though the MamC$_{\Delta 1-9}$-GFP fusion lacks part of the putative Sec-pathway signal, it is not possible to exclude the Sec pathway as a transort mechanism, as the residual part of the signal sequence might have accounted for the protein fraction that was inserted into the MM. For all fusion proteins, except for full length MamC-GFP and MamC$_{1-116}$-GFP, a putatively false positive signal with the size of the MamC-GFP fusion (39.5 kDa) was observed in the membrane protein fraction. The size of this unspecific signal did not shift even if truncated versions of MamC with reduced sizes were analyzed. The absence of signals in the cytoplasmic protein fraction, despite of the microscopical detection of cytoplasmic fluorescence and the presence of several smaller bandsin the immunoblot, indicated that the GFP fusions of truncated MamC variants were not stable, but degraded rapidly. Therefore, the cytoplasmic fluorescence observed for GFP fusions of different MamC variants can either be explained by inefficient targeting of the fusion proteins or by degradation products.

In conclusion, it was not possible to identify a distinct signal that entails the magnetosome-directed targeting of fusion proteins with this approach. The deletion of N-terminal regions and of larger regions from the C-terminus results in mistargeting and protein degradation. Only the last nine C-terminal amino acids are dispensable for the correct localization of MamC-GFP. This is in agreement with a comparison of the MamC sequences from *M. gryphiswaldense*, *M. magneticum*, *M. magnetotacticum*, the magnetic vibrio MV-1 and the magnetic coccus MC-1, which has shown that the C-terminus is less conserved than the rest of the protein (data not shown). After all, the magnetosome-specific targeting of MamC could be mediated not by a single signal peptide but by an interface composed of several residues or sequence stretches, which are distributed over the primary protein structure. In future experiments, the determinants of MamC-targeting may be identified by analysis of MamC-versions with single amino acid substitutions.
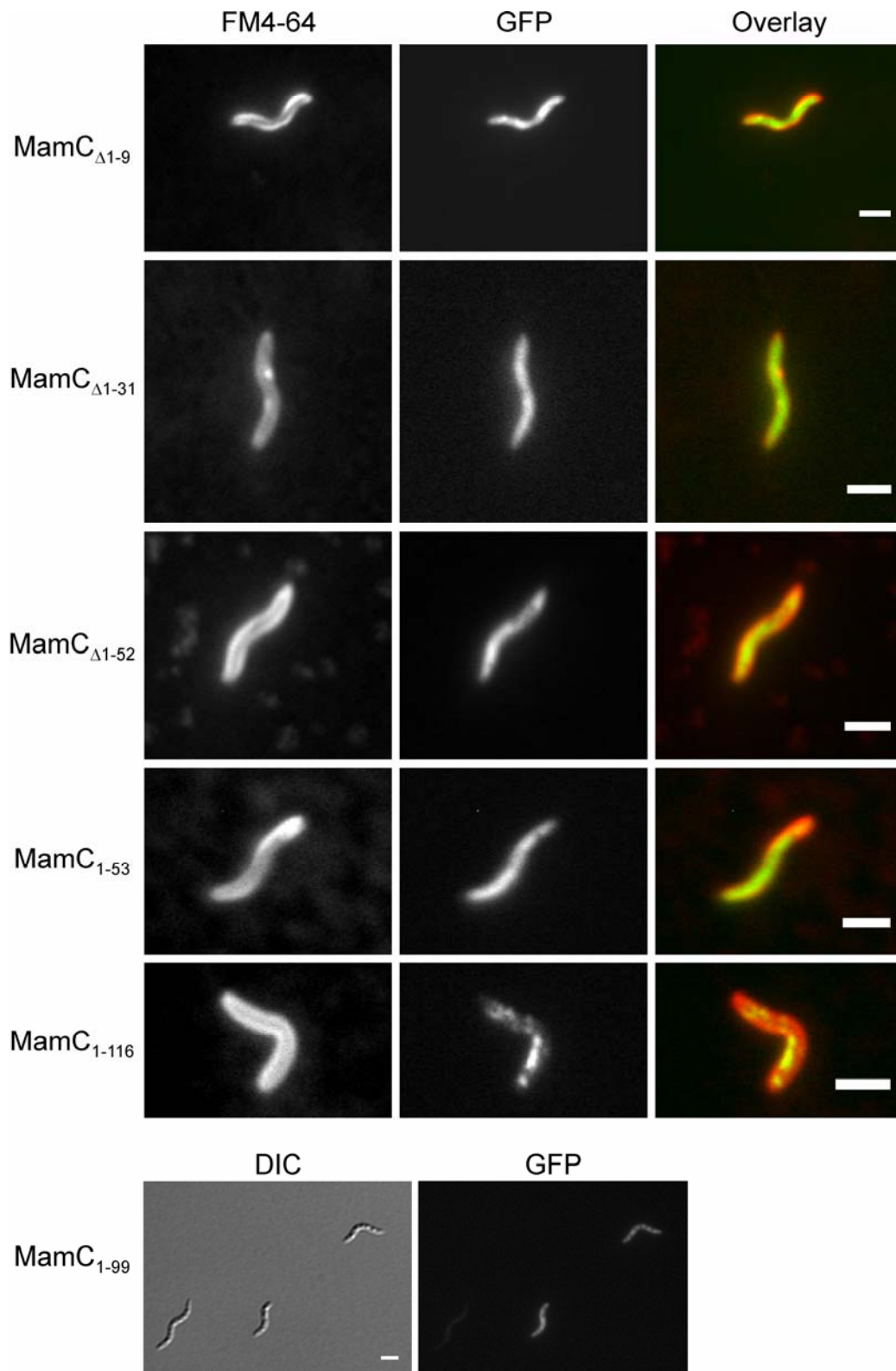
Figure 5: *In vivo* **localization of translational fusions of truncated versions of MamC and GFP.** To construct the fusion proteins truncated variants of *mamC* were PCR amplified (Primer sequences are listed in the supplementary in table 1), cloned into pJET1.2/blunt (Fermentas**,** St. Leon-Rot, Germany) or pGEMT-Easy (Promega, Madison, Wisconsin) and sequenced. The truncated *mamC* genes were subcloned into pCL5 (Manuscript 1) in front of the *egfp* gene. The constructed plasmids were transferred to *M. gryphiswaldense* by conjugation and analyzed by fluorescence microscopy as described in Manuscript 1. Since the fluorescence of MamC$_{1-99}$ –GFP was very weak, membrane staining with FM4-64 was omitted to avoid artefacts caused by weak

FM4-64 fluorescence in the GFP channel. A DIC micrograph is shown, to illustrate the position and the shape of the cells. Scale bars are 2 μm.
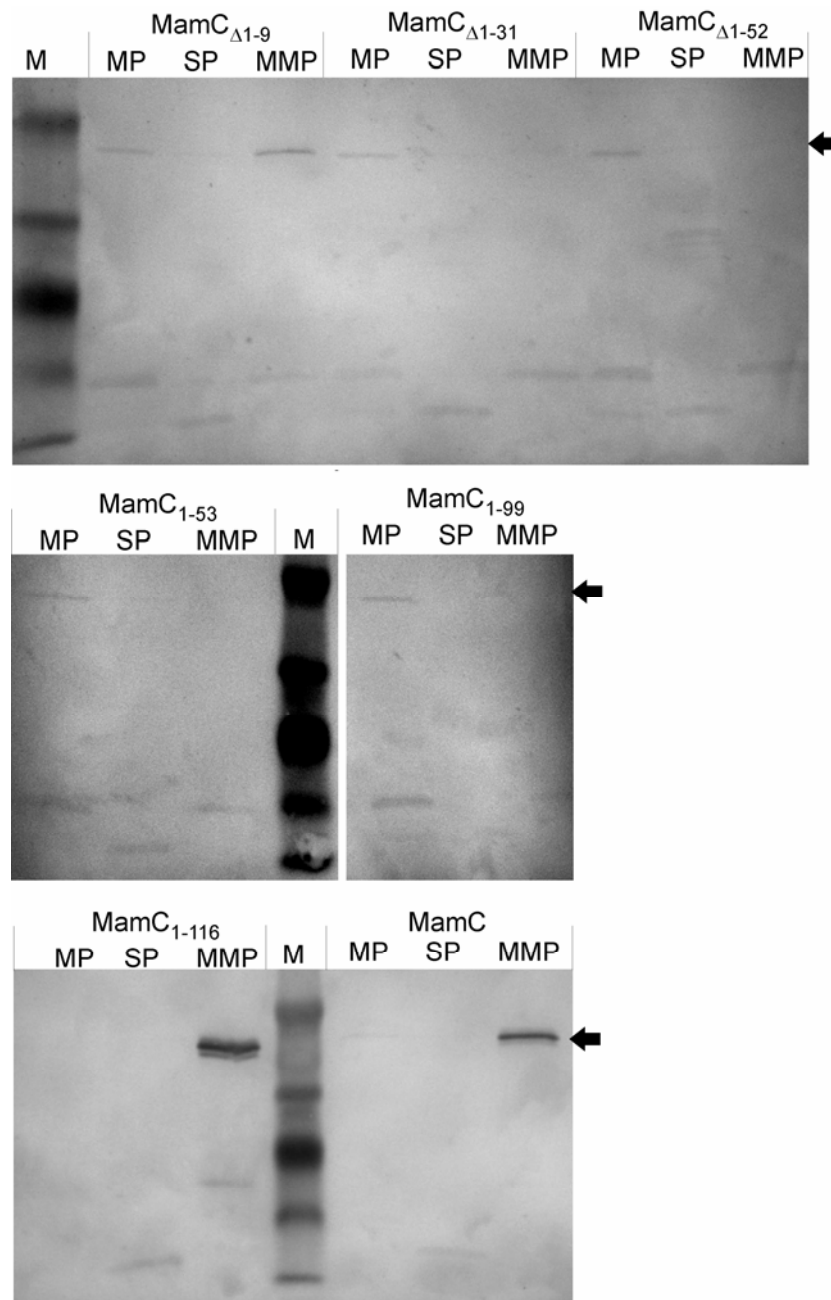
Figure 6: Immunoblot analysis of the localization of MamC-truncations fused to GFP. *M. gryphiswaldense* cultures expressing different truncated versions of MamC fused to GFP were cultivated in sealed 2 l flask with a culture volume of 1.7 l and air in the headspace for 24 h at 28°C. Magnetosomes were purified and cellular proteins were fractionated into soluble (SP) and membrane proteins (MP) (Manuscript 1). The protocol for immunoblot detection was modified from Manuscript 1. Briefly, 7.5 μg of MMP (MMP), SP and MP of each culture were separated by SDS-PAGE (12% gels) and blotted onto nitrocellulose membranes. For detection rabbit Anti-GFP antibody was used in a 1:1000 dilution as a primary antibody and shrimp alkaline phosphatase labelled anti-rabbit-IgG was in a 1:2000 dilution as a secondary antibody. The size of MamC-GFP is indicated by black arrows.

Localization of MamC-GFP in non-magnetic M. gryphiswaldense cells

It was of interest to investigate the localization of MamC-GFP and MamF-GFP in cells that were cultivated without iron and under aerobic conditions, because magnetite formation is inhibited under these conditions. These experiments were intended to analyze the localization of MMP in non-magnetic cells and to identify a potential role of magnetite in the targeting of magnetosome proteins.

In both non-magnetic cultures, the localization of MamC-GFP and MamF-GFP was virtually identical to the localization of both proteins in magnetic cells (Figure 7, Figure 4). This indicates that the localization of magnetosome vesicles and proteins is not altered under magnetite suppressing conditions. This also means that magnetite synthesis is not required for the correct targeting of MamC- or MamF-GFP. Since magnetite crystals are not required for the correct localization of the fusion proteins, other MMP must facilitate the magnetosome-specific targeting of MamC and MamF.
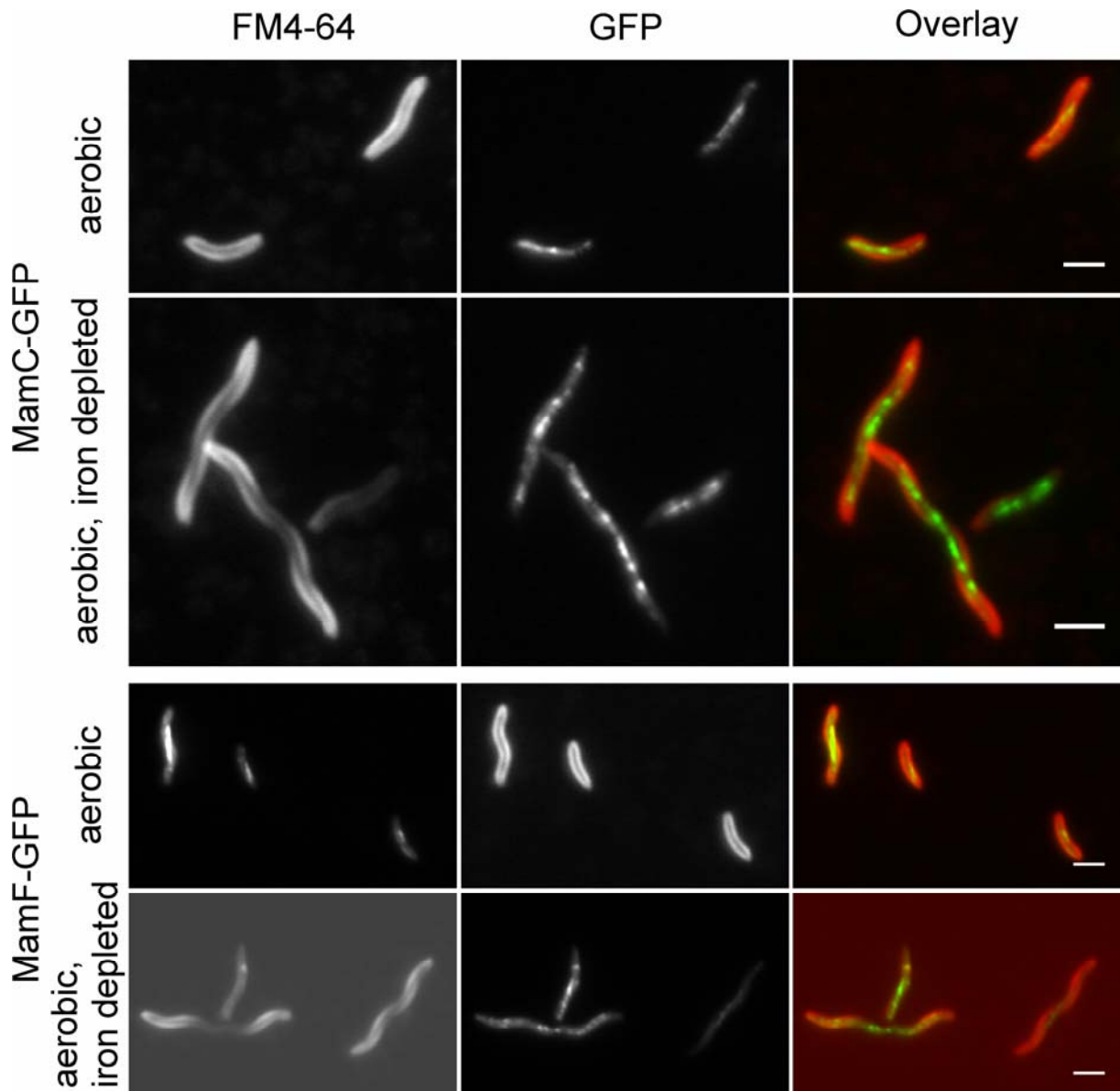
Figure 7: Fluorescence microscopy of MamC- and MamF-GFP in non-magnetic *M. gryphiswaldense* MSR-1 wild type cells. *M. gryphiswaldense* harbouring pCL6 (MamC-GFP) or pCL7 (MamF-GFP) (Manuscript 1) were cultivated for three passages under aerobic conditions in 15 ml polypropylene tubes with a 5 ml culture volume either in flask standard medium (FSM) (Heyen *et al.* 2003) or for iron depletion experiments in low iron medium (LIM) (Faivre *et al.* 2008a). Both methods resulted in non-magnetic cells with a cellular magnetism (C_{mag}) (Schüler *et al.* 1995) below 0.01. Staining and imaging was carried out as described in Manuscript 1. Scale bars are 2 µm.

Localization of MamC-GFP in mutants of M. gryphiswaldense

In the next set of experiments it was studied whether the localization of MamC-GFP is dependent on the presence of one or more magnetosome proteins. Initially, the localization of MamC-GFP was studied in four different non-magnetic mutants, namely MSR-1B, *ΔmamB*, *ΔmamM*, *ΔmamJKL*. Strain MSR-1B is a spontaneous mutant that lacks a 40 kb region of the magnetosome island including the *mms6-*, the *mamDC-* and the *mamAB-* operon (Schübbe *et al.* 2003), whereas the *ΔmamB*, *ΔmamM*, *ΔmamJKL* mutants were constructed by site-specific mutagenesis (Junge 2008; E. Katzmann, unpublished). In all non-magnetic mutants MamC-GFP formed one or several fluorescent spots and did not localize in a linear structure at midcell, which was observed in the wild type (Figure 4; Figure 8). The fluorescent spots presumably represent MamC-GFP inclusion bodies, which may be formed because of inefficient MamC-GFP targeting in the non-magnetic mutants. This interpretation is in agreement with the preliminary phenotypic characterization of the strain MSR-1B and *ΔmamJKL* mutant, which suggests that magnetosome vesicles are absent from these mutants (K. Junge, G. Wanner, D. Schüler; E. Katzmann, unpublished). Hence, MamC-GFP cannot be inserted into magnetosome vesicles in these strains. However, empty magnetosome vesicles in a chain-like arrangement were detected by thin section TEM in the *ΔmamB* mutant, and similar vesicular structures were observed in the *ΔmamM* mutant (Junge 2008; E. Katzmann, unpublished). Thus the mislocalization of MamC-GFP in these strains may be attributed either to a lower number of target organelles in the mutants or to the lack of specific proteins in the MM that are required for the correct insertion of MamC.

A punctuate localization pattern of MamC-GFP, which was similar to the localization of MamC-GFP in non-magnetic cells, was observed in the *ΔmamK* mutant, in which the magnetosome chain alignment is disturbed and several short chains are observed instead of one long continuous magnetosome chain (E. Katzmann, unpublished). This finding indicates that the MamK protein is required for the correct assembly of proteins in the MM and is required for the proper localization of MamC. However, since *ΔmamK* only contains a reduced number of magnetosomes compared to the wild type (E. Katzmann, unpublished), it is also possible that a fraction of MamC-GFP is inserted in the magnetosome vesicles correctly, whereas excessive MamC-GFP is mislocalized.

In a Δ*mamJ* mutant magnetosomes are clustered in three dimensional aggregates (Scheffel *et al.* 2006a). The localization of MamC-GFP in patches with a diameter of up to 1 µm (Figure 8) is consistent with the magnetosome directed targeting of MamC-GFP in the

Δ*mamJ* mutant. Hence, the results indicate that MamC-GFP is targeted specifically to the magnetosome compartments even if MamJ is absent and if magnetosome vesicles are not arranged in chains.

In Δ*mamC* and Δ*mamGFDC* mutants, which produce magnetosomes with reduced sizes, MamC-GFP localized in a linear signal at midcell, which was reminiscent of the localization pattern in wild type cells (Figure 8). In conclusion, these experiments demonstrated that neither native MamC nor other constituents of the *mamGFDC* operon are required for the magnetosome-specific targeting of MamC. In the future, the localization of MamC-GFP in the Δ*mamK,* Δ*mamJ,* Δ*mamC* and Δ*mamGFDC* mutants should be verified by immunoblot analysis.

At this stage it can be excluded that neither MamJ nor the proteins encoded by the *mamGFDC* operon are required to direct MamC to the magnetosome vesicle. The aberrant localization of MamC-GFP in several different mutants suggests that the lack of a single protein, i.e. MamK, MamB or MamM, has an effect either on the number of magnetosome vesicles or on the assembly of MMP in magnetosome vesicles. A promising approach for future experiments is to identify interaction partners of MamC by bacterial two hybrid analysis or by co-immunoprecipitation.
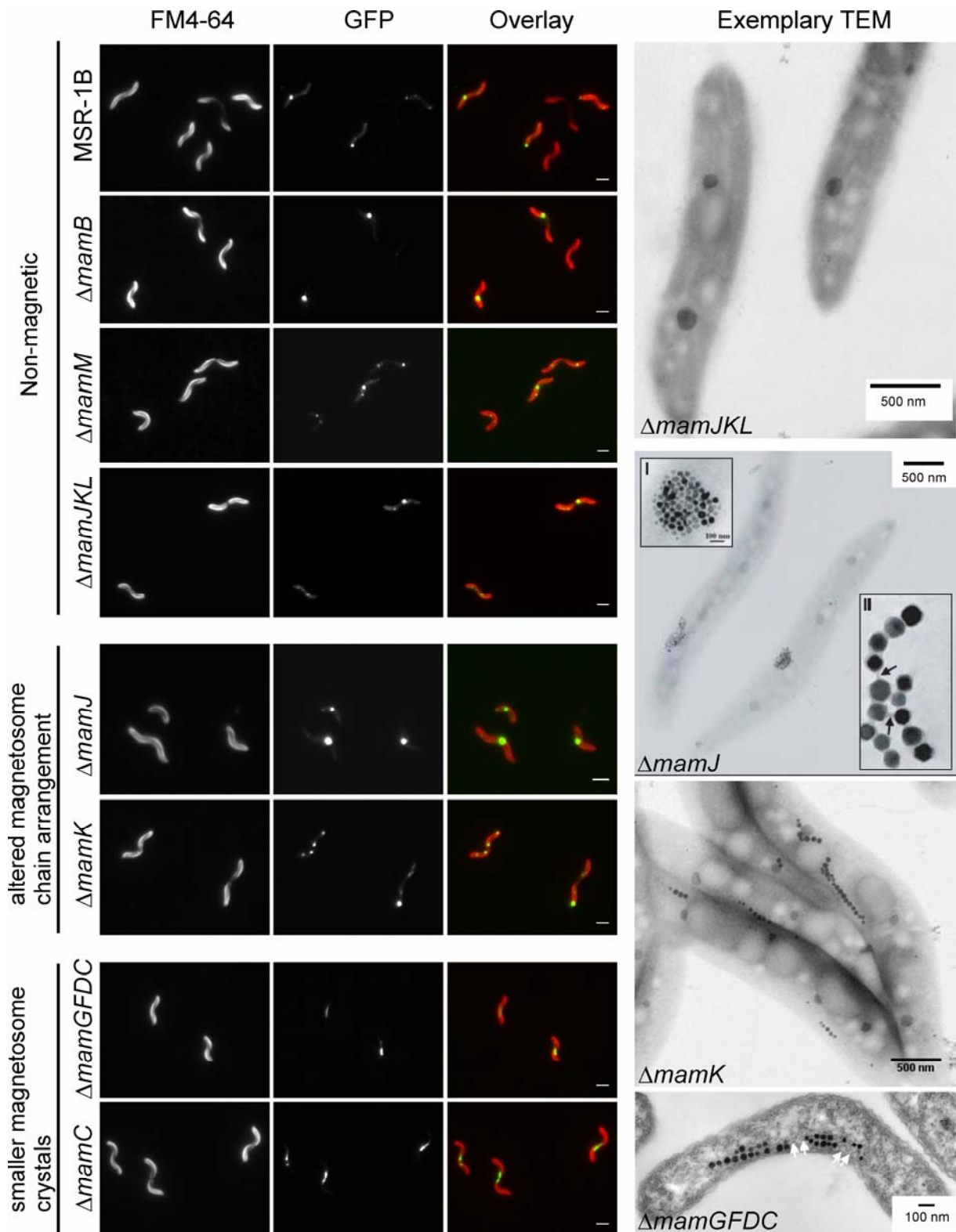
Figure 8: *In vivo* **localization of MamC-GFP in different mutants of** *M. gryphiswaldense.* MamC-GFP was expressed from the pCL6 plasmid (Manuscript 1) in different mutants of *M. gryphiswaldense*. The available mutants included the non-magnetic mutants MSR-1B (Schübbe *et al.* 2003), Δ*mamB*, Δ*mamM* (Junge 2008), Δ*mamJKL* (constructed by E. Katzmann, unpublished), the Δ*mamJ* (Scheffel *et al.* 2006a) and Δ*mamK* (constructed by E. Katzmann, unpublished) mutants with altered magnetosome chain arrangement and the Δ*mamC* (Scheffel *et al.* 2008) and Δ*mamGFDC* (Scheffel *et al.* 2008) mutants with smaller magnetosome crystal sizes. Membrane-staining with FM4-64, conjugation and microscopy was done as described previously

(Manuscript 1). To illustrate the phenotypes of the different mutants TEM pictures of representative mutants are shown. The picture of the non-magnetic Δ*mamJKL* mutant and the Δ*mamK* mutant was provided by E. Katzmann. The Δ*mamJ* micrograph was taken from Scheffel *et al.* (2006a). The thin section of the Δ*mamGFDC* mutant was made by G. Wanner (Scheffel *et al.* 2008). If not indicated otherwise in the figure, the scale bars are 2 μm.

Analysis of promoters for efficient and inducible gene expression in *M. gryphiswaldense*

Until now, protein expression in *M. gryphiswaldense* and other MTB has been limited by lack of an appropriate expression system. Incomplete complementation of mutants and weak expression of fusion proteins expressed in *M. gryphiswaldense* have indicated that the previously used *E. coli* P_{lac} and P_{tac} promoters are not efficient in the α-proteobacteria *M. gryphiswaldense* and *M. magneticum* (Komeili *et al.* 2006; Komeili *et al.* 2004; Pradel *et al.* 2006; Scheffel *et al.* 2008; Scheffel *et al.* 2006a; Scheffel *et al.* 2007; Manuscript 1; K. Junge, unpublished). Only a single study in *M. magneticum* has reported a system for the expression of fusion proteins. A luciferase-based assay showed that from six tested putative promoters the highest expression was obtained with the promoter of a putative peroxiredoxin gene (P_{msp3}) (Yoshino *et al.* 2005b). However, peroxiredoxins are involved in the response to oxidative stress (Seaver *et al.* 2001), and their regulation may prevent the expression of genes under microaerobic or anaerobic conditions. To identify efficient promoters for gene expression in *M. gryphiswaldense,* the expression of GFP from several sequences of putative and previously identified promoters from *M. gryphiswaldense* and *E. coli* were investigated.

The promoter of the mamGFDC operon (P_{mamDC}) is a strong promoter in *M. gryphiswaldense*

In total, six sequences of either putative or predicted promoters in *M. gryphiswaldense* were analyzed (P_{mamDC}, P_{mamAB}, P_{apdA}, P_{msp3}, P_{rpsJ}, P_{rplK} and P_{ure}). With the BPROM promoter prediction tool (http://linux1.softberry.com/berry.phtml?topic=bprom&group=programs&subgroup=gfindb, last accessed 08.12.08) -35 and -10 regions with high similarities to *E. coli* promoters were identified for all sequences except of the putative ribosomal promoter P_{rplK} (Manuscript 2, Figure 1). However, the promoters from *M. gryphiswaldense* were not functional in *E. coli* (Manuscript 2, Figure 2). The inactivity of α-proteobacterial promoters in *E. coli* is a common phenomenon. For example, promoters from *Caulobacter crescentus* and *Sinorhizobium meliloti* are also not active in *E. coli* (MacLellan *et al.* 2006; Malakooti *et al.* 1995; Smit *et al.*

1984). Promoter activity in *M. gryphiswaldense* was analyzed by fluorescence microscopy, fluorometry and immunoblot analysis. These studies demonstrated that all *M. gryphiswaldense* promoters except of the putative P*ure* promoter activate GFP expression more efficiently than the *E. coli* P*lac* promoter (Manuscript 2, Figure 2). The magnetosomal promoter P*mamDC*, which was previously identified by primer extension analysis in *M. gryphiswaldense* (Schübbe 2006) promotes GFP expression more efficiently than homologues of the highly active *M. magneticum* promoters P*msp3* and P*mms16* (in *M. gryphiswaldense* called P*apdA*) (Yoshino *et al.* 2005b). P*mamDC* activity is even higher than the activity of the putatively strong ribosomal promoters P*rpsJ* (rpsJ: MGR3815 ribosomal protein S10) and P*rplK* (rplK: MGR3801 ribosomal protein L11).

The analysis of three truncated versions of P*mamDC* showed that a 96 bp fragment, containing only four bases upstream of the -35 region, is sufficient for the efficient expression of GFP (Manuscript 2, Figure 5). This indicates that neither transcription factors nor upstream promoter elements like A-tract sequences are required for efficient transcription from P*mamDC*. In future experiments, the short 96 bp fragment could be incorporated in a primer to simplify cloning, and it could reduce the frequency of unwanted recombinations between plasmid-borne and chromosomal P*mamDC*.

To investigate the applicability of P*mamDC* as a tool for the production of genetically engineered magnetosomes, the promoter was used for expression of a MamC-ZZ fusion protein in *M. gryphiswaldense*. The MamC-ZZ protein consists of the MM anchor protein MamC and an antibody-binding ZZ domain, which is a derivative of the staphylococcal protein A (Löwenadler *et al.* 1987). Immunoblot analysis of different cell fractions showed that the antibody binding protein was highly expressed and specifically targeted to the MM (Manuscript 2, Figure 6). In addition, it was shown that purified MamC-ZZ magnetosomes bind rabbit antibodies in aqueous suspensions (Manuscript 2, Figure 6). Hence, these particles can be used for the purification of antibodies as previously described with ZZ-modified bacterial polyester granules (Brockelbank *et al.* 2006). The utilization of the highly efficient P*mamDC* promoter and the availability of *M. gryphiswaldense* mutants with magnetosomes displaying altered magnetic properties could be used for the production of ZZ-modified magnetosomes with improved properties for magneto-immunoassays.

P*tet* is an inducible promoter in M. gryphiswaldense

A putative P*ure* promoter that might be induced in the presence of urea or under nitrogen-limitation (D'Orazio *et al.* 1993; Friedrich *et al.* 1977) and the widely used P*tet* promoter from the *E. coli* Tn10 Tc^R gene (Skerra 1994) were analyzed with GFP as a reporter.

While no inducing conditions for P_{ure} could be identified, fluorometry and microscopy showed that the P_{tet} promoter can be induced in *M. gryphiswaldense* by the addition of 5-50 ng ml^{-1} anhydrotetracycline (Manuscript 2, Figure 3). Although P_{tet} is not as active as P_{mamDC}, this promoter is a valuable addition to the *M. gryphiswaldense* genetic toolbox. The tightly regulated P_{tet} promoter could be used for the expression of deleterious proteins or for the expression of GFP fusions for cell cycle-dependent protein localization studies.

The expression of GFP from different promoters is not homogeneous in all cells of a population

The results also show that GFP is a useful transcriptional reporter in *M. gryphiswaldense*. One major advantage of GFP in comparison to other transcriptional reporters is its detectability at a single cell level by fluorescence microscopy or flow cytometry. Flow cytometry revealed that GFP was heterogeneously expressed in populations of *M. gryphiswaldense* from all promoters. Even with strong promoters like P_{mamDC} the proportion of fluorescent cells was not higher than 60 % of all cells. Inhomogeneous gene expression in isogenic cell populations is frequently observed in bacteria (Davidson *et al.* 2008; Siegele *et al.* 1997) and might be caused by variations of growth rates and protein synthesis, different cell-cycle stages, or the stochasticity of gene expression (Elowitz *et al.* 2002; Roostalu *et al.* 2008; Strovas *et al.* 2007). For future applications of genetically engineered magnetosomes, it is of significance that not all magnetosomes display functional moieties in equal amounts. It is important to use sufficiently large amounts of magnetosomes so that variations in the degree of functionalization of single magnetosomes do not affect the results.

Part II: Production of magnetosomes for the development of diagnostic applications

Investigations on the applicability of magnetosomes from *M. gryphiswaldense* in *in vitro* applications, such as magnetic separation procedures and immunoassays as well as in *in vivo* applications like MRI required the constant supply of large amounts of magnetosomes. In order to guarantee that variations of magnetosome characteristics from different charges were minimal, a previously developed oxystat fermentation procedure for *M. gryphiswaldense* (Heyen *et al.* 2003) was adapted to maintain constant pH, oxygen partial pressure and temperature during cultivation. In total, a culture volume of 440 l was produced with the 20 l oxystat fermenter system for the purification of magnetosomes (~ 400 mg Fe). Initially, only the wild type strain *M. gryphiswaldense* MSR-1 was cultivated. Later on, the strain MSR-1K, which produces superparamagnetic magnetite crystals with reduced sizes (Figure 9) (Hoell *et al.* 2004; Ullrich *et al.* 2005), was cultivated. Superparamagnetic particles do not maintain a permanent magnetic moment and do not interact magnetically as strongly as single-magnetic-domain particles in the absence of an external magnetic field. Therefore, the MSR-1K magnetosomes have been less susceptible to aggregation and have been advantageous for chemical modifications of the MM (Bülent Ceyhan, Universität Dortmund, personal communication).
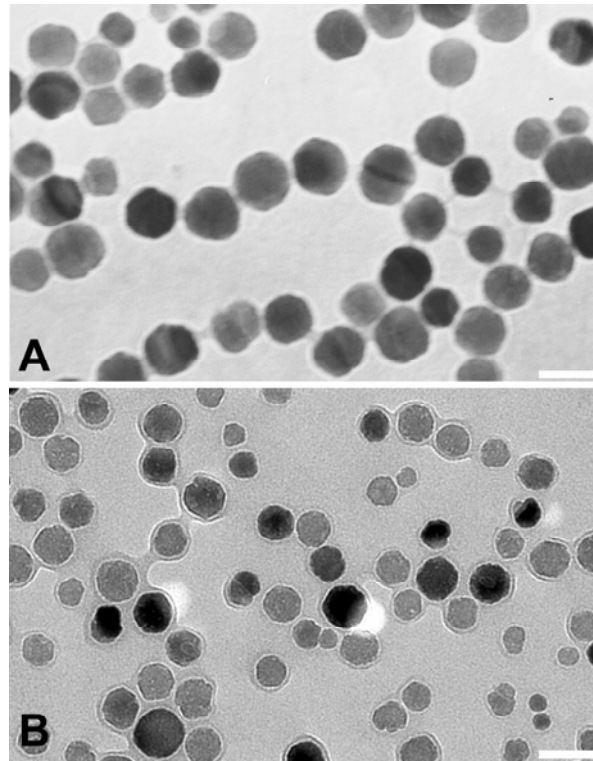
Figure 9: Transmission electron micrographs of purified magnetosomes from *M. gryphiswaldense* MSR-1 (A) and *M. gryphiswaldense* MSR1-K (B). Scale bars are 50 nm.

Optimization of the magnetosome purification procedure for biotechnological applications

In previous studies, magnetosomes were purified mainly for biochemical studies (Grünberg *et al.* 2004). Therefore, the purity of the isolated magnetosomes was the only concern. For biotechnological applications, it was also important that the MM remains intact during the purification procedure. The MM represents a coating of the magnetite crystal, which is essential for the magnetosome dispersibility and for the chemical modification of magnetosomes. Hence, it was necessary to optimize the previously developed procedure by Grünberg *et al.* (2004) for biotechnical applications. The magnetosome purification procedure involves three main steps, i.e. cell lysis, magnetic separation and density gradient centrifugation. While the previously used cell lysis procedure by French Press was found most appropriate for the extraction of intact magnetosomes, it was observed that magnetosomes are highly susceptible to mechanical forces after cell lysis. During the magnetic separation step, magnetosomes are retained in a special magnetic column (C-MACS, Miltenyi-Biotech, Germany) while non-magnetic cellular components pass through the column. It is essential not to apply forces other than gravity and to limit the flow speed to a maximum of 10 ml/minute to avoid sheering of the MM and magnetosome aggregation (Figure 10). The next step is the density fractionation of magnetosomes by centrifugation through a sucrose cushion. The sucrose concentration was increased to 60 % w/w to improve

the purity of the magnetosomes. To minimise MM sheering, the sedimented magnetosomes were resuspended by incubation for about 16 h at 4°C in extraction buffer.

Using a specifically adapted magnetic separation stand, the purified magnetosomes can be easily separated from aqueous suspensions (Figure 11). The magnetic separation stand was also used for the testing of magnetosome stability in different chemical environments (Manuscript 1, Figure 6) and for the magnetic separation of molecules that interact with genetically engineered magnetosomes (Manuscript 2; Figure 6).
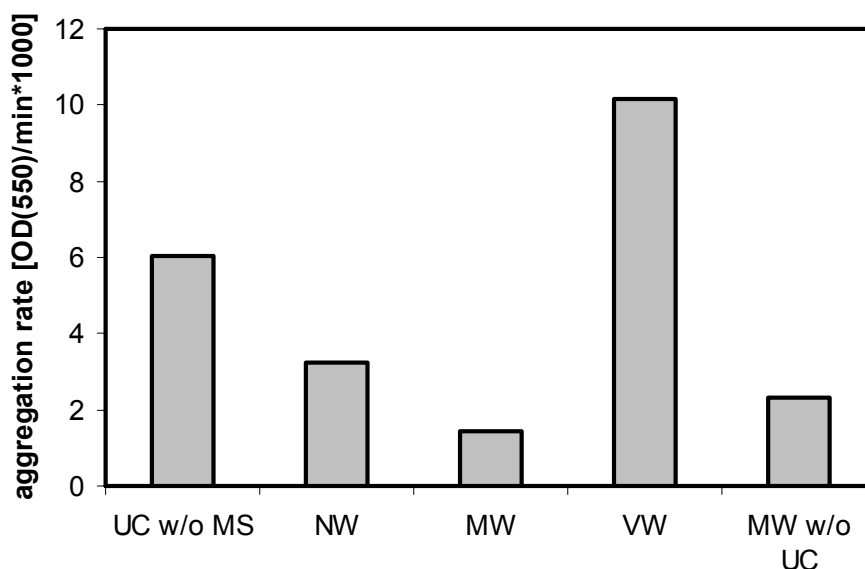
Figure 10: Effect of different purification procedures on the aggregation of magnetosomes. Magnetosomes from the same batch of cells were purified by different methods and resuspended in buffer (10 mM Hepes, 1 mM EDTA, pH 7.4) to an OD_{550} of 0.5. The decrease of turbidity was plotted against the time, and the aggregation rate was calculated from the slope of the curve. UC w/o MS: density gradient centrifugation (60 % sucrose), without magnetic separation, NW: normal purification procedure; density gradient centrifugation (60 % sucrose) and magnetic separation with the application of mild suction (Flow speed ~30 ml/min), MW: mild purification procedure; density gradient centrifugation (60 % sucrose) and magnetic separation with gravity flow during the magnetic column separation step and reduction of the flow speed to ~10 ml/min, VW: vigorous washing procedure; density gradient centrifugation (60 % sucrose) and magnetic separation with the application of extensive suction (Flow speed > 100 ml/min). MW w/o UC: mild purification without density gradient centrifugation.

Figure 11: Purified magnetosomes are easily separated from aqueous suspensions in a specifically adapted magnetic separation stand. The magnetic separation stand was designed for the magnetic separation of magnetosomes from suspensions in 1.5 and 2.0 ml reaction tubes or from 15 ml polypropylene tubes. High energy permanent magnets (neodynium-iron-boron and samarium cobalt magnets) facilitated the separation of magnetosomes from suspensions within 1-5 min. The tube in the back and the tube in the magnetic separation stand contain aliquots of the same magnetosome suspension.

Using the pure and intact magnetosomes from the *M. gryphiswaldense* strains MSR-1 and MSR-1K it was possible to develop several novel applications. In the following, two studies are discussed, which investigated possibilities for the chemical modification of isolated magnetosomes with biomolecules and their application in immunoassays. In addition, the main findings of three studies that investigated the potential of purified magnetosomes as contrast agents for magnetic resonance imaging (MRI) of specific cell types will be presented.

Oligonucleotide- and antibody- modified magnetosomes generated by streptavidin-biotin chemistry

In general, it is possible to functionalize magnetosomes either by genetic approaches within the cell or by chemical procedures after purification from the cells. As genetic tools that are required for the genetic modification of magnetosomes were not available at the onset of this thesis, chemical functionalization procedures were investigated in parallel. In previous studies the modification of magnetosomes from *M. magneticum* was achieved by glutaraldehyde-induced crosslinking for the immobilization of proteins on the magnetosome surface (Matsunaga *et al.* 1987; Matsunaga *et al.* 2001). Amine-modified oligonucleotides were attached to the MM with the heterobifunctional reagent N-succinimidyl 3-(2-

pyridyldithio) propionate (Sode *et al.* 1993). Similar reagents were also used for the production of myosin conjugated magnetosomes, which interact with actin filaments and for the production of biotinylated magnetosomes (Amemiya *et al.* 2005; Tanaka *et al.* 1997). Despite the utilization of several different procedures, a systematic comparison of different procedures was not carried out.

Instead of the functionalization of magnetosomes with one specific moiety, a modular approach was developed for the functionalization of purified magnetosomes from *M. gryphiswaldense*. In a first step, different procedures for the biotinylation of magnetosomes were investigated. In the second step, the biotinylated magnetosomes were conjugated to different biotinylated biomolecules, such as antibodies or oligonucleotides, with streptavidin as a coupling reagent. Purified magnetosomes from *M. gryphiswaldense* were reacted with two biotinylation reagents: (i) the biotin lipid, biotin-DPPE [(1,2-dipalmitoyl-*sn*-glycero-3-phosphoethanolamine-*N*-(biotinyl) (disodium salt)], which integrates into the MM non-specifically and (ii) NHS-biotin [sulfo-*N*-hydroxy-succinimide esters sodium salt], which forms covalent bonds with free amino groups. For a quantitative comparison of the efficiencies of both biotinylation procedures, streptavidin was attached to the biotinylated magnetosomes. After addition of Cy5- and biotin-labelled oligonucleotides the amount of magnetosome-bound streptavidin was quantified by fluorometric measurement of Cy5. The experiment has shown that the use of biotin-DPPE results in the immobilization of two- to threefold more streptavidin on the magnetosome surface than use of NHS-biotin, which interacts specifically with lysine residues. However, the reproducibility of the results was lower with use of biotin-DPPE, which indicates that addition of the biotin-lipid also caused aggregation of the magnetosomes (Manuscript 3).

Using streptavidin-biotin chemistry, the biotinylated magnetosomes could be further functionalized with biotinylated oligonucleotides and antibodies. Bifunctional magnetosomes were generated by addition of two different oligonucleotides in equimolar ratio. The modified magnetosomes were used (i) for detection of specific target oligonucleotides immobilized on a glass slide, (ii) for DNA directed assembly of three dimensional binary networks of oligonucleotide-coated gold nanoparticles and oligonucleotide-modified magnetosomes, and (iii) for detection of antigens in a sandwich immunoassay (Manuscript 3).

Magneto-Immuno-PCR

The ultra sensitive detection and quantification of specific proteins within complex biological matrices is of vital importance in the fields of clinical diagnostics, agriculture, drug development and doping control (Borgono *et al.* 2006; Chassy 2002; Matsakas *et al.* 2005;

Scaros *et al.* 2005; Zolg *et al.* 2004). For development of a highly sensitive and automatable protein detection method, it was of interest to combine the use of magnetic particles for antigen-capture and antigen-enrichment with the ultra sensitive immuno-PCR procedure, which combines an enzyme-linked-immunosorbent assay (ELISA) with the amplification power of PCR (Niemeyer *et al.* 2007).

Streptavidin-modified, superparamagnetic magnetosomes purified from the *M. gryphiswaldense* strain MSR-1K (Manuscript 3) and commercially available streptavidin-coated, micrometric beads (Roche) were used to develop systems for the detection of hepatitis B surface antigen (HBsAg). After incubation with biotinylated HBsAg-antibody, the magnetic beads and the modified magnetosomes were used to separate HBsAg from spiked human serum. The antigen was detected either by ELISA with a conjugate of alkaline-phosphatase or by real-time Immuno-PCR with an anti-HBsAg-Imperacer^{TM} conjugate (Chimera Biotec). The experiments have shown that the magnetosome-assisted immuno-PCR (magneto immuno-PCR) is 125 fold more sensitive than the analogous magnetosome-ELISA (Manuscript 4). Comparison of the performance of modified magnetosomes with commercially available streptavidin coated micrometric magnetic beads revealed that the sensitivity of the assay is increased 25-fold if magnetosomes are used. In addition, the linear dynamic range for quantification is increased from 200 - 8 ng/ml with commercially available magnetic beads to 200 ng/ml - 320 pg/ml with magnetosomes. These results clearly demonstrate that magnetosomes are advantageous to synthetic magnetic microbeads for the development of highly sensitive magneto-immuno-PCR procedures. The greatest advantage of the magnetosome-based procedures is that it is automatable and could be adapted for high-throughput applications (Manuscript 4).

Utilization of magnetosomes as contrast agents for magnetic resonance imaging

Magnetic nanoparticles are being vigorously researched as the next generation of MRI contrast agents (Corot *et al.* 2006; Sun *et al.* 2008a). MRI is a non-invasive, non-harmful method to obtain clinical images and to visualize different tissues *in vivo*. The differentiation of tissues with similar chemical composition can be achieved with special contrast agents (Sun *et al.* 2008a). Iron oxide nanoparticles are currently the preferred contrast agents for the monitoring of specific cell types and tissues (Bulte *et al.* 2004). Initial *in vitro* studies have indicated that bacterial magnetosomes might represent an alternative to chemically produced iron oxide particles as magnetosomes can be detected at low concentrations (0.6-0.9 nM Fe) in an aqueous buffer in a 1.5 Tesla whole body scanner (Herborn *et al.* 2003). Magnetosomes were also successfully employed to detect microtumors in rat livers by MRI (Reszka 2000). In

addition, MRI can be used to monitor cell migration of specifically labelled cells during pathological processes. It is of particular interest to monitor the trafficking of macrophages, because these cells are well-known effectors and regulators of the inflammatory response, which migrate to regions of acute inflammation (Bulte *et al.* 2004).

Labelling of macrophages with magnetosomes

The magnetic resonance relaxation properties of magnetosomes embedded in agarose were measured *in vitro* to test if magnetosomes can be used as contrast agents for the labelling of macrophages in MRI (Manuscript 5). Interestingly, the R_2 relaxivity of magnetosomes was 2-3 fold higher than of commercially available magnetic nanoparticles (Resovist®, Schering, Berlin), which indicates that a lower dosage of magnetosomes is required to observe the same signal change compared to Resovist®. Mouse macrophages (J77A.1), which were incubated with magnetosomes, took up magnetosomes by phagocytosis and could be detected by MRI. After injection of magnetosomes into mice and induction of peritonitis, initial *ex vivo* experiments have indicated that it is possible to visualize the position of acute inflammations by MRI (Manuscript 5, Figure 6).

Fluorescently labelled magnetosomes as biomodal probes for magnetic resonance and near infrared fluorescence optical imaging

One of the fastest growing areas in the field of molecular imaging is the development of fluorescence-based methods for the detection of pathologic changes *in vivo* (Weissleder *et al.* 2008). While these methods provide high sensitivity, spatial and temporal resolution, they are limited in tissue penetration (Ballou *et al.* 2005). Therefore, macroscopic fluorescence-based imaging methods and MRI are complementary methods and bimodal contrast agents, which could be used in both applications, are a desired material.

For the development of bimodal contrast agents, purified magnetosomes were covalently labelled with a Succinimdyl-ester-modified near infrared fluorescent dye (DY-676), which reacts with accessible amino groups. Flow cytometry was employed to verify that fluorescently labelled magnetosomes (FM676) were synthesized. Cultured mouse macrophages (J774) that were treated with the bimodal contrast agent (FM676) took up FM676 agent by phagocytosis. The modified magnetosomes were visible in endosomes by ultrathin section microscopic analysis, and the intracellular colocalization of dense structures observed by phase contrast microscopy and near infrared fluorescence signals confirmed that FM676 was taken up in the cells and remained stable during uptake. Imaging of FM676 treated macrophages in a small-animal-near-infrared-fluorescence-imager and by MRI

demonstrated that fluorescently labelled magnetosomes (FM676) can be readily detected by both methods. Due to the unique magnetic properties of the magnetosome crystal, the FM676 particles display high transversal relaxivities compared to Resovist® (Schering, Berlin, Germany) and increase the sensitivity of MRI. In conclusion, the utilization of fluorescently labelled magnetosomes as bimodal contrast agents for optical and magnetic resonance imaging of inflammatory processes is yet another highly promising application of purified magnetosomes from *M. gryphiswaldense*.

Labelling of dendritic cells with magnetosomes

In addition to macrophages, dendritic cells (DC) represent a further cell type that is potentially capable of magnetosome phagocytosis. Like macrophages DC belong to the group of antigen presenting cells and are essential for the activation of T cells. In most tissues DC are present in an immature state. Upon induction by an immunological stimulus they mature to active antigen presenting cells and migrate to the lymphoid organs, where they interact with antigen-specific T cells (Banchereau *et al.* 1998). DC loaded with specific antigens are under clinical investigation as cellular vaccines (Figdor *et al.* 2004). Since the success of these procedures largely depends on the accurate administration and migration of DC, procedures for the non-invasive monitoring of DC migration need to be developed. It was demonstrated by magnetic separation, transmission electron microscopy and quantification of the cellular iron content that DC take up magnetosomes purified from *M. gryphiswaldense* as well as synthetic lipid-iron-oxide nanoparticles by phagocytosis. DC containing either biogenic or synthetic magnetic nanoparticles were visualized by MRI *in vitro*. *In vivo* MRI of C57BL/6 mice, which received injections of magnetic nanoparticles containing DC, showed hypointense signals in the draining lymph nodes close to the injection site after 24 h. In control experiments with non-modified DC no signals were detected. In addition, the presence of large amounts of iron in the draining lymphnodes was verified by histological analysis. These data show that magnetosomes can be used for the magnetic labelling of DC and to monitor the localization of labelled DC *in vivo*. In future, genetically engineered magnetosomes, which display certain antigenic proteins or peptides, could be used to load DC with antigens and create cellular vaccines, which can be monitored *in vivo* by MRI.

Outlook

The genetic tools that were developed in this study will be of great value for many future applications. Using MamC as a MM anchor protein and the highly efficient P_{mamDC} promoter, it will be possible to express different functional moieties on the MM, as it was exemplified with GFP and the antibody binding ZZ-protein. For instance, it might be possible to express enzymatic functions on the magnetosome surface for the production of catalysts that can be separated after a reaction magnetically.

As a positional marker for magnetosome vesicles in living cells, MamC-GFP is also of great cell biological interest. The protein could be employed in live-cell and time-lapse imaging studies to elucidate the dynamics of magnetosome vesicle localization and magnetosome chain assembly during cell division. For this purpose, it will be also of interest to express fluorescently labelled cell division proteins such as Fts proteins in *M. gryphiswaldense* and study the localization of the magnetosome chain and the cell division machinery simultaneously.

While we have shown that MamC is specifically targeted to the magnetosome compartment, it is still unclear how proteins are assembled in the MM. The herein presented results indicate that the correct positioning of MamC relies on the presence of other proteins in the MM. In future, studies will be required to identify interaction partners of MamC and other MMP by methods such as bacterial-two-hybrid assays or co-immunoprecipitation.

In this study a procedure for the production of highly pure and intact magnetosomes was developed. These magnetosomes were used successfully in a number of applications. However, it is still a long way to the development of a commercially competitive magnetosome-based product. First of all, it would be of advantage to lower the production costs for magnetosomes. This could be achieved by scale up and optimization of the fermentation procedure, such as the development of a fed batch system as described recently (Sun *et al.* 2008c). Another option is the isolation of strains with increased magnetosome production. For *in vitro* applications, such as procedures for DNA and protein detection, in future, genetically engineered magnetosomes could be used instead of chemically functionalized particles. *In vivo* applications, such as MRI, will require studies on the immunogenicity of bacterial magnetosomes.

References

Amann R., Peplies J. and Schüler D. (2006). Diversity and taxonomy of magnetotactic bacteria. <u>Microbiology Monographs - Magnetoreception and magnetosomes in bacteria</u>. D. Schüler. Heidelberg, Springer**:** 25–36.

Amemiya Y., Arakaki A., Staniland S., Tanaka K. and Matsunaga T. (2007) Controlled formation of magnetite crystal by partial oxidation of ferrous hydroxide in the presence of recombinant magnetotactic bacterial protein Mms6. *Biomater.* **28:**5381-5389

Amemiya Y., Tanaka T., Yoza B. and Matsunaga T. (2005) Novel detection system for biomolecules using nano-sized bacterial magnetic particles and magnetic force microscopy. *J. Biotech.* **120:**308-314

Arató B., Szanyi Z., Flies C.B., Schüler D., Frankel R.B., Buseck P.R. and Pósfai M. (2005) Crystal-size and shape distributions of magnetite from uncultured magnetotactic bacteria as a potential biomarker. *Am. Min.* **90:**1233-1241

Baeuerlein E., Schüler D., Reszka R. and Päuser S. (1998) Specific magnetosomes, method for the production and use thereof. *Patent PCT/DE 98/00668*

Balkwill D., Maratea D. and Blakemore R.P. (1980) Ultrastructure of a magnetotactic spirillum. *J. Bacteriol.* **141:**1399-1408

Ballou B., Ernst L.A. and Waggoner A.S. (2005) Fluorescence imaging of tumors *in vivo*. *Curr. Med. Chem.* **12:**795-805

Banchereau J. and Steinman R.M. (1998) Dendritic cells and the control of immunity. *Nature* **392:**245-252

Barry S.E. (2008) Challenges in the development of magnetic particles for therapeutic applications. *Int. J. Hyperthermia* **24:**451-466

Bazylinski D.A., A. Garratt-Reed and R.B. Frankel (1994) Electron-microscopic studies of magnetosomes in magnetotactic bacteria. *Microsc. Res. Tech.* **27:**389-401

Bazylinski D.A. and Schübbe S. (2007a) Controlled biomineralization by and applications of magnetotactic bacteria. *Adv. Appl. Microbiol.* **62:**21-62

Bazylinski D.A. and Williams T.J. (2007b). Ecophysiology of magnetotactic bacteria. <u>Microbiology Monographs - Magnetoreception and magnetosomes in bacteria</u>. D. Schüler, Springer Verlag Berlin Heiderlberg**:** 37-75.

Blakemore R.P. (1975) Magnetotactic bacteria. *Science* **190:**377-379

Borgono C.A., Kishi T., Scorilas A., Harbeck N., Dorn J., Schmalfeldt B., Schmitt M. and Diamandis E.P. (2006) Human kallikrein 8 protein is a favorable prognostic marker in ovarian cancer. *Clin. Cance.r Res.* **12:**1487-1493

Brockelbank J.A., Peters V. and Rehm B.H.A. (2006) Recombinant *Escherichia coli* strain produces a ZZ domain displaying biopolyester granules suitable for immunoglobulin G purification. *Appl. Environ. Microbiol.* **72:**7394-7397

Bulte J.W. and Kraitchman D.L. (2004) Iron oxide MR contrast agents for molecular and cellular imaging. *NMR Biomed.* **17:**484–499

Chassy B.M. (2002) Food safety evaluation of crops produced through biotechnology. *J. Am. Coll. Nutr.* **21:**166S-173

Coker V.S., Pearce I.P., Lang C., Van der Laan G., Pattrick R.A.D., Telling N., Schüler D., Arenholz E. and Lloyd J.R. (2007) Cation site occupancy of biogenic magnetite compared to polygenic ferrite spinels determined by X-ray magnetic circular dichroism. *Eur. J. Min.* **19:**707-716

Corot C., Roberta P., Idéea J.-M. and Port M. (2006) Recent advances in iron oxide nanocrystal technology for medical imaging. *Adv. Drug Deliv. Rev.* **58:**1471-1504

D'Orazio S.E.F. and Collins C.M. (1993) The plasmid-encoded urease gene cluster of the family *enterobacteriaceae* is positively regulated by UreR, a member of the AraC family of transcriptional activators. *J. Bacteriol.* **175:**3459-3467

Davidson C.J. and Surette M.G. (2008) Individualtiy in bacteria. *Annu. Rev. Genet.* **42:**253-268

DeLong E.F., Frankel R.B. and Bazylinski D.A. (1993) Multiple evolutionary origins of magnetotaxis in bacteria. *Science* **259:**803-806

Devouard B., Posfai M., Hua X., Bazylinski D.A., Frankel R.B. and Buseck P.B. (1998) Magnetite from magnetotactic bacteria: Size distributions and twinning. *Am. Min.* **83:**1387-1398

Drepper T., Eggert T., Circolone F., Heck A., Krausz U., Guterl J.-K., Wendorff M., Losi A., Gartner W. and Jaeger K.-E. (2007) Reporter proteins for *in vivo* fluorescence without oxygen. *Nat. Biotech.* **25:**443-445

Eberbeck D., Janke V., Hartwig S., Heyen U., Schüler D., Albrecht M. and Trahms L. (2005) Blocking of magnetic moments of magnetosomes measured by magnetorelaxometry and direct observation by magnetic force microscopy. *J. Magn. Magn. Mater.* **289:**70-73

Elowitz M.B., Levine A.J., Siggia E.D. and Swain P.S. (2002) Stochastic gene expression in a single cell. *Science* **297:**1183-1186

Faivre D., Boettger L., Matzanke B. and Schüler D. (2007) Intracellular magnetite biomineralization in bacteria proceeds by a distinct pathway involving membrane-bound ferritin and an iron(II) species. *Angew. Chem. Int. Ed.* **46:**8495

Faivre D., Menguy N., Posfai M. and Schüler D. (2008a) Environmental parameters affect the physical properties of fast-growing magnetosomes. *Am. Min.* **93:**463-469

Faivre D. and Schüler D. (2008b) Magnetotactic bacteria and magnetosomes. *Chem. Rev.* **108:**4875-4898

Farina M., Esquivel D.M.S. and Lins de Barros H. (1990) Magnetic iron-sulphur crystals from a magnetotactic microorganism. *Nature* **343:**256-258

Figdor C.G., de Vries I.J.M., Lesterhuis W.J. and Melief C.J.M. (2004) Dendritic cell immunotherapy: Mapping the way. *Nat. Med.* **10:**475-480

Flies C.B., Jonkers H.M., de Beer D., Bosselmann K., Böttcher M.E. and Schüler D. (2005) Diversity and vertical distribution of magnetotactic bacteria along chemical gradients in freshwater microcosms. *FEMS Microbiol. Ecol.* **52:**185-195

Frankel R.B. and Blakemore R. (1979) Magnetite in freshwater magnetotactic bacteria. *Science* **203:**1355-1356

Frankel R.B., Papaefthymiou G.C., Blakemore R.P. and O'Brian W. (1983) Fe_3O_4 precipitation in magnetotactic bacteria. *Biochim. Biophys. Acta* **763:**147-159

Frankel R.B., Williams T.J. and Bazylinski D.A. (2007). Magneto-Aerotaxis. <u>Microbiology Monographs - Magnetoreception and magnetosomes in bacteria</u>. D. Schüler. Heidelberg, Springer. **3:** 1.

Friedrich B. and Magasanik B. (1977) Urease of *Klebsiella aerogenes*: control of its synthesis by glutamine synthetase. *J. Bacteriol.* **131:**446-452

Fukuda Y., Okamura Y., Takeyama H. and Matsunaga T. (2006) Dynamic analysis of a genomic island in Magnetospirillum sp. strain AMB-1 reveals how magnetosome synthesis developed. *FEBS Lett.* **580:**801-812

Gorby Y.A., Beveridge T.J. and Blakemore R. (1988) Characterization of the bacterial magnetosome membrane. *J. Bacteriol.* **170:**834-841

Grünberg K., Müller E.C., Otto A., Reszka R., Linder D., Kube M., Reinhardt R. and Schüler D. (2004) Biochemical and proteomic analysis of the magnetosome membrane in *Magnetospirillum gryphiswaldense*. *Appl. Environ. Microbiol.* **70:**1040-1050

Grünberg K., Wawer C., Tebo B. M. and Schüler D. (2001) A large gene cluster encoding several magnetosome proteins is conserved in different species of magnetotactic bacteria. *Appl. Environ. Microbiol.* **67:**4573-4582

Guo L., Huang J., Zhang X., Lic Y. and Zheng L. (2008) Bacterial magnetic nanoparticles as drug carriers. *J. Mater. Chem.* **18:**5993–5997

Gupta A.K. and Gupta M. (2005) Synthesis and surface engineering of iron oxide nanoparticles for biomedical applications. *Biomater.* **26:**3995-4021

Handrick R., Reinhardt S., Schultheiss D., Reichart T., Schüler D., Jendrossek V. and Jendrossek D. (2004) Unraveling the function of the *Rhodospirillum rubrum* activator of polyhydroxybutyrate (PHB) degradation: the activator is a PHB-granule-bound protein (phasin). *J. Bacteriol.* **186:**2466-2475.

Hansen M.C., Palmer R.J., Udsen C., White D.C. and Molin S. (2001) Assessment of GFP fluorescence in cells of *Streptococcus gordonii* under conditions of low pH and low oxygen concentration. *Microbiology* **147:**1383-1391

Heim R., Prasher D.C. and Tsien R.Y. (1994) Wavelength mutations and posttranslational autoxidation of green fluorescent protein. *Proc. Natl. Acad. Sci. USA* **91:**12501-12504

Herborn C.U., Papanikolaou N., Reszka R., Grünberg K., Schüler D. and Debatin J.F. (2003) Magnetosomes as biological model for iron binding: relaxivity determination with MRI. *Rofo. Fortschr. Geb. Rontgenst. Neuen Bildgeb. Verfahr.* **175:**830-834.

Hergt R., Hiergeist R., Zeisberger M., Schüler D., Heyen U., Hilger I. and Kaiser W.A. (2005) Magnetic properties of bacterial magnetosomes as diagnostic and therapeutic tools. *J. Magn. Magn. Mater.* **293:**80-86

Heyen U. and Schüler D. (2003) Growth and magnetosome formation by microaerophilic *Magnetospirillum* strains in an oxygen-controlled fermentor. *Appl. Microbiol. Biotechnol.* **61:**536-544

Hoell A., Wiedenmann A., Heyen U. and Schüler D. (2004) Nanostructure and field-induced arrangement of magnetosomes studied by SANSPOL. *Physica B* **350:**e309-e313

Ito A., Shinkai M., Honda H. and Kobayashi T. (2005) Medical application of functionalized magnetic nanoparticles. *J. Biosci. Bioeng.* **100:**1-11

Jogler C., Kube M., Schübbe S., Ullrich S., Teeling H., Bazylinksi D.A., Reinhardt R. and Schüler D. (2008) Comparative analysis of magnetosome gene clusters in magnetotactic bacteria provides further evidence for horizontal gene transfer. *Environ. Microbiol.* **in press**

Jogler C. and Schüler D. (2006). Genetic analysis of magnetosome biomineralization. Microbiology Monographs - Magnetoreception and magnetosomes in bacteria. D. Schüler. Heidelberg, Springer.

Junge K. (2008). Die Funktion der CDF-Transporter MamB und MamM beim magnetosomalen Eisentransport in *Magnetospirillum gryphiswaldense*. Fachbereich Biologie/Chemie. Bremen, Universität Bremen. **Dissertation**

Kirschvink J.L. (1982) Paleomagnetic evidence for fossil biogenic magnetite in western Crete. *Earth Planet. Sci. Lett.* **59:**388-392

Komeili A., Li Z., Newman D.K. and Jensen G.J. (2006) Magnetosomes are cell membrane invaginations organized by the actin-like protein MamK. *Science* **311:**242-245

Komeili A., Vali H., Beveridge T.J. and Newman D. (2004) Magnetosome vesicles are present prior to magnetite formation and MamA is required for their activation. *Proc. Natl. Acad. Sci. USA* **101:**3839-3844

Kopp R.E., Nash C.Z., Kobayashi A., Weiss B.P., Bazylinski D.A. and Kirschvink J.L. (2006) Ferromagnetic resonance spectroscopy for assessment of magnetic anisotropy and magnetostatic interactions: A case study of mutant magnetotactic bacteria. *J. Geophys. Res. [Solid Earth]* **111:**15

Kopp R.E. and Kirschvink J.L. (2008) The identification and biogeochemical interpretation of fossil magnetotactic bacteria *Earth Sci. Rev.* **86:**42-61

Laurent S., Forge D., Port M., Roch A., Robic C., Elst L.V. and Muller R.N. (2008) Magnetic iron oxide nanoparticles: Synthesis, stabilization, vectorization, physicochemical characterizations, and biological applications. *Chem. Rev.* **108:**2064-2110

Lins U. and Farina M. (1998) Magnetosome size distribution in uncultured rod-shaped bacteria as determined by electron microscopy and electron spectroscopic imaging. *Microsc. Res. Tech.* **42:**459-464

Löwenadler B., Jansson B., Paleus S., Holmgren E., Nilsson B., Moks T., Palm G., Josephson S., Philipson L. and Uhlén M. (1987) A gene fusion system for generating antibodies against short peptides. *Gene* **58:**87-97

Lu A.H., Salabas E.L. and Schuth F. (2007) Magnetic nanoparticles: Synthesis, protection, functionalization, and application. *Angew. Chem. Int. Ed.* **46:**1222-1244

MacLellan S.R., MacLean A.M. and Finan T.M. (2006) Promoter prediction in the rhizobia. *Microbiology* **152:**1751-1763

References

Maeda Y., Yoshino T., Takahashi M., Ginya H., Asahina J., Tajima H. and Matsunaga T. (2008) Noncovalent immobilization of streptavidin on *in vitro-* and *in vivo-* biotinylated bacterial magnetic particles. *Appl. Environ. Microbiol.* **74:**5139-5145

Malakooti J., Wang S.P. and Ely B. (1995) A consensus promoter sequence for *Caulobacter crescentus* genes involved in biosynthetic and housekeeping functions. *J. Bacteriol.* **177:**4372-4376

Mann S., Sparks N.H.C., Frankel R.B., Bazylinski D.A. and Jannash H.W. (1990) Biomineralization of ferrimagnetic greigite (Fe_3S_4) and iron pyrite (FeS_2) in a magnetotactic bacterium. *Nature* **343:**258-260

Matsakas A. and Diel P. (2005) The growth factor myostatin, a key regulator in skeletal muscle growth and homeostasis. *Intl. J. Sports Med.* **26:**83-89

Matsunaga T., Arakaki A. and Takahori M. (2002) Preparation of luciferase-bacterial magnetic particle complex by artificial integration of MagA-luciferase fusion protein into the bacterial magnetic particle membrane. *Biotechnol. Bioeng.* **77:**614-618.

Matsunaga T. and Kamiya S. (1987) Use of magnetic particles isolated from magnetotactic bacteria for enzyme immobilization. *Appl. Microbiol. Biotechnol.* **26:**328-332

Matsunaga T., Nakamura C., Burgess J.G. and Sode S. (1992) Gene transfer in magnetic bacteria: Transposon mutagenesis and cloning of genomic DNA fragments required for magnetosome synthesis. *J. Bacteriol.* **174:**2748-2753

Matsunaga T., Nakayama H., Okochi M. and Takeyama H. (2001) Fluorescent detection of cyanobacterial DNA using bacterial magnetic particles on a MAG-microarray. *Biotechnol. Bioeng.* **73:**400-405.

Matsunaga T., Okamura Y., Fukuda Y., Wahyudi A.T., Murase Y. and Takeyama H. (2005) Complete genome sequence of the facultative anaerobic magnetotactic bacterium *Magnetospirillum sp.* strain AMB-1. *DNA Res.* **12:**157-166

Matsunaga T., Sato R., Kamiya S., Tanaka T. and Takeyama H. (1999) Chemiluminescence enzyme immunoassay using Protein A-bacterial magnetite complex. *J. Magn. Magn. Mater..* **194:**126-131

Moskowitz B.M., Frankel R.B., Flanders P.J., Blakemore R.P. and Schwartz B.B. (1988) Magnetic properties of magnetotactic bacteria. *J. Magn. Magn. Mater.* **73:**273-288

Niemeyer C.M., Adler M. and Wacker R. (2007) Detecting antigens by quantitative immuno-PCR. *Nat. Protocols* **2:**1918-1930

Okamura Y., Takeyama H., Sekine T., Sakaguchi T., Wahyudi A.T., Sato R., Kamiya S. and Matsunaga T. (2003) Design and Application of a New Cryptic-Plasmid-Based

Shuttle Vector for *Magnetospirillum magneticum*. *Appl. Environ. Microbiol.* **69:**4274-4277

Osaka T., Matsunaga T., Nakanishi T., Arakaki A., Niwa D. and Iida H. (2006) Synthesis of magnetic nanoparticles and their application to bioassays. *Anal. Bioanal. Chem.* **384:**593-600

Pankhurst Q.A., Connolly J., Jones S.K. and Dobson J. (2003) Applications of magnetic nanoparticles in biomedicine. *J. Phys. D: Appl. Phys.* **36:**R167-R181

Phillips G.J. (2001) Green fluorescent protein - a bright idea for the study of bacterial protein localization. *FEMS Microbiol. Lett.* **204:**9-18

Pradel N., Santini C., Bernadac A., Fukumori Y. and Wu L. (2006) Biogenesis of actin-like bacterial cytoskeletal filaments destined for positioning prokaryotic magnetic organelles. *Proc. Natl. Acad. Sci. USA* **103:**17485-17489

Reid B.G. and Flynn G.C. (1997) Chromophore formation in green fluorescent protein. *Biochemistry* **36:**6786-6791

Reszka R. (2000). Applications for magnetosomes in medical research. <u>Biomineralization</u>. E. Baeuerlein. Weinheim, Wiley-VCH**:** 81-92.

Richter M., Kube M., Bazylinski D.A., Lombardot T., Glockner F.O., Reinhardt R. and Schüler D. (2007) Comparative genome analysis of four magnetotactic bacteria reveals a complex set of group-specific genes implicated in magnetosome biomineralization and function. *J. Bacteriol.* **189:**4899-4910

Roostalu J., Jõers A., Luidalepp H., Kaldalu N. and Tenson T. (2008) Cell division in Escherichia coli cultures monitored at single cell resolution. *BMC Microbiology* **8:68:**

Rudner D.Z., Pan Q. and Losick R.M. (2002) Evidence that subcellular localization of a bacterial membrane protein is achieved by diffusion and capture. *Proc. Natl. Acad. Sci. USA* **99:**8701-8706

Scaros O. and Fisler R. (2005) Biomarker technology roundup: from discovery to clinical applications, a broad set of tools is required to translate from the lab to the clinic. *Biotechniques* **Suppl:**30-32

Scheffel A. (2007). Molekulare und strukturelle Untersuchungen zur Bildung von Magnetosomen und zur Assemblierung von Magnetosomenketten in *Magnetospirillum gryphiswaldense*. <u>Fachbereich Biologie/Chemie</u>. Bremen, Universität Bremen. **Dissertation**

Scheffel A., Gärdes A., Grünberg K., Wanner G. and Schüler D. (2008) The major magnetosome proteins MamGFDC are not essential for magnetite biomineralization in

Magnetospirillum gryphiswaldense, but regulate the size of magnetosome crystals. *J. Bacteriol.* **190:**377-386

Scheffel A., Gruska M., Faivre D., Linaroudis A., Graumann P.L., Plitzko J.M. and Schüler D. (2006a) An acidic protein aligns magnetosomes along a filamentous structure in magnetotactic bacteria. *Nature* **440:**110-115

Scheffel A. and Schüler D. (2006b). Magnetosomes in magnetotactic bacteria. <u>Microbiology Monographs: Complex intracellular structures in prokaryotes</u>. J.M. Shively. Berlin / Heidelberg, Springer. **1**.

Scheffel A. and Schüler D. (2007) The acidic repetitive domain of the *Magnetospirillum gryphiswaldense* MamJ protein displays hypervariability but is not required for magnetosome chain assembly. *J. Bacteriol.* **189:**6437-6446

Schleifer K.H., Schüler D., Spring S., Weizenegger M., Amann R., Ludwig W. and Köhler M. (1991) The genus *Magnetospirillum* gen. nov., description of *Magnetospirillum gryphiswaldense* sp. nov. and transfer of *Aquaspirillum magnetotacticum* to *Magnetospirillum magnetotacticum* comb. nov. *Syst. Appl. Microbiol.* **14:**379-385

Schübbe S. (2005). Untersuchungen zur molekularen Organisation und regulation der *mam*-Gene in *Magnetospirillum gryphiswaldense* MSR-1. <u>Fachbereich Biologie/Chemie</u>. Bremen, Universität Bremen**. Dissertation**.

Schübbe S., C. Würdemann, J. Peplies, U. Heyen, C. Wawer, F.O. Glöckner and D. Schüler (2006) Transcriptional organization and regulation of magnetosome operons in *Magnetospirillum gryphiswaldense. Appl. Environ. Microbiol.* **72:**5757-5765

Schübbe S., Kube M., Scheffel A., Wawer C., Heyen U., Meyerdierks A., Madkour M.H., Mayer F., Reinhardt R. and Schüler D. (2003) Characterization of a spontaneous nonmagnetic mutant of *Magnetospirillum gryphiswaldense* reveals a large deletion comprising a putative magnetosome island. *J. Bacteriol.* **185:**5779-5790

Schüler D. (2004). Biochemical and genetic analysis of the magnetosome membrane in *Magnetospirillum gryphiswaldense*. <u>Biomineralization</u>. E. Baeuerlein. Weinheim, Wiley-VCH.

Schüler D. (2008) Genetics and cell biology of magnetosome formation in magnetotactic bacteria. *FEMS Micobiol. Rev.* **32:**654-672

Schüler D. and Baeuerlein E. (1998) Dynamics of iron uptake and Fe_3O_4 biomineralization during aerobic and microaerobic growth of *Magnetospirillum gryphiswaldense*. *J. Bacteriol.* **180:**159-162

Schüler D. and Frankel R.B. (1999) Bacterial magnetosomes: microbiology, biomineralization and biotechnological applications. *Appl. Microbiol. Biotechnol.* **52:**464-473

Schüler D. and Köhler M. (1992) The isolation of a new magnetic spirillum. *Zentralbl. Mikrobiol.* **147:**150-151

Schüler D., Uhl R. and Baeuerlein E. (1995) A simple light scattering method to assay magnetism in *Magnetospirillum gryphiswaldense. FEMS Microbiol. Lett.* **132:**139-145

Schultheiss D., Handrick R., Jendrossek D., Hanzlik M. and Schüler D. (2005) The presumptive magnetosome protein Mms 16 is a PHB-granule bounded protein (phasin) in *Magnetospirilum gryphiswaldense. J. Bacteriol.* **187:**2416-2425

Schultheiss D., Kube M. and Schüler D. (2004) Inactivation of the flagellin gene *fla*A in *Magnetospirillum gryphiswaldense* results in nonmagnetotactic mutants lacking flagellar filaments. *Appl. Environ. Microbiol.* **70:**3624-3631

Schultheiss D. and Schüler D. (2003) Development of a genetic system for *Magnetospirillum gryphiswaldense. Arch. Microbiol.* **179:**89-94

Schwertmann U. and Cornell R.M. (1991). <u>Iron oxides in the Laboratory : Preparation and characterization</u>. Weinheim, VCH, Weinheim.

Seaver L.C. and Imlay J.A. (2001) Alkyl hydroperoxide reductase is the primary scavenger of endogenous hydrogen peroxide in *Escherichia coli. J. Bacteriol.* **183:**7173–7181

Shu X., Shaner N.C., Yarbrough C.A., Tsien R.Y. and Remington J.S. (2006) Novel chromophores and buried charges control color in mFruits. *Biochemistry* **45:**9639-9647

Siegele D.A. and Hu J.C. (1997) Gene expression from plasmids containing the *araBAD* promoter at subsaturating inducer concentrations represents mixed populations *Proc. Natl. Acad. Sci. USA* **94:**8168–8172

Skerra A. (1994) Use of the tetracycline promoter for the tightly regulated production of a murine antibody fragment in Escherichia coli. *Gene* **151** 131-135

Smit J. and Agabian N. (1984) Cloning of the major protein of the *Caulobacter crescentus* periodic surface layer: detection and characterization of the cloned peptide by protein expression assays. *J. Bacteriol.* **160:**1137-1145

Sode K., Kudo S., Sakaguchi H., Nakamura N. and Matsunaga T. (1993) Application of bacterial magnetic particles for highly selective mRNA recovery system. *Biotechnol. Tech.* **7:**688-694

References

Southward C.M. and Surette M.G. (2002) The dynamic microbe: green fluorescent protein brings bacteria to light. *Mol. Microbiol.* **45:**1191-1196

Sparks N.H.C., Courtaux L., Mann S. and Board R.G. (1986) Magnetotactic bacteria are widely distributed in sediments in the UK. *FEMS Microbiol. Lett.* **37:**305-308

Spring S., Amann R., Ludwig W., Schleifer K.-H., van Gemerden H. and Petersen N. (1993) Dominating role of an unusualmagnetotactic bacterium in the microaerobic zone of a freshwater sediment. *Appl. Environ. Microbiol.* **50:**2397-2403

Staniland S., Williams W., Telling N., Van der Laan G., Harrison A. and Ward B. (2008) Controlled cobalt doping of magnetosomes *in vivo*. *Nat. Nanotechnol.* **3:**158-162

Strovas T.J., Sauter L.M., Guo X.F. and Lidstrom M.E. (2007) Cell-to-cell heterogeneity in growth rate and gene expression in *Methylobacterium extorquens* AM1. *J. Bacteriol.* **189:**7127-7133

Sun C., Lee J.S.H. and Zhang M.Q. (2008a) Magnetic nanoparticles in MR imaging and drug delivery. *Adv. Drug Deliv. Rev.* **60:**1252-1265

Sun J.-B., Duan J.-H., Dai S.-L., Ren J., Guo L., Jiang W. and Li Y. (2008b) Preparation and anti-tumor efficiency evaluation of doxorubicin-loaded bacterial magnetosomes: Magnetic nanoparticles as drug carriers isolated from *Magnetospirillum gryphiswaldense*. *Biotechnol. Bioeng.* **101:**1313-1320

Sun J.-B., Zhao F., Tang T., Jiang W., Tian J.-s., Li Y. and Li J.-L. (2008c) High-yield growth and magnetosome formation by *Magnetospirillum gryphiswaldense* MSR-1 in an oxygen-controlled fermentor supplied solely with air. *Appl. Microbiol. Biotechnol.* **79:**389-397

Tanaka M., Okamura Y., Arakaki A., Tanaka T., Takeyama H. and Matsunaga T. (2006) Origin of magnetosome membrane: proteomic analysis of magnetosome membrane and comparison with cytoplasmic membrane. *Proteomics* **6:**5234-5247

Tanaka T. and Matsunaga T. (2000) Fully automated chemiluminescence immunoassay of insulin using antibody-protein A-bacterial magnetic particle complexes. *Anal. Chem.* **72:**3518-3522

Tanaka T., Takeda H., Ueki F., Obata K., Tajima H., Takeyama H., Goda Y., Fujimoto S. and Matsunaga T. (2004) Rapid and sensitive detection of 17 beta-estradiol in environmental water using automated immunoassay system with bacterial magnetic particles. *J. Biotechnol.* **108:**153-159

Tanaka T., Yamasaki H., Tsujimura N., Nakamura N. and Matsunaga T. (1997) Magnetic control of bacterial magnetite-myosin conjugate movement on actin cables. *Mater. Sci. Eng. , C* **5:**121-124

Taoka A., Asada R., Wu L. and Fukumori Y. (2007) Polymerization of the actin-like protein MamK, which is associated with magnetosomes. *J. Bacteriol.* **189:**8737-8740

Thiesen B. and Jordan A. (2008) Clinical applications of magnetic nanoparticles for hyperthermia. *Int. J. Hyperthermia* **24:**467-474

Thomas-Keprta K.L., Bazlinski D.A., Kirschvink J.L., Clemett S.J., McKay D.S., Wentworth S.J., Vali H., Gibson Jr. E.K. and Romanek C.S. (2000) Elongated prismatic crystals in AL84001 carbonate globules : Potential Martian Magnetofossils. *Geochim. Cosmochim. Acta* **64:**4049-4081

Ullrich S., Kube M., Schübbe S., Reinhardt R. and Schüler D. (2005) A Hypervariable 130-Kilobase Genomic Region of *Magnetospirillum gryphiswaldense* Comprises a Magnetosome Island Which Undergoes Frequent Rearrangements during Stationary Growth. *J. Bacteriol.* **187:**7176-7184

Valdivia R.H. and Falkow S. (1996) Bacterial genetics by flow cytometry: rapid isolation of Salmonella typhimurium acid-inducible promtoers by differential fluorescence induction. *Mol. Microbiol.* **22:**367-378

Wadhams G.H., Martin A.C., Porter S.L., Maddock J.R., Mantotta J.C., King H.M. and Armitage J.P. (2002) TlpC, a novel chemotaxis protein in *Rhodobacter sphaeroides*, localizes to a discrete region in the cytoplasm. *Mol. Microbiol.* **46:**1211-1221

Wall M.A., Socolich M. and Ranganathan R. (2000) The structural basis for red fluorescence in the tetrameric GFP homolog DsRed. *Nature Struct. Biol.* **7:**1133-1138

Weissleder R. and Pittet M.J. (2008) Imaging in the era of molecular oncology. *Nature* **452:**580-589

Wu W., He Q. and Jiang C. (2008) Magnetic iron oxide nanoparticles: synthesis and surface functionalization strategies. *Nanoscale Res. Lett.* **3:**397-415

Yoshino T., Kato F., Takeyama H., Nakai K., Yakabe Y. and Matsunaga T. (2005a) Development of a novel method for screening of estrogenic compounds using nano-sized bacterial magnetic particles displaying estrogen receptor. *Analyt. Chim. Acta* **532:**105-111

Yoshino T. and Matsunaga T. (2005b) Development of efficient expression system for protein display on bacterial magnetic particles. *Biochem. Biophys. Res. Commun.* **338:**1678-1681

Yoshino T. and Matsunaga T. (2006) Efficient and stable display of functional proteins on bacterial magnetic particles using Mms13 as a novel anchor molecule. *Appl. Environ. Microbiol.* **72:**465-471

Yoshino T., Takahashi M., Takeyama H., Okamura Y., Kato F. and Matsunaga T. (2004) Assembly of G protein-coupled receptors onto nanosized bacterial magnetic particles using Mms16 as an anchor molecule. *Appl. Environ. Microbiol.* **70:**2880-2885

Yoza B., Arakaki A., Maruyama K., Takeyama H. and Matsunaga T. (2003a) Fully automated DNA extraction from blood using magnetic particles modified with a hyperbranched polyamidoamine dendrimer. *J. Biosci. Bioeng.* **95:**21-26

Yoza B., Arakaki A. and Matsunaga T. (2003b) DNA extraction using bacterial magnetic particles modified with hyperbranched polyamidoamine dendrimer. *J. Biotechnol.* **101:**219-228

Zahn M. (2001) Magnetic fluid and nanoparticle applications to nanotechnology. *J. Nanoparticle Res.* **3:**73-78

Zhang C., Xing X.H. and Lou K. (2005) Rapid detection of a GFP-marked *Enterobacter aerogenes* under anaerobic conditions by aerobic fluorescence recovery. *FEMS Microbiol. Lett.* **249:**211-218

Zolg J.W. and Langen H. (2004) How industry is approaching the search for new diagnostic markers and biomarkers. *Mol. Cell. Proteomics* **3:**345-354

Supplementary

Table 1: Primer sequences for truncation experiments

Primer name	Sequence
mamCfwXhoI	CTCGAGAGGACAACAGCGATGAGCTTTC
mamCrevNdeI	CATATGGGCCAATTCTTCCCTCAG
mamCrevNdeI267ct	CATATGGGCGGCGACGCCGGCGATTAG
mamCrevNdeI349ct	CATATGGTCGGACGCTGTCGCCTC
mamCrevNdeI159ct	CATATGTTCCTTGCCGGTGTCGATG
mamCfwXhoI28ct	CTCGAGATGGCGAAATCCGTCCCTGGAATC
mamCfwXhoI94ct	CTCGAGATGAATGCCCGCCTTTTGAAGGAC
mamCfwXhoI157ct	CTCGAGATGGAAGCCGCCGGCGCCGGGCTTG

Table 2: Plasmids used for MamC truncation experiments

Plasmid	Description	Source
pCL5	pBBR1MCS1 + 10 glycine linker + *egfp*	Article 6
pBBRMamC(Δ1-9)-GFP	pCL5 + PCR product from mamCrevNde/mamCfwXhoI28ct	This study
pBBRMamC(Δ1-31)-GFP	pCL5 + PCR product from mamCrevNde/mamCfwXhoI94ct	This study
pBBRMamC(Δ1-52)-GFP	pCL5 + PCR product from mamCrevNde/mamCfwXhoI157ct	This study
pBBRMamC(1-53)-GFP	pCL5 + PCR product from mamCfwXhoI/mamCrevNdeI159ct	This study
pBBRMamC(1-99)-GFP	pCL5 + PCR product from mamCfwXhoI/mamCrevNdeI267ct	This study
pBBRMamC(1-116)-GFP	pCL5 + PCR product from mamCfwXhoI/mamCrevNdeI349ct	This study
pBBRMamC(29-53)-GFP	pCL5 + PCR product from mamCfwXhoI28ct/mamCrevNdeI349ct	This study

Manuscript 1

Expression of GFP fused to magnetosome proteins in microaerophilic

magnetotactic bacteria

Claus Lang, Dirk Schüler*

Ludwig-Maximillians-Universität München

Department Biologie I, Bereich Mikrobiologie

Maria-Ward-Str. 1a

80638 München

*Corresponding author: dirk.schueler@lrz.uni-muenchen.de

Abstract

The magnetosomes of magnetotactic bacteria are prokaryotic organelles consisting of a magnetite crystal bounded by a phospholipid bilayer that contains a distinct set of proteins with various functions. Because of their unique magnetic and crystalline properties, magnetosome particles are potentially useful as magnetic nanoparticles in a number of applications, which in many examples requires the coupling of functional moieties to the magnetosome membrane. In this work we studied the use of green fluorescent protein (GFP) as reporter for magnetosomal localization and expression of fusion proteins in the microaerophilic *Magnetospirillum gryphiswaldense* by flow cytometry, fluorescence microscopy, and biochemical analysis. Although optimum conditions for high fluorescence and magnetite synthesis were mutually exclusive, we established oxygen-limited growth conditions, which supported growth, magnetite biomineralization, and GFP fluorophore formation at reasonable rates. Under these optimized conditions we studied the subcellular localization and expression of the GFP-tagged magnetosome proteins MamC, MamF, and MamG by fluorescence microscopy and immunoblotting. While all fusions specifically localized at the magnetosome membrane, MamC-GFP displayed the strongest expression and fluorescence. MamC-GFP-tagged magnetosomes purified from cells displayed strong fluorescence, which was sensitive towards detergents, but stable under a wide range of temperature and salt concentrations. In summary, our data demonstrate the use of GFP as a reporter for protein localization under magnetite forming conditions and the utility of MamC as an anchor for magnetosome-specific display of heterologous gene fusions.

Introduction

The magnetosomes of magnetotactic bacteria are specialized organelles for magnetic orientation that consist of membrane-enveloped crystals of a magnetic iron mineral (1, 34). In strains of *Magnetospirillum*, magnetosomes are synthesized by magnetite (Fe_3O_4) precipitation within specific vesicles formed by the magnetosome membrane (MM), which invaginates from the cytoplasmic membrane and contains a number of specific proteins that are involved in the synthesis of functional magnetosome particles (7, 9, 16, 44). Increasing efforts in interdisciplinary research are aimed at understanding how magnetotactic bacteria achieve their outstanding control over the properties of the magnetic mineral crystals, and their assembly into highly ordered chain-like structures (2, 15). Recently, magnetotactic bacteria have emerged as powerful models for the study of cell biology and organelle formation in prokaryotes, as magnetosomes display many common features of eukaryotic organelles (15). In addition, the uniform sizes, crystal habits, and magnetic characteristics of magnetosomes have attracted interest in their use as magnetic nanoparticles with superior properties (20-22), and a number of potential applications such as magnetic separation and detection of analytes, the use as contrast agents in magnetic resonance imaging (MRI), or their use in magnetic hyperthermia have been suggested for magnetic nanoparticles derived from magnetic bacteria (13, 24, 52, 55). Many of these applications require the functionalization of isolated magnetosome particles, e.g. by the magnetosome-specific display of functional moieties, such as enzymes, antibody binding proteins, protein tags, or oligonucleotides (22). This has been mostly achieved by chemical coupling of specific ligands to lipids or proteins of the MM (4, 26, 45, 48). Alternatively, the use integral magnetosome membrane proteins (MMPs) as anchor for the magnetosome-specific display of heterologous proteins fused to them has been suggested (22, 53, 54). For example, luciferase was used as a reporter for magnetosome directed expression of genetic fusions to the Mms13 protein of *M. magneticum* (27). Another protein that is useful as a reporter for expression and intracellular localization of magnetosome proteins is the *green fluorescent protein* (GFP). Use of GFP fusions has revolutionized the understanding of subcellular organization and membrane targeting in model bacteria such as *Escherichia coli, Bacillus subtilis* and *Caulobacter crescentus* (25, 41). In addition, GFP was used as molecular marker in various environmental microorganisms (23) and has served as a powerful transcriptional reporter to measure real-time gene expression in single living cells by flow cytometry or microscopy (3). GFP-assisted fluorescence microscopy has already been used to study the subcellular localization of several magnetosome proteins in the magnetotactic bacteria *M. magneticum* and *M. gryphiswaldense.*

Investigated proteins include the MamA protein, which is presumably involved in the activation of magnetosomes, as well as the acidic MamJ protein and the actin-like MamK protein, both of which control the intracellular assembly of magnetosome chains. Although these examples already demonstrated its principal usefulness in MTB, the use of GFP expression as intracellular marker of magnetosome localization can be problematic. Magnetite crystals are formed in these microaerophilic organisms only at low oxygen concentrations below 10 mbar (14), while on the other hand the use of GFP at micro- or anaerobiosis is limited since the maturation of the protein requires molecular oxygen during the last step of fluorophore maturation (12, 30). Accordingly, it has been noticed that fluorescence intensities and the proportion of fluorescent cells were rather low and varied considerably under microoxic growth conditions, and so far, the application of GFP in relationship to magnetite formation in magnetic bacteria has not been addressed systematically.

This study was intended to investigate the expression of GFP in the microaerophilic *M. gryphiswaldense* at various oxygen levels by flow cytometry and fluorescence microscopy. Cultivation conditions were optimized with respect to growth, biomineralization of magnetite crystals as well as the maximum expression of GFP and fluorophore formation. We further analyzed by fluorescence microscopy and immunoblotting the subcellular localization of the GFP-tagged magnetosome proteins MamC, MamF, and MamG, which were previously shown to be involved in the size control of growing magnetite crystals (32). The GFP modified fluorescent magnetic nanoparticles were purified from bacterial cells, and the stability of expression and fluorescence of MamC-GFP-labelled magnetosomes was studied *in vitro* under various conditions. These studies served (i) to characterize GFP modified magnetosomes as a novel biomaterial, which might be useful for biomedical applications, and (ii) as a prerequisite for future experiments using magnetosome proteins as an anchor for magnetosome-specific display of heterologous gene fusions.

Materials and Methods

Strains and growth conditions

Escherichia coli strains DH5α and TOP10 (TOP10 chemically competent cells, Invitrogen, Karlsruhe, Germany) were used as hosts for cloning. For conjugation experiments the *E. coli* strain S17-1 was used (40). *E. coli* strains were grown on Luria-Bertani at 37°C, the medium was supplemented with kanamycin or ampicillin (50 μg/ml) if appropriate. Throughout this study the *M. gryphiswaldense* strain R3/S1, which is a spontaneous

rifampicin and streptomycin resistant mutant of the *M. gryphiswaldense* strain MSR-1 was used (38). *M. gryphiswaldense* was routinely grown microaerobically at 28°C under moderate shaking (100 rpm) in modified FSM medium using 27 mM pyruvate as a carbon source as described previously (14). For cultivation on petri dishes agar was added to 1.5% wt/vol to FSM medium.

Fermentor production of fluorescent magnetosomes

R3/S1(pCL6) was cultivated in a modified Biostat A Twin dual vessel laboratory fermentor (B. Braun Biotech International, Melsungen, Germany) in LSM medium as described previously (14). Oxygen electrodes (InPro6000; Mettler Toledo, Gießen, Germany) were calibrated with nitrogen and a microoxic gas mixture (1% oxygen in nitrogen) or synthetic air (flow rate 3 L min^{-1}) as described by Heyen and Schüler (14). The medium (10 liters) was inoculated with a 1-liter preculture grown in a 2-liter flask containing air in the headspace. The fermentor was inoculated to an initial cell density of approximately 1×10^7 cells ml^{-1}. During cultivation agitation (150 rpm), temperature (28°C) and pH (7.0) were maintained constant. Bacteria were grown microaerobically at 0.125 or 2 mbar oxygen until the stationary phase for 24 h. Alternatively, bacteria were cultivated aerobically at 200 mbar oxygen for 16 h and subsequently shifted to 0.2 mbar, as indicated in the experiments.

Molecular genetic techniques

If not otherwise specified, standard DNA procedures were employed (31). Cloned genes and fusion constructs were sequenced using BigDye terminator v3.1 chemistry on an ABI 3700 capillary sequencer (Applied Biosystems, Darmstadt, Germany). Sequence data were analyzed with Lasergene 6 (DNAstar Inc. Madison, WI). Primers were purchased from Carl Roth GmbH (Karlsruhe, Germany) and MWG Biotech (Ebersberg, Germany). The primer sequences are listed in Table 1.

Table 1: Primers used in this study. Restriction sites that were incorporated in the primer are indicated in bold and the sequence region encoding for the glycine-linker is written in italics.

Primer name	Target gene	Sequence
CL1	*egfp*	**catatg**g*ggaggcggaggcggtggcggaggtggcgga*gtgagcaagggcgaggag
CL2	*egfp*	gt**ggatcc**ttacttgtacagctcgtc
CL3	*mamG*	**ctcgag**ggagatcagatgatcaagggcatc
CL4	*mamG*	**catatg**agcaggctcggcggaggc
CL5	*mamF*	**ctcgag**agggcaaagcaatggccgagac
CL6	*mamF*	**catatg**gatcagggcgactacatggctg
CL7	*mamC*	**ctcgag**aggacaacagcgatgagctttc
CL8	*mamC*	**catatg**ggccaattcttccctcag

Construction of GFP-Fusion proteins

In this study the GFPmut1 variant, which is also termed EGFP (enhanced GFP), was used (5, 23). The *egfp* gene was PCR amplified (Taq-Mastermix, Promega, Heidelberg, Germany) from the pEGFPN-1 (BD Biotech) plasmid using the CL1 forward primer, which adds a *Nde*I restriction site and a ten glycine linker to the 5' end of the *egfp* gene, and reverse primer CL2. The PCR product was cloned into pGEMT-Easy (Promega) to yield pCL1. The *mamC* (CL7, CL8), *mamF* (CL5, CL6) and *mamG* (CL3, CL4) genes were amplified with the corresponding primer pairs (indicated in parentheses) using genomic DNA of *M. gryphiswaldense* R3/S1 as a template. The PCR products were cloned into pGEMT-Easy (Promega) and transformed into $CaCl_2$ competent DH5α to generate pCL2-4. The *egfp* gene was subcloned from pCL1 into the *Eco*RI site of the pBBRMCS-2 (18) plasmid to yield the plasmids pCL5. Colony PCR was performed to screen for plasmids in which *egfp* was present in the same orientation as the P_{lac} promoter. Translational fusions of *mamC*, *mamF* and *mamG* with *egfp* connected via a ten glycine linker were constructed by ligating the respective *mam* genes from pCL2, pCL3 and pCL4 into the *Nde*I and *Xho*I sites of the pCL5 vector to generate the plasmids pCL6, pCL7 and pCL8, respectively. For a complete list of plasmids used in this study refer to Table 2. The plasmids harboring the *mam-egfp* fusions were transferred into *M. gryphiswaldense* R3/S1 by conjugation from *E. coli* S17-1 as described previously (39).

Table 2: Plasmids used in this study

Plasmid name	description	Source
pEGFPN-1	GFP expression vector, Ap	BD Biotech
pGEMT-Easy	Cloning vector, Ap	Promega
pCL1	pGEMT-Easy + 10 glycine linker + *egfp*	This study
pCL2	pGEMT-Easy + *mamC*	This study
pCL3	pGEMT-Easy + *mamF*	This study
pCL4	pGEMT-Easy + *mamG*	This study
pBBR1-MCS2	mobilizable broad host range vector, Km	Kovach et al (11)
pCL5	pBBR1-MCS2 + 10G*egfp* from pCL1	This study
pCL6	pCL5 + *mamC* from pCL1	This study
pCL7	pCL5 + *mamF* from pCL2	This study
pCL8	pCL5 + *mamG* from pCL3	This study

Fluorescence microscopy

M. gryphiswaldense R3/S1 strains bearing the plasmids pCL5-pCL8 were grown in 15 ml polypropylene tubes with sealed screw caps and a culture volume of 11 ml to stationary phase. The cell membranes were stained with the membrane stain FM4-64 (Invitrogen, Karlsruhe, Germany) at a final concentration of 1.5 µM. The stained cells were immobilized on agarose pads (FSM medium excluding yeast extract and peptone, but supplemented with 1% agarose). Immobilized cells were imaged with an Olympus BX61 microscope equipped with a 100x UPLSAPO100XO objective with a numerical aperture of 1.40 and an Olympus F-View II camera. Images were captured and analyzed using Olympus cell^M and ImageJ 1.36b software. For the microscopic visualization of fluorescent magnetosomes approximately 15 µl of a magnetosome suspension with a magnetosome concentration corresponding to an iron concentration of 10 mM were spotted on a microscopic slide. After placement of a bar magnet next to the microscopic slide the fluorescent magnetosomes were imaged with a Zeiss LSM510 microscope equipped with a 10x objective and a Photometrics Coolsnap HQ camera.

Analytical procedures

Cell growth and magnetism were measured turbidimetrically at 565 nm. The average magnetic orientation of cell suspensions was assayed as previously described (36). Briefly, an external magnetic field was employed to align cells at different angles relative to the light beam. The ratio of the resulting maximum and minimum extinction (C_{mag}) correlates with the

average number of magnetic particles per cell and was used as a semi-quantitative assessment of magnetite formation (a $C_{mag} = 0$ was assumed for non-magnetic cells).

For the determination of iron concentration of magnetosome suspensions, magnetosomes were sedimented by centrifugation, resuspended in 65% HNO_3 and incubated at 99°C overnight to dissolve the magnetite crystals. The iron content of the solution was determined with a modified version (47) of the ferrozine assay (42).

The protein concentration of the cell lysate (CL), the non-magnetic (NF), soluble (SP), membranous (MP) and magnetosome protein fractions were assessed with a bicinchoninic protein quantification kit (Sigma, Munich, Germany) according to manufacturer's instructions.

The magnetosome bound fluorescence was quantified with an Infinite 500 96well fluorescence reader using I-Control v1.2.7.0 software (Tecan, Crailsheim, Germany). The excitation wavelength was 485 nm (20 nm bandwidth) and emission was recorded at 535 nm (25 nm bandwidth). Different dilutions of magnetosomes (0-10 mM iron) were prepared in triplicate in 100 µl EP (10 mM Hepes, 1 mM EDTA pH7.4) in a black 96-well Nunclon plate. The value for each sample was averaged from 10 reads over an integration period of 20 µs.

Flow cytometry

Flow cytometry was performed with a FACScalibur flow cytometer (Becton-Dickinson) equipped with an argon laser emitting at 488 nm. GFP fluorescence was recorded in the FL-1 channel. Cells of *M. gryphiswaldense* R3/S1 and derivatives bearing the plasmids pCL5 to pCL8 were washed in phosphate-buffered saline and resuspended in phosphate-buffered saline in a 1:100 dilution to maintain a counting speed between 300 and 1000 events s^{-1}. Unless otherwise indicated, 50 000 events were counted. Data were analyzed using FlowJo software (Treestar). Untransformed R3/S1 was used as a non-fluorescent standard. Contaminating cell debris and media constituents were excluded from the analysis based on forward (FSC) and side scatter (SSC) data. To estimate the proportion of fluorescent cells a threshold for fluorescence was set to the fluorescent intensity below which 99% of untransformed R3/S1 were detected.

Isolation of magnetosomes

The procedure for magnetosome purification was modified after Grünberg et al. (9). *M. gryphiswaldense* strains were exposed to air in sealed 5L flasks (Schott, Mainz, Germany) containing 4L modified FSM medium. The cultures were inoculated with 400 ml overnight culture to a cell density of approximately $1x10^7$ cells ml^{-1}. The cultures were incubated at

28°C at moderate shaking (120 rpm). Stationary phase cultures were harvested by centrifugation, washed with WB (20 mM Hepes, 1 mM EDTA pH 7.4) and finally resuspended in RB (50 mM Hepes, 1 mM EDTA, 0.1 mM PMSF pH7.4). Cells were disrupted by three passages through a French Press at 1260 bar. Cell debris was removed by centrifugation at 800 g for 5 min. The cleared cell lysate was passed through a MACS magnetic separation column placed between Sm-Co magnets (Miltenyi, Bergisch Gladbach, Germany) to separate magnetosomes from the non-magnetic fraction. The column bound magnetosomes were washed with ten column volumes (50 ml) of EP, HP (10 mM Hepes, 200 mM NaCl, 1 mM EDTA pH7.4) and water before the magnetic field was removed and the magnetosomes were eluted in EP. Subsequently the magnetosomes were centrifuged through an 8-ml sucrose cushion (60% [wt/wt] in EP) at 200 000 x g for 90 min. Due to their high specific density, magnetosomes sediment at the bottom of the tube, whereas other cellular constituents are retained by the sucrose cushion. Finally, the magnetosomes were resuspended in 2 ml EP.

The NF, which was not retained by the magnetic column, was subjected to centrifugation at 4000 g for 60 min to remove residual cell debris. The supernatant was subjected to 2h of centrifugation at 100 000 g to separate the cellular membranes from the soluble protein fraction. The sedimented membrane fraction was resuspended in EP and centrifuged a second time at 100 000 g for 2h. The membrane proteins were resuspended in EP supplemented with 1% sodium dodecyl sulfate (SDS).

SDS-PAGE and Western blot analysis

Polyacrylamide gels were prepared according to the procedure of Laemmli (19). Protein samples from different cellular fractions were resuspended in electrophoresis sample buffer (62.5 mM Tris-HCl pH 6.8, 0.1M DTT, 1.6% SDS, 5% glycerol, 0.002% bromophenol blue) and denatured at 100°C for 5 min. Fifteen micrograms of protein was loaded onto the gels. For SDS-PAGE analysis of the relative abundances of fusion proteins present in the MM, MMP were separated on 15% (wt/vol) gels and proteins were visualized by coomassie brilliant blue staining. For Western blot analysis 10% (wt/vol) gels were used, and following electrophoresis proteins were transferred onto nitrocellulose membranes (Protran, Whatman, Germany) by electroblotting. The membranes were blocked for 2h at room temperature. An anti-GFP antibody (Santa Cruz, Biotechnology, Inc.) or an anti-MamC antibody (8) was added to the blocking solution in 1:1000 or 1:500 dilution, respectively, and incubated for 1h at room temperature. The membrane was washed several times with Tween-Tris-buffered saline and Tris-buffered saline (TBS) before alkaline phosphatase-labeled goat anti-rabbit IgG

antibody (Santa Cruz, Biotechnology, Inc.) was added in 1:1000 dilution in TBS (Tris buffered saline). After incubation at room temperature for 45 min the membrane was washed with TBS and the BCIP (5-bromo-4-chloro-3-indolyl-phosphate)/ nitroblue tetrazolium) detection reagent (Roche Diagnostics, Mannheim, Germany) was used for detection.

Stability assays of magnetosome fluorescence

A stock solution with a defined magnetosome concentration (2 mM iron) was prepared in EP and dispensed in 100 µl portions into 1.5 ml reaction tubes. Magnetosomes were magnetically separated for two minutes by attaching a neodymium magnet to the side of the tube. The supernatant was aspirated, and the magnetosomes were resuspended in 100 µl of a buffer containing the desired constitution. For pH testing, buffer S (40 mM boric acid, 40 mM phosphoric acid) was adjusted with sodium hydroxide to pH values of pH 3 to pH 11 (51). Stability to detergents was tested by resuspending magnetosomes in buffer S (pH 8) containing different SDS or triton X-100 concentrations from 0 to 1% (w/v). To investigate the effect of guanidinium chloride, the magnetosomes were resuspended in buffer S (pH 8) containing between 0 and 1 M guanidinium chloride. The influence of sodium chloride was tested with buffer S (pH 8) supplemented with 0, 0.1, 0.5, 1, 2 and 4 M sodium chloride. After the magnetosome suspensions were incubated for 1 h at 4°C, the magnetosomes were separated magnetically as described above, resuspended in buffer S (pH 8) and the fluorescence was quantified with a fluorescence reader. The influence of the storage temperature was tested by incubating magnetosome suspensions in buffer S (pH 8) at temperatures between -20 and 70°C for 12 h followed by a magnetic separation, resuspension in the same buffer, and fluorescence quantification as described above.

Results

Optimization of growth conditions for maximum GFP fluorophore formation and magnetite synthesis

Synthesis of magnetite crystals in *M. gryphiswaldense* occurs only below an oxygen partial pressure of 10 mbar (14, 35, 50). In initial experiments, we noticed that under these microoxic conditions only a small and highly variable proportion of cells expressing GFP were fluorescent, and the emitted signal was rather weak and varied between different growth experiments (C. Lang and D. Schüler, unpublished observation). As we reasoned that poor GFP fluorescence expression was due to limited availability of oxygen for fluorophore biosynthesis, we performed a number of experiments in order to establish growth conditions

that would provide both strong GFP expression and magnetite biomineralization. First, cells expressing GFP from the *lac* promoter on pCL5 were grown in sealed batch flask cultures with various headspace-to-volume ratios and under different headspace oxygen concentrations. As shown in Table 3 the proportion of fluorescent cells and magnetic orientation (as monitored by C_{mag}) displayed an inverse dependence on the aeration. For example, under standard cultivation conditions (1% oxygen in the culture headspace), which are used for maximal magnetite production, only 8.5 % of the cells displayed significant fluorescence. The highest proportion of fluorescent cells (~ 22 %) was found at the highest aeration of 21 % oxygen in the headspace. However, cells were completely devoid of magnetite crystals (C_{mag} = 0) under these conditions. The proportion of fluorescent cells and the average intensity increased with the oxygen availability, and both magnetite formation and fluorescence intensity were reasonably high if the headspace-to-liquid ratio was approximately 1:4, and air was used in the headspace (Table 3). Next, we investigated the fluorescence of GFP fused to the MMPs MamG, MamC, and MamF, respectively, under these optimized conditions. The expression and intracellular localization of these three proteins was of primary interest as they represent the most abundant proteins in the MM, are tightly bound to the magnetosome by several transmembrane domains, and thus are promising candidates for anchors to display fusion proteins on the surface of magnetosome particles (9, 32). Like with unfused GFP, cultures expressing GFP fused to the MamC, MamF, and MamG, from the plasmids pCL6, pCL7 and pCL8, respectively, displayed reasonable magnetite formation and high fluorescence, and large proportions of fluorescent cells were obtained in flask cultures grown under the optimized conditions described before. However, the fusions displayed different fluorescence intensities, and the highest fluorescence was observed with MamC-GFP followed by MamF-GFP and MamG-GFP (Figure 1, Table 3).

In summary, the best compromise with respect to magnetite formation and GFP fluorescence was obtained in flask cultures with growth-limiting oxygen supply, in which oxygen concentrations declined from high initial levels in the medium with increasing cell numbers, eventually reaching low dissolved oxygen concentrations permitting magnetite synthesis (14, 35). As this is accompanied by a change of conditions during growth, further experiments were performed in an oxystat fermentor, which allowed the precise maintenance of a constant oxygen partial pressure over the entire incubation period (14). Cells expressing MamC-GFP from pCL6 were highly magnetic at 0.12 mbar oxygen, however, only 10.8 % of the R3/S1(pCL6) cells exhibited fluorescence levels above that of the untransformed control. On the contrary, fluorescence intensities and the proportions of fluorescent cells (26.1%) were

highest at an oxygen partial pressure of 200 mbar, which however entirely repressed magnetite synthesis. At an intermediate oxygen partial pressure of 2 mbar the culture produced magnetite, but only 15.8% of the cells was fluorescent, and the average fluorescence was low with an intensity only 22% higher than that of the culture grown at 0.12 mbar oxygen (Table 3).

As we concluded from these experiments that strong fluorescence and maximum magnetite synthesis are mutually exclusive at any constant oxygen level, shift experiments were performed, in which the cells were initially grown for 16 hours under fully oxic conditions (200 mbar) to an OD_{565} of 0.310, and then shifted to microoxic conditions (0.2 mbar) for eight hours. This treatment resulted in a magnetic culture with 20.3 % fluorescent cells and a fluorescence intensity that had increased by 50% compared to the microoxically grown culture (Table 3). In addition, we attempted first to incubate the bacteria under microoxic conditions and subsequently induce GFP maturation by exposure to air. However these experiments were unsuccessful as the fluorescence did not increase over an incubation period of 6 h, and cells ceased growth after the shift (data not shown).
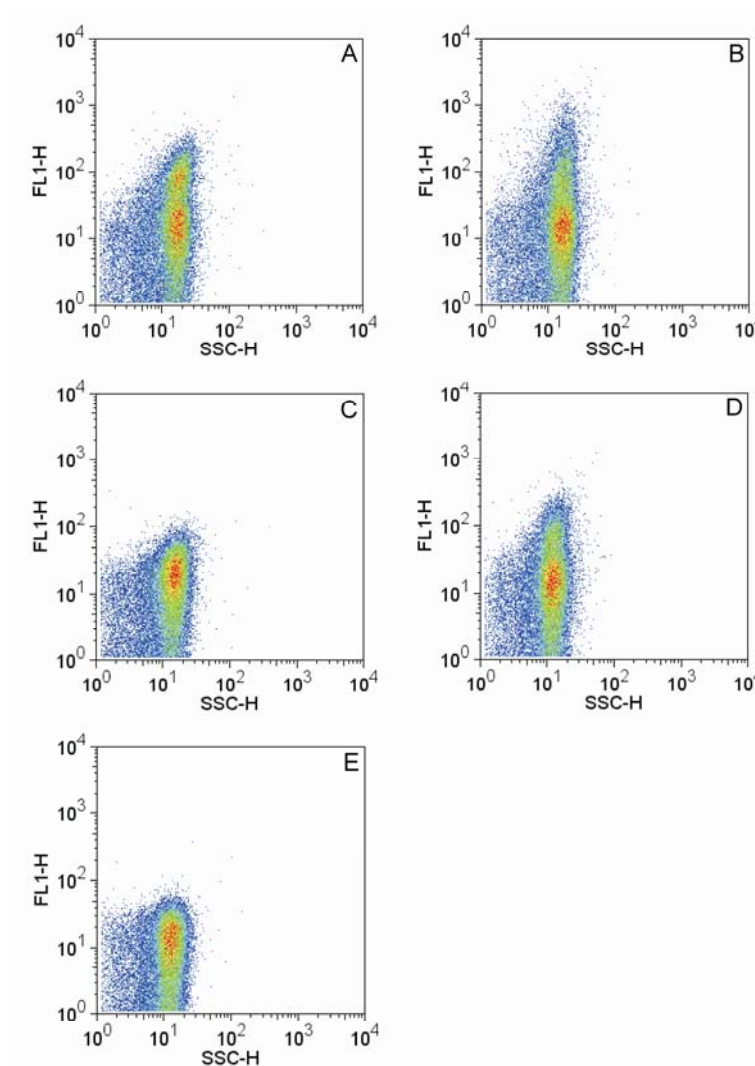
Figure 1: Flow cytometrical analysis of *M. gryphiswaldense* R3/S1 expressing either GFP (pCL5) (A), MamC-GFP (pCL6) (B), MamG-GFP (pCL8) (C) or MamF-GFP (pCL7) (D). The analysis of the untransformed *M. gryphiswaldense* strain is shown in panel (E). The fluorescence intensity (FL1-H) of each event was plotted against the side scatter (SSC).

Table 3: Flow cytometric analysis of different GFP and GFP-fusion expressing derivatives of *M. gryphiswaldense* cultivated under different conditions.

Strains	Culture conditions	Growth stage (OD)	Magnetism (C_{mag})	Average Fluorescence	Cell proportion above threshold (%)
M. gryphiswaldense (pCL5)	1% oxygen 100 ml culture in 1 L flask	0.095	1.7	18.1	8.5
M. gryphiswaldense (pCL5)	10% oxygen 100 ml culture in 1 L flask	0.183	1.5	41.9	20.0
M. gryphiswaldense (pCL5)	21% 100 ml culture in 1 L flask	0.138	0.0	52.3	20.4
M. gryphiswaldense (pCL5)	21% oxygen, 100 ml culture in 500 ml flask	0.224	0.0	50.1	22
M. gryphiswaldense (pCL5)	21% oxygen, 400 ml culture in 500 ml flask	0.220	1.7	42.6	19.7
M. gryphiswaldense (pCL5)	21% oxygen, 4L culture in 5L flask	0.408	2.0	30.8	22.3
M. gryphiswaldense (pCL6)	21% oxygen, 4L culture in 5L flask	0.532	1.9	42	22
M. gryphiswaldense (pCL7)	21% oxygen, 4L culture in 5L flask	0.408	1.7	15.6	5.3
M. gryphiswaldense (pCL8)	21% oxygen, 4L culture in 5L flask	0.416	1.5	24.9	17
M. gryphiswaldense (pCL6)	0.12 mbar oxygen, 10 L fermenter	0.624	1.3	22.8	10.8
M. gryphiswaldense (pCL6)	2 mbar oxygen, 10 L fermenter	0.540	1.6	27.8	15.8
M. gryphiswaldense (pCL6)	200 mbar oxygen, 10 L fermenter	0.480	0.2	46.2	26.1
M. gryphiswaldense (pCL6)	200 mbar oxygen for 16 h + 0.2 mbar for 8 h, 10 L fermenter	0.624	1.3	42.4	20.3

The GFP fusions to MamC, MamF and MamG are specifically expressed in the MM

In vivo localization of GFP fusions of MamC, MamF and MamG

Next, we studied the expression and subcellular localization of GFP fusions of the GFP-tagged MamC, MamF, and MamG proteins by fluorescence microscopy under conditions of magnetite formation. In cells expressing MamC-GFP, MamF-GFP, and MamG-GFP the fluorescence was typically observed as linear signals along the cell axis at midcell, where the magnetosome chain is usually located (Figure 2). With all three fusions the signals either appeared predominantly as 0.5 to 2 µm straight, or less frequently, as punctuated lines. The linear signals were either observed at the concave side of the cells or at the shortest connection from one turn to the next, which is consistent with a localization along the axis of the twist of the helical cells. In MamC-GFP-expressing cells the signal was occasionally observed as a single bright fluorescent spot at midcell. No significant fluorescence was associated with the cytoplasmic membrane for any of the fusions. However, some fluorescence was detectable in the cytoplasm of cell expressing MamF-GFP and MamG-GFP (approximately 100% and 50% above background fluorescence of the medium), whereas the MamC-GFP fusions display almost no cytoplasmic fluorescence (<10% above background). Control cells expressing unfused GFP displayed fluorescence evenly distributed over the cytoplasm (Figure 2).
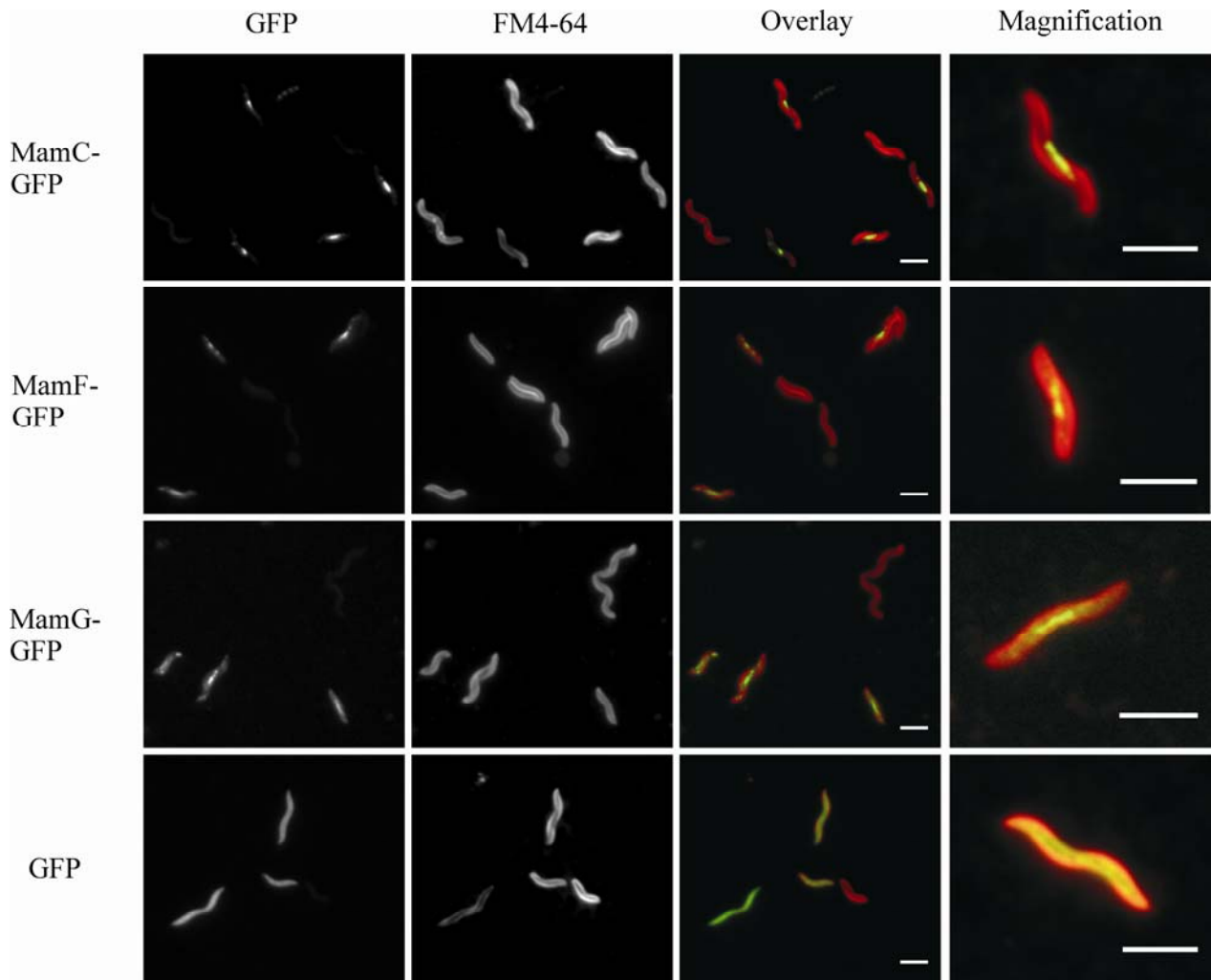
Figure 2: Fluorescence micrographs of *M. gryphiswaldense* R3/S1 strains expressing MamC-GFP (pCL6), MamF-GFP (pCL7), MamG-GFP (pCL8) or GFP (pCL5). In the first column the GFP fluorescence signals are shown. In the second column the signals of the membrane stain FM4-64 are shown for the same cells displayed in the first column and in the third column the overlays of the GFP (green) and FM4-64 (red) signals are displayed. The fourth column shows an enlargement of an overlay of a single representative cell. Scale bars are 3 μm.

Immunoblot analysis MamC-, MamF- and MamG-GFP localization

The localization and expression of GFP fusions were further studied by SDS-PAGE and immunodetection in cell fractions prepared from fluorescent and magnetic cells. An additional protein band of the expected size of the MamC-GFP fusion protein (40 kDa) was detected by Coomassie stain in magnetosomes from cells expressing MamC-GFP (Figure 3A, top). Bands corresponding to MamF-GFP (40.1 kDa) and MamG-GFP (35.5 kDa) were below detection by Coomassie but were recognized with an anti-GFP antibody (Figure 3A, bottom). In addition, a band of roughly 20 kDa was immunodetected in the magnetosome fractions from all of the GFP fusions, and further bands representing products of proteolytic cleavage

were visible in MM preparations from MamF-GFP and MamG-GFP, indicating that these fusions were partially degraded in the cells (Figure 3A, bottom).

Immunodetection of the MamC-GFP fusion by an anti-MamC antibody revealed the strongest signal in the MMP fraction, whereas a weak band of this size was also recognized in the NF, the MP, and the CL, but not the SP (Figure 3B). Native, unfused MamC recognized by anti-MamC as a band of 12.5 kDa displayed an identical subcellular distribution to that of MamC-GFP. The presence of low levels of MamC and MamC-GFP in the NF and the MP is probably caused by magnetosome membranes, which evaded the magnetic separation procedure such as empty magnetosome vesicles, vesicles containing immature magnetite crystals and MMs which were detached during the purification procedure. The intensity of the MamC-GFP band was approximately 80% of that of the MamC band, indicating that both the fusion and the native protein are expressed in comparable quantities (Figure 3B). MamF-GFP and MamG-GFP were exclusively detected as weak bands only in the MMP fraction, but were below detection in other subcellular fractions including the entire CL (data not shown), which indicates that MamF-GFP and MamG-GFP are present only in small amounts, due to either strong degradation or poor expression. For comparison, unfused GFP was recognized by an anti-GFP antibody at the expected size of approximately 27 kDa in the CL, the NF and in the SP, but not in the MP or the MMP (Figure 3C).
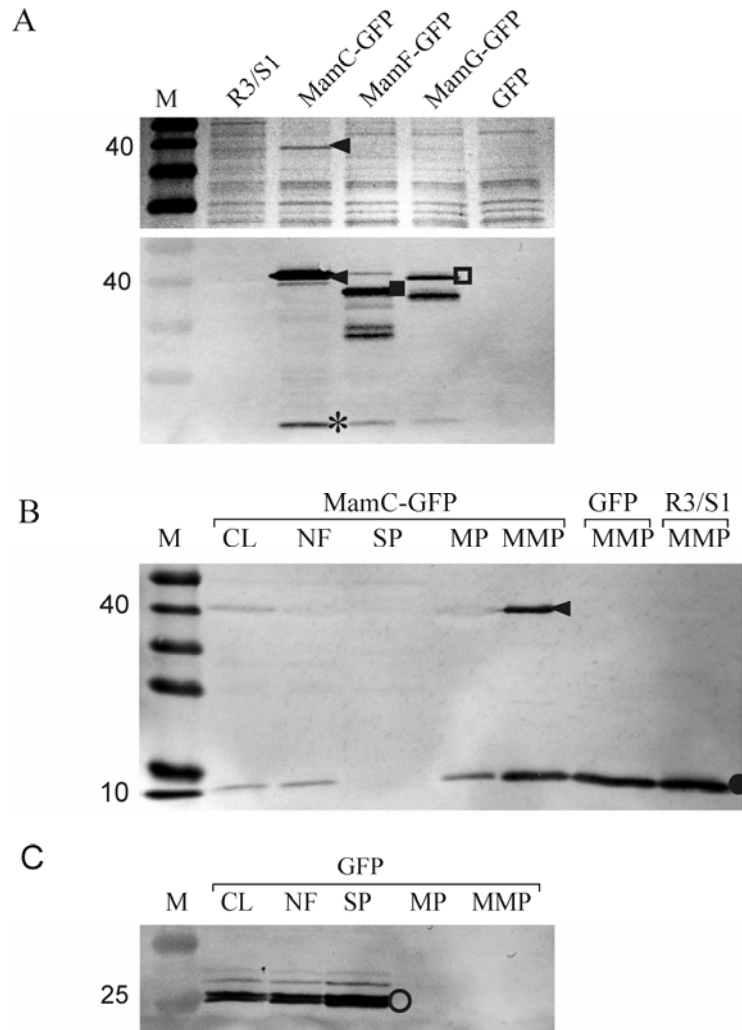
Figure 3: Detection of GFP fusion proteins in isolated magnetosomes and other cell fractions. M – marker, CL – cell lysate, NF – non-magnetic fraction, SP – soluble protein, MP – membrane protein, MMP – magnetosome membrane protein

A: Detection of GFP fusion proteins on isolated magnetosomes. Upper panel: SDS-PAGE of purified MMPs from the *M. gryphiswaldense* R3/S1 strain, and derivatives harbouring the plasmids pCL5 (GFP), pCL6 (MamC-GFP), pCL7 (MamF-GFP) and pCL8 (MamG-GFP). The MamC-GFP signal is indicated by an arrow (◄). Lower panel: Immunoblot of an identical gel as shown in the upper panel probed with an anti-GFP antibody. Besides the MamC-GFP signal (◄), signals for MamF-GFP (■) and MamG-GFP (□) are observed. In addition a putatively non-specific signal (*) is detected at a size of 20 kDa in the magnetosome fraction of MamC-GFP, MamF-GFP and MamG-GFP expressing cells.

B: Immundetection of MamC (•) and MamC-GFP (◄) in different cell fractions of R3/S1(pCL6) (MamC-GFP) and in the magnetosome membrane fractions of R3/S1(pCL5) (GFP) and R3/S1 with an anti-MamC antibody.

C: Immunodetection of GFP (○) in different cell fractions of R3/S1(pCL5) (GFP) with an anti-GFP antibody.

Isolated magnetosomes expressing GFP fusions to MamC, MamF and MamG display stable fluorescence *in vitro*

The next question was whether GFP fusions expressed on magnetosomes retain functionality *in vitro,* as *in vitro* stability would a prerequisite for any future application of proteins genetically fused to magnetosome proteins. Freshly isolated magnetosomes expressing MamC-GFP, MamF-GFP or MamG-GFP, displayed strong fluorescence, which was visible under the fluorescence microscope in form of bundles of chains that formed in the presence of an ambient magnetic field (Figure 4, also see supplemental materials). MamC-GFP magnetosomes displayed the highest fluorescence, while the fluorescence of MamF-GFP and MamG-GFP magnetosomes of cells from identical cultures was approximately threefold (MamF-GFP) and fivefold (MamG-GFP) lower (Figure 5). The stability of fluorescent magnetosomes was tested by measuring the fluorescence after incubation in various conditions including different pH, temperatures, salt and detergent concentrations (Figure 6). The highest fluorescence intensity was retained between pH 8 and pH 9, which is close to the reported optimum pH of GFP (29), and at pH 11 the intensity was still 20% of the value at pH 9, whereas fluorescence was abolished at acidic pH below pH 6. At pH 7 only 60 % of the intensity was retained. The fluorescence intensity was equally high if magnetosomes were stored at temperatures below 24°C or frozen at -20°C. Temperature increase to 30°C or 50°C led to a decrease (~20%) of fluorescence, and after storage at 70°C only approximately 15% of the fluorescence of magnetosomes stored at 4°C was retained. In addition, the particles incubated at this high temperature rapidly agglomerated, indicating that the membrane enclosing the particles became disturbed, probably due to denaturation. Sodium chloride had a quenching effect on the magnetosome fluorescence only at a high concentration of 4 M, and guanidinium chloride reduced the fluorescence intensity to roughly 50% at a concentration of 1 M. However, the detergents SDS and triton X-100 lead to a loss of approximately 80 % of the magnetosome bound fluorescence at a concentration of 0.05 %, probably due to solubilization and loss of MamC-GFP. Remarkably, a fluorescence of approximately 20% was retained even at higher detergent concentrations, which might be due to nonspecific adsorption of MamC-GFP to the surfaces of magnetite crystals after membrane solubilization.
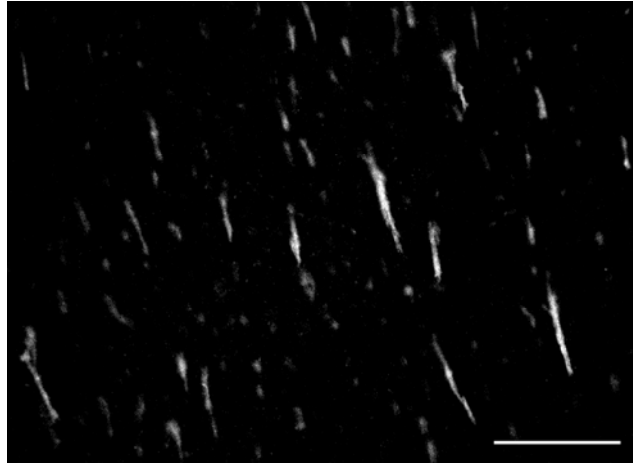
Figure 4: Fluorescence micrographs of magnetosome particles isolated from R3/S1 (pCL6). The magnetosome particles aggregated into bundles of chains in the presence of an ambient magnetic field. The scale bar is 100 μm.
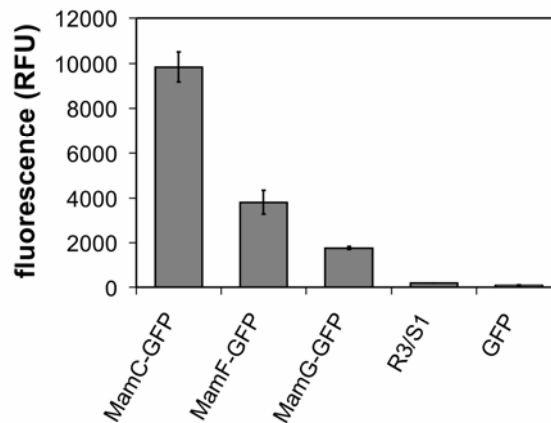

Figure 5: Fluorescene measurements of magnetosomes isolated from the R3/S1 strain or R3/S1 derivatives harbouring the plasmids pCL5 (GFP), pCL6 (MamC-GFP), pCL7 (MamF-GFP) and pCL8 (MamG-GFP). Fluorescence was quantified on 100 μl aliquots of magnetosome suspensions containing a magnetosome amount equivalent to 5 mM iron.
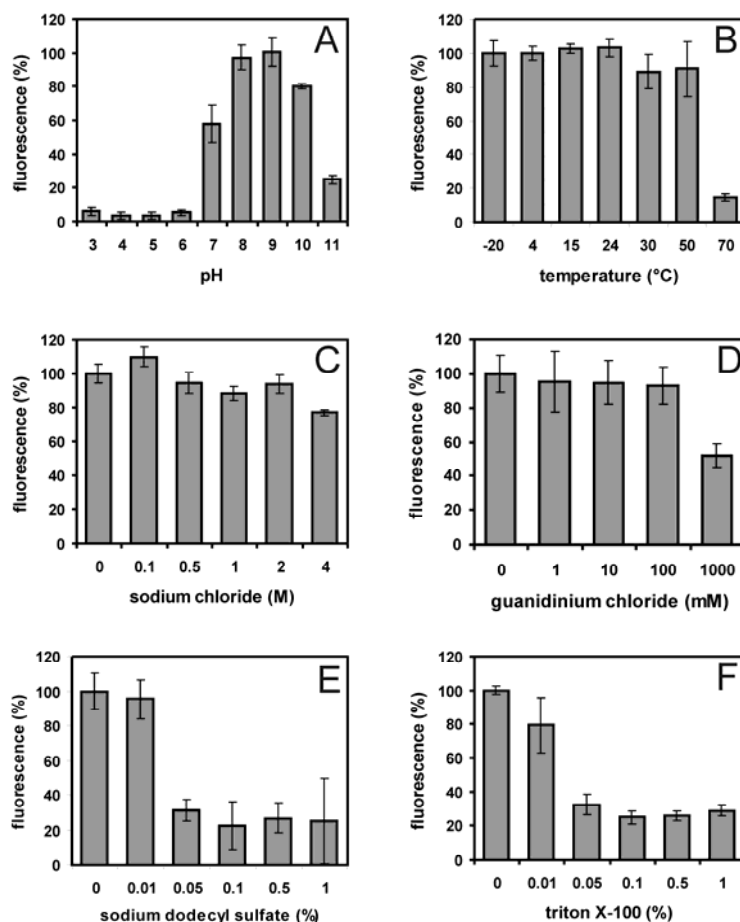
Figure 6: *In vitro* **stability of fluorescent magnetosomes purified from R3/S1(pCL6)** (A) Effect of the pH of the buffer on magnetosome fluorescence. (B) Thermal stability of the magnetosome-bound fluorescence (C-F) Fluorescence of magnetosomes incubated with different amounts of sodium chloride (C), guanidinium chloride (D), sodium dodecyl sulphate (E) or triton X-100 (F). Following an incubation period of one hour, the magnetosomes were magnetically separated and resuspended in buffer S pH 8 to remove unbound fluorophores. Subsequently, the stability of the magnetosomes was assessed by fluorescence quantification. The error bars represent the standard deviations, which were calculated from four independent experiments.

Discussion

Although GFP has been used previously as a tag to follow the subcellular localization of magnetosome proteins in microaerophilic magnetotactic bacteria (16, 17, 33, 37), its expression and activity under the microoxic conditions required for magnetite synthesis have not yet been assessed systematically. However, they are crucial for correlating protein localization with the position of magnetite crystals and chains. Here, we have demonstrated that the optimum requirements for fluorophore formation and magnetite synthesis are mutually exclusive, and no permanent growth condition was found to permit high fluorescence and magnetite synthesis simultaneously. Magnetite synthesis occurs only below 10 mbar (14), whereas GFP requires molecular oxygen during fluorophore maturation, which limits its use in oxygen-limited systems (30). This problem has been partially overcome in a variety of anaerobic and microaerophilic bacteria by shifting anaerobically grown cells to oxic conditions after growth to stimulate fluorophore formation. For example, in *Enterobacter aerogenes* a 60 min shift from anaerobic to aerobic conditions was sufficient to double fluorescence (56). Hansen et al. found that the GFP variant GFPmut3* displayed fluorescence in *Streptococcus gordonii* with 0.1 ppm dissolved oxygen. In the same study, it was also observed that fluorescence was activated in an anaerobically grown, non-fluorescent *S. gordonii* biofilm by a 20 min shift to aerobic conditions (11). In anaerobically grown *Rhodobacter sphaeroides* GFP was visualized after 4h of aeration by vigorous shaking (49) . An abrupt shift from anoxic or microoxic conditions to oxic conditions did not induce fluorophore formation in *M. gryphiswaldense* in our experiments, but inhibited further growth. The highest percentage of both fluorescent and magnetic cells were obtained, when fluorophore formation and magnetite synthesis became sequentially induced, if culture conditions were chosen that provided gradually decreasing oxygen levels during the incubation due to the increasing oxygen consumption of cells. Although the proportion of fluorescent cells never reached 100%, nearly all cells under these conditions contained magnetosome chains (data not shown). Our data also show that even under high oxygen tensions only 22-26% of the cells displayed significant fluorescence intensities. This may be attributed to a low expression level of GFP from the *lac* promoter. In addition a dependence of protein expression on the cell cycle within a heterogeneous population, and stochasticity of gene expression might be involved, as described for other bacteria (6, 43).

Of all tested fusions, the MamC-GFP fusion displayed the highest fluorescence both *in vivo* and on isolated magnetosomes, which was consistent with the highest abundance of both the fusion and the unfused MamC protein, which displayed similar expression levels. In

contrast, MamF-GFP and MamG-GFP fusions were below detection by Coomassie in MM preparations. The immunodetection of several proteolytic degradation products of MamF- and MamG-GFP fusions indicated that these proteins are less stable. GFP fusions to MamF and MamG were substantially more weakly expressed than their unfused counterparts. This could be explained either by a bias in targeting to the MM, or by a relatively low expression from the *lac* promoter present on the vector backbone, which makes future expression studies of native or inducible promoters highly desirable.

The GFP fusions of MamC, MamF and MamG displayed nearly identical localization patterns, and the extension of the linear fluorescence signal correlated well with the typical length and position of the magnetosome chain. Results of localization studies are in agreement with previous biochemical studies (9), and with the immunogold-labeling studies of Mam12, which is orthologous to MamC in *M. magnetotacticum.* However, due to the weak immunogold signals, the immunogold-labeling experiments were not fully conclusive regarding the intracellular Mam12 localization (46). In contrast, the observed localization of MamC-GFP as a bright dot at midcell might indicate that the intracellular localization of the MamC protein along the chain is variable and may change over the cell cycle. The absence of strong fluorescence and immuno-signals from different compartments of cells expressing GFP fusions to either MamC, MamF or MamG indicated that these hydrophobic proteins are targeted exclusively to the MM. This is in contrast to other, more hydrophilic magnetosome proteins, which showed a variable and slightly different subcellular localization. For instance, in *M. magneticum,* GFP fusions of the protein MamA, which is postulated to be involved in the "activation" of magnetite precipitation and regulation of magnetosome chain length, showed a growth stage dependent localization pattern. During exponential phase, a filamentous structure was seen, which reached from pole to pole and stationary cells displayed more punctuated signals at midcell (17). GFP fused to MamK, which is an actin-like protein presumably forming the cytoskeletal magnetosome filament, localized as straight lines that extended through most of the cell (16). Similar to MamK and MamA, GFP fused to the MamJ protein of *M. gryphiswaldense*, which is predicted to attach magnetosome vesicles to the magnetosome filament, localized as long filaments extending from pole to pole (33). While the localization of these hydrophilic proteins clearly extended the length of the magnetosome chains, the linear fluorescent signals corresponding to the MamGFC-GFP fusions seem to be confined to the position of the chain of magnetite crystals. Remarkably, none of the MamGFC-GFP proteins were found to be associated with the cytoplasmic membrane (CM), although MamGFC represent hydrophobic proteins with a predicted

localization in the CM. Hence, our data indicate that MamC, MamF and MamG are targeted to the MM by a highly specific mechanism, which seems different from that of other MMPs, such as MamA, MamJ and MamK. It is possible that certain magnetosome membrane proteins such as MamA, MamJ and MamK display a different localization pattern to MamC, MamF and MamG as they interact with the magnetosome filament, whereas MamC, MamF and MamG, which are part of the magnetosome membrane, are predominantly associated with mature magnetsomes.

The utilization of magnetic nanoparticles for many applications generally requires a specifically functionalized particle surface (reviewed in reference 22). For example, it is very attractive to specifically display foreign polypeptides, such as enzymes, fluorophores, or coupling groups on the surface of particles, and the genetic modification of magnetosome associated proteins may provide an elegant way to construct multifunctionalized magnetic nanoparticles. In our study, the MamC-GFP fusion protein retained functionality *in vitro* and remained attached with the magnetosomes after their isolation from disrupted cell, as indicated by robust magnetosome-specific fluorescence under a variety of storage and incubation conditions. Such GFP-coupled magnetosomes might be useful as fluorescence-labeled magnetic nanoparticles in several applications, such as bimodal contrast agents for the fluorescent and magnetic resonance imaging of macrophages (24). In addition to GFP, other functional moieties, such as enzymes, antibody binding proteins, receptors, peptide hormones, growth factors, autobiotinylation signals, and protein tags for "click chemistry" could be expressed on the magnetosome particle by use of magnetosome specific anchor proteins. Previous studies in *M. magneticum* attempted to use either the MagA or Mms16 proteins as membrane anchors for magnetosome-specific display of fusions proteins (28, 53). However, it has been challenged that MagA and Mms16 (renamed as ApdA in *M. gryphiswaldense*) are native constituents of the MM, but in fact may rather represent contaminations from other subcellular compartments that become non-specifically associated with the magnetosomes particles upon cell disruption (10, 34, 37). Magnetosomes modified with a luciferase fusion of the magnetosome protein Mms13, which is an ortholog of MamC, had more than 400-fold-higher luminescence intensity than Mms16-luciferase-modified magnetosomes in *M. magneticum* AMB-1 (53). This is in agreement with our results that demonstrate that GFP fused to MamC displayed strong and stable fluorescence *in vitro*. MamC seems to represent a useful, perhaps universal anchor for magnetosome display of other proteins for several reasons. First, MamC is tightly attached to the magnetite crystal surface, and its association has been shown to be resistant to proteolysis, and chemical stress (9). Second, as the most

abundant magnetosome protein, it is highly expressed. By densitometric quantification we roughly estimated the number of MamC-GFP copies per magnetosome particle to be 50 to 100 (data not shown). In addition, as an anchor, MamC is not likely to interfere with the function of the added moiety because of its relatively small size, and its hydrophilic C-terminus is accessible for the expression of fusion proteins. Conversely, MamC fusions with heterologous proteins are not expected to interfere with magnetosome formation, as it has been demonstrated that the deletion of MamC had only a minor effect on magnetite synthesis (32).

In conclusion, we established cultivation conditions for the expression of GFP in *M. gryphiswaldense.* Under these growth conditions, it is possible to use GFP as fluorescent tag for subcellular protein localization or as reporter gene to study gene expression in correlation to magnetite synthesis within the same cell. Furthermore, the use of MamC as an anchor for future functionalization of magnetosomes for biotechnological applications has been demonstrated.

References

1. **Bazylinski, D. A., and R. B. Frankel.** 2004. Magnetosome formation in prokaryotes. Nat. Rev. Microbiol. **2:**217-230.

2. **Bazylinski, D. A., and S. Schübbe.** 2007. Controlled biomineralization by and applications of magnetotactic bacteria. Adv. Appl. Microbiol. **62:**21-62.

3. **Bumann, D., and R. H. Valdivia.** 2007. Identification of host-induced pathogen genes by differential fluorescence induction reporter systems. Nat. Protoc. **2:**770-777.

4. **Ceyhan, B., P. Alhorn, C. Lang, D. Schüler, and C. M. Niemeyer.** 2006. Semi-synthetic biogenic magnetosome nanoparticles for the detection of proteins and nucleic acids. Small **2:**1251.

5. **Cormack, B. P., R. H. Valdivia, and S. Falkow.** 1996. FACS-optimized mutants of the green fluorescent protein (GFP). Gene **173:**33-38.

6. **Elowitz, M. B., A. J. Levine, E. D. Siggia, and P. S. Swain.** 2002. Stochastic gene expression in a single cell. Science **297:**1183-1186.

7. **Gorby, Y. A., T. J. Beveridge, and R. Blakemore.** 1988. Characterization of the bacterial magnetosome membrane. J. Bacteriol. **170:**834-841.

8. **Grünberg, K.** 2005. Biochemische und molekulabiologische Untersuchung der Magnetosomenmembran von *Magnetospirillum gryphiswaldense*. Doctoral thesis. Universität Bremen, Bremen.

9. **Grünberg, K., E. C. Müller, A. Otto, R. Reszka, D. Linder, M. Kube, R. Reinhardt, and D. Schüler.** 2004. Biochemical and proteomic analysis of the magnetosome membrane in *Magnetospirillum gryphiswaldense*. Appl. Environ. Microbiol. **70:**1040-1050.

10. **Handrick, R., S. Reinhardt, D. Schultheiss, T. Reichart, D. Schüler, V. Jendrossek, and D. Jendrossek.** 2004. Unraveling the function of the *Rhodospirillum rubrum* activator of polyhydroxybutyrate (PHB) degradation: the activator is a PHB-granule-bound protein (phasin). J. Bacteriol. **186:**2466-75.

11. **Hansen, M. C., R. J. Palmer, C. Udsen, D. C. White, and S. Molin.** 2001. Assessment of GFP fluorescence in cells of *Streptococcus gordonii* under conditions of low pH and low oxygen concentration. Microbiology **147:**1383-1391.

12. **Heim, R., D. C. Prasher, and R. Y. Tsien.** 1994. Wavelength mutations and posttranslational autooxidation of green fluorescent protein. Proc. Natl. Acad. Sci. U S A **91:**12501-12504.

13. **Hergt, R., R. Hiergeist, M. Zeisberger, D. Schüler, U. Heyen, I. Hilger, and W. A. Kaiser.** 2005. Magnetic properties of bacterial magnetosomes as diagnostic and therapeutic tools. J. Magn. Magn. Mat. **293:**80-86.

14. **Heyen, U., and D. Schüler.** 2003. Growth and magnetosome formation by microaerophilic *Magnetospirillum* strains in an oxygen-controlled fermentor. Appl. Microbiol. Biotechnol. **61:**536-544.

15. **Komeili, A.** 2007. Molecular mechanisms of magnetosome formation. Annu. Rev. Biochem. **76:**351-66.

16. **Komeili, A., Z. Li, D. K. Newman, and G. J. Jensen.** 2006. Magnetosomes are cell membrane invaginations organized by the actin-like protein MamK. Science **311:**242-245.

17. **Komeili, A., H. Vali, T. J. Beveridge, and D. Newman.** 2004. Magnetosome vesicles are present prior to magnetite formation and MamA is required for their activation. Proc. Natl. Acad. Sci. U. S. A. **101:**3839-3844.

18. **Kovach, M. E., P. H. Elzer, D. S. Hill, G. T. Robertson, M. A. Farris, R. M. Roop, 2nd, and K. M. Peterson.** 1995. Four new derivatives of the broad-host-range cloning vector pBBR1MCS, carrying different antibiotic-resistance cassettes. Gene **166:**175-6.

19. **Laemmli, U. K.** 1970. Cleavage of structural proteins during the assembly of the head of bacteriophage T4. Nature **227:**680-5.

20. **Lang, C., and D. Schüler.** 2006. Biogenic nanoparticles: production, characterization, and application of bacterial magnetosome. J. Phys.: - Condens. Matter **18:**S2815-S2828.

21. **Lang, C., and D. Schüler.** 2006. Biomineralization of magnetosomes in bacteria: Nanoparticles with potential applications, p. 107-124. *In* B. Rehm (ed.), Microbial Bionanotechnology: Biological Self-assembly Systems and Biopolymer-based Nanostructures. Horizon bioscience, Wymondham.

22. **Lang, C., D. Schüler, and D. Faivre.** 2007. Synthesis of magnetite nanoparticles for bio- and nanotechnology: Genetic engineering and biomimetics of bacterial magnetosomes. Macromol. Biosci. **7:**144-151.

23. **Larrainzar, E., F. O'Gara, and J. P. Morrissey.** 2005. Applications of autofluorescent proteins for *in situ* studies in microbial ecology. Annu. Rev. Microbiol. **59:**257-77.

24. **Lisy, M.-R., A. Hartung, C. Lang, D. Schüler, W. Richter, J. R. Reichenbach, W. A. Kaiser, and I. Hilger.** 2007. Fluorescent bacterial magnetic nanoparticles as bimodal contrast agents. Invest. Radiol. **42:**235-241.

25. **Margolin, W.** 2005. FtsZ and the division of prokaryotic cells and organelles. Nat. Rev. Mol. Cell Biol. **6:**862-871.

26. **Matsunaga, T., H. Nakayama, M. Okochi, and H. Takeyama.** 2001. Fluorescent detection of cyanobacterial DNA using bacterial magnetic particles on a MAG-microarray. Biotechnol. Bioeng. **73:**400-405.

27. **Matsunaga, T., T. Suzuki, M. Tanaka, and A. Arakaki.** 2007. Molecular analysis of magnetotactic bacteria and development of functional bacterial magnetic particles for nano-biotechnology. Trends Biotechnol. **25:**182-8.

28. **Matsunaga, T., H. Togo, T. Kikuchi, and T. Tanaka.** 2000. Production of luciferase-magnetic particle complex by recombinant *Magnetospirillum* sp AMB-1. Biotechnol. Bioeng. **70:**704-709.

29. **Patterson, G. H., S. M. Knobel, W. D. Sharif, S. R. Kain, and D. W. Piston.** 1997. Use of the green fluorescent protein and its mutants in quantitative fluorescence microscopy. Biophys. J. **73:**2782-2790.

30. **Reid, B. G., and G. C. Flynn.** 1997. Chromophore formation in green fluorescent protein. Biochemistry **36:**6786-6791.

31. **Sambrook, J., and D. Russel, W.** 2001. Molecular cloning: A laboratory manual (3rd edn.). Cold Spring Harbor Laboratory Press, Cold Spring Harbor, NY.

32. **Scheffel, A., A. Gärdes, K. Grünberg, G. Wanner, and D. Schüler.** 2007. The major magnetosome proteins MamGFDC are not essential for magnetite biomineralization in *Magnetospirillum gryphiswaldense*, but regulate the size of magnetosome crystals. J. Bacteriol. **190:**377-386.

33. **Scheffel, A., M. Gruska, D. Faivre, A. Linaroudis, P.L. Graumann, J. M. Plitzko, and D. Schüler.** 2006. An acidic protein aligns magnetosomes along a filamentous structure in magnetotactic bacteria. Nature **440:**110-115.

34. **Schüler, D.** 2004. Molecular analysis of a subcellular compartment: The magnetosome membrane in *Magnetospirillum gryphiswaldense*. Arch. Microbiol. **181:**1-7.

35. **Schüler, D., and E. Baeuerlein.** 1998. Dynamics of iron uptake and Fe_3O_4 biomineralization during aerobic and microaerobic growth of *Magnetospirillum gryphiswaldense*. J. Bacteriol. **180:**159-162.

36. **Schüler, D., R. Uhl, and E. Baeuerlein.** 1995. A simple light scattering method to assay magnetism in *Magnetospirillum gryphiswaldense*. FEMS Microbiol. Lett. **132:**139-145.

37. **Schultheiss, D., R. Handrick, D. Jendrossek, M. Hanzlik, and D. Schüler.** 2005. The presumptive magnetosome protein Mms16 is a PHB-granule bounded protein (phasin) in *Magnetospirilum gryphiswaldense*. J. Bacteriol. **187:**2416-2425.

38. **Schultheiss, D., M. Kube, and D. Schüler.** 2004. Inactivation of the flagellin gene *fla*A in *Magnetospirillum gryphiswaldense* results in nonmagnetotactic mutants lacking flagellar filaments. Appl. Environ. Microbiol. **70:**3624-3631.

39. **Schultheiss, D., and D. Schüler.** 2003. Development of a genetic system for *Magnetospirillum gryphiswaldense*. Arch. Microbiol. **179:**89-94.

40. **Simon, R., U. Priefer, and A. Pühler.** 1983. A broad host range mobilisation system for *in vivo* genetic engineering: transposon mutagenesis in Gram-negative bacteria. Biotechnology **1:**784-791.

41. **Southward, C. M., and M. G. Surette**. 2002. The dynamic microbe: green fluorescent protein brings bacteria to light. Mol. Microbiol. **45:**1191-6.

42. **Stookey, L. L.** 1970. Ferrozine - a new spectrophotometric reagent for iron. Anal. Chem. **42:**779-781.

43. **Strovas, T. J., L. M. Sauter, X. F. Guo, and M. E. Lidstrom.** 2007. Cell-to-cell heterogeneity in growth rate and gene expression in *Methylobacterium extorquens* AM1. J. Bacteriol. **189:**7127-7133.

44. **Tanaka, M., Y. Okamura, A. Arakaki, T. Tanaka, H. Takeyama, and T. Matsunaga.** 2006. Origin of magnetosome membrane: proteomic analysis of magnetosome membrane and comparison with cytoplasmic membrane. Proteomics **6:**5234-47.

45. **Tanaka, T., H. Yamasaki, N. Tsujimura, N. Nakamura, and T. Matsunaga.** 1997. Magnetic control of bacterial magnetite-myosin conjugate movement on actin cables. Mater. Sci. Eng. , C **5:**121-124.

46. **Taoka, A., R. Asada, H. Sasaki, K. Anzawa, L.-F. Wu, and Y. Fukumori.** 2006. Spatial localizations of Mam22 and Mam12 in the magnetosomes of *Magnetospirillum magnetotacticum*. J. Bacteriol. **188:**3805-3812.

47. **Viollier, E., P. W. Inglett, K. Hunter, A. N. Roychoudhury, and P. Van Cappellen.** 2000. The ferrozine method revisited: Fe(II)/Fe(III) determination in natural waters. Appl. Geochem. **15:**785-790.

48. **Wacker, R., B. Ceyhan, P. Alhorn, D. Schüler, C. Lang, and C. M. Niemeyer.** 2007. Magneto-Immuno PCR: A homogeneous immunoassay based on biogenic magnetosome nanoparticles. Biochem. Biophys. Res. Commun. **357:** 391-396.

49. **Wadhams, G. H., A. C. Martin, S. L. Porter, J. R. Maddock, J. C. Mantotta, H. M. King, and J. P. Armitage.** 2002. TlpC, a novel chemotaxis protein in *Rhodobacter sphaeroides*, localizes to a discrete region in the cytoplasm. Mol. Microbiol. **46:**1211-1221.

50. **Yang, C. D., H. Takeyama, T. Tanaka, and T. Matsunaga.** 2001. Effects of growth medium composition, iron sources and atmospheric oxygen concentrations on production of luciferase-bacterial magnetic particle complex by a recombinant *Magnetospirillum magneticum* AMB-1. Enzyme Microbial. Technol. **29:**13-19.

51. **Yoong, P., R. Schuch, D. Nelson, and V. A. Fischetti.** 2006. PlyPH, a bacteriolytic enzyme with a broad pH range of activity and lytic action against *Bacillus anthracis*. J. Bacteriol. **188:**2711-2714.

52. **Yoshino, T., F. Kato, H. Takeyama, K. Nakai, Y. Yakabe, and T. Matsunaga.** 2005. Development of a novel method for screening of estrogenic compounds using nano-sized bacterial magnetic particles displaying estrogen receptor. Analyt. Chim. Acta **532:**105-111.

53. **Yoshino, T., and T. Matsunaga.** 2006. Efficient and stable display of functional proteins on bacterial magnetic particles using Mms13 as a novel anchor molecule. Appl. Environ. Microbiol. **72:**465-471.

54. **Yoshino, T., M. Takahashi, H. Takeyama, Y. Okamura, F. Kato, and T. Matsunaga.** 2004. Assembly of G protein-coupled receptors onto nanosized bacterial magnetic particles using Mms16 as an anchor molecule. Appl. Environ. Microbiol. **70:**2880-2885.

55. **Yoza, B., A. Arakaki, and T. Matsunaga.** 2003. DNA extraction using bacterial magnetic particles modified with hyperbranched polyamidoamine dendrimer. J. Biotechnol. **101:**219-228.

56. **Zhang, C., X. H. Xing, and K. Lou.** 2005. Rapid detection of a GFP-marked *Enterobacter aerogenes* under anaerobic conditions by aerobic fluorescence recovery. FEMS Microbiol. Lett. **249:**211-218.

Manuscript 2

Analysis of promoters for efficient and inducible gene expression in

M. gryphiswaldense

Claus Lang, René Uebe, Dirk Schüler*

Ludwig-Maximillians-Universität München

Department Biologie I, Bereich Mikrobiologie

Großhadernerstr. 4

82152 Planegg-Martinsried

*Corresponding author: dirk.schueler@lrz.uni-muenchen.de

Abstract

Magnetospirillum gryphiswaldense is a widely used model organism to study the biomineralization of magnetosomes, which are unique prokaryotic organelles. Analysis of the formation of magnetosomes as well as their functionalization for bionanotechnological application has been hampered by the relative shortage of tools for genetic manipulation of *M. gryphiswaldense* and other magnetotactic bacteria. To develop an expression system for *M. gryphiswaldense* we estimated gene expression from known and predicted genuine *M. gryphiswaldense* promoters as well as several widely used *E. coli* promoters using GFP as a reporter. Highest level of GFP expression was observed with the magnetosomal P_{mamDC} promoter. In addition, the *E. coli* P_{tet} promoter was efficiently induced by anhydrotetracycline in *M. gryphiswaldense,* even though absolute expression levels from P_{tet} were lower than from P_{mamDC}. The usefulness of P_{mamDC} as a gene expression tool was further demonstrated by magnetosome-specific display of a translational fusion of the magnetosome protein MamC and the antibody binding "ZZ" domain. This resulted in the generation of antibody-binding magnetic nanoparticles that could be used for magnetic separation of antibodies and for immunoassays.

Introduction

The ability of magnetotactic bacteria (MTB) to orient in geomagnetic fields is based on the formation of magnetosomes, which are intracellular organelles consisting of nanocrystals of the magnetic iron oxide magnetite (Fe_3O_4) that are formed within a distinct subcellular compartment provided by the magnetosome membrane (MM) (39). The two strains *Magnetospirillum magneticum* and *M. gryphiswaldense* have recently emerged as model systems to study the biomineralization and cell biology of magnetosome formation as well as potential applications of these bacterial magnetic nanoparticles. A magnetosome-specific subset of proteins was identified that are presumably involved in vesicle formation, magnetosome-directed iron transport, magnetite crystallization, and magnetosome chain assembly (12, 18, 19, 32, 35-37, 48). Although the genetic analysis of MTB is still complicated by a relative shortage of genetic tools, recently methods became available for transformation and mutagenesis of *M. magneticum* and *M. gryphiswaldense*. In addition, GFP was successfully used as a reporter to study the localization of proteins involved in magnetosome formation and chain assembly *in vivo* (18, 19, 36, 37). Flow cytometry was

used to study the use of GFP in microaerophilic MTB, and optimized growth conditions for both GFP fluorophore formation and magnetite biomineralization were established (23).

Because of their unique magnetic characteristics, magnetosomes have attracted bio- and nanotechnological attention in applications such as magnetic separation, magnetic resonance imaging, or magnetic hyperthermia (5, 14, 27, 31, 52), which require the immobilization of functional moieties on the magnetosome surface. This can be achieved either by chemical modification of purified magnetosomes or by genetic modification of MM proteins (22, 24, 31).

Despite the demand for efficient and inducible expression systems, only one study reported a system for the expression of fusion proteins in the MM of *M. magneticum*. Using luciferase as a reporter several putative promoters driving the expression of highly abundant membrane and magnetosome proteins were studied. The highest expression of luciferase was observed with the promoter of a putative peroxiredoxin gene (P_{msp3}) (53). In *M. gryphiswaldense* an *E. coli* P_{lac} promoter was recently used for the expression of GFP fusion proteins that were specifically targeted to the magnetosome compartment (23). In another study of *M. gryphiswaldense*, three promoters (P_{mamAB}, P_{mamDC} and P_{mms}) that drive the expression of magnetosomal operons were identified by primer extension analysis. By quantitative real-time RT-PCR and microarray analysis it was shown that the three promoters are highly transcribed under magnetite-inducing conditions, i.e. at microaerobiosis and in the presence of micromolar amounts of iron (38).

In order to identify genuine promoters for gene expression in *M. gryphiswaldense* we investigated the expression of GFP from putative and previously identified promoters of *M. gryphiswaldense*, several homologues of promoters previously identified in *M. magneticum,* as well as the P_{lac} and P_{tet} promoters of *E. coli*, which have been widely used in many different bacteria. Using fluorescence microscopy, fluorometry, immunoblot analysis and flow cytometry we show that P_{mamDC} is a highly efficient promoter in *M. gryphiswaldense*. Although GFP expression was not uniform within the cell population, we demonstrate that P_{mamDC} can be used for magnetosome-specific expression of a fusion protein comprising the "ZZ" domain of protein A and the MM protein MamC, resulting in magnetic nanoparticles which specifically interact with rabbit IgG antibodies.

Materials and Methods

Bacterial strains, media, and growth conditions

Escherichia coli strain DH5α was used as a host for cloning and the *E. coli* strain BW29427 (*thrB1004 pro thi rpsL hsdS lacZ*ΔM15 RP4-1360 Δ(*araBAD*)567 Δ*dapA1341::[erm pir* (wt)]) (Datsenko, K. and Wanner B.L. unpublished) was used for conjugation experiments. *E. coli* strains were grown on Luria-Bertani (LB) at 37°C. If appropriate the medium was supplemented with kanamycin (25 µg ml^{-1}) or ampicillin (50 µg ml^{-1}). For cultivation of strain BW29427 LB was supplemented with DL-α,ε-diaminopimelic acid to 1 mM. Throughout this study the *M. gryphiswaldense* strain R3/S1 was used (41). *M. gryphiswaldense* was routinely grown microaerobically at 30°C at moderate shaking (100 rpm) in modified FSM medium using 27 mM lactate as a carbon source as described previously (15). For cultivation on petri dishes agar was added to 1.5% w/v to FSM medium.

Construction of vectors

If not specified otherwise DNA methods were conducted according to standard procedures (34). Primers were purchased from Sigma-Aldrich (Munich, Germany). The primer sequences are listed in Table 1. Cloned genes and fusion constructs were sequenced using BigDye terminator v3.1 chemistry on an ABI 3730 48 capillary sequencer (Applied Biosystems). Sequence data was analyzed with Vector NTI 10.3 (Invitrogen).

In this study the GFPmut1 variant, which is also termed EGFP, was used (6, 25). The *egfp* gene was PCR amplified (Taq-Mastermix, Promega) from the pEGFPN-1 (BD Biotech) plasmid using the *egfpfw* forward primer, which adds a *NdeI* restriction site to the 5' end of the *egfp* gene, and reverse primer CL2, which introduces a *BamHI* site. The PCR product was cloned into pGEMT-Easy (Promega) to yield pGEMegfp. The plasmid pBBRegfp was generated by subcloning the *egfp* gene from pGEMegfp into the *EcoRI* site of the pBBR1MCS-2 (20) plasmid downstream of the P$_{lac}$ promoter. The P$_{lac}$ promoter was excised by restriction enzyme digestion with *NsiI* and *ApaI,* and the vector was religated after Mung Bean nuclease (New England Biolabs) treatment to yield the promoterless GFP reporter plasmid pBBRpl.

Putative promoter regions of P$_{mamDC}$, P$_{mamAB}$, P$_{msp3}$, P$_{apdA}$, P$_{ure}$, P$_{rplK}$ and P$_{rpsJ}$ were PCR amplified with Taq polymerase (Fermentas) from genomic DNA of *M. gryphiswaldense* R3/S1 as a template with primers that generate a *XhoI* or *HindIII* (P$_{rplK}$) site at the 5' end, and a *NdeI* or *VspI* (P$_{msp3}$) site at the 3' end of the fragments. The PCR fragments were 200 to 400 bp long and included the intergenic region upstream from the start codon to the next open

reading frame. To facilitate cloning into the *NdeI* restriction site a CAT triplet was inserted in front of the start codon. The PCR products were cloned into pGEMT-Easy and sequenced. The promoter fragments were subcloned into the *XhoI* or *HindIII* and *NdeI* restriction sites of pBBRpl resulting in the plasmids pBBRPmamDC, pBBRPmamAB, pBBRPmsp3, pBBRPapdA, pBBRPure, pBBRPrplK and pBBRPrpsJ.

The P$_{tet}$ promoter was amplified together with the *tetR* repressor gene in two steps employing splicing by overlap extension PCR from the plasmid pASK-IBA5 to eliminate an internal *NdeI* restriction site. In the first round two PCR fragments were produced by amplification with the primer pairs *ptetfw/ptetintrev* and *ptetintfw/ptetrev* (16). In the second PCR round these products were used as template for the primers ptetfw/ptetrev. The PCR fragment was cloned into pCR2.1 TOPO (Invitrogen) to yield plasmid pCRPtet. The promoter/repressor fragment was then subcloned into the *NdeI* and *XhoI* restriction sites of pBBRpl.

Shortened P$_{mamDC}$ promoter fragments were PCR amplified with the forward primers PmamDC96, PmamDC262, PmamDC163 and the reverse primer PmamDCrev and cloned into pGEMT-Easy. Using the *Nde*I and *Xho*I restriction sites the P$_{mamDC}$ fragments were subcloned into pBBRpl to generate pBBRPdc96, pBBRPdc163 and pBBRPdc262.

For the construction of a MamC-ZZ fusion protein the *ezz* gene, which codes for the antibody binding ZZ-protein domain, was PCR amplified with primers zzfw/zzrev from pEZZ18 (GE Healthcare) and cloned into pGEM-T Easy. The ZZ-fragment was then cloned into the *XbaI* and *NdeI* restriction sites of the pCL6 vector (23) to replace the *egfp* gene with the *ezz* gene and create the *mamC-ezz* fusion construct pBBRCZZ. The P$_{mamDC}$ promoter was amplified with PmamDCfw/PmamDCx1rev and cloned into pJET1.2/blunt (Fermentas). The P$_{mamDC}$ fragment was released from the resulting pJET1.2 derivative pJETPdcx1 and cloned into the *XhoI* site of pBBRCZZ upstream of the *mamC-ezz* fusion to yield pBBRPdcCZZ.

For a complete list of plasmids used in this study refer to Table 2. The plasmids were transferred into *M. gryphiswaldense* R3/S1 by conjugation from *E. coli* BW29427 as described previously (42).

Table 1: Primers used in this study. Restriction sites that were incorporated in the primer are indicated in bold.

Primer name	Sequence
egfpfw	**CATATG**GTGAGCAAGGGCGAGGAG
CL2	GT**GGATCC**TTACTTGTACAGCTCGTC
papdAfw	**CTCGAG**GAGCCTCTCCATTAAACAATG
papdArev	**CATATG**CTTGAATTCCTCCAACCGGGGGTATG
prplKfw	**AAGCTT**GGCATCAAGGTTTCGGAAG
prplKrev	**CATATG**TTTACCCTACCTCTGGTCG
prpsJfw	**CTCGAG**GTCCTTCG GGATCGCTTG AC
prpsJrev	**CATATG**ATTCACGTCATCCGTTAAATC
purerev	**CATATG**GTGGTTATGCGCTGCTCAAAATC
purefw	**CTCGAG**CTTTTCTCGATCCGGGAAAAATAC
PmamDCrev	**CATATG**CTGATCTCCGGCAAGTGTATG
PmamDCfw	**CTCGAG**CAATGACCACCACCACCTTA AAC
PmamABfw	**CTCGAG**ATGGCGCAAAGATGTGACGT C
PmamABrev	**CATATG**TCCCGTCACAATTCACCTCC
pmsp3fw	**CTCGAG**GAACTCCAAAAGCAAGGCTATTTAC
pmsp3rev	**ATTAAT**CCGAAAGCTCCTTGAATCAAAAG
ptetfw	**CTCGAG**CTTCCGGCTGGCTGGTTTATTG
ptetrev	**CATATG**TTTTTGCCCTCGTTATCTAG
ptetintrev	CCGCAGATGATCAATTCAAGGCCGAATAAG
ptetintfw	CTTGAATTGATCATCTGCGGATTAGAAAAAC
PmamDC96	**CTCGAG**CTTTTTCGCTTTACTAGCTC
PmamDC262	**CTCGAG**GCACCCTGTTTGGCAGGC
PmamDC163	**CTCGAG**ATAACTCTATTTTTGCACACCC
PmamDCxlrev	**CTCGAG**GATCTCCGGCAAGTGTATGCAC
zzfw	GCTGCA**CATATG**GCGCAACACGATGAAGCC
zzrev	CCA**TCTAGA**AATATTACCGCCAGCCATTG

Table 2: Plasmids used in this study list

Plasmid name	Description	Source
pEGFPN1	GFP expression vector; Ap	BD Biotech
pGEMT-Easy	Cloning vector; Ap	Promega
pBBR1MCS-2	Mobilizable broad-host-range vector; Km	Kovach et al. (18)
pASK-IBA5	Tetracycline inducible expression vector	IBA-Go
pCR2.1 – TOPO	Cloning vector; Ap	Invitrogen
pGEMegfp	pGEMT-Easy + *egfp*	This study
pBBRegfp	pBBR1MCS-2 + *egfp* from pGEMegfp	This study
pBBRpl	Promoterless GFP-reporter vector based on pBBRegfp	This study
pGEMPmamDC	pGEMT-Easy + P_{mamDC}	This study
pGEMPmamAB	pGEMT-Easy + P_{mamAB}	This study
pGEMPure	pGEMT-Easy + P_{ure}	This study
pGEMPapdA	pGEMT-Easy + P_{mms16}	This study
pGEMPmsp3	pGEMT-Easy + P_{msp3}	This study
pGEMPrplK	pGEMT-Easy + P_{rplK}	This study
pGEMPrpsJ	pGEMT-Easy + P_{rpsJ}	This study
pBBRPmamDC	pBBRpl + P_{mamDC} from pGEMPmamDC	This study
pBBRPmamAB	pBBRpl + P_{mamAB} from pGEMPmamAB	This study
pBBRPure	pBBRpl + P_{ure} from pGEMPure	This study
pBBRPapdA	pBBRpl + P_{mms16} from pGEMPapdA	This study
pBBRPmsp3	pBBRpl + P_{msp3} from pGEMPmsp3	This study
pBBRPrpLK	pBBRpl + P_{rplK} from pGEMPrplK	This study
pBBRPrpsJ	pBBRpl + P_{rpsJ} from pGEMPrpsJ	This study
pCRPtet	pCR2.1 + P_{tet}	This study
pBBRPtet	pBBRpl + P_{tet}	This study
pGEMPdc96	pGEMT-Easy + 96 bp fragment of P_{mamDC}	This study
pGEMPdc163	pGEMT-Easy + 163 bp fragment of P_{mamDC}	This study
pGEMPdc262	pGEMT-Easy + 262 bp fragment of P_{mamDC}	This study
pBBRPdc96	pBBRol + 96 bp fragment of P_{mamDC} from pGEMPdc96	This study
pBBRPdc163	pBBRol + 163 bp fragment of P_{mamDC} from pGEMPdc163	This study
pBBRPdc262	pBBRol + 262 bp fragment of P_{mamDC} from pGEMPdc262	This study
pEZZ18	Protein A gene fusion vector; Ap	GE Healthcare
pGEMZZ	pGEMT-Easy + "ZZ" protein domain	This study
pCL6	pBBR1MCS-2 + MamC-GFP	(23)
pBBRCZZ	exchange of GFP with ZZ function in pCL6	This study
pJETPdcx1	pJET1.2 + P_{mamDC}	This study
pBBRPdcCZZ	pBBRCZZ + P_{mamDC} from pGEMPdcx1	This study

Promoter activity assays

For promoter activity assays *E. coli* cells were grown in LB to an OD_{600} of 0.5. *M. gryphiswaldense* strains were cultivated in triplicates microaerobically in 3 ml culture volumes in 6-well culture plates under a microoxic atmosphere (1% oxygen, 99% nitrogen). The cultures were grown to early stationary phase for 20-22 h in FSM medium (15). Induction of the P_{tet} promoter was achieved by the addition of different concentrations of anhydrotetracycline after 16 hours of microaerobic cultivation. The fluorescence was

quantified after an additional 4 hour period of cultivation. To study the induction of the P_{tet} promoter over time *M. gryphiswaldense* harbouring pBBRPtet was grown aerobically in triplicates in 100 ml volume for 16 hours. After this incubation period 10 ng ml^{-1} anhydrotetracycline were added to each culture, and the fluorescence was quantified at different time points during a 7 h period of continued incubation.

Fluorescence microscopy

For microscopic investigation *E. coli* cells and *M. gryphiswaldense* cells were immobilized on agarose pads (FSM medium excluding yeast extract and peptone, but supplemented with 1% agarose). The immobilized cells were imaged with an Olympus IX81 microscope equipped with a 100x UPLSAPO100XO objective with a numerical aperture of 1.40 and a Hamamatsu Orca ER camera. Images were captured and analyzed using Olympus cell^M software.

Detection of GFP fluorescence with a fluorescence reader

M. gryphiswaldense and *E. coli* strains expressing GFP from different promoters were washed and resuspended in phosphate buffered saline to an OD_{565} of 0.5. The expression of GFP was quantified from 100 μl aliquots of the cell suspension with an Infinite 500 96-well fluorescence reader using I-Control v1.2.7.0 software (Tecan). The excitation wavelength was 485 nm (20-nm bandwidth), and emission was recorded at 535 nm (25-nm bandwidth). The value for each sample was averaged from 10 reads over an integration period of 20 μs.

Immunoblot analysis

Either 10 μg of whole cell protein for analysis of GFP expression from different promoters or 7.5 μg of protein from different cell fractions for detection of MamC-ZZ were separated by SDS-polyacrylamide (12%) gel electrophoresis (PAGE) according to the procedure of Laemmli (21). After electrophoresis, proteins were transferred onto nitrocellulose membranes (Protran; Whatman) by electroblotting. The membranes were blocked for 2 h at room temperature. An anti-GFP antibody (Santa Cruz Biotechnology) was added to the blocking solution at a 1:1,000 dilution and the mixture was incubated for 1 h at room temperature. The membrane was washed several times with Tris-buffered saline (TBS) (20mM Tris, 0.5M NaCl, pH7.5) and TTBS (TBS, 0.05% v/v Tween 20, pH 7.5) before alkaline phosphatase-labelled goat anti-rabbit immunoglobulin G antibody (Santa Cruz, Biotechnology) was added at a 1:1,000 dilution in TBS. After incubation at room temperature

for 45 min, the membrane was washed with TBS, and the nitroblue tetrazolium/BCIP (5-bromo-4-chloro-3-indolylphosphate) detection reagent (Roche Diagnostics) was used for detection.

Flow cytometry

Flow cytometry was conducted with a FACScalibur flow cytometer (Becton-Dickinson). The GFP fluorescence was excited with a 488 nm argon laser. Cells of *M. gryphiswaldense* R3/S1 and derivatives that express GFP from different promoters were washed and resuspended in phosphate-buffered saline at a 1:100 dilution to maintain a counting speed between 300 and 2,000 events s^{-1}. For each sample 50,000 events were counted. Cytometry data were analyzed with FlowJo (Treestar) software. Contaminating cell debris and medium constituents were excluded from the analysis based on forward and side scatter data. To estimate the proportion of fluorescent cells, a threshold for fluorescence was set to the fluorescence intensity below which 99% of untransformed *M. gryphiswaldense* cells, which served as a non-fluorescent standard, were detected.

Isolation of magnetosomes and cell fractionation

Magnetosome isolation and cell fractionation was done as described previously (23) with the only exception that the cells were lysed with a benchtop constant cell disruptor (Constant Systems) at a pressure of 1.35 kbar instead of a French press.

Antibody-binding assay

Triplicates of magnetosomes from *M. gryphiswaldense* R3/S1, and derivatives with pBBRPdcX1CZZ and pCL6 were diluted to a concentration of 1 mM Fe in 500 µl blocking solution (TBS + milk powder). The samples were incubated for 30 min at room temperature before rabbit GFP-Antibody was added at a 1:2,000 dilution. After incubation for 45 min magnetosomes were collected magnetically and resuspended in TBS. After an additional magnetic separation step a conjugate of shrimp alkaline phosphatase (SAP) and goat-anti-rabbit antibody was added in a 1:2000 dilution in TBS. After an incubation period of 45 min, the magnetosomes were magnetically separated and washed with TBS three times. After the third magnetic collection of the magnetosomes the particles were resuspended in 200 µl TBS of which 100 µl were incubated with 100 µl Attophos SAP detection reagent (Roche) for 5 min. Fluorescence was detected with an Infinite 500 96-well fluorescence reader using I-Control v1.2.7.0 software (Tecan). The excitation wavelength was 430 nm (20 nm bandwidth)

and emission was recorded at 535 nm (25 nm bandwidth). The value for each sample was averaged from 10 reads over an integration period of 20 μs.

Results

Sequence analysis of putative promoters in *M. gryphiswaldense*

We investigated several genomic fragments from *M. gryphiswaldense* harbouring potential promoter sequences, including putative P_{mamDC}, P_{mamAB}, P_{apdA}, P_{msp3}, P_{rpsJ}, P_{rplK} and P_{ure} sequences. The P_{mamDC} and P_{mamAB} promoters were mapped previously in *M. gryphiswaldense* (38). Genomic regions homologous to the P_{mms16} (P_{apdA}) and the P_{msp3} promoters which were described previously in *M. magneticum* (53) were analyzed. As the homologue of *M. magneticum* Mms16 is a PHB-granule-bound phasin in *M. gryphiswaldense*, designated ApdA, the promoter is named P_{apdA} in this organism (40). In addition, genomic regions upstream of large ribosomal gene clusters, which potentially encode the strong *rpsJ* (rpsJ: MGR3815 ribosomal protein S10) and *rplK* (rplK: MGR3801 ribosomal protein L11) promoters, were analyzed. P_{rpsJ} was previously used as a strong and constitutive promoter for heterologous gene expression in *Streptomyces avermitilis* (17). In *E. coli* P_{rplK} is the major promoter for ribosomal genes *rplKAJL* and *rpoBC* (RNA polymerase subunits β, β') (2, 9). We also analyzed the region upstream of a putative urease operon (MGR3989-MGR3978), which may encode a putative urea or nitrogen-limitation inducible promoter P_{ure} (7, 11) and the P_{tet} promoter from the *E. coli* Tn10 Tc[R] gene, which can be induced by addition of anhydrotetracyline in a wide range of bacteria (4, 44, 50).

Analysis of the putative promoter regions with the bacterial promoter prediction tool BPROM (Softberry) showed that sequences with similarity to the canonical sequence motif of *E. coli* promoters are present in all regions except for the region upstream of the *rplK* gene (Figure 1). The predicted transcription start points for the P_{mamAB} and P_{mamDC} promoter are identical to those identified experimentally (38). Highest similarity to an *E. coli* promoter sequence was found by BPROM analysis in the region upstream of the *msp3* gene. All putative -35 and -10 promoter sequences are divergent to each other and to the canonical sequences of *E. coli* (-35: TTGACA, -10: TATAAT) (13, 26) and the α-proteobacterium *Sinorhizobium meliloti* (-35: CTTGAC, -10: CTATAT) (29). By sequence alignment the highest similarity to the canonical sequences from *E. coli* and *S. meliloti* was found for P_{mamAB}, with a match of 5 (of 6) nucleotides at the -35 position and a match of 5 (of 6) nucleotides at the -10 position to both canonical sequences. The predicted -35 and -10

sequences show only a weak conservation with the previously described *M. gryphiswaldense* P*mms* promoter (-35: CCGTCT, -10: ATTCCA) (38) (Figure 1).

P*mamDC* (Linear discriminant function (LDF): 3.34)
      42   37
tt**ttcgct**ttactagctcttagttctccaa**taaatt**ccctgc**g**tc…38bp…cc*ggag*atcag**ATG**

P*mamAB* (LDF: 2.99)
      83   64
gc**ttgtca**accgacctcgattcgttgc**tatagt**ccgtgcgaa**t**t*ggagg*tgaattgtgacgggaATG

P*apdA* (LDF: 2.76)
      60   43
ga**ttgaaa**agatcggcatc**ttgcatcat**tgcgat**g**at…104bp…tt*ggagga*attcaag**ATG**

P*msp3* (LDF: 4.43)
      32   70
gc**ttggcg**gatgaagattgtcg**gggtaatat**aatttc**g**ta…13bp…tt*ggag*ttccctaATG

P*rpsJ* (LDF: 1.13)
      45   33
tc**ttgcac**ctgctaccgagtct**ctgtataaa**accgcc**t**tc…114bp…ac*gga*tgacgtgaat**ATG**

P*ure* (LDF: 4.08)
   3   80
aa**tacaaa**gaaacaattcagaaata**ttgtaaaat**agatga**t**gccgtgattttgagcagcgcataaccac**ATG**

P*tet* (LDF: 4.55)
      66   54
tg**ttgaca**ctctatcattgatag**agttatttt**accact**C**cc…50bp…ac*gagg*gcaaaaa**ATG**

Figure 1: Prediction of promoter regions using the BPROM (Softberry, Inc) promoter prediction tool. Predicted -35 and -10 regions (bold), transcriptional start sites (bold, enlarged), putative ribosomal binding sites (bold, italics) and start codons (bold, capitals) are highlighted in the figure. In addition the score values of the promoter prediction are indicated above the corresponding -35 and -10 regions. The Linear discriminant function (LDF), which combines characteristics describing functional motifs and oligonucleotide composition of *E. coli* σ^{70} promoter sites (for comparison *E. coli* P*lac* LDF: 4.38 and P*bad* LDF: 4.24) is displayed for the different promoters.

Experimental identification of genuine promoters in *M. gryphiswaldense*

Putative promoters were cloned upstream of a promoterless GFP reporter gene. *E. coli* cells transformed with transcriptional fusions of *M. gryphiswaldense* promoters to the GFP reporter showed almost no fluorescence upon microscopic inspection (Figure 2A). Fluorescence levels for every promoter from *M. gryphiswaldense* were even below 20% of the uninduced *E. coli*-P*lac* promoter (Figure 2B), indicating that promoters from *M. gryphiswaldense* are poorly expressed in this organism. In contrast *M. gryphiswaldense* strains harbouring GFP fusions of P*mamDC*, P*mamAB*, P*msp3*, P*apdA* displayed strong fluorescence, whereas weaker fluorescence was observed with P*rpsJ*, P*rplK* and *E. coli*-P*lac*, and virtually no fluorescence was seen in strains harbouring the P*ure*, *E. coli*-P*tet*, and the promoterless control (Figure 2C, Figure 2D).

Analysis of cell lysates from the different *M. gryphiswaldense* reporter strains by an anti-GFP-immunoblot showed the highest amounts of GFP was produced from P_{mamDC}, followed by P_{msp3}, P_{apdA}, P_{mamAB}, P_{rplK} and P_{lac} (P_{mamDC}>>P_{msp3}, P_{apdA}>P_{mamAB}>>P_{rplK}> *E. coli*-P_{lac}). No GFP production was detected in the strain with the promoterless GFP construct (Fig 2E). These results confirmed that the level of fluorescence in fact is correlated to the amount of GFP.
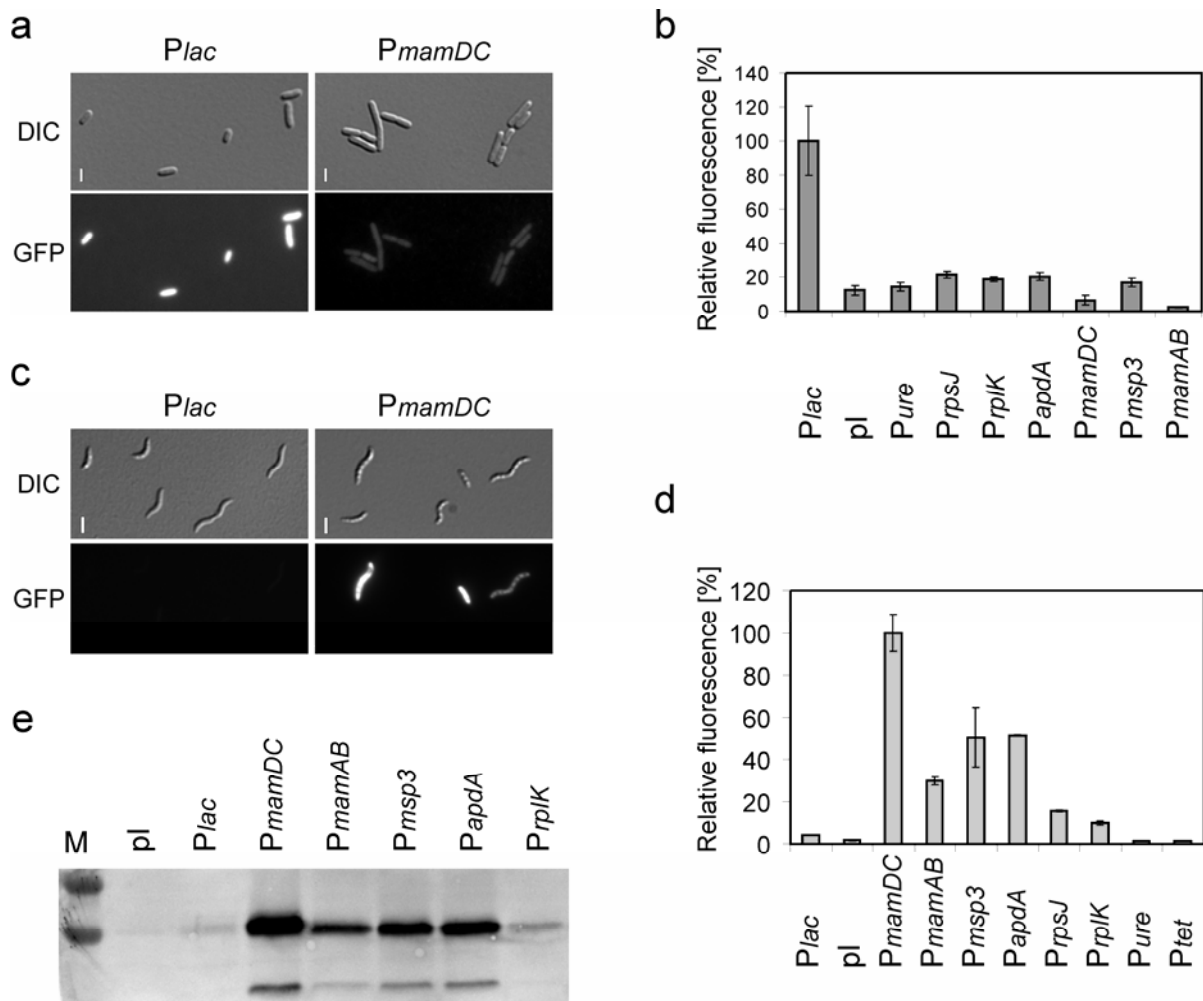

Figure 2: Expression of GFP from different promoters in *E. coli* and *M. gryhiswaldense.* (a) Fluorescence microscopy of *E. coli* cells expressing GFP from P_{lac} or P_{mamDC} promoter (exposure time: 1 s). (b) Fluorescence quantification of GFP production from *E. coli* strains expressing GFP from different promoters. (c-e) Analysis of GFP expression from different promoters in *M. gryphiswaldense* by (c) fluorescence microscopy (exposure time: 0.5 s), (d) fluorometry and (e) immunoblot. The error bars reflect the standard deviation calculated from three independent experiments. DIC – differential interference contrast, pl – promoterless control, M – molecular weight marker

P_{tet} is an inducible promoter in *M. gryphiswaldense*

To test if P_{ure} can be induced in *M. gryphiswaldense* under nitrogen limitation and in the presence of urea, we tried combinations of different media constituents (1-4 mM sodium

nitrate, 0.075-0.3% w/v soy peptone, 0 or 50 mM urea), but were unable to detect GFP expression under any condition (data not shown). In contrast, GFP expression from the P_{tet} promoter was observed four hours after the addition of 2.5 ng ml^{-1} anhydrotetracycline (Figure 3A). Maximum GFP fluorescence was detected between 5-50 ng ml^{-1} anhydrotetracycline, whereas a concentration of 100 ng ml^{-1} resulted in a reduced GFP expression (Figure 3A). GFP production could be detected already 20 min after induction and increased for 4 hours after induction to remain then constant (Figure 3B). Flow cytometric analysis of the P_{tet} – GFP construct showed that the uninduced P_{tet} promoter produced nearly as little fluorescence as the promoterless GFP construct, which is indicative for a tight regulation. In the induced culture the expression level from P_{tet} was about as high as from P_{rplK}, but tenfold lower than from P_{mamDC}. The proportion of fluorescent cells increased after induction from 2.4 % about tenfold to 26.3 % of the population (Figure 4).
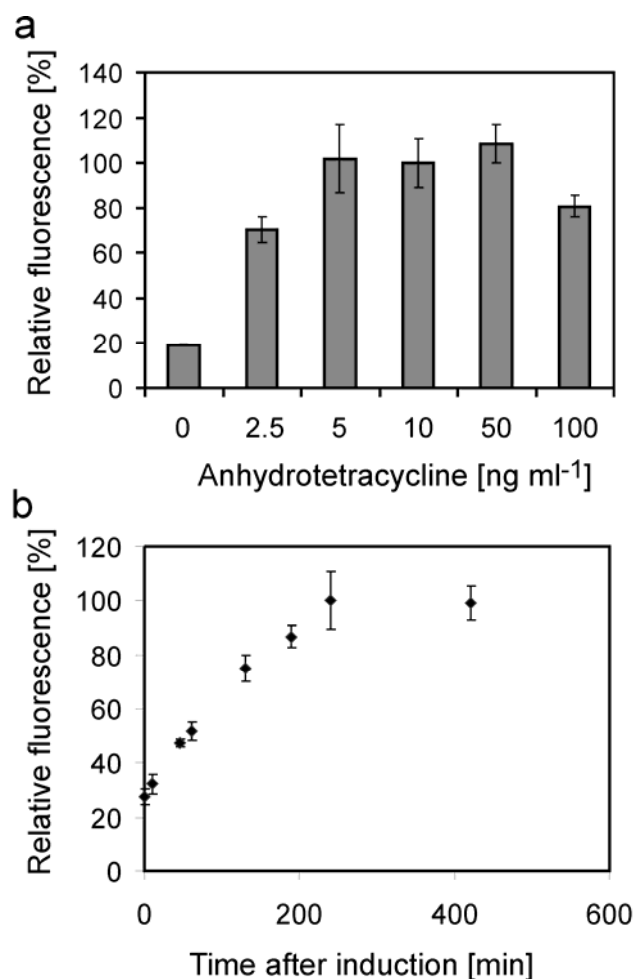
Figure 3: Induction of GFP expression from the P_{tet} promoter in *M. gryphiswaldense*. (a) Quantification of fluorescence four hours after addition of different concentrations of the inducer anhydrotetracycline. (b) Quantification of culture average fluorescence at different time points after addition of 10 ng ml^{-1} anhydrotetracycline. Standard deviations calculated from three independent experiments are indicated.

GFP is heterogeneously expressed from different promoters in *M. gryphiswaldense*

Comparison of the average fluorescence intensities by flow cytometry showed that cells containing the P_{mamDC} – GFP construct fluoresced on average twice as much as cells, expressing GFP from P_{msp3} or P_{apdA} (Figure 4). However, these experiments also revealed that not all cells within a given population uniformly expressed GFP, but that a variable fraction of the cells was non-fluorescent (Figure 4). Low proportions of fluorescent cells were observed with weak promoters such as P_{ure} (1.96 %) and $P_{tet\ (uninduced)}$ (2.67 %). For the intermediate-strength promoters P_{lac}, P_{rplK}, $P_{tet\ (\ induced)}$, P_{rpsJ} and P_{mamAB} the proportions of fluorescent cells (from 8.52 % to 56.5 %) correlated well with the increased average fluorescence intensities, whereas higher average fluorescence produced by the stronger promoters P_{msp3}, P_{mamDC} and P_{apdA} was not correlated with a higher proportion of fluorescent cells (56.3-50.3%).
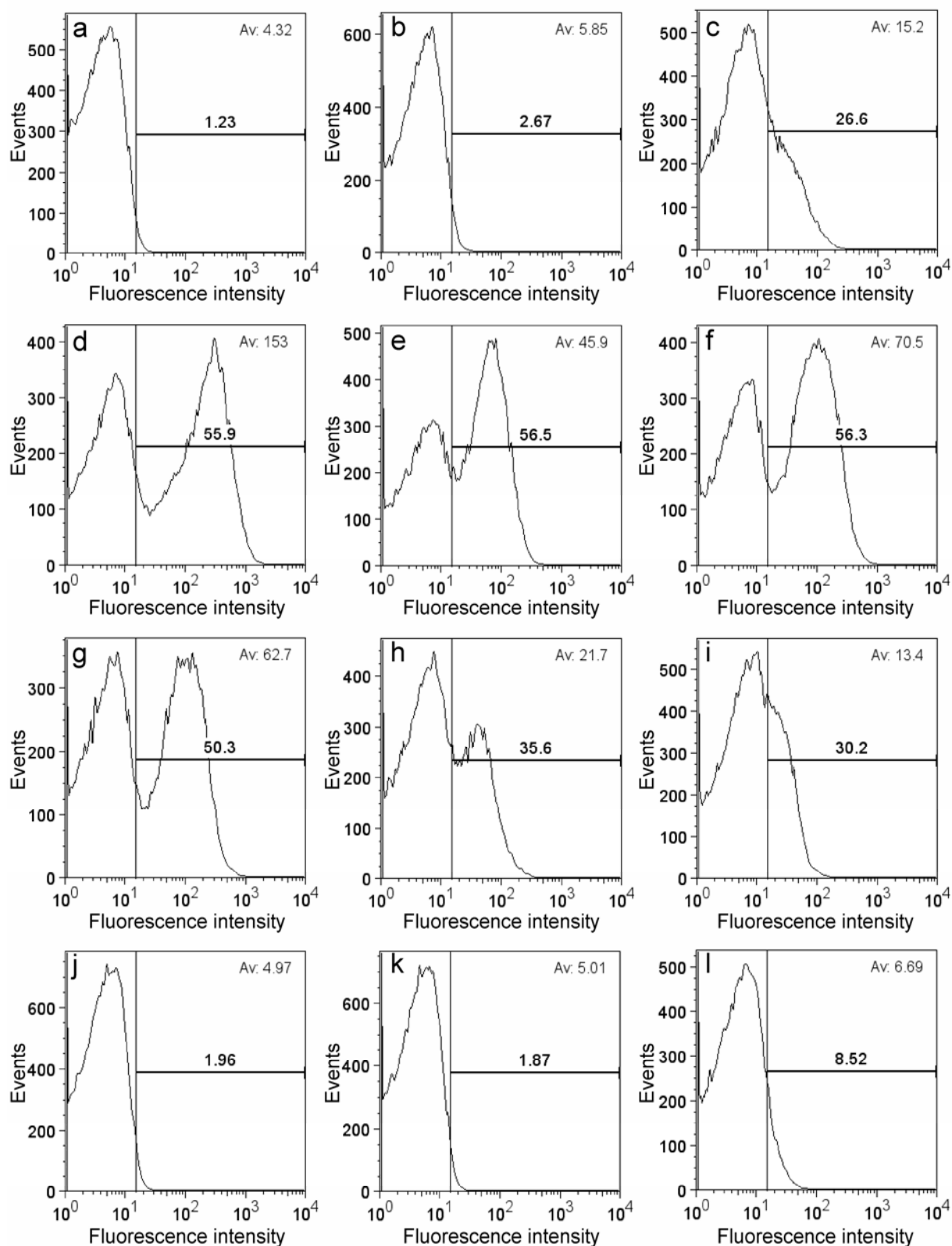
Figure 4: Flow cytometry of *M. gryphiswaldense* (a) and strains expressing GFP from different plasmids.
(b) pBBRPtet uninduced; (c) pBBRPtet induced; (d) pBBRPmamDC; (e) pBBRPmamH; (f) pBBRPmsp3; (g) pBBRPapdA ; (h) pBBRPrpsJ; (i) pBBRPrplK; (j) pBBRPure; (k) pBBRpl (promoterless); (l) pBBRegfp (P*lac*). The proportion of fluorescent cells is shown in bold, and the average fluorescence intensity is displayed in the upper right corner.

A 96 bp P$_{mamDC}$ promoter fragment is sufficient for efficient expression of GFP

In order to identify potential regulatory sequences and the minimal part required for efficient expression, three different truncations of the P$_{mamDC}$ promoter region were constructed. In addition to the 325 bp DNA fragment which was described above, a 262 bp version (P$_{mamDC262}$), a 163 bp (P$_{mamDC163}$) version, and a 96 bp (P$_{mamDC96}$) version were cloned upstream of the *egfp* reporter gene. No differences were detected between the different P$_{mamDC}$ truncations after growth under standard conditions (Figure 5) as well as after growth under oxic and iron limiting conditions (data not shown).
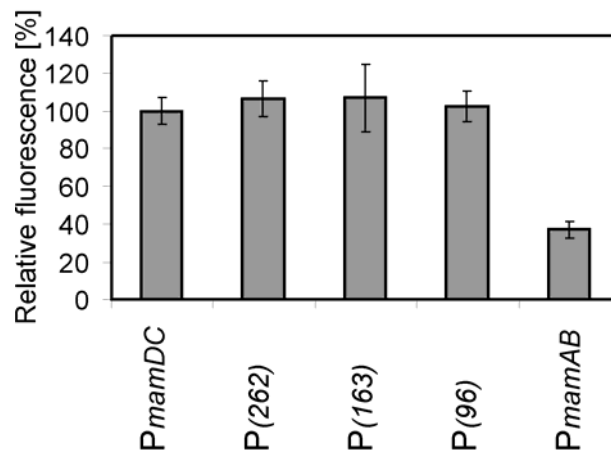
Figure 5: Fluorescence quantification of GFP expression from the P$_{mamDC}$ and truncated versions P$_{mamDC262}$, P$_{mamDC163}$ and P$_{mamDC96}$. Standard deviations calculated from three independent experiments are indicated.

P$_{mamDC}$ allows strong expression of recombinant fusions proteins for display in the magnetosome membrane

In order to demonstrate the potential of P$_{mamDC}$ a fusion of MamC, which has previously been identified as an efficient magnetosome membrane anchor protein (23) with the antibody-binding ZZ domain was expressed from P$_{mamDC}$. The ZZ domain is a derivative of protein A (28) and has been previously demonstrated to be functional in *M. magneticum* (54). By immunoblot analysis of different cell fractions with a rabbit anti-GFP antibody as a primary antibody, whose constant region tightly interacts with the ZZ protein domain, we detected weak expression of the MamC-ZZ fusion protein in the cell lysate in the membrane protein fraction. A strong signal was obtained in the magnetosome membrane fraction (Figure 6A), which demonstrates that MamC-ZZ is efficiently targeted to this compartment. Next, we tested if native MamC-ZZ modified magnetosomes bind antibodies to generate antibody-displaying magnetic nanoparticles. After incubation of MamC-ZZ modified, unmodified and GFP-displaying magnetosomes with rabbit anti-GFP antibody we detected the highest

abundance of the rabbit anti-GFP antibody with a shrimp-alkaline-phosphatase labelled goat anti-rabbit-antibody on the surface of MamC-ZZ modified magnetosomes (Figure 6B). The signal was substantially stronger than the signal observed for MamC-GFP modified magnetosomes, which were produced by expression of the MamC-GFP fusion from the P_{lac} promoter (23) (Figure 6B). These results demonstrate that MamC-ZZ modified magnetosomes efficiently bind rabbit antibodies. In addition, MamC-ZZ magnetosomes, which were not incubated with the rabbit anti-GFP antibody, yielded a weak signal, which indicates that MamC-ZZ modified antibodies also interact weakly with goat antibody, if also much weaker than with rabbit antibodies (Figure 6B).
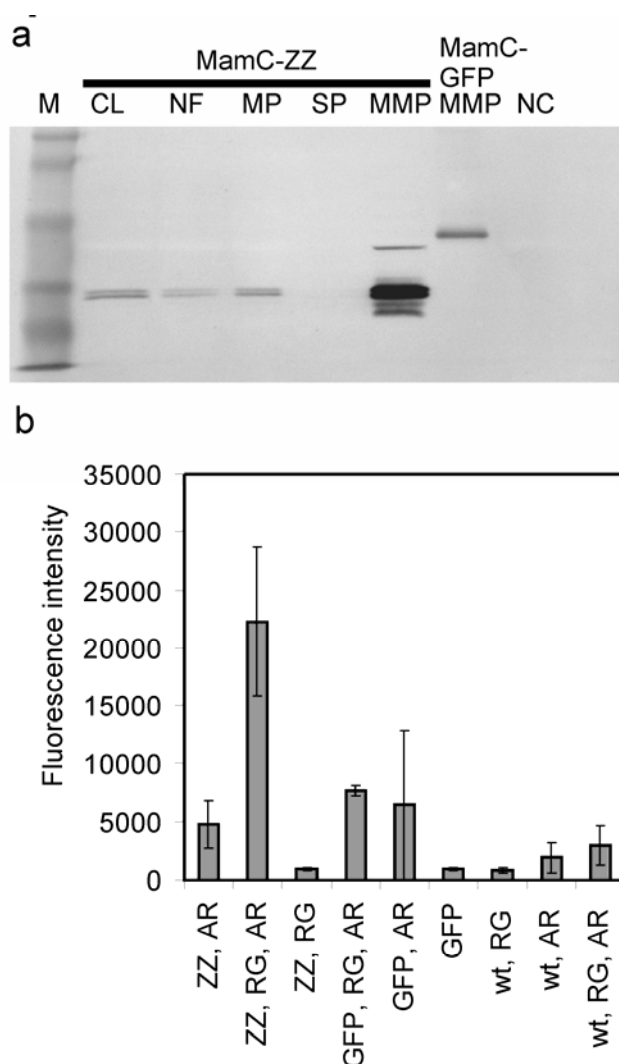
Figure 6: Expression of a MamC-ZZ fusion protein in *M. gryphiswaldense* for the production of antibody-binding magnetosomes. (a) Detection of the MamC-ZZ protein in different cell fractions of *M. gryphiswaldense* pBBRPdcCZZ using a rabbit Anti-GFP-antibody. As a positive control MamC-GFP modified magnetosome and as a negative control MamC-Strep modified magnetosomes were utilised. M – molecular weight marker, CL – cell lysate, NF – non-magnetic fraction, MP – membrane protein fraction, SP – soluble protein fraction, MMP – magnetosome membrane protein fraction (b) Antibody-binding assay of MamC-ZZ modified magnetosomes.

The strongest signal was observed with magnetosomes purified from *M. gryphiswaldense* pBBRPdcCZZ (ZZ), which were treated with a primary rabbit Anti-GFP antibody (RG) and a shrimp alkaline phosphate conjugate of a goat Anti-Rabbit antibody (AR). ZZ-Magnetosomes which were only treated with one antibody, MamC-GFP modified magnetosomes (GFP) and non-modified magnetosomes (wt) were included as controls. Standard deviations calculated from three replicates are indicated.

Discussion

In this study we compared previously predicted magnetosomal promoter sequences P_{mamDC} and P_{mamAB} (38) with the heterologous regions of P_{mms16} (in *M. gryphiswaldense* P_{apdA}) and P_{msp3}, and with putative promoter sequences of ribosomal proteins (P_{rpsJ} and P_{rplK}) and a putative promoter of an urease operon (P_{ure}) in *M. gryphiswaldense*. Sequence analysis showed that all tested sequences, with the exception of the upstream region of *rplK,* contained a region with high similarity to an *E. coli* promoter sequence. Nevertheless, promoter sequences from *M. gryphiswaldense* did not activate GFP expression in *E. coli*. Their observed inactivity in *E. coli* is in agreement with results of previous studies on promoters from α-proteobacteria and was described, for example, for promoters from *S. meliloti* (29), and *Caulobacter crescentus* (30, 45). In *M. gryphiswaldense* six of seven tested native promoters were considerably more active than the *E. coli* P_{lac} promoter that has been used in previous studies in this organism. The strongest promoter in *M. gryphiswaldense* was P_{mamDC} followed by P_{msp3}, P_{apdA}, P_{mamAB}, P_{rpsJ} and P_{rplK}.

As the predicted and previously identified promoter sequences (38) show only weak conservation, it is currently not possible to deduce a consensus sequence for promoters in *M. gryphiswaldense*. In addition, a correlation of the promoter sequences with the expression level might be obscured, as the expression level might be affected by additional promoter regions such as A-tract sequences upstream of the -35 element, transcriptional regulators, and different ribosomal binding sites.

The use of GFP as reporter enabled us to estimate its expression in individual cells by flow cytometry. This revealed that GFP was heterogeneously expressed within a given population of cells, and that even strong promoters such as P_{mamDC} did not further increase the proportion of fluorescent cells above 60%. At this point it is unclear why such a large proportion of cells was inactive with respect to GFP expression. However, inhomogeneous gene expression in an isogenic population of cells was frequently observed in bacteria (8, 43) and might be caused by cell-cycle dependent effects, stochasticity of gene expression or variations of growth rates and protein synthesis between individual cells (33, 47, 10). As a

similar pattern was observed with several different promoters, it is unlikely that promoter-specific gene regulatory mechanisms are involved. However, further studies are required to understand the reason for the heterogeneity of protein expression and to raise the proportion of cells that express a heterologous protein.

The range of potentially inducible promoters in MTB is rather limited. The widely used arabinose and xylose inducible promoters are presumably non-functional in *M. gryphiswaldense*, because *M. gryphiswaldense* is incapable of sugar utilization. Likewise, the vanillate-inducible promoter from *Caulobacter crescentus* (49) was not functional in *M. gryphiswaldense* (data not shown) and the activity of the putative *M. gryphiswaldense* promoter P$_{ure}$ was unaffected by nitrogen limitation or the presence of urea. In contrast, our results demonstrate that the P$_{tet}$ promoter can be induced in *M. gryphiswaldense* by the addition of 5-50 ng ml^{-1} anhydrotetracycline. Expression from P$_{tet}$ was tightly regulated, and although the fully induced P$_{tet}$ promoter is not as strong as the P$_{mamDC}$ promoter in *M. gryphiswaldense*, the availability of an inducible promoter is an important addition to the *M. gryphiswaldense* genetic toolbox. For instance P$_{tet}$ can be useful in future experiments for the regulated expression of deleterious proteins, or in studies of cell cycle-dependent protein localization using GFP-fusions.

Although the use of GFP in microaerophilic bacteria requires caution because of the oxygen-dependence of GFP fluorescence (23), our results also demonstrate that GFP is an effective transcriptional reporter in magnetotactic bacteria. In comparison to other transcriptional reporters such as β-galactosidase (*lacZ*), luciferase (*luc*) and β-glucuronidase (*gusA*), the major advantages of GFP is that it is readily detected at a single cell level by fluorescence microscopy or flow cytometry. The combination of fluorescent proteins as transcriptional reporter with flow cytometry or fluorescence microscopy can be used to investigate the heterogeneity of populations and study the bacterial physiological state of individual cells (46). In addition, the pBBRpl plasmid could be used in future studies to monitor the activity of other clonable promoters, and in combination with flow cytometry it might be possible to identify differentially expressed promoters from *M. gryphiswaldense* and related MTB as previously described in other organisms (3, 51).

Our data show that P$_{mamDC}$ is the strongest promoter so far identified in *M. gryphiswaldense* and was even stronger than the homologues of the previously identified promoters P$_{msp3}$ and P$_{mms16}$ of *M. magneticum* (53). Truncation experiments of the P$_{mamDC}$ promoter showed that a 96 bp region upstream of the GFP start codon is sufficient for efficient gene expression. This region contains only four bases upstream of the -35 region,

which indicates that neither an A-tract promoter sequence or transcription factors are required for efficient P*mamDC* transcription. For future applications the short 96 bp fragment will facilitate its cloning and also reduce the chance of unwanted recombination between plasmid-borne and chromosomal P*mamDC*.

Another important application for an expression system in magnetotactic bacteria is the display of chimeric proteins on magnetosomes to generate functional biogenic nanoparticles (22, 24, 31). Besides selection of an appropriate polypeptide anchor, which is firmly attached to the magnetite particle, this approach requires robust and abundant expression of the chimeric protein in a large proportion of cells. We demonstrated that a translational fusion of the magnetosome membrane protein MamC with the antibody-binding ZZ domain (MamC-ZZ) was highly expressed from P*mamDC* and inserted into the magnetosome membrane. The purified ZZ-modified magnetosomes, which selectively bind rabbit antibodies, can be used for magneto-immunoassays (54), or for purification of antibodies, as described with ZZ-modified bacterial polyester granules (1). One particular advantage of *M. gryphiswaldense* as a host for production of such genetically functionalized magnetosomes is that several mutant strains with average magnetosome size between 24 and 37 nm are available (35), which makes it possible to produce a wide range of magnetic nanoparticles with engineered biochemical and physicochemical characteristics. In conclusion, our results indicate that our expression system is a powerful tool for the display of engineered proteins on the surface of magnetosomes to generate functionalized magnetic nanoparticles for bio- and nano-technological applications.

Acknowledgments

We are indebted to Martin Thanbichler for donation of plasmids containing the P$_{tet}$ and P$_{van}$ promoters. We are grateful to Markus Kador and Michael Boshart for providing help and access to the flow cytometer. We also thank Torsten Pirch and Kirsten Jung for access to the fluorescence reader as well as Anna Pollithy and Ivaylo Kostadinov for help with cloning. The project was funded by German Research Foundation grant SPP 1104 and the "Nanobiotechnology" program of the German Federal Ministry of Education and Research.

References

1. **Brockelbank, J. A., V. Peters, and B. H. A. Rehm.** 2006. Recombinant *Escherichia coli* strain produces a ZZ domain displaying biopolyester granules suitable for immunoglobulin G purification. Appl. Environ. Microbiol. **72:**7394-7397.

2. **Brückner, R., and H. Matzura.** 1981. *In vivo* synthesis of a polycistronic messenger RNA for the ribosomal proteins L11, L1, L10 and L7/12 in *Escherichia coli*. Mol. Gen. Genet. **183:**277-282.

3. **Bumann, D., and R. H. Valdivia.** 2007. Identification of host-induced pathogen genes by differential fluorescence induction reporter systems. Nat. Protoc. **2:**770-777.

4. **Carroll, P., D. G. N. Muttucumaru, and T. Parish.** 2005. Use of a tetracycline-inducible system for conditional expression in *Mycobacterium tuberculosis* and *Mycobacterium smegmatis*. Appl. Environ. Microbiol. **71:**3077-3084.

5. **Ceyhan, B., P. Alhorn, C. Lang, D. Schüler, and C. M. Niemeyer.** 2006. Semi-synthetic biogenic magnetosome nanoparticles for the detection of proteins and nucleic acids. Small **2:**1251-1255.

6. **Cormack, B. P., R. H. Valdivia, and S. Falkow.** 1996. FACS-optimized mutants of the green fluorescent protein (GFP). Gene **173:**33-38.

7. **D'Orazio, S. E. F., and C. M. Collins.** 1993. The plasmid-encoded urease gene cluster of the family *Enterobacteriaceae* is positively regulated by UreR, a member of the AraC family of transcriptional activators. J. Bacteriol. **175:**3459-3467.

8. **Davidson, C. J., and M. G. Surette.** 2008. Individualtiy in Bacteria. Annu. Rev. Genet. **42:**253-268.

9. **Downing, W. L., and P. P. Dennis.** 1987. Transcription products from the *rpIKAJL-rpoBC* gene cluster. J. Mol. Biol. **194:**609-620.

10. **Elowitz, M. B., A. J. Levine, E. D. Siggia, and P. S. Swain.** 2002. Stochastic gene expression in a single cell. Science **297:**1183-1186.

11. **Friedrich, B., and B. Magasanik.** 1977. Urease of *Klebsiella aerogenes*: control of its synthesis by glutamine synthetase. J. Bacteriol. **131:**446-452.

12. **Grünberg, K., E. C. Müller, A. Otto, R. Reszka, D. Linder, M. Kube, R. Reinhardt, and D. Schüler.** 2004. Biochemical and proteomic analysis of the magnetosome membrane in *Magnetospirillum gryphiswaldense*. Appl. Environ. Microbiol. **70:**1040-1050.

13. **Harley, C. B., and R. P. Reynolds.** 1987. Analysis of *E. coli* promoter sequences. Nucleic Acids Res. **15:**2349-2361.

14. **Hergt, R., R. Hiergeist, M. Zeisberger, D. Schüler, U. Heyen, I. Hilger, and W. A. Kaiser.** 2005. Magnetic properties of bacterial magnetosomes as diagnostic and therapeutic tools. J. Magn. Magn. Mat. **293:**80-86.

15. **Heyen, U., and D. Schüler.** 2003. Growth and magnetosome formation by microaerophilic *Magnetospirillum* strains in an oxygen-controlled fermentor. Appl. Microbiol. Biotechnol. **61:**536-544.

16. **Horton, R. M., H. D. Hunta, S. N. Ho, J. K. Pullen, and L. R. Pease.** 1988. Engineering hybrid genes without the use of restriction enzymes: gene splicing by overlap extension. Gene **77:**61-68.

17. **Komatsu, M., M. Tsuda, S. Omura, H. Oikawa, and H. Ikeda.** 2008. Identification and functional analysis of genes controlling biosynthesis of 2-methylisoborneol. Proc. Natl. Acad. Sci. USA **105:**7422–7427.

18. **Komeili, A., Z. Li, D. K. Newman, and G. J. Jensen.** 2006. Magnetosomes are cell membrane invaginations organized by the actin-like protein MamK. Science **311:**242-245.

19. **Komeili, A., H. Vali, T. J. Beveridge, and D. Newman.** 2004. Magnetosome vesicles are present prior to magnetite formation and MamA is required for their activation. Proc. Natl. Acad. Sci. USA **101:**3839-3844.

20. **Kovach, M. E., P. H. Elzer, D. S. Hill, G. T. Robertson, M. A. Farris, R. M. Roop, 2nd, and K. M. Peterson.** 1995. Four new derivatives of the broad-host-range cloning vector pBBR1MCS, carrying different antibiotic-resistance cassettes. Gene **166:**175-6.

21. **Laemmli, U. K.** 1970. Cleavage of structural proteins during the assembly of the head of bacteriophage T4. Nature **227:**680-5.

22. **Lang, C., and D. Schüler.** 2006. Biogenic nanoparticles: production, characterization, and application of bacterial magnetosome. J. Phys.: - Condens. Matter **18:**S2815-S2828.

23. **Lang, C., and D. Schüler.** 2008. Expression of green fluorescent protein fused to magnetosome proteins in microaerophilic magnetotactic bacteria. Appl. Environ. Microbiol. **74:**4944-4953.

24. **Lang, C., D. Schüler, and D. Faivre.** 2007. Synthesis of magnetite nanoparticles for bio- and nanotechnology: Genetic engineering and biomimetics of bacterial magnetosomes. Macromol. Biosci. **7:**144-151.

25. **Larrainzar, E., F. O'Gara, and J. P. Morrissey.** 2005. Applications of autofluorescent proteins for *in situ* studies in microbial ecology. Annu. Rev. Microbiol. **59:**257-77.

26. **Lisser, S., and H. Margalit.** 1993. Compilation of *E. coli* mRNA promoter sequences. Nucleic Acids Res. **21:**1507-1516.

27. **Lisy, M.-R., A. Hartung, C. Lang, D. Schüler, W. Richter, J. R. Reichenbach, W. A. Kaiser, and I. Hilger.** 2007. Fluorescent bacterial magnetic nanoparticles as bimodal contrast agents. Invest. Radiol. **42:**235-241.

28. **Löwenadler, B., B. Jansson, S. Paleus, E. Holmgren, B. Nilsson, T. Moks, G. Palm, S. Josephson, L. Philipson, and M. Uhlén.** 1987. A gene fusion system for generating antibodies against short peptides. Gene **58:**87-97.

29. **MacLellan, S. R., A. M. MacLean, and T. M. Finan.** 2006. Promoter prediction in the rhizobia. Microbiology **152:**1751-1763.

30. **Malakooti, J., S. P. Wang, and B. Ely.** 1995. A consensus promoter sequence for *Caulobacter crescentus* genes involved in biosynthetic and housekeeping functions. J. Bacteriol. **177:**4372-4376.

31. **Matsunaga, T., T. Suzuki, M. Tanaka, and A. Arakaki.** 2007. Molecular analysis of magnetotactic bacteria and development of functional bacterial magnetic particles for nano-biotechnology. Trends Biotechnol. **25:**182-188.

32. **Pradel, N., C.-L. Santini, A. Bernadac, Y. Fukumori, and L.-F. Wu.** 2006. Biogenesis of actin-like bacterial cytoskeletal filaments destined for positioning prokaryotic magnetic organelles. Proc. Natl. Acad. Sci. USA **103:**17485–17489.

33. **Roostalu, J., A. Jõers, H. Luidalepp, N. Kaldalu, and T. Tenson.** 2008. Cell division in *Escherichia coli* cultures monitored at single cell resolution. BMC Microbiol. **8:68**.

34. **Sambrook, J., and D. Russel, W.** 2001. Molecular cloning: A laboratory manual (3rd edn.). Cold Spring Harbor Laboratory Press, Cold Spring Harbor, NY.

35. **Scheffel, A., A. Gärdes, K. Grünberg, G. Wanner, and D. Schüler.** 2007. The major magnetosome proteins MamGFDC are not essential for magnetite biomineralization in *Magnetospirillum gryphiswaldense,* but regulate the size of magnetosome crystals. J. Bacteriol. **190:**377-386.

36. **Scheffel, A., M. Gruska, D. Faivre, A. Linaroudis, P. L. Graumann, J. M. Plitzko, and D. Schüler.** 2006. An acidic protein aligns magnetosomes along a filamentous structure in magnetotactic bacteria. Nature **440:**110-115.

37. **Scheffel, A., and D. Schüler.** 2007. The acidic repetitive domain of the *Magnetospirillum gryphiswaldense* MamJ protein displays hypervariability but is not required for magnetosome chain assembly. J. Bacteriol. **189:**6437-6446.

38. **Schübbe, S., C. Würdemann, J. Peplies, U. Heyen, C. Wawer, F. O. Glöckner, and D. Schüler.** 2006. Transcriptional organization and regulation of magnetosome operons in *Magnetospirillum gryphiswaldense*. Appl. Environ. Microbiol. **72:**5757-5765.

39. **Schüler, D.** 2008. Genetics and cell biology of magnetosome formation in magnetotactic bactereria. FEMS Microbiol. Rev. **32:**654-672.

40. **Schultheiss, D., R. Handrick, D. Jendrossek, M. Hanzlik, and D. Schüler.** 2005. The presumptive magnetosome protein Mms16 is a PHB-granule bounded protein (phasin) in *Magnetospirilum gryphiswaldense*. J. Bacteriol. **187:**2416-2425.

41. **Schultheiss, D., M. Kube, and D. Schüler.** 2004. Inactivation of the flagellin gene *fla*A in *Magnetospirillum gryphiswaldense* results in nonmagnetotactic mutants lacking flagellar filaments. Appl. Environ. Microbiol. **70:**3624-3631.

42. **Schultheiss, D., and D. Schüler.** 2003. Development of a genetic system for *Magnetospirillum gryphiswaldense*. Arch. Microbiol. **179:**89-94.

43. **Siegele, D. A., and J. C. Hu.** 1997. Gene expression from plasmids containing the *araBAD* promoter at subsaturating inducer concentrations represents mixed populations. Proc. Natl. Acad. Sci. USA **94:**8168–8172.

44. **Skerra, A.** 1994. Use of the tetracycline promoter for the tightly regulated production of a murine antibody fragment in *Escherichia coli*. Gene **151:**131-135.

45. **Smit, J., and N. Agabian.** 1984. Cloning of the major protein of the *Caulobacter crescentus* periodic surface layer: detection and characterization of the cloned peptide by protein expression assays. J. Bacteriol. **160:**1137-1145.

46. **Strovas, T. J., and M. E. Lidstrom.** 2008. Analyzing bacterial physiology at the single-cell level. Microbe **3:**239-244.

47. **Strovas, T. J., L. M. Sauter, X. F. Guo, and M. E. Lidstrom.** 2007. Cell-to-cell heterogeneity in growth rate and gene expression in *Methylobacterium extorquens* AM1. J. Bacteriol. **189:**7127-7133.

48. **Tanaka, M., Y. Okamura, A. Arakaki, T. Tanaka, H. Takeyama, and T. Matsunaga.** 2006. Origin of magnetosome membrane: proteomic analysis of magnetosome membrane and comparison with cytoplasmic membrane. Proteomics **6:**5234-47.

49. **Thanbichler, M., A. Iniesta, and L. Shapiro.** 2007. A comprehensive set of plasmids for vanillate- and xylose-inducible gene expression in *Caulobacter crescentus*. Nucleic Acids Res. **35:**e137.

50. **Thanbichler, M., and L. Shapiro.** 2006. MipZ, a spatial regulator coordinating chromosome segregation with cell division in *Caulobacter*. Cell **126:**147-162.

51. **Valdivia, R. H., and S. Falkow.** 1996. Bacterial genetics by flow cytometry: rapid isolation of *Salmonella typhimurium* acid-inducible promoters by differential fluorescence induction. Mol. Microbiol. **22:**367-378.

52. **Wacker, R., B. Ceyhan, P. Alhorn, D. Schüler, C. Lang, and C. M. Niemeyer.** 2007. Magneto-Immuno PCR: A homogeneous immunoassay based on biogenic magnetosome nanoparticles. Biochem. Biophys. Res. Commun. **357:**391-396.

53. **Yoshino, T., and T. Matsunaga.** 2005. Development of efficient expression system for protein display on bacterial magnetic particles. Biochem. Biophys. Res. Commun. **338:**1678-1681.

54. **Yoshino, T., and T. Matsunaga.** 2006. Efficient and stable display of functional proteins on bacterial magnetic particles using Mms13 as a novel anchor molecule. Appl. Environ. Microbiol. **72:**465-471.

Manuscript 3

Semisynthetic biogenic magnetosome nanoparticles for the detection of proteins and nucleic acids**

Bülent Ceyhan, Petra Alhorn, Claus Lang, Dirk Schüler, and Christof M. Niemeyer*

[*]   Dr. B. Ceyhan, P. Alhorn, Prof. Dr. C. M. Niemeyer Universitt Dortmund, Fachbereich Chemie Biologisch-Chemische Mikrostrukturtechnik Otto-Hahn Strasse 6, 44227 Dortmund (Germany) Fax: (+ 49)231-755-7082 E-mail: christof.niemeyer@uni-dortmund.de

C. Lang, Dr. D. Schüler, Max-Planck Institut für Marine Mikrobiologie, Abteilung Mikrobiologie, Celsiusstrasse 1, 28359 Bremen (Germany)

Keywords:

Analytical methods; DNA; Magnetosomes; Magnetotactic bacteria; Nanostructures

Manuscript

Currently there is great interest in the preparation of functional magnetic nanoparticles (MNPs) with respect to their application in various fields of biomedical diagnostics and nanosciences.[1–3] For example, biofunctionalized MNPs have been used for the *in vitro* detection of proteins[4–6] and nucleic acids,[7, 8] the *in vivo* detection of cell surface[9] and cytosolic[10, 11] proteins, and the signal enhancement of biomolecular detection assays,[12–16] as probes for magnetic resonance imaging (MRI),[9, 10, 17–21] and as reagents for hyperthermia magnetotherapy.[22–24] Until now, synthetic MNPs have been used almost exclusively for these applications although they often do not fully match the high requirements with respect to uniform size and morphology, biocompatibility, and high magnetization capabilities. By contrast, biogenic MNPs, such as the bacterial magnetosome particles (MPs) derived from various magnetotactic bacteria, reveal a number of advantages.[25, 26] In particular, the almost monodisperse MPs possess an unusually high magnetization, display unique shapes and sizes, which depend on the producing bacterial species, and are typically in the range of 35– 120 nm in diameter.[27] Their resulting superparamagnetic or ferrimagnetic properties potentially make them highly useful in many (biomedical) applications. MPs are organelles consisting of membrane-enclosed magnetite crystals that are thought to direct bacterial swimming towards growth-favoring microoxic zones at the bottom of natural waters.[28] The magnetosome membrane is comprised of phospholipids and a specific set of proteins[29, 30] and it therefore offers a large biocompatible surface, which is accessible for synthetic chemical manipulations for the attachment of artifical functional moieties.[31, 32]

We report here the modification of biogenic magnetosome particles, 1, by a modular synthetic chemical approach (Figure 1). Initially, biotin groups were coupled to the magnetosome membrane of MPs produced by the magnetotactic bacterium Magnetospirillum gryphiswaldense; these MPs are 38 nm in size (mature crystals), have cuboctahedral shapes, and have a monocrystalline core consisting of magnetite.[29, 33] Two different strategies were used, namely, the incorporation of the biotinylated lipid biotin-DPPE, 2, or the covalent modification of the proteins within the magnetosome membrane by using NHS-biotin, 3.[34] After this, the membrane-bound biotin groups of the resulting MPs 4a and 4b were used for attachment of the protein streptavidin (STV, 5), thereby leading to STV-functionalized MPs 6a and 6b, respectively. The resulting biotin-binding capacity of particles 6 was then used for

116

the attachment of functional biomolecular entities, such as biotinylated DNA oligonucleotides (7 and 8 for DNA sequences; see Table 1) and/or biotinylated antibodies (9). The resulting MPs, 10–14, were evaluated for their suitability to serve as probes for the detection of complementary targets, nucleic acids, and proteins that are specifically recognized by the MP-bound DNA oligomers or antibodies, respectively.

Table 1. Oligonucleotide sequences used in this study.

Compound	Sequence
7	5'-biotin-TCC TGT GTG AAA TTG TTA TCC GCT-3'
8	5'-GCA CTT GAG AGC (dT12)-biotin-3'
linker 17	5'-GCT CTC AAG TGC GAT CTC TTC ACC-3'
15	5'-SH-(dT12) GGT GAA GAG ATC-3'

In the course of the chemical modification of the MPs, summarized in Figure 1, we investigated the biotinylation rate of MPs 4, the number of DNA moieties attached to MPs 10, and the hybridization capacities of 10, by using fluorescence-based assays,[34] similarly to previously described procedures.[35, 36] For example, for the determination of the DNA moieties attached to MPs 10a and 10b, doubly labeled 5'-biotin, 3'-Cy5 oligonucleotides 7 were coupled to either MPs 6a and 6b. After removal of unbound DNA oligomers and repeated magnetic separation/redispersion, the fluorescence of the Cy5-labeled MPs 10a and 10b was measured with a fluorimeter, and the fluorescence signals of Cy5 (measured at 670 nm) were converted into molar concentrations of the Cy5-modified oligonucleotide by using a standard linear calibration curve.[34] The results, summarized in Table S1 in the Supporting Information, indicated that the functionalization of the MPs by means of the biotin-DPPE route led to about two-to threefold higher surface coverages with STV and oligonucleotides than those obtained by the NHS-based biotinylation route. On average, about 120 and 40 STV molecules were bound to 6a and 6b, respectively. Notably, the reproducibility was lower in the case of 6a, a fact suggesting that the lipid modification was accompanied by aggregation mediated by the magnetosome membrane of the MPs, as discussed below. Independently of the biotinylation method, the number of oligonucleotides bound per MP was about 1.5–2-fold higher than the number of STV molecules, which suggests that each STV molecule was bound preferentially to just a single biotin moiety present on the magnetosomes. The DNA-hybridization capacities of particles 10 were found to be about 45% for both biotinylation routes (Table S1 in the Supporting Information). It should be noted that this hybridization

capacity is in good agreement with that observed for DNA-modified gold nanoparticles (DNA–AuNPs) of about 5–45 % depending on the oligonucleotide length and surface coverage.[35]
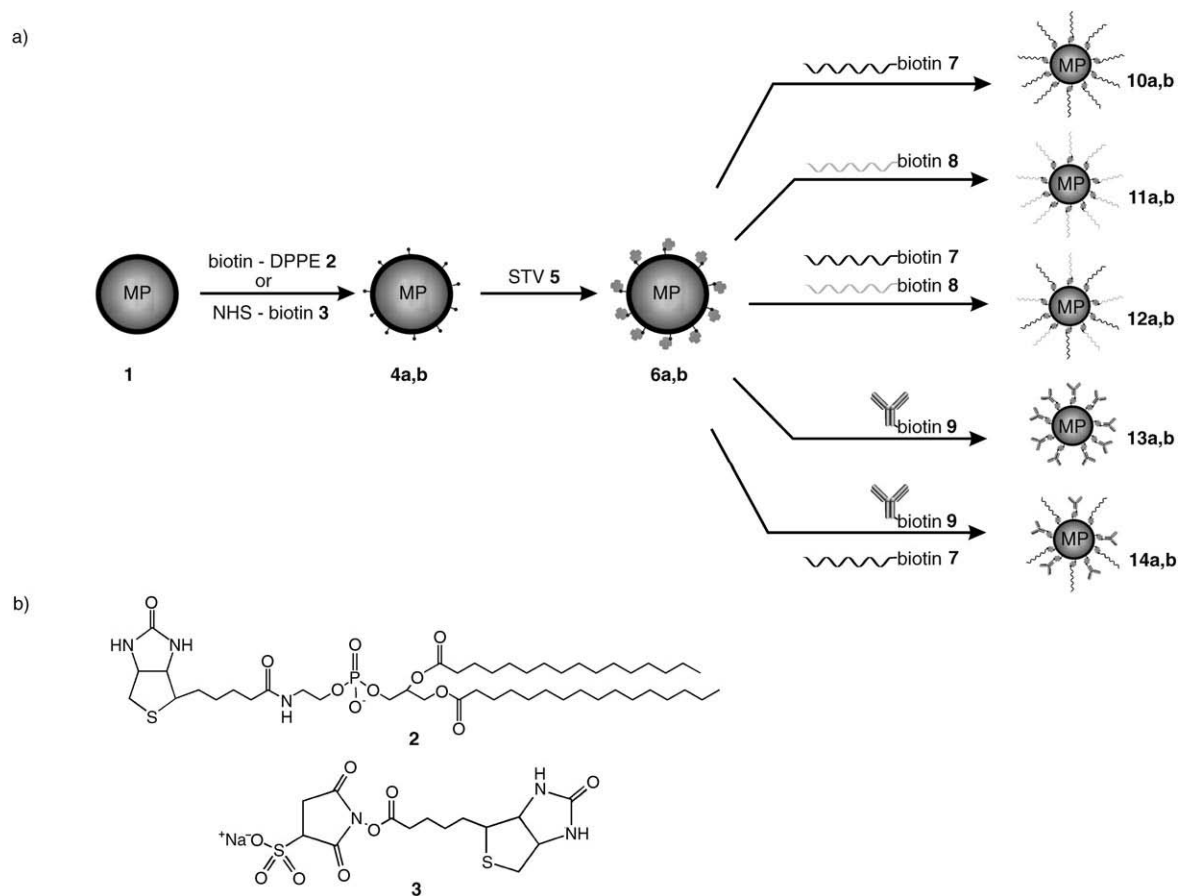

Figure 1. a) Schematic drawing of the preparation of oligofunctional DNA-and/or protein-modified magnetosome particles. Biotin groups were attached to the magnetosome membrane of MPs 1 either by incorparation of [1,2-dipalmitoyl-sn-glycero-3-phosphoethanolamine-N-(biotinyl) (sodium salt)] (biotin-DPPE, 2) or by the covalent modification of the proteins within the magnetosome membrane by using sulfo-N-hydroxysuccinimide ester sodium salt (NHS-biotin, 3). Magnetosomes modified with 2 are labeled a, while magnetosomes modified with 3 are labeled b. The surface-bound biotin groups of the resulting MPs 4a and 4b were used to bind streptavidin (STV, 5), and the resulting STV-functionalized MPs 6a and 6b were functionalized with biotinylated DNA oligomers 7 and 8 and/or antibody 9. b) Chemical structures of the biotinylated modifiers 2 and 3.

To evaluate the functionality of the DNA–MP conjugates, particles 11a and 11b were allowed to hybridize with gold nanoparticle conjugates (DNA–AuNP 16), prepared from thiolated oligonucleotide 15 (for oligonucleotide sequence, see Table 1) and citrate-stabilized gold nanoparticles,[34, 36] together with the complementary DNA linker 17 (for oligomer sequence, see Table 1) to facilitate aggregation of heterodimeric aggregates comprised of the AuNPs and the MPs. Spectroscopic analysis of the hybridization showed the characteristic red

shift and damping of the AuNPs plasmon absorption band, thus confirming that the oligomer moities of 11 a and 11 b were indeed capable of binding complementary targets (see Figure S2 in the Supporting Information). Precipitated MP–AuNP hybrid materials, formed from 38-nm MP 11b and 11-nm DNA–AuNP 16, were also investigated by transmission electron microscopy (TEM). To this end, the binary particle aggregates were purified by magnetic separation to remove unbound AuNPs from the solution, before the aggregates were resuspended and immobilized on the TEM grids. Typical TEM images of the binary particle aggregates are shown in Figure 2. The presence of extended three-dimensional aggregates of two different-sized particles can be clearly observed (Figure 2a).

Due to the specificity of DNA hybridization, we expected a periodic heterodimeric structure of the nanoparticle networks, as was observed previously in the aggregation of different-sized DNA–AuNPs by Mirkin and co-workers.[37] Although satellite-like structures were observed in some areas of the TEM images (Figure 2c), the hybrid structures, in general, revealed only a low degree of order. Nonetheless, in comparison to the control experiment lacking linker 17 (Figure 2 d), the increased amount of small AuNPs bound to the larger MPs clearly indicated successful formation of binary nanoparticle networks. We reasoned that this result might be caused by some irreversible aggregation, possibly associated with a cohesion of the magnetosome membrane of the MPs occurring during the conjugate synthesis and magnetic purification steps. Indeed, dynamic light-scattering measurements revealed a slight increase in the hydrodynamic diameter of the MPs subsequent to their conversion into DNA–MP conjugates, regardless of the synthesis route (Figure S3 in the Supporting Information). These results supported our assumption that the MPs were partially aggregated and the formation of small aggregates of MPs might interfere with the formation of ordered binary network structures upon hybridization with DNA– AuNPs.
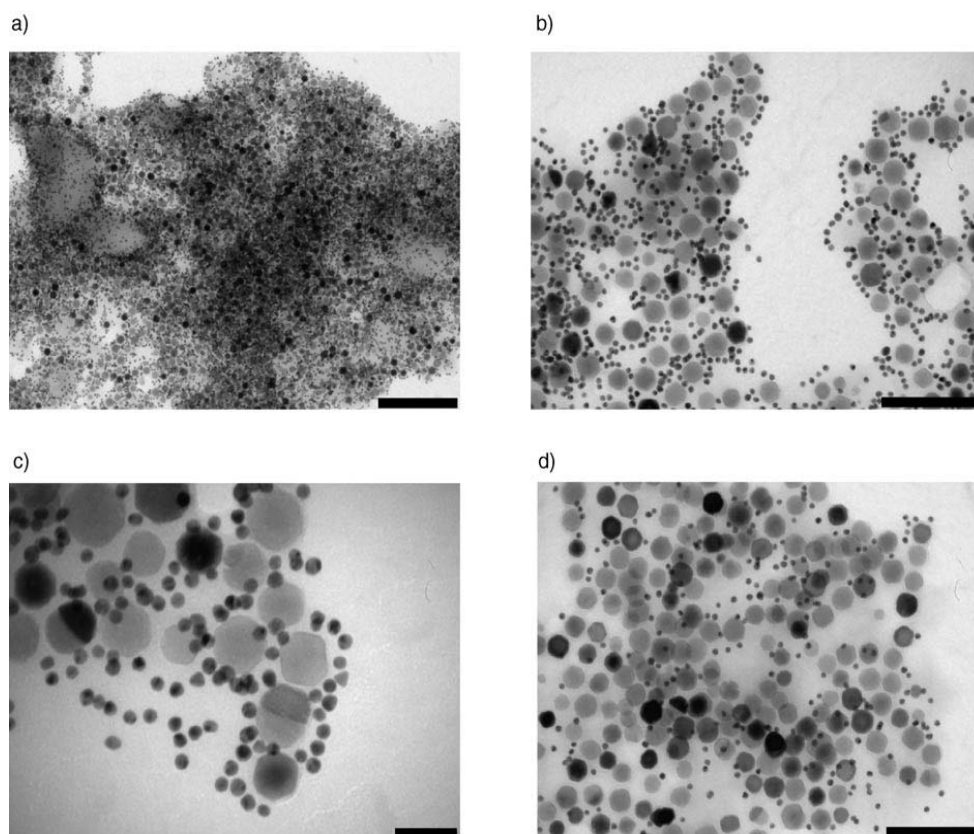
Figure 2. **TEM images of binary network aggregates obtained from DNA-linked MP11b (38 nm in diameter) and DNA–AuNP16 (11 nm in diameter) connected by a complementary DNA linker oligonucleotide.** A control sample lacking the linker is shown in d). Scale bars: a) 500 nm; b) and d) 200 nm; c) 50 nm.

To further elucidate functionality, STV-modified MPs 6a were converted into difunctional DNA conjugates 12a by coupling an equimolar ratio of two biotinylated oligonucleotides, 7 and 8, similarly to the procedure described previously for the preparation of di-and oligofunctional DNA– AuNPs.[36] Here, the resulting DNA–MPs 12 were used in a solid-phase DNA-directed immobilization assay (Figure 3a), such that particle-bound oligomer 7 was used to facilitate binding to complementary capture oligomers bound to a microtiter plate, while the second particle-bound oligomer 8 was used for generating a layer of AuNPs through hybridization with AuNP conjugate 16 by means of the complementary DNA linker 17. We had previously used a similar assay for the study of difunctional DNA–AuNPs.[38] Subsequent to the formation of the AuNP layer, a silver development step was carried out for signal detection. As shown in Figure 3b, photometric measurements of the precipitated silver revealed that layer formation led to an increase in absorbance at 490 nm. Control experiments lacking the DNA linker oligomer 17 showed no such increase in absorbance. Therefore, these results confirm the specificity of DNA hybridization of the bifunctional DNA–MP conjugates.

To take advantage of the modular concept of our synthesis (Figure 1 a), we also investigated whether proteins can be bound to the STV-tagged MPs 6. To this end, 6a was incubated with a mixture containing equimolar ratios of biotinylated DNA 7 and biotinylated antibody anti-mouse immunoglobulin G (IgG, 9). This led to the formation of the difunctional MP conjugate 14a, which was then employed for the detection of mouse IgG, used as a model antigen in a sandwich immunoassay (Figure 4a). To this end, known amounts of the antigen were first immobilized on microplates by using physisorbed capture antibodies (polyclonal anti-mouse IgG) and, subsequently, 14 a was allowed to bind to the immobilized antigens. The DNA oligomers of the difunctional MP conjugate 14a were then utilized to capture DNA–STV–alkaline phosphatase conjugate 19 by means of specific DNA hybridization. Signal detection was carried out by the addition of the fluorogenic alkaline phosphatase substrate Attophos and fluorescence measurements (Figure 4a). While high signal intensities indicated the successful binding of the antigen in the case of 14 a, no such result was observed in the control experiments carried out with monofunctional MP conjugates, containing either only biotinylated anti-mouse IgG (MP 13a) or only biotinylated DNA oligomer 7 (MP 10a). These results again confirmed the successful functionalization of the magnetosomes by our chemical-modificiation approach.
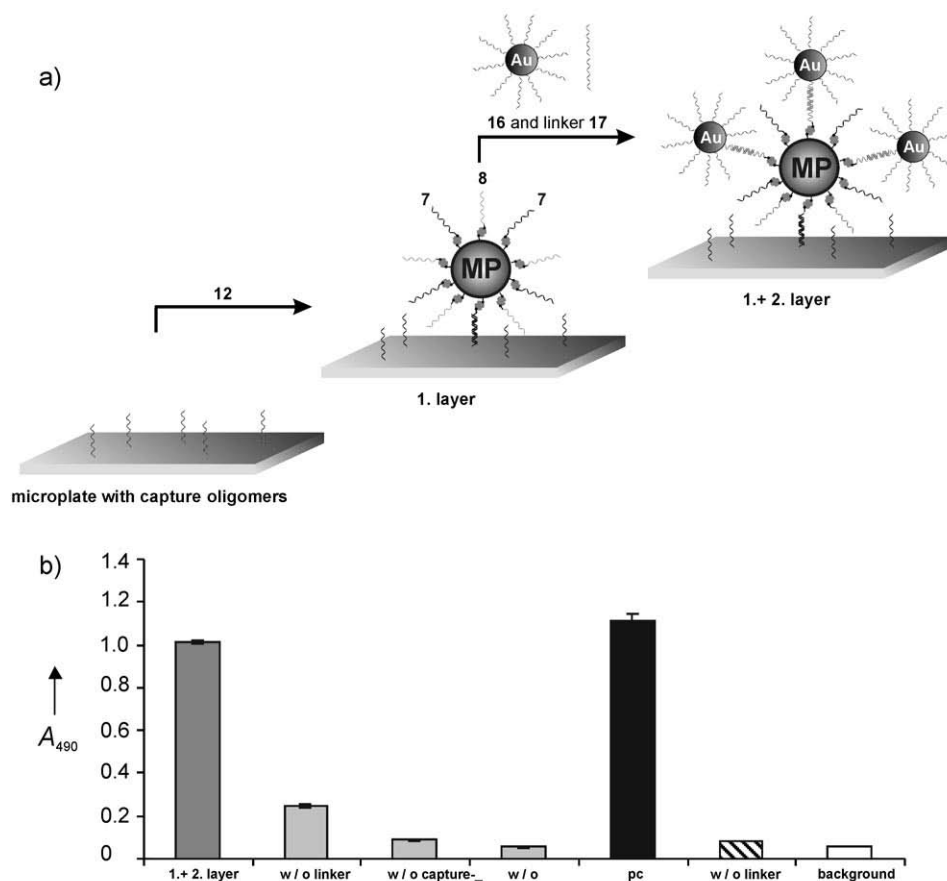
Figure 3. DNA-directed generation of a surface-bound double layer by using difunctional DNA–MPs and monofunctional DNA–gold nanoparticle conjugates on a microplate. a) Schematic drawing of the assay. A surface-bound magnetosome layer was generated by hybridization of the particle-bound sequence 7 of difunctional MP 12a to biotinylated complementary capture oligomers immobilized on STV-coated microplates. The magnetosome-bound sequence 8 of the immobilized MP 12a was then used for binding of DNA–AuNPs 16 through linker oligomer 17. The immobilization of DNA–AuNPs to the first layer was detected by absorbance measurements at 490 nm subsequent to silver enhancement. The drawing is not to scale. b) Signal intensities after the silver enhancement. The darkgray bar on the left side corresponds to the signal obtained by hybridization of MP 12, linker 17, and DNA–Au conjugate 16. The three light gray bars show the signal intensities of various negative controls, namely, the hybridization procedure in the absence of linker 17, capture oligomers, or MP 12, respectively. The blackbar demonstrates the signal intensity of a positive control reaction, in which 16 was directly immobilized in the absence of MP 12 through linker 17 by using biotinylated capture oligomer 8 attached to the STV microplate. The hatched blackbar represents the signal intensity of the immobilization of 16 without linker oligomer 17. The white bar represents the background signal of the silver solution.
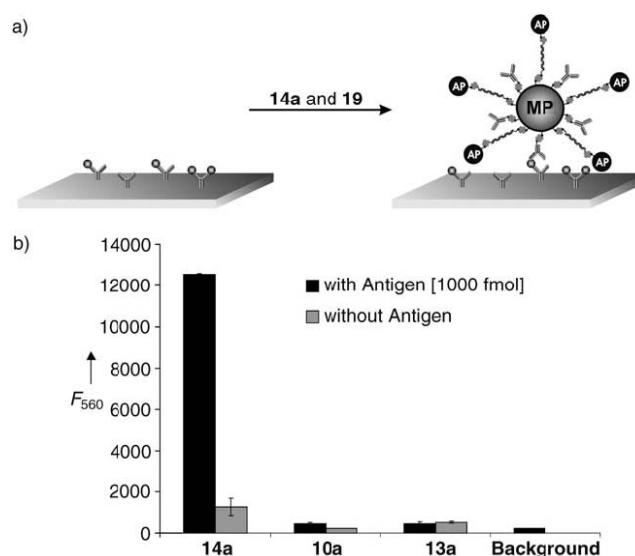
Figure 4. Utilization of antibody/DNA-functionalized biogenic MPs as reagents in a sandwich immunoassay. a) Schematic drawing. The antigen (mouse IgG, represented by gray spheres) was bound by surface-attached capture antibodies through specific immunosorption on a microplate. Subsequently, immobilized antigen was labeled with anti-mouse-IgG-functionalized MP 14a. The magnetosomebound DNA oligomer 7 of MP 14a was then used for binding of a complementary DNA–STV–alkaline phosphatase conjugate 19, which comprises DNA–STV conjugate 18 and biotinylated alkaline phosphatase. Subsequent to the binding of MP 14a to the immobilized antigens, Attophos was added as the alkaline phosphatase substrate for fluorescence signal detection. MP 14a and 19 were mixed before they were added to the immobilized antigens on the microplate. The drawing is not to scale. b) Fluorescence signal intensities obtained in the immunoassay. Signal intensities were only observed in the presence of difunctional MP 14a, whereas no signals were generated in the presence of monofunctional magnetosomes 11 or 13.

In conclusion, we have reported here the modular functionalization of biogenic magnetosome nanoparticles isolated from the magnetotactic bacterium *M. gryphiswaldense.* Based on either covalent or noncovalent modification of the magnetosome membrane with biotin moieties and employment of streptavidin as a connector, DNA oligonucleotides were bound the magnetosomes, thus leading to semisynthetic hybrid particles with specific binding capabilities for complementary DNA. The DNA–magnetosome conjugates were successfully used as reagents in a protein detection assay, and we anticipate further developments of such particles for the analysis of protein microarrays, which are increasingly important in immunological diagnostics and proteome research.[39] Moreover, because magnetosome biomineralization in magnetotactic bacteria is under genetic control, magnetosome particles of different sizes and shapes[40] or functionalized magnetosomes displaying heterologous fusion proteins can be generated by genetic engineering.[28,41] One may also envision the development of new classes of biogenic nanoparticle probes with applications in bioanalytics,

imaging, and other fields of nanobiotechnology.

References

[1] A. K. Gupta, M. Gupta, Biomaterials 2005, 26, 3995 –4021.

[2] A. Ito, M. Shinkai, H. Honda, T. Kobayashi, J. Biosci. Bioeng. 2005, 100, 1 –11.

[3] G. Reiss, A. Hutten, Nat. Mater. 2005, 4, 725–726.

[4] J. M. Perez, L. Josephson, T. O'Loughlin, D. Hogemann, R. Weissleder, Nat. Biotechnol. 2002, 20, 816–820.

[5] J. M. Nam, C. S. Thaxton, C. A. Mirkin, Science 2003, 301, 1884–1886.

[6] H. Gu, K. Xu, C. Xu, B. Xu, Chem. Commun. 2006, 941–949.

[7] J. Wang, G. Liu, A. Merkoci, J. Am. Chem. Soc. 2003, 125, 3214–3215.

[8] J. M. Perez, T. O'Loughlin, F. J. Simeone, R. Weissleder, L. Josephson, J. Am. Chem. Soc. 2002, 124, 2856–2857.

[9] E. A. Schellenberger, D. Hogemann, L. Josephson, R. Weissleder, Acad. Radiol. 2002, 9 (Suppl 2), S310 –S311.

[10] R. Weissleder, A. Moore, U. Mahmood, R. Bhorade, H. Benveniste, E. A. Chiocca, J. P. Basilion, Nat. Med. 2000, 6, 351–355.

[11] H. W. Kang, L. Josephson, A. Petrovsky, R. Weissleder, A. Bogdanov, Jr., Bioconjugate Chem. 2002, 13, 122–127.

[12] E. Katz, L. Sheeney-Haj-Ichia, A. F. Bckmann, I. Willner, Angew. Chem. 2002, 114, 1399 –1402; Angew. Chem. Int. Ed. 2002, 41, 1343–1346.

[13] L. Sheeney-Haj-Ichia, E. Katz, J. Wasserman, I. Willner, Chem. Commun. 2002, 158–159.

[14] Y.Weizmann, F. Patolsky, E. Katz, I. Willner, ChemBioChem 2004, 5, 943–948.

[15] E. Katz, R. Baron, I. Willner, J. Am. Chem. Soc. 2005, 127, 4060–4070.

[16] D. L. Graham, H. A. Ferreira, P. P. Freitas, Trends Biotechnol. 2004, 22, 455–462.

[17] U. Schoepf, E. M. Marecos, R. J. Melder, R. K. Jain, R. Weissleder, Biotechniques 1998, 24, 642–651.

[18] D. Hoegemann, L. 110–114; Josephson, R. Weissleder, J. P. Basilion, Bioconjugate Chem. 2000, 11, 941 –946.

[19] D.Hoegemann, V. Ntziachristos, L. Josephson, R. Weissleder, Bioconjugate Chem. 2002, 13, 116–121.

[20] Y. M. Huh, Y. W. Jun, H. T. Song, S. Kim, J. S. Choi, J. H. Lee, S. Yoon, K. S. Kim, J. S. Shin, J. S. Suh, J. Cheon, J. Am. Chem. Soc. 2005, 127, 12387–12391.

[21] E. T. Ahrens, R. Flores, H. Xu, P. A. Morel, Nat. Biotechnol. 2005, 23, 983–987.

[22] A. Jordan, R. Scholz, P. Wust, H. Fhling, J. Magn. Magn. Mater. 1999, 201, 413–419.

[23] A. Jordan, R. Scholz, P. Wust, T. Schiestel, H. Schmidt, R. Felix, J. Magn. Magn. Mater. 1999, 194, 185–196.

[24] M. Johannsen, U. Gneveckow, L. Eckelt, A. Feussner, N. Waldofner, R. Scholz, S. Deger, P. Wust, S. A. Loening, A. Jordan, Int. J. Hyperthermia 2005, 21, 637–647.

[25] D. Schüler, R. B. Frankel, Appl. Microbiol. Biotechnol. 1999, 52, 464–473.

[26] D. A. Bazylinski, R. B. Frankel, Nat. Rev. Microbiol. 2004, 2, 217–230.

[27] B. M. Moskowitz, Rev. Geophys. 1995, 33, 123 –128.

[28] A. Scheffel, M. Gruska, D. Faivre, A. Linaroudis, J. M. Plitzko, D. Schüler, Nature 2006, 440, 110-114 corrigendum: A. Scheffel M. Gruska, D. Faivre, A. Linaroudis, P. L. Graumann, J. M. Plitzko, D. Schüler, Nature 2006, 441, 248.

[29] K. Grünberg, E. C. Müller, A. Otto, R. Reszka, D. Linder, M. Kube, R. Reinhardt, D. Schüler, Appl. Environ. Microbiol. 2004, 70, 1040–1050.

[30] A. Komeili, Z. Li, D. K. Newman, G. J. Jensen, Science 2006, 311, 242–245.

[31] N. Nakamura, J. G. Burgess, K. Yagiuda, S. Kudo, T. Sakaguchi, T. Matsunaga, Anal. Chem. 1993, 65, 2036–2039.

[32] Y. Amemiya, T. Tanaka, B. Yoza, T. Matsunaga, J. Biotechnol. 2005, 120, 308–314.

[33] U. Heyen, D. Schüler, Appl. Microbiol. Biotechnol. 2003, 61, 536–544.

[34] Detailed experimental protocols for the biotinylation and STV modfication of MPs, the determination of the surface coverage of DNA-containing MPs, the DNA-directed immobilization, and the immunoassay are available in the Supporting Information.

[35] L. M. Demers, C. A. Mirkin, R. C. Mucic, R. A. Reynolds, R. L. Letsinger, R. Elghanian, G. Viswanadham, Anal. Chem. 2000, 72, 5535–5541.

[36] C. M. Niemeyer, B. Ceyhan, P. Hazarika, Angew. Chem. 2003, 115, 5944–5948; Angew. Chem. Int. Ed. 2003, 42, 5766– 5770.

[37] R. C. Mucic, J. J. Storhoff, C. A. Mirkin, R. L. Letsinger, J. Am. Chem. Soc. 1998, 120, 12674–12675.

[38] P. Hazarika, B. Ceyhan, C. M. Niemeyer, Small 2005, 1, 844– 848.

[39] M. F. Templin, D. Stoll, M. Schrenk, P. C. Traub, C. F. Vohringer, T. O. Joos, Trends Biotechnol. 2002, 20, 160–166.

[40] Experiments carried out with smaller MPs (diameter of (29+-1) nm) produced from mutant strain MSR-1K of magnetotactic bacteria confirmed that the modification procedures described here led to similar DNA–MP conjugates with similar functionality. Typical surface

coverages and microplate binding assays are shown in Table S1 and Figures S4 and S5, respectively, in the Supporting Information.

[41] T. Yoshino, T. Matsunaga, Appl. Environ. Microbiol. 2006, 72, 465–471

Manuscript 4

Magneto Immuno-PCR: A homogeneous immunossay based on biogenic

magnetosome nanoparticles

Ron Wacker[1], Bülent Ceyhan,[2] Petra Alhorn,[2] Dirk Schüler,[3] Claus Lang,[3] and
Christof M. Niemeyer[2]*

[1] Dr. R. Wacker, Chimera Biotec GmbH, Emil-Figge-Str. 76A, D-44227 Dortmund

[2] Prof. Dr. C. M. Niemeyer, Dr. B. Ceyhan, P. Alhorn, Universität Dortmund, Fachbereich
Chemie, Biologisch-Chemische Mikrostrukturtechnik, Otto-Hahn Str. 6, D-44227 Dortmund

[3] Dipl. Biol. C. Lang, PD Dr. D. Schüler, Max-Planck Institut für marine Mikrobiologie,
Abteilung Mikrobiologie, Celsiusstrasse 1, D-28359 Bremen

[*] corresponding author: christof.niemeyer@uni-dortmund.de

Abstract:

We describe an innovative modification of the Immuno-PCR technology for automatable high sensitive antigen detection. The Magneto-Immuno-PCR (M-IPCR) is based on antibody-functionalized biogenic magnetosome nanoparticles revealing major advantages over synthetic magnetic particles. The general principle of the M-IPCR is similar to that of a two-sided (sandwich) immunoassay. However, antibody-functionalized magnetosome conjugates were employed for the immobilization and magnetic enrichment of the signal generating detection complex enabling the establishment of a surface independent immunoassay. To this end, the M-IPCR was carried out by simultaneously tagging the antigen with the reagent for read-out, i.e., a conjugate comprising the specific antibody and DNA fragments, in the presence of the antibody-functionalized magnetosomes. To demonstrate the general functionality of the M-IPCR, the detection of recombinant Hepatitis B surface Antigen (HBsAg) in human serum was established. We observed a detection limit of 320pg/ml of HBsAg using the M-IPCR, which was about 100-fold more sensitive than the analogous Magneto-ELISA, established in parallel for comparison purposes.

Keywords: Immuno PCR · Real-time Immuno-PCR · Biomarker · Magnetosome · Hepatitis B · Automatization · Protein Analytics

Introduction:

In the field of clinical diagnostics a biomarker is defined as any biochemical compound, for instance a protein, which can be used to accurately and sensitively monitor health status or diagnose the progress of disease and the effects of treatment of individuals.[1, 2] Furthermore in various fields of interest, such as agriculture,[3] drug development[4] or doping control,[5] the detection of biological markers are of fast growing importance. Currently researchers spend more and more time to identify proteins in human body, animals or plants as markers for specific physiological conditions of organisms. This increasing effort in research is reflecting the need for new biomarkers facing the requirements of today's fast growing biotechnological and pharmaceutical industry.[4, 6] To support these requirements, novel technologies are needed allowing for the precise detection and quantification of this new challenging generation of biomarkers, which may occur in very low concentrations within complex biological matrices.[7-10]

Immuno-PCR (IPCR), first described by Sano et al.,[11] has nowadays evolved to an established methodology for the ultra sensitive analysis of biomarkers.[12] IPCR combines the

standard ELISA technology with the signal amplification power and fast read-out of the real-time PCR. As the consequence, IPCR not only does lead to a 100- to 10,000-fold gain in sensitivity compared to conventional ELISA,[13-15] but it also reveals a very broad linear dynamic range of up to five orders of magnitude.[14, 16] Additional advantages of IPCR include minimized sample volume requirements, high tolerances against drug and matrix effects and its adaptability for the detection of basically any antigen.[17]

To further increase the performance of IPCR as a standard laboratory routine, reduction and automation of the various assay steps is an important goal, and the use of magnetic nanoparticles (MPs) may provide a solution for the establishment of automated one-step immunoassays.[18-20] Key requirements for the efficient use of such MPs comprise their uniform size and morphology, biocompatibility and high magnetization capabilities. To address these issues, we have recently developed biogenic bacterial magnetosome particles, derived from the magnetotactic bacterium *Magnetospirillum gryphiswaldense*, which were modified with oligonucleotides and antibodies by synthetic chemical means.[21] These magnetosome conjugates have a number of advantages over conventional synthetic MP. Magnetosomes are membrane-enveloped magnetite crystals which are formed intracellulary via a genetically controlled biomineralization process. This ensures uniform particle shape and a narrow size distribution. The ferrimagnetic single magnetic domain particles possess a high magnetic susceptibility, in addition mutants producing smaller, superparamagnetic particles are available.[22][23, 24]

We here report on the development on the development of an IPCR variant, called Magneto Immuno-PCR (M-IPCR), which is based on the chemically modified magnetosome nanoparticles, bearing streptavidin molecules at the magnetosome membrane.[21] To elucidate the performance of M-IPCR we chose the detection of recombinant Hepatitis B surface Antigen (HBsAg) in human serum as model system. The general scheme of this assay is based on a two-sided (sandwich) immunoassay (Figure 1). However, while in standard immunoassays the capture antibodies are typically bound to the solid-phase, we here used antibody-functionalized biogenic magnetosome particles as the capture phase. The particles were mixed with the commercially available DNA-anti HBsAg antibody conjugate directly within the biological matrix (i.e., blood serum), and subsequent to the formation of the detection complex, the magnetosomes were collected using an external magnetic field.
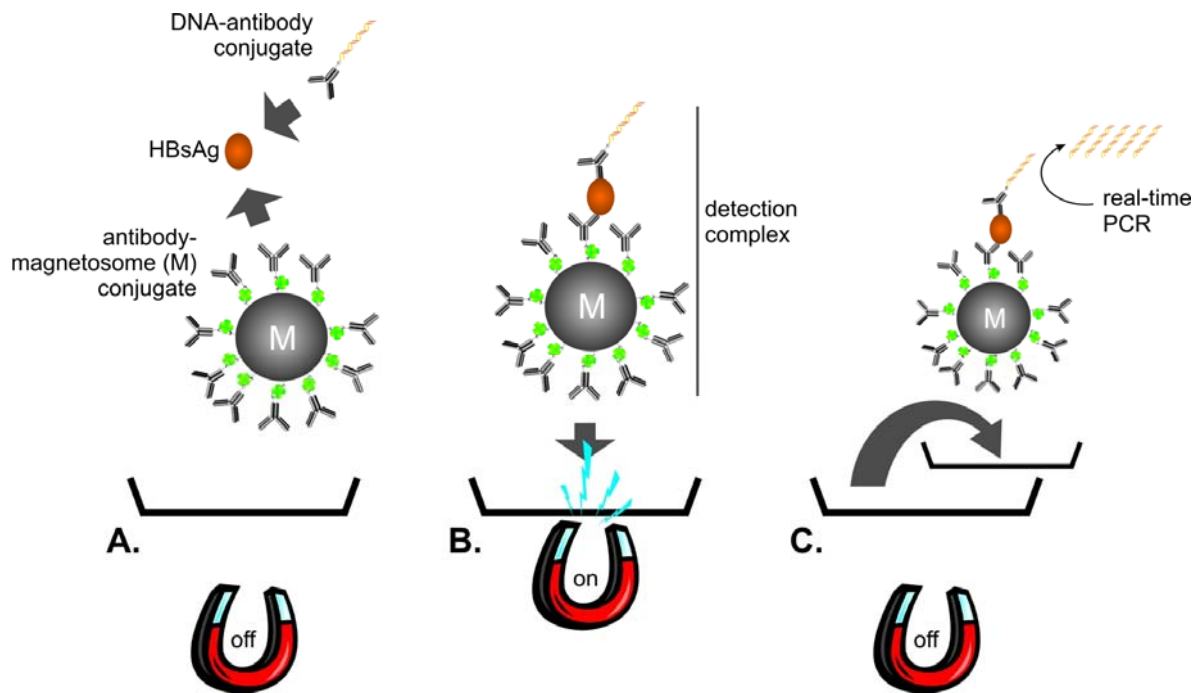
Figure 1: Schematic drawing of the Magneto Immuno-PCR (M-IPCR). **A**: HBsAg specific magnetosome-antibody conjugate and DNA-antibody conjugate are incubated simultaneously with the serum sample containing HBsAg resulting in a signal-generating immunocomplex. **B**: The immunocomplex is concentrated using an external magnetic field. Subsequent washing steps permit the removal of unbound materials. **C**: After resuspension, a defined volume of the magnetosome solution is transferred to a microplate containing the PCR mastermix to enable real-time PCR detection of the immobilized antigen.

In a first step, we established a Magneto-ELISA (M-ELISA) protocol as the model system for evaluation of the magnetosome properties. Therein the DNA-antibody conjugate was exchanged against an antibody-alkaline-phosphatase conjugate, thus allowing for the direct comparison of the two assays. Moreover, to evaluate the M-IPCR in a wider context, we compared our magnetosome-based capture phase with commercial magnetic microbeads which were functionalized with the respective antibody. Both M-IPCR were compared to each other as well as to the analogous M-ELISA with respect to sensitivity, linearity, standard deviation and recovery rates.

Results and Discussion:

To facilitate the M-IPCR, streptavidin (STV)-functionalized magnetosomes were used to prepare the capture phase using the convenient coupling with biotinylated antibodies. Synthesis and purification of the STV-functionalized magnetosomes was carried out as previously described.[21] In brief, the magnetosome membrane was initially biotinylated using NHS-biotin, and the membrane-bound biotin groups were then used to bind the STV. The STV-functionalized magnetosomes were coupled with biotinylated anti-HBsAg antibody and

the resulting particles were washed using magnetic separation (see Experimental section). The M-IPCR assay was carried out in microplates to which, subsequent to incubation, a magnetic rack was attached to facilitate the magnetic collection of the particles.

A first set of experiments was carried out to establish a general protocol for the assay schematically depicted in Figure 1. Serial dilutions of samples containing the antigen, recombinant HBsAg, spiked in standardized human serum, were divided into two aliquots. One aliquot was mixed with the commercial anti-HBsAg Imperacer™ conjugate for real-time Immuno-PCR (hereafter termed as M-IPCR) and the other with alkaline-phosphatase (AP)-antibody conjugate for fluorescence detection (hereafter termed as M-ELISA). Subsequent to incubation of the mixtures for 30 min, antibody-functionalized magnetosomes were added to the aliquot, incubated for 60 min and concentrated at the bottom of the microplate wells using the magnetic rack. The particles were briefly washed and resuspended in 50 µl ddH$_2$O, and aliquots of 1 µl, 5 µl or 10 µl were transferred to another microplate containing the PCR mastermix to carry out real-time PCR. For M-ELISA, the fluorescence substrate AttoPhos (Roche) was added to some of the transferred aliquots in the second microplate, and a fluorescence was determined at λ = 560 nm using a microplate reader.

As shown in **Figure 2**, quantification of the signals revealed a limit of detection for M-IPCR (**Figure 2A**) of 320 pg/ml for 1 µl and 5 µl of transferred volumes and 1.6 ng/ml for 10 µl. The main reason for these findings is the standard deviation (SD). The average SD of 2.3% (1 µl) and 1.0% (5 µl) in the assays carried out with the lower volumes transferred enabled a higher sensitivity than with larger volumes transferred (10 µl) which showed an SD of 10.9%. In comparison, the M-ELISA (**Figure 2B**) revealed an optimal detection limit of 40 ng/ml for all three volumes transferred and average SDs of 8.3% (1 µl), 14.2% (5 µl), and 13.3% (10 µl), respectively. Therefore, an about 125-fold increase in sensitivity was observed for the M-IPCR as compared to M-ELISA. These results demonstrate that the increase in sensitivity, typically obtained by using Immuno-PCR instead of the analogous ELISA,[12] could also be achieved with this IPCR variant.

The reason for the increased error rates in the M-IPCR at larger transfer volumes is likely a consequence of inhibitory effects of the magnetosomes on the PCR amplification. This hypothesis arose from a control experiment in which the PCR mastermix was directly added to the washed and dried detection complex. No quantifiable signals along with very high standard deviations were observed in this case for M-IPCR. In contrast, no significant influence was observed for M-ELISA (data not shown). Therefore, transfer volumes of 5 µl

appeared to be the optimal compromise between the increase in PCR template concentration and the minimization of the inhibitory effects of the magnetosomes.

We also investigated whether the use of biogenic magnetosomes is advantageous over the use of synthetic magnetic beads in our M-IPCR assay. Using the same protocol for M-IPCR (5 µl transfer volume) we, thus, exchanged the antibody-functionalized magnetosomes with antibody-functionalized commercial STV-coated magnetic beads (Roche).
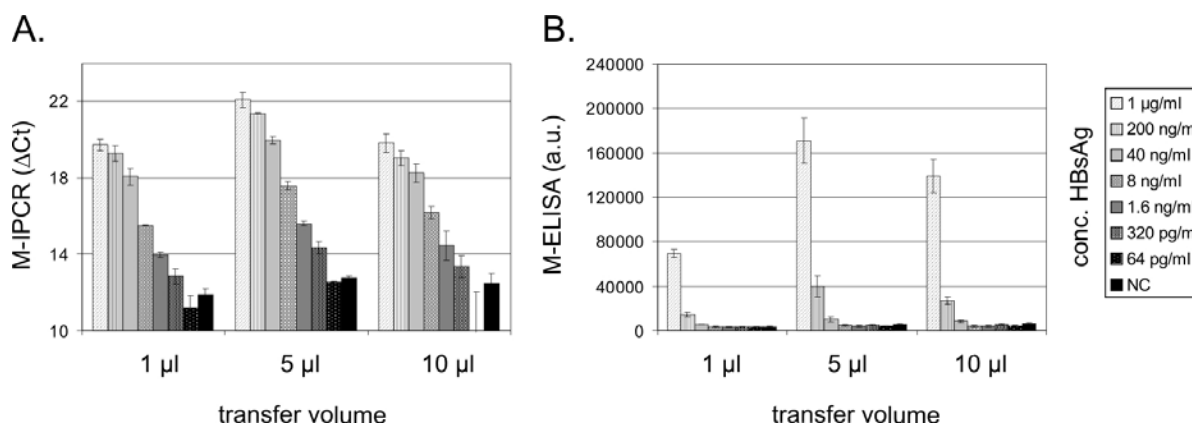

Figure 2: Magneto Immuno-PCR (M-IPCR, **A**) and Magneto ELISA (M-ELISA, **B**) for the detection of Hepatitis B surface Antigen (HBsAg) in human serum samples. While both technologies are functional the M-IPCR shows a maximum sensitivity of 320 pg/ml compared to 40 ng/ml in M-ELISA. Different volumes of 1 µl, 5 µl or 10 µl of the resuspended magentosomes (see **Figure 1**) were used for real-time PCR (M-IPCR) or fluorescence detection (M-ELISA).

As shown in **Figure 3**, the use of biogenic magnetosomes revealed a 25-fold increased sensitivity of 320 ng/ml, compared to the limit of detection (LOD) of 8 ng/ml HBsAg in standardized human serum using the commercial beads. The LOD is typically defined as the value of NC to which three times the value of the average standard deviation (SD) is added. Here, the average percentage SD for the M-IPCR using biogenic magnetosomes was only 0.9%. Thus, the cut off value for the LOD calculates to $DC_t = 13.20$. The magnetic microbeads, in contrast, showed an average SD of 2.2% and a cut-off $DC_t = 15.71$. This result was mainly due to the reduced signal to noise ratio and a slight increase in average SD in the case of the magnetic beads. However, both techniques showed linear regressions with $R^2 = 0.99$ (biogenic magnetosomes) and $R^2 = 0.98$ (magnetic particles). The use of magnetosomes resulted in a linear dynamic range of quantification for 200 ng/ml-320 pg/ml). In contrast, the magnetic microbeads only revealed a linear dynamic range of quantification of 200-8 ng/ml. Comparable results were obtained in M-ELISA (Data not shown). Furthermore, the recovery rates were calculated using the linear regression of the spiked serum samples.

The individual recovery rates determined by this method are listed in Table 1. Biogenic magnetosomes revealed average recovery rates of 103% ± 22% while this value was 105% ± 33% for the magnetic microbeads. These results, again, confirmed the good performance of the M-IPCR protocol using biogenic magnetosomes.

The initial results reported here clearly demonstrate that the biogenic magnetosomes posses a higher performance than long established synthetic magnetic microbeads. Most likely, this enhanced performance results from their smaller size, monodispersity, and higher magnetization [21,23]. However, the use of the biogenic magnetosomes also showed some disadvantages during the handling steps of the assay. In particular, a limited tolerance against detergents, high salt concentrations and repeated centrifugation steps was observed, which most likely stems from the limited stability of the magnetosome's biological membrane [21]. Nonetheless, the protocol reported here overcomes these limitations and further optimization of the production and modification processes of the magnetosomes should further increase the scope of applications of these biological nanoparticles [21].
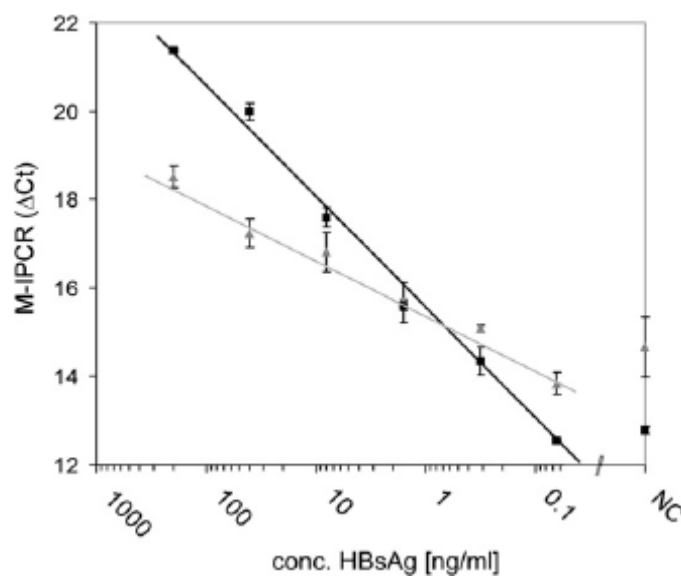
Figure 3: Comparison of Magneto Immuno-PCR (M-IPCR) using the biogenic magnetosomes (black squares) or commercial magnetic beads (gray triangles). Both techniques showed linear regressions. The use of magnetosomes resulted in improved limit of detection (LOD) with 320 pg/ml and decreased standard deviations. This led to a 25-fold higher sensitivity, compared to the magnetic beads. The microbeads showed and LOD if 8 ng/ml.

Table 1: Average recovery rates (%) for HBsAg were re-calculated by using the linear regression and the spiked serum samples of the calibration curve.

	M-IPCR	
	Biogenic magnetosomes	Magnetic beads
200 ng/ml	94	116
40 ng/ml	137	58
8 ng/ml	82	133
1.6 ng/ml	70	89
320 pg/ml	115	151
64 pg/ml	117	83
Average	103	105
SD	23	31
%	21.8	29.9

Individual and average values are shown for Magneto Immuno-PCR (M-IPCR).

Conclusions:

We here reported on the development of a homogeneous Immuno-PCR assay based on antibody-functionalized biogenic magnetosome nanoparticles. Using a clinical relevant sample system, i.e., the detection of Hepatitis B surface Antigen (HBsAg) in human serum, an initial protocol for M-IPCR was established and some major advantages of the magnetosomes in combination with Immuno-PCR were demonstrated in a comparative study.

Compared to the analogous Magneto-ELISA a more than 100-fold improvement of the sensitivity was observed, correlating very well with the typical sensitivity improvement accessible by converting a given ELISA into an Immuno-PCR assay.[12] The direct comparison of the magnetosomes with commercial magnetic beads as magnetic carriers showed that the use of magnetosomes led to better signal to noise ratios, reduced standard deviations and an about 25-fold increase in sensitivity, thus demonstrating the advantages of using these novel compounds for high sensitivity IPCR protocols. Furthermore the magnetosome-based M-IPCR revealed a good dynamic range in quantification and excellent recovery rates. Another major advantage of the M-IPCR results from its independency of special solid phase materials, i.e. particular microplates with high protein binding capacity, high thermostability and size compatibility with customary real-time PCR cyclers, which are needed for standard Immuno-PCR protocols.

In summary we demonstrated a powerful new automatable immunoassay platform combining the established Immuno-PCR technology with the advantages of functionalized biogenic magnetosome nanoparticles. The promising results obtained here face the challenges of new technology developments with respect to high-sensitivity, high-throughput diagnostics of biomarkers.

Experimental Section:

Magnetic Capture Conjugate Preparation:

Synthesis and purification of the antibody-functionalized biogenic magnetosome particles (MP) was carried out by a modular synthetic chemical approach, as previously described.[21] In brief, biotin groups were initially coupled to the magnetosome membrane of predominantly superparamagnetic magnetosomes, isolated from the mutant strain *M. gryphiswaldense* MSR-1K, using sulfo-N-hydroxy-succinimide ester sodium salt (NHS-biotin). Following, the membrane-bound biotin groups were used to attach the protein Streptavidin (STV), thereby leading to STV-functionalized magnetosomes.

Magnetic capture particles of STV-functionalized magnetosomes and biotinylated antibodies were prepared by mixing 10 nM stock-solutions of STV-functionalized magnetosomes (in TED buffer containing 20 mM Tris-HCl, 5mM EDTA, pH 7.5) and 20-fold excess (2.9 µM stock-solution) of biotinylated monoclonal anti-HBsAg IgG (clone NE3, IBT Reutlingen, biotinylated with NHS-Biotin (Pierce) according to manufacturers instructions) in a 96well PCR microplate (Applied Biosystems). After incubation for 30 min at room temperature, the mixtures were immobilized using a magnetic microplate (Dynal) and washed with 100 µl TE (10 mM Tris buffer, 5 mM EDTA pH 7.5). After an additional incubation for 20 min in MSTE-B (10 mM Tris buffer, pH 7.5, 5 mM EDTA) containing 0.1 mg/ml reagent grade DNA (Roche), 0.5% milk powder (Oxoid) and 800 µM D-biotin (Sigma) the MPs were washed again and diluted to a final concentration of 3.3 nM in TE.

For comparison, commercial STV-functionalized magnetic beads (Roche) were used. The functionalization with anti-HBsAg IgG was done according to manufacturers instructions. After an additional incubation for 20 min in MSTE-B the antibody-functionalized magnetic beads (MB) were immobilized using a magnetic microplate, washed with 100 µl TETBS (20 mM Tris-Cl buffer, pH 7.5, 150 mM NaCl, 5 mM EDTA, 0.01% (w/v) Tween-20) and diluted to a final concentration of 167 µg/ml in TE.

Detection Conjugate Preparation:

The alkaline-phosphatase (AP)-antibody conjugate for M-ELISA was prepared by incubating 1 µl STV-AP (Roche) and 10 pmol (4.8 µM stock-solution) of the biotinylated monoclonal anti-HBsAg IgG (clone NF5, IBT Reutlingen, biotinylated with NHS-Biotin (Pierce) according to manufacturers instructions) to a total volume of 10 µl TE. After 10 min

incubation the conjugate was diluted to a final concentration of 20 nM in MSTE-B. The DNA-antibody conjugate (HBsAg Imperacer™ Kit, Chimera Biotec) was diluted 1:10 in MSTE-B.

Magneto Immuno-PCR and ELISA:

To reduce nonspecific binding of the reagents, the PCR microplate was pretreated for 12 hours with blocking solution (Chimera Biotec). The microplate was washed twice with WashBuffer A (Chimera Biotec) and serial dilutions of the antigens were applied. The antigen used was Hepatitis B surface Antigen (HBsAg, recombinant, IBT) ranging from 1 µg/ml to 0.5 pg/ml in standardized human serum (BISEKO, Biotest).

For M-IPCR the DNA-antibody conjugates were added directly to 30 µl of the antigen samples to a final dilution of 1:60. For M-ELISA the AP-antibody conjugate was added directly to 30 µl of the antigen samples to a final concentration of 2 nM. The mixture was incubated for 30 minutes under orbital shaking.

Following antibody-functionalized magnetosomes (to a final concentration of 0.8 nM) or antibody-functionalized magnetic beads (to a final concentration of 5 µg/well) were added. The mixture was incubated for 60 minutes under orbital shaking. Subsequent to complex immobilization using a magnetic microplate and washing twice by adding and removing 50 µl TE the complex is resuspend in 50 µl ddH$_2$O.

A microplate (TopYield® modules, Nunc) was prepared by adding 30 µl per well PCR Mastermix (HBsAg Imperacer™ Kit, Chimera Biotec) for M-IPCR or 50 µl per well AttoPhos (Roche) for M-ELISA. Different amounts of 1, 5 or 10 µl resuspended detection complex were transferred to the TopYield® modules and for M-IPCR real-time PCR was done according to the HBsAg Imperacer™ Kit protocol (Chimera Biotec) using an ABIPrism 7000 real-time PCR cycler (Applied Biosystems). For M-ELISA fluorescence read-out was carried out after 20 min incubation under orbital shaking using a Victor[2] multilabel reader (Perkin Elmer).

References:

[1]   O. Scaros, R. Fisler, *Biotechniques* **2005**, *Suppl*, 30.

[2]   M. Schmitt, N. Harbeck, M. G. Daidone, N. Brynner, M. J. Duffy, J. A. Foekens, F. C. Sweep, *Int J Oncol* **2004**, *25*, 1397.

[3]   B. M. Chassy, *J Am Coll Nutr* **2002**, *21*, 166S.

[4]   J. W. Zolg, H. Langen, *Mol Cell Proteomics* **2004**, *3*, 345.

[5]   A. Matsakas, P. Diel, *Int J Sports Med* **2005**, *26*, 83.

[6]   M. J. F. Austin, L. Babiss, *The AAPS Journal* **2006**, *8*.

[7]   R. P. Valle, C. Chavany, T. A. Zhukov, M. Jendoubi, *Expert Rev Mol Diagn* **2003**, *3*, 55.

[8]   Q. Y. He, J. F. Chiu, *J Cell Biochem* **2003**, *89*, 868.

[9]   E. F. Petricoin, D. K. Ornstein, L. A. Liotta, *Urol Oncol* **2004**, *22*, 322.

[10]   K. R. Calvo, L. A. Liotta, E. F. Petricoin, *Biosci Rep* **2005**, *25*, 107.

[11]   T. Sano, C. L. Smith, C. R. Cantor, *Science* **1992**, *258*, 120.

[12]   C. M. Niemeyer, M. Adler, R. Wacker, *Trends Biotechnol* **2005**, *23*, 208.

[13]   K. Sugawara, D. Kobayashi, K. Saito, D. Furuya, H. Araake, A. Yagihashi, T. Yajima, K. Hosoda, T. Kamimura, N. Watanabe, *Clin Chim Acta* **2000**, *299*, 45.

[14]   K. Lind, M. Kubista, *J Immunol Methods* **2005**, *304*, 107.

[15]   M. Adler, M. Langer, K. Witthohn, J. Eck, D. Blohm, C. M. Niemeyer, *Biochem Biophys Res Commun* **2003**, *300*, 757.

[16]   C. M. Niemeyer, M. Adler, D. Blohm, *Anal Biochem* **1997**, *246*, 140.

[17]   M. Adler, R. Wacker, C. M. Niemeyer, *Biochem Biophys Res Commun* **2003**, *308*, 240.

[18]   A. K. Gupta, M. Gupta, *Biomaterials* **2005**, *26*, 3995.

[19]   A. Ito, M. Shinkai, H. Honda, T. Kobayashi, *J Biosci Bioeng* **2005**, *100*, 1.

[20]   G. Reiss, A. Hutten, *Nat Mater* **2005**, *4*, 725.

[21]   B. Ceyhan, P. Alhorn, C. Lang, D. Schüler, C. M. Niemeyer, *Small* **2006**, 1251.

[22]   A. Hoell, A. Wiedenmann, U. Heyen, D. Schüler, *Phys. B* **2004**, *350*, e309.

[23]   D. Schüler, R. B. Frankel, *Appl Microbiol Biotechnol* **1999**, *52*, 464.

[24]   D. A. Bazylinski, R. B. Frankel, *Nat Rev Microbiol* **2004**, *2*, 217.

Manuscript 5

Labelling of macrophages using bacterial magnetosomes and their characterization by magnetic resonance imaging

Annegret Hartung[a,d,] Marcus R. Lisy[b], Karl-Heinz Herrmann[a], Ingrid Hilger[b], Dirk Schüler[e], Claus Lang[e], Matthias E. Bellemann[d], Werner A. Kaiser[c], Jürgen R. Reichenbach[a]*

[a]Medical Physics Group, Institute for Diagnostic and Interventional Radiology, Friedrich-Schiller University, Jena, Germany

[b]Experimental Radiology, Institute for Diagnostic and Interventional Radiology, Friedrich-Schiller University, Jena, Germany

[c]Institute for Diagnostic and Interventional Radiology, Friedrich-Schiller University, Jena, Germany

[d]Department of Biomedical Engineering, University of Applied Sciences, Jena, Germany

[e]Max-Planck Institute for Marine Microbiology, Bremen, Germany

*Corresponding author. annegret.hartung@med.uni-jena.de

Abstract

This work investigated macrophages labeled with magnetosomes for the possible detection of inflammations by MR molecular imaging. Pure magnetosomes and macrophages containing magnetosomes were analyzed using a clinical 1.5 T MR-scanner. Relaxivities of magnetosomes and relaxation rates of cells containing magnetosomes were determined. Peritonitis was induced in two mice. T_1, T_2 and T_2* weighted images were acquired following injection of the probes. Pure magnetosomes and labeled cells showed slight effects on T_1, but strong effects on T_2 and T_2* images. Labeled macrophages were located with magnetic resonance imaging (MRI) in the colon area, thus demonstrating the feasibility of the proposed approach.

Keywords: Magnetosome; Macrophage; Magnetic resonance imaging; Molecular imaging; Iron particle; Inflammation

Cell migration is frequently involved in pathological processes, such as the formation of metastatic lesions in cancer, or the infiltration of blood-borne or lymphoid inflammatory cells in a variety of diseases, such as angiogenesis, multiple sclerosis, rheumatoid arthritis and tissue or organ rejection. Since macrophages are well-known effectors and regulators of the inflammatory response, visualization of the infiltration of these cells into the host tissue or assessment of their reaction with respect to therapeutic interventions would be of high diagnostic value. In addition, their biological purpose to internalize any foreign particles makes macrophages an interesting target for molecular imaging [1].

Molecular imaging can be defined as the non-invasive, quantitative and reproducible imaging and monitoring of targeted macromolecules and/or biological processes in living organisms [2]. To visualize cells and tissues *in vivo* special probes, however, are needed, which bind to the target with high affinity and which are detectable with a high sensitivity by the imaging modality. In recent years molecular imaging has been performed with different imaging modalities, including positron emission tomography (PET), single photon emission computer tomography (SPECT) or near infrared fluorescence spectroscopy (NIRF). Although these techniques show high sensitivity for the used probes, they commonly lack anatomic resolution which is needed for reliable diagnosis. On the other hand, magnetic resonance imaging (MRI) shows high soft tissue contrast with excellent spatial resolution without using any ionizing radiation, but with significantly lower label sensitivity compared to optical methods, for instance. The present study investigates the applicability of iron oxide particles

of bacterial origin (magnetosomes) to label macrophages for MR molecular imaging. Therefore, *in vitro* experiments as well as first animal experiments were performed to characterize the relaxation properties of these biogenic nanoparticles and their ability to visualize the inflammatory response with MRI.

The magnetosomes were obtained from the Max Planck Institute for Marine Microbiology (Bremen, Germany) and used as MR contrast agent [3]. These biogenic iron oxide nanoparticles are produced by the magnetotactic bacteria *Magnetospirillum gryphiswaldense*. They consist of an iron oxide core (Fe_3O_4) with a diameter of 42 nm that is surrounded by a bio membrane (5 nm) resulting in an overall diameter of approximately 50 nm.

To investigate the magnetic relaxation properties of the nanoparticles the optically labeled magnetosomes were diluted in two identical series of different concentrations with iron contents ranging from 3 to 129 µmol/l Fe. Agarose (0.4 g) (Sigma-Aldrich, Steinheim, Germany) and 19.6 ml phosphate buffered saline (PBS) were heated to 70°C for solubilization of the agarose and the magnetosome ferrofluid was diluted with the agarose gel. The samples were placed into 500 µl reaction tubes which were kept on ice until the samples solidified. Iron content of the samples was calculated from the ferrofluid iron content and the known dilution of the samples (Figure 1(a)).

To prove the internalization of the magnetosomes by the macrophages three samples of J774A.1 mouse macrophages (Cell Lines Service, Heidelberg, Germany) were cultivated until confluence in culture bottles with DMEM (Dulbecco's modified Eagle medium) and 10% (v/v) heat-inactivated fetal calf serum (37°C, 5 CO_2, 95% humidity). Afterwards, the medium was removed and replaced by 10 ml DMEM with 10 % (v/v) fetal calf serum and 770 µl magnetosomes (equivalent 100 µg Fe/ml solution). The macrophages were incubated with the magnetosomes for 3 h (37°C, 5 % CO_2, 95 % humidity). To remove non-internalized magnetosomes the cells were washed six times, each time with 15 ml PBS buffer (100 mM, pH 7.4). To avoid cell aggregation which would compromise a homogeneous dispersion of cells in the samples and, thus, influence the cell counts necessary for the MRI experiments, 10 ml PBS with 2 mM ethyl diamine tetra acetic acid (EDTA) were added. Cells were carefully removed from the culture bottles and counted in an Abbe-Zeiss counting cell chamber. The cells were fixated in 5 % (w/v) paraformaldehyd (Fischar, Heidelberg, Germany) for another 15 min at room temperature. Afterwards the macrophages were washed with PBS/EDTA. Each of the three macrophage suspensions was diluted twice to identical series of cell samples with cell counts ranging from 0 – 2000 cells/µl. The samples were

placed in 500 µl reaction tubes and sedimented at 300×*g* for 5 min. The cell pellets were re-suspended in PBS 2 % (w/v) agarose (Sigma Aldrich, Steinheim, Germany) and kept on ice until the samples solidified (Figure 1(b)).
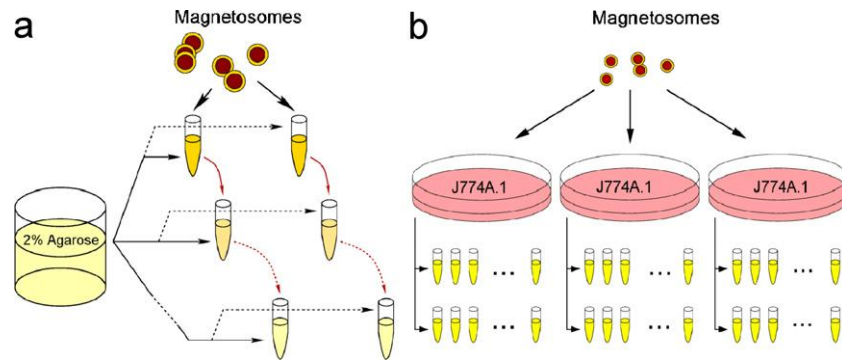

Figure 1. Schematics of the *in vitro* experiments. (a) For the investigation of the relaxation properties the magnetosome ferrofluid was diluted into two identical series of samples with iron contents ranging from 3 to 129 µmol/l. To gain a homogenous dispersion of nanoparticles inside the sample, 2 % agarose gel was used to fixate the magnetosomes. (b) The properties of magnetosomes internalized by macrophages were investigated by incubating three solutions of mouse macrophages (J77A.1) with magnetosomes. Two identical series of cell samples up to 2000 cells/µl were prepared from each solution.

MR imaging was performed on a clinical 1.5 T scanner (Magnetom Sonata, Siemens Medical Solutions, Erlangen, Germany) to determine the relaxation properties of the magnetosomes and to prove the internalization of the marker by macrophages *in vitro*. Four samples were placed at a time in a small surface coil with a diameter of 30 mm. T_1 relaxation times were determined by using an IR Turbo-FLASH sequence (TR = 4000 ms, TE = 2.73 ms, TI = 175 – 3000 ms, FOV = 50 mm, slice thickness = 5 mm, flip angle = 8°, matrix = 64×64, NEX = 4). For the T_2 measurements a single-echo spin-echo sequence was used with varying echo times (TR = 3000 ms, TE = 11, 30, 60 and 120 ms, FOV = 60 mm, matrix = 192×256, slice thickness = 5 mm, flip angle = 90°). Finally, T_2^* relaxation times were measured with a multi-echo gradient echo sequence (TR = 100 ms, 12 echoes, TE = 4.52 – 80 ms, FOV = 60 mm, matrix = 128×92, slice thickness = 5 mm, flip angle = 21°, NEX = 10). Relaxation times were determined by applying a ROI-based analysis of the MR images and fitting the ROI signals to the appropriate exponential functions. With the known iron content of the pure magnetosome samples, the corresponding relaxivities R_1, R_2 and R_2^* were calculated. The relaxivity is a characteristic measure of any MR contrast agent and denotes the ability of magnetic compounds to increase the relaxation rates of the surrounding water proton spins.

All animal studies were performed in accordance with the guidelines for animal research of the regional animal committee. To evaluate the labeling of the macrophages with the magnetosomes in an animal model, peritonitis was induced in two mice by an intraperitoneal injection of 3 mg Zymosan A (Sigma Aldrich, Steinheim, Germany) in 500 µl physiological saline solution. Both animals received an intravenous injection of magnetosomes (100 mg/kg) after 90 min. Administration of Zymosan A is known to produce a time-dependent cell accumulation in the peritoneal cavity according to the typical profile of an acute inflammatory response. Resident peritoneal macrophages initially disappear from the peritoneal cavity due to generalized activation and adhesion to the internal mucosa layers. The macrophage population then reappears due to a genuine monocyte recruitment and the number of macrophages steadily increases between 6 and 24 h after injection. The amount of macrophages diminishes after 48 h [4].

MR imaging of the first mouse was performed 6 h after inducing the peritonitis. A T_2* weighted, 3D dual-echo gradient echo sequence was performed (TR = 60 ms, TE = 19 and 50 ms, 64 slices, slice thickness = 1 mm, FOV = 100 mm, matrix = 192×120, NEX = 10). Before the MR imaging the mouse was sacrificed with ether and placed in the small loop coil. The second mouse was subjected to a second injection of magnetosomes after 18 h. MR imaging was performed 24h after inducing the peritonitis, when the inflammatory response and thus the amount of macrophages in the peritoneal cavity reached its maximum [4]. This mouse was also sacrificed with ether before imaging and placed in the small loop coil. Additionally, a 1 ml reaction tube filled with water was placed in the coil. 3D, T_2-weighted turbo-spin-echo images (TR = 400 ms, TE = 57 ms, 40 slices, slice thickness = 0.6 mm, FOV = 80 mm, matrix = 192, flip angle = 180°, NEX = 1) were acquired in this case. Besides the T_2* properties of iron oxide nanoparticles, resulting in a strong decrease in signal intensity, there is also R_1 relaxivity associated with these particles, which results in a in a signal increase using T_1 weighted sequences. At low iron concentrations a T_1 enhancing effect can be observed, whereas at higher doses the susceptibility phenomenon balances the T_1 effect [5]. Several studies [6-8] reported significant T_1 effects due to the presence of superparamagnetic iron oxide particles, especially in inflammatory tissue. Therefore, 3D, T_1 weighted dual-echo gradient-echo images (TR = 20 ms, TE = 2.49 and 4.76 ms, 40 slices, slice thickness = 0.6 mm, FOV = 80 mm, matrix = 128, flip angle = 90°, NEX = 4) were acquired.

Iron oxide nanoparticles are known to produce a significant T_2* effect [5, 9, 10]. The iron oxide core of the magnetosomes, as for every SPIO-based contrast agent, produces

magnetic field inhomogeneities around the particle. If protons pass through the area around the nanoparticle, basically two effects occur. First the fluctuating, local magnetic fields associated with the particles enable the protons to release their energy to the surrounding environment faster than without the contrast agent. This process accelerates T_1 relaxation. On the other hand, the field inhomogeneities produced by the iron oxide core speed up the dephasing of the transverse magnetization and therefore the MR signal decay (Figure 2). The MR scan also shows that suspending the magnetosomes in 2 % agarose gel does not ensure a homogenous dispersion of the nanoparticles inside the sample. The resulting inhomogeneities lead to higher standard deviations in the ROI. Nevertheless, distinct signal decay with increasing iron content can be seen in the MR image as well.
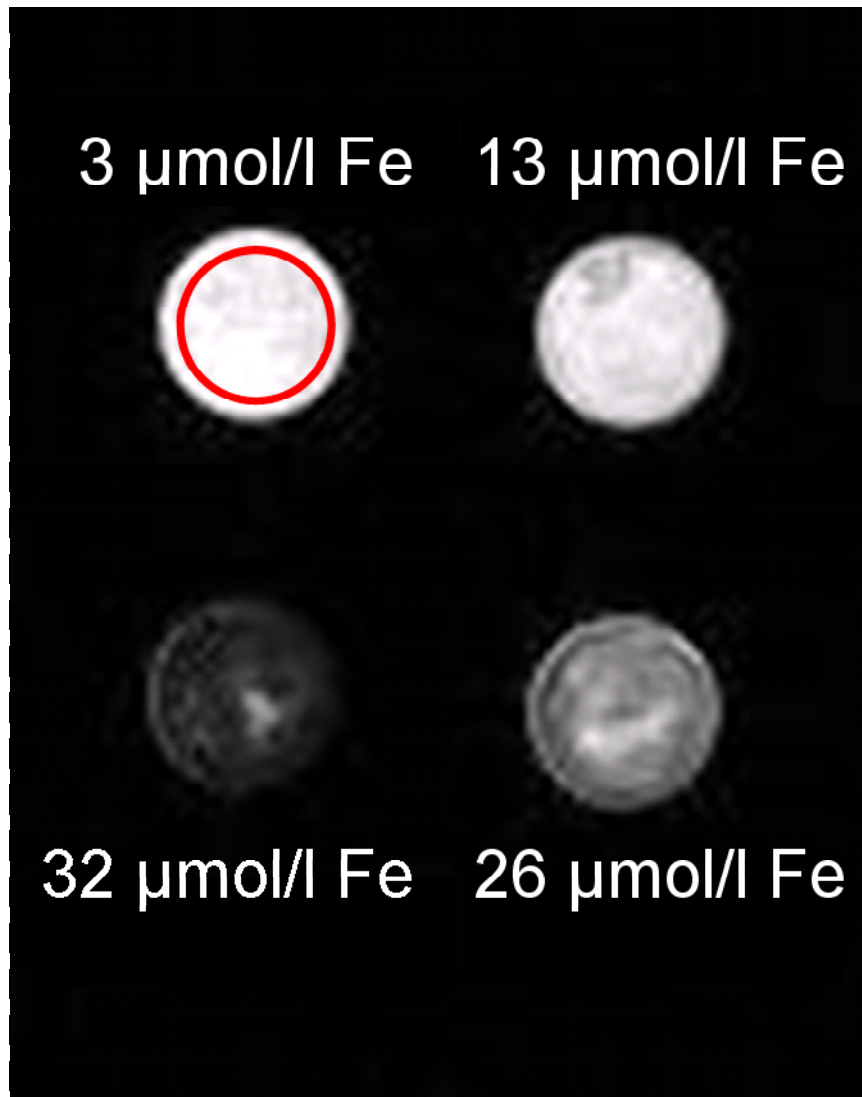
Figure 2. Spin-echo image in coronal orientation of four samples of magnetosomes in 2 % agarose gel (TR/TE = 3000/11 ms). ROIs (as indicated in red) were used for analysis. Although the magnetosomes were suspended and fixated in the gel, the image shows that the nanoparticles were not dispersed homogenously inside the sample. Nevertheless, the signal decay with increasing iron concentration is clearly seen.

For the magnetosomes in agarose gel a relatively low R_1 relaxivity of 3.2 ± 0.4 $(\text{mM} \times \text{s})^{-1}$ was determined. This is in rough agreement with the findings for typical iron containing contrast agents, such as, for example, Resovist[®] (Schering, Berlin) with an R_1 of 9.5 $(\text{mM} \times \text{s})^{-1}$ [11]. Usually, T_1 enhancement is observed during the vascular phase of the nanoparticles and by using minimal echo times in order to prevent the T_2* effect of iron oxide from overriding the signal enhancement from T_1 shortening. As soon as they are removed from the blood pool by the reticuloendothelial system (RES), T_1 enhancement is predominantly seen in edemas which are characteristic for inflammatory processes. It has also been reported that restricted water diffusion and/or particle diffusion, e.g., by compartmentalization, limits the T_1 effect of iron oxide nanoparticles in cells. This observation is in agreement with previous reports of marked T_1 effects of USPIO in blood (non-compartmentalized) as opposed to the T_1 effect of USPIO in liver, spleen or bone marrow (compartmentalized). Due to its similar properties to human tissue the fixation of the magnetosomes in 2 % agarose gel produces an environment comparable with compartmentalized USPIO and therefore restricts the T_1 effect [12-14].

As expected the magnetosomes revealed a large R_2 relaxivity of 526 ± 56 mM s^{-1} and an even higher R_2* relaxivity of 1198 ± 342 mM s^{-1}. The internalization of iron oxide nanoparticles leads to high concentrations of iron in the phagolysosomes of macrophages that cause very effective signal decays [9]. Compared to Resovist[®] ($R_2 = 230$ mM s^{-1}) [11] the R_2 relaxivity of magnetosomes is thus considerably higher. Consequently, the iron dose which would have to be administrated to observe a similar signal change on T_2-weighted images is distinctly lower for magnetosomes compared to Resovist[®].

The relaxation properties of the three measured solutions of macrophages incubated with magnetosomes were found to be similar to that of the pure magnetosomes. As can be seen from Figure 3 the effect of different numbers of cells on $1/T_1$ remains quite small. All three series of cell samples showed good agreement with a mean value of approximately $1/T_1 \approx 0.45$ s^{-1} and small standard deviations. For series 3 a slight increase of the relaxation time rate was observed for the samples with cell counts larger than 600 cells/µl. For $1/T_2$ (Figure 4) a more pronounced effect was observed. Again, series 3 showed a stronger dependency of $1/T_2$ on the cell count compared to series 1 and 2. The strongest effects, however, were observed for $1/T_2$* (Figure 5). The high relaxation rate of the sample with 100 cells/µl should be considered as an outlier. Overall, the standard deviations in Figure 5 are larger compared

to that in Figure 4, because local magnetic inhomogeneities are not compensated by the multi-echo gradient echo sequence and lead to additional signal cancellation.
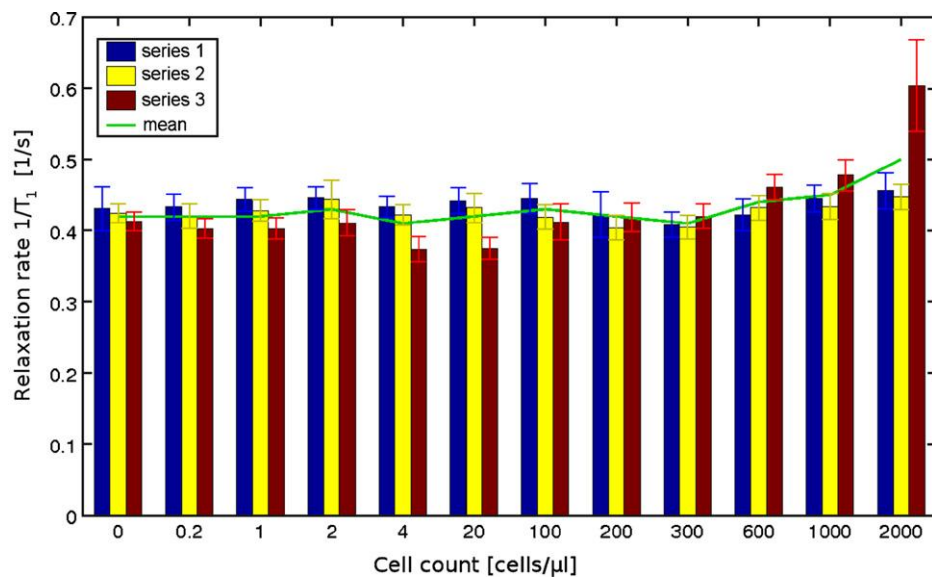

Figure 3. T_1 relaxation rates plotted *vs*. cell counts for the three series of cell samples. The mean relaxation rate $1/T_1$ remains relatively constant for all series up to roughly 600 cells/µl. Series 3 shows an increase in $1/T_1$ for the highest cell count which was not observed with the other two series.
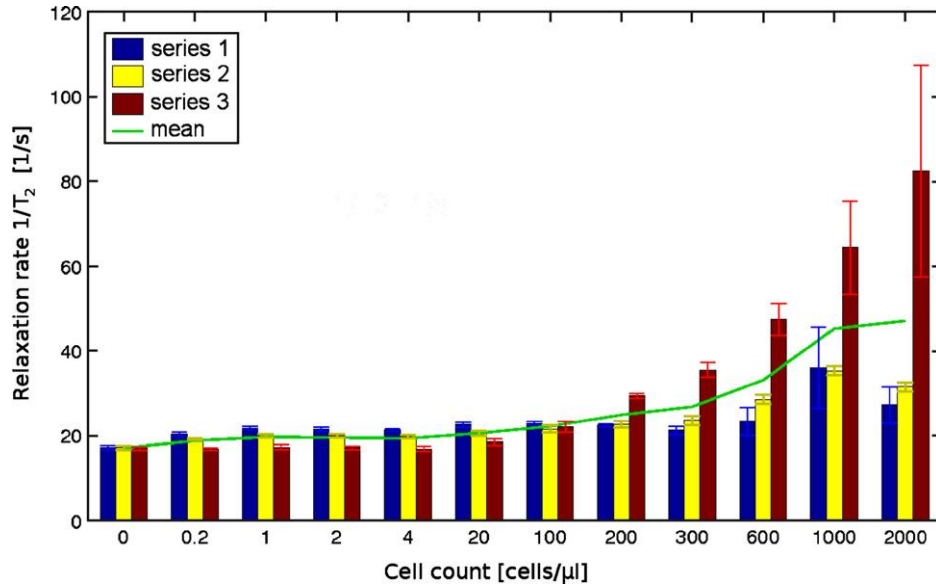

Figure 4. T_2 relaxation rate vs. cell counts of the three series of cell samples. Again, the increase of $1/T_2$ in series 3 is stronger than for series 1 and 2, indicating most likely a larger amount of internalized magnetosomes.
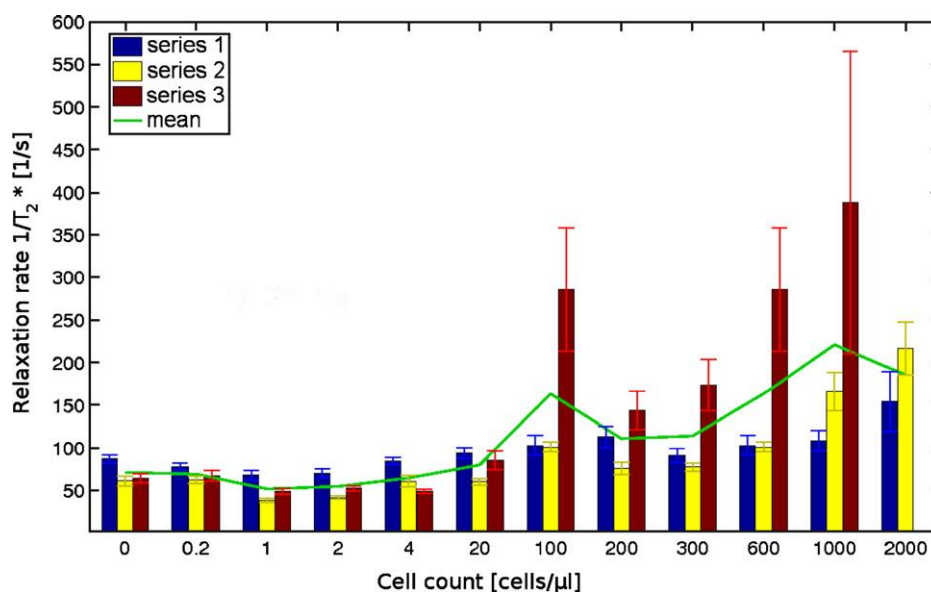
Figure 5. T_2* relaxation rate vs. cell counts of the three series of cell samples. Increases of $1/T_2$* are observed beyond 2000 cells/µl for series 1, beyond 1000 cells/µl for series 2 and beyond 200 cells/µl for series 3.

For all relaxation rates $1/T_1$, $1/T_2$ and $1/T_2$* sample series 1 and 2 revealed similar behavior, whereas the values obtained for series 3 showed stronger deviations. Since the phagocytic capacity of macrophages fluctuates [15] the cells in this series most likely internalized more magnetosomes compared to the cells in series 1 and 2. This would also explain the observation that for series 3 changes in $1/T_2$ and $1/T_2$* occur consistently at lower cell numbers.

MRI was able to demonstrate the uptake of the magnetosomes by macrophages *in vitro*. MR imaging of the first mouse with induced peritonitis, revealed a signal decrease on the sagittal T_2* weighted images (Figure 6(a), red arrows) in the area of the peritoneum between colon and abdominal wall. A similar effect was observed in the second animal after 24 h. The coronal T_2 weighted images show a signal decrease around an intestinal loop on the right side as well (Figure 6(b), red arrows). In the T_1 weighted image the same structure occurs bright due to the T_1 effect of USPIO (Figure 6(c), red arrows). Both the signal decay on the T_2* and T_2 weighted images and the T_1 enhancement in inflammatory tissue are typical for superparamagnetic iron oxide nanoparticles. The injected magnetosomes were obviously removed from the blood pool by monocytes, which migrated to the focus of inflammation in the peritoneal cavity. In all MR images the liver occurred dark (Figure 6(a-c); yellow arrows). This observation confirms that for high iron concentrations and restricted water diffusion the T_2* effect of iron oxide nanoparticles overrides the T_1 enhancement.
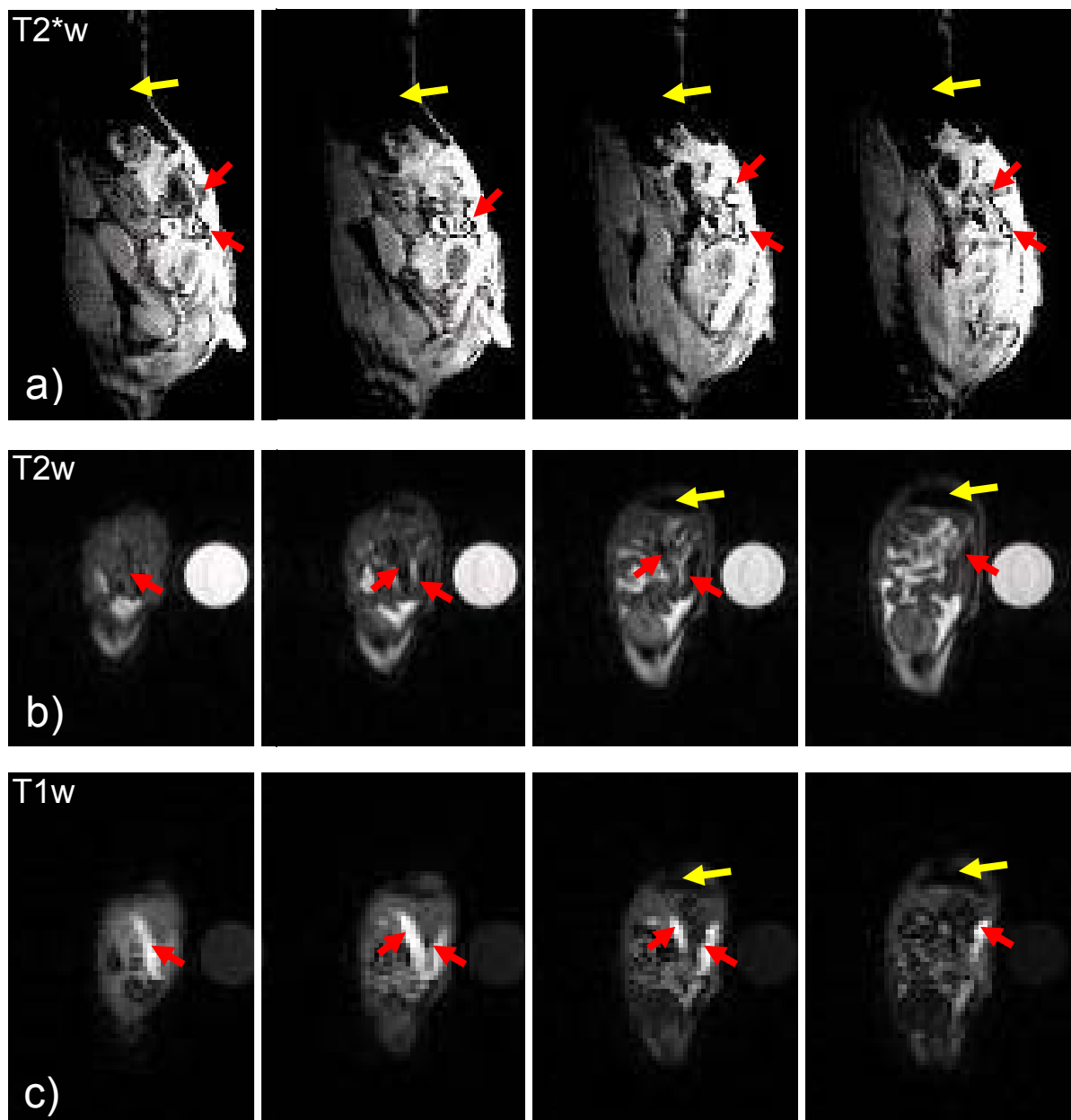
Figure 6. *Ex vivo* MR animal imaging. (a) T_2^* weighted images 6 h after inducing the peritonitis. The hypointense signal in the liver (yellow arrows) shows that the injected macrophages were effectively removed from the blood pool by the RES. Areas of signal loss are also seen near the abdominal wall due to an accumulation of magnetosome containing macrophages in the peritoneum surrounding the colon (red arrows). MRI of the second mouse (b and c) was performed after 24 h. In the coronal T_2 weighted images a hypointense area is seen in the left colon (red arrows). The same structure is reproduced hyperintensely in the T_1 weighted images of the same animal (c). The liver shows again strong signal loss in both the T_2 and the T_1 weighted images (yellow arrows).

In summary, as demonstrated by MRI, macrophages were successfully labeled with magnetosomes and characterized with respect to their MR relaxation properties. These

organelles consist of membrane-enclosed magnetite crystals that are thought to help to direct bacterial swimming towards growth-favoring microoxic zones at the bottom of natural waters [3]. Consequently, they form an interesting class of iron containing contrast agent for MRI applications.

In a pilot *ex vivo* animal study we were able to identify the inflammation caused by the induced peritonitis on the MR images by applying magnetosomes. One limitation, however, is related to the inferior sensitivity and resolution of the used clinical MR scanner, which makes it difficult to interpret the images properly. Nevertheless, we were still able to prove the feasibility of this approach even with a human whole-body scanner. Further studies are certainly necessary to investigate this animal model *in vivo* with a larger number of animals. Higher field strengths and dedicated coils would help to increase the available signal-to-noise ratio.

One interesting and very elegant approach would be to combine the used iron oxide particles with optical markers as a bimodal probe to improve the sensitivity. The use of such a bimodal agent would be highly advantageous as it allows a direct corroboration of the *in vivo* MRI images by, for instance, fluorescent histology or *in vivo* optical imaging. Fluorescence can greatly aid with *in vitro* as well as *in vivo* studies as it can serve as a surrogate marker of contrast agent uptake without recourse to immunohistochemical staining whereas MRI makes it possible to visualize detailed anatomy repeatedly and non-invasively *in vivo* [16].

References

[1]   M. Rudin, Molecular Imaging-Basic Principles and Appplications in Biomedical Research, Imperial College Press, 2005.

[2].   D. L. J. Thorek, A. K. Chen. et al., Ann. Biomed. Eng. 34 (2006) 23.

[3].   A. Scheffel, M. Gruska, D. Faivre, et al., Nature. 440 (2006) 110.

[4].   M. N. Ajuebor, R. J. Flower, R. Hannon, et al., J. Leukoc. Biol. 63 (1998) 108.

[5].   C. Corot, K. G. Petry, R. Trivedi et al., Invest. Radiol. 39 (2004) 619.

[6].   A. M. Lutz, C. Seemayer, C. Corot et al., Radiology 233 (2004) 149.

[7].   G. Simon, H. Daldrup-Link, J. von Vopelius-Feldt, et al., Röfo. 178 (2006) 20.

[8].   Q. G. de Lussanet, W. H. Backes, A. W. Griffioen, et al., Radiology 229 (2003) 429.

[9].   S. A. Schmitz, Röfo. 174 (2002) 469.

[10].   Y. L. Wu, Q. Ye, L. M. Foley et al., Proc. Natl. Acad. Sci. 103 (2006) 1852.

[11].   N. Kato, M. Takahashi, T. Tsuji et al., Invest. Radiol. 34 (1999) 551.

[12].   G. H. Simon, J. Bauer, O. Saborovski et al., Eur. Radiol. 16 (2006) 738.

[13].   G. H. Simon, J. von Vopelius-Feldt, et al., J. Magn. Reson. Imaging 23 (2006)720.

[14].   S. Saini, R. R. Edelman, P. Sharma, et al., Am. J. Roentgenol. 164 (1995) 1147.

[15].   S. Metz, G. Bonaterra, M. Rudelius et al., Eur. Radiol. 14 (2004) 1851.

[16].   M. Modo, Current Stem Cell Res. Ther. 1 (2006) 55.

Manuscript 6

Fluorescent bacterial magnetic nanoparticles as bimodal contrast agents

Marcus-René Lisy, PhD,[+]* Annegret Hartung, MS,* Claus Lang, MS,† Dirk Schüler, PhD,†
Walter Richter, PhD,‡ Jürgen R. Reichenbach, PhD,* Werner A. Kaiser, MD, MS,* and
Ingrid Hilger, PhD*

*Institute for Diagnostic and Interventional Radiology, Friedrich-Schiller-University Jena, Jena, Germany;

†Department Biologie I Bereich Mikrobiologie, Ludwig-Maximillians-Universität München, München, Germany; and

‡Center for Electron Microscopy of the Medical Faculty, Friedrich-Schiller-University Jena, Jena, Germany.

[+]corresponding author: marcus.lisy@med.uni-jena.de

Abstract

Objectives: The purpose of this study was to assess whether fluorochrome-coupled bacterial magnetic nanoparticles can be used as bimodal contrast agent for both magnetic resonance imaging (MRI) and near-infrared fluorescence optical (NIRF) imaging of cultured macrophages.

Materials and Methods: Bacterial magnetic nanoparticles (magnetosomes, particle diameter: 42 nm) were harvested from *Magnetospirillum gryphiswaldense* and characterized by using MRI. After covalent coupling to the fluorescent dye DY-676 ($\lambda_{abs.}/\lambda_{em.}$= 676 nm/701 nm, Dyomics, Jena, Germany), the fluorescent magnetosomes were analyzed by fluorescence-activated cell sorting. Subsequently, murine macrophages *J774* were incubated with the bimodal contrast agent (3 hours) and examined by a whole-body near infrared small animal imaging system as well as by using a 1.5 T clinical MR system. Moreover, labeled cells were characterized using confocal laser scanning microscopy (CLSM) and ultrathin section transmission electron microscopy.

Results: Characterization of the nanoparticles by MRI revealed R_1 and R_2 relaxivities of 3.2 mM^{-1}s^{-1} and 526 mM^{-1} s^{-1}, respectively. Fluorochrome-coupled magnetosomes exhibited increased fluorescence intensities at wavelengths >670 nm. Macrophages that were incubated with the contrast agent showed a significant fluorescence emission in the near infrared range as imaged with a whole body NIR imaging system, FACS analysis and CLSM. Moreover, CLSM data showed the greatest fluorescence intensities within intracellular compartments and colocalized with the magnetosomes. With MRI, both T1 and T2 relaxation times were substantially shortened at concentrations greater than 600 cells/μL.

Discussion and Conclusion: Macrophages could be labeled with fluorescent magnetosomes, and they were successfully imaged using both a 1.5 T MR scanner as well as with NIRF optical methods. The use of this bimodal contrast agent for diagnostic purposes may benefit from the excellent spatial resolution of the MRI and the high sensitivity of the fluorescence imaging.

Key Words: molecular imaging, bimodal contrast agents, bacterial nanoparticles, magnetic resonance imaging, optical imaging

Introduction

In the recent years, significant progress has been achieved in regard to the imaging of cells and molecular markers detection of early pathologic changes *in vivo*. This new field in diagnostic imaging called molecular imaging deals with both the development of sophisticated imaging techniques and contrast agents for cell labeling and their clinical application.[1] For example, superparamagnetic iron oxide nanoparticles such as the clinically approved Resovist (Schering, Berlin, Germany) are used for contrast-enhanced magnetic resonance imaging (MRI) of the liver[2] and magnetic labelling of stem cells, to monitor cell trafficking.[3,4] Moreover, recent investigations showed the suitability of paramagnetic contrast agents like Gadofluorine M[5] or Gadolinium-Fullerenol[6] for stem cell labeling and MRI. Besides the excellent spatial resolution, one limitation of MRI is its low sensitivity for tracers or contrast agents, which are important for the detection of cellular or molecular changes in a nanomolar scale.[7] This might lead to the underdiagnosis of early disease stages. The limited sensitivity of MRI can be overcome by the combination with fluorescence optical imaging methods. Optical imaging is being used in cell biology research for a long time and has entered now the field of *in vivo* diagnostic imaging. For example, the detection of both the Her-2/neu protein expressed in 30% of breast cancers[8] as well as phosphatidylserin in apoptotic tumor cells[9] in an animal model using high affinity contrast agents with covalently bound near infrared fluorescent dyes (Cy 5.5) were described recently.

In the long term, the combination of both imaging technologies could provide a powerful tool for clinical diagnostics because the high sensitivity of the optical system may complement the superior spatial resolution of the magnetic resonance technique. In first studies, by using Cy5.5-labeled cross-linked iron oxide nanoparticles, apoptotic T cells could be successfully detected *in vitro*[9] as well as *in vivo* in a gliosarcoma tumor model in mice.[10] Moreover, recent interesting developments of bimodal contrast agents were focused on functionalized quantum dots with a paramagnetic coating.[11]

A new source of magnetic nanoparticles is provided by biomineralization. Here, we describe a bimodal contrast agent for MRI and fluorescence optical imaging, which consists of bacterial magnetic nanoparticles, so-called magnetosomes, isolated from the magnetic bacterium *Magnetospirillum gryphiswaldense,*[12] to which a near infrared fluorescent dye is covalently bound. In contrast to most synthetic magnetic nanoparticles, the magnetite crystals of magnetosomes display a narrow size distribution (mean diameter of mature particles is 42 ± 9 nm). Their ferrimagnetic single domain permits detection with clinical MRI devices even at very low concentrations[13] and because of their biologic membrane they are able to be

153

coupled to fluorochromes or even to be functionalized with antibodies. The fluorochrome DY-676 (Dyomics GmbH, Jena, Germany) used in this study is characterized by its absorption and emission maxima of $\lambda_{abs.}/\lambda_{em.} = 676$ nm/701 nm, where an increased light penetration into tissue was reported.[14] To demonstrate the bimodal features of contrast agent and its applicability in biologic systems, macrophages in culture were used. One of the typical features of these cells comprises their phagocytotic activity, by which it is possible to simply accumulate magnetic nanoparticles as described previously.[15] Particularly the following issues were addressed: (1) What are the particle properties in relation to MR and NIR optical imaging and (2) is it possible to label macrophages with the bimodal magnetic nanoparticles *in vitro* and image them using both MR and NIR optical methods?

Materials and Methods

Preparation and Characterization of the Bimodal Contrast Agent FM676

Magnetic nanoparticles were obtained from cells of the magnetic bacterium *M. gryphiswaldense* (Figure 1A), which were grown under microaerobic conditions in an oxystat fermentor as described previously.[16] Bacteria were cultured in a medium containing 50 μM ferric citrate at 28°C. For isolation of magnetosomes, cells were disrupted in a French press and fractionated as described elsewhere.[13,17] Purified magnetosomes were enveloped by the intact magnetosome membrane (Figure 1B), which prevents the isolated magnetic particles from agglomeration.[14] The relaxivities and the potential to shorten T_1 and T_2 relaxation times of magnetosomes dissolved in water with 2% agarose have been estimated with the clinical 1.5 T MR-scanner Magnetom Sonata (Siemens Medical Solutions, Erlangen, Germany) using a turbo flash sequence or a single echo spin echo sequence. Afterward, magnetosomes were covalently bound to the fluorochrome DY-676 via the activated NHS-ester according to the manufacturer's protocol. A solution of 275 nmol reactive dye in 100 μL of 50 mM $NaHCO_3$-buffer (pH 9.0) was added to 900 μL of a suspension of magnetic nanoparticles containing about 1.44 mg Fe/mL (Figure 2). After 3 hours of reaction, magnetosomes were washed carefully with phosphate-buffered saline (0,1 M, pH 8.5) in a magnet stand (Promega, Mannheim, Germany) until no more dye was detected in the supernatant. Optical properties of these fluorescent magnetic nanoparticles named *FM676* were tested on a FACSCalibur analytical instrument with the CellQuest software (Becton Dickinson, Heidelberg, Germany).
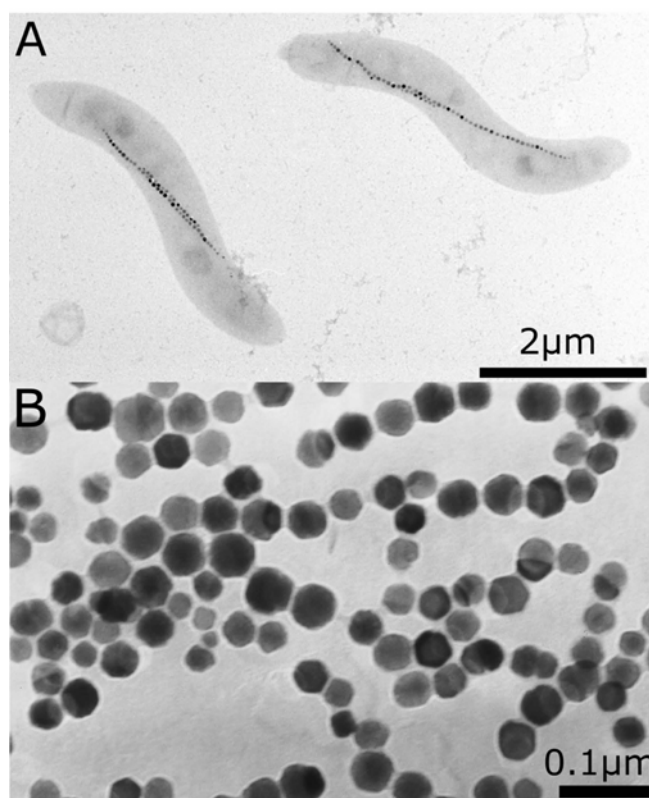
Figure 1. Light and electron microscopy image of magnetosomes. Top, magnetosomes located within the cytoplasm *of M. gryphiswaldense*. Bottom, isolated magnetosomes, which are enveloped by the magnetosome membrane.
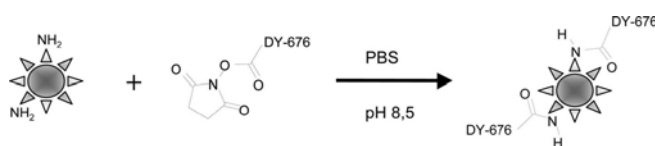

Figure 2. Schematic illustration on coupling the fluorescent dye DY-676 via reactive NHS-ester to magnetosome membrane. Amino groups in the magnetosomes biomembrane react with the activated ester of the fluorochrome forming a covalent amid bound.

Cell Culture

To assess the applicability of the bimodal contrast agent for the detection of labeled cells, we used the mouse macrophage cell line *J774* (Cell lines service, Heidelberg, Germany). A total of 5×10^6 cells were cultured at 37°C in a 5% CO_2 atmosphere and incubated with FM676 (each sample with 44 µg Fe per milliliter of medium), native magnetosomes, or with medium only for 3 hours. After washing carefully to remove all non phagocyted magnetosomes, cells were harvested for further characterization.

Imaging of Labelled and Unlabelled Macrophages

To verify macrophage cell labeling, 10^5 cells were sedimented, air-dried on Histobond object slides (Marienfeld, Bad Mergentheim, Germany), and embedded with Permafluor (Immunotech, Marseille, France). Confocal laser scanning microscopy (CLSM) was performed using a LSM510 system with the LSM510 image examiner software (Zeiss, Jena, Germany). For ultrathin section transmission electron microscopy, harvested cells were fixed with glutaraldehyde, embedded in Araldite CY212 (Agar Scientific Ltd., Stansted, Essex) and TEM was performed using the EM 900 electron microscope (Zeiss, Oberkochen, Germany).

To assess the imaging feasibility of the bimodal contrast agent FM676, we used both a bio-optical planar near infrared fluorescence small animal imager (bonSAI, Siemens Medical Solutions, Erlangen, Germany) as well as the 1.5 T MR scanner Magnetom Sonata. Macrophages, which were previously incubated with native magnetosomes, with FM676 or with medium only, were placed in 1.5-mL reaction tubes and embedded in water with 2% (wt/vol) agarose to avoid signal artifacts caused by sedimentation of the cells during data acquisition. NIRF images were recorded using the 660/735 nm filter system for excitation and emission at an acquisition time of 0.5 seconds with binning factor 2 (matrix size 512 x 696 pixel). Fluorescence signals were detected with a charge-coupled device camera (pixel size 4.6 x 4.6 μm). Images were analyzed semiquantitatively on the basis of regions of interests using the integrated *syngo* software. MR imaging was performed with 0.5-mL reaction tubes containing either macrophages (0 and 10^7 cells/mL in 2% wt/vol agarose) labeled with FM676 or unlabeled controls using an inversion recovery sequence and a single echo spin echo sequence, respectively.

Results

Characterization of the isolated bacterial magnetosomes from *M. gryphiswaldense* revealed a longitudinal relaxivity of $R_1 = 3.2 \pm 0.4$ mM^{-1}s^{-1} and a transversal relaxivity of R_2 = 526 ± 56 mM^{-1}s^{-1} (Figure 3) as determined with a 1.5 T clinical MR scanner. Fluorochrome-coupled magnetosomes FM676 showed distinctly higher fluorescence intensities >670 nm in comparison to native magnetosomes as shown by histogram blots of the FACS analysis (Figure 4).

Ultrathin section electron microscopic analysis of cultured mouse macrophages *J774* incubated with FM676 and fixed with glutardialdehyde showed electron dense granules inside the cytoplasmic region (Figure 5). The observed structures containing FM676 exhibited an endosomal character, which indicates an active uptake of the contrast agent. Moreover, the

use of CLSM showed that the cells that were incubated with FM676 revealed distinct fluorescence intensities >700 nm within intracellular compartments colocalized with accumulations of nanoparticles as detected by fluorescence and particle-filled dense structures as observed by phase-contrast microscopy (Figure 6A–C). In contrast to this, cells that were incubated with native magnetosomes revealed no fluorescence at all, although accumulations of nanoparticles were present (Figure 6D–E).

The obtained NIRF macroscopic images (Figure 7) of reaction tubes containing each a suspension of 10^6 cells in water with 2% (wt/vol) agarose clearly showed that only those macrophages that had internalized FM676 exhibited increased fluorescence intensities (1768 ± 54 arbitrary units) in the near-infrared range as compared with controls incubated with medium or native magnetosomes only (136 ± 11 and 128 ± 5 a.u., respectively). The obtained semiquantitative values are presented as results of 3 different experiments ± standard deviations.

The relaxation times of unlabeled cells were found to be of $T_1 = 2400 ± 32$ milliseconds and $T_2 = 70.0 ± 1.0$ milliseconds by using a 1.5 T clinical MR scanner, whereas labeling with FM676 lead to a substantial decrease of relaxation times to $T_1 = 1258 ± 196$ milliseconds and $T_2 = 7.7 ± 0.9$ milliseconds (Figure 8 right) and a successful detection by MRI.
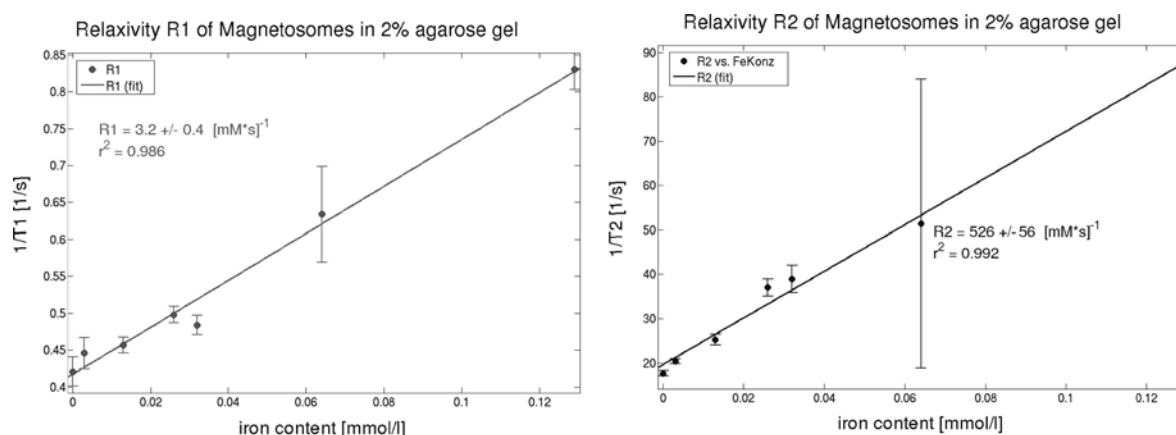
Figure 3. Longitudinal relaxivity $R_1 = 3.2 ± 0.4$ mM^{-1}s^{-1}(left) and transversal relaxivity R2 = 526 ± 56 mM^{-1}s^{-1} (right) of magnetosomes in water with 2% (wt/vol) agarose as determined by using a clinical 1.5 T MR-scanner.
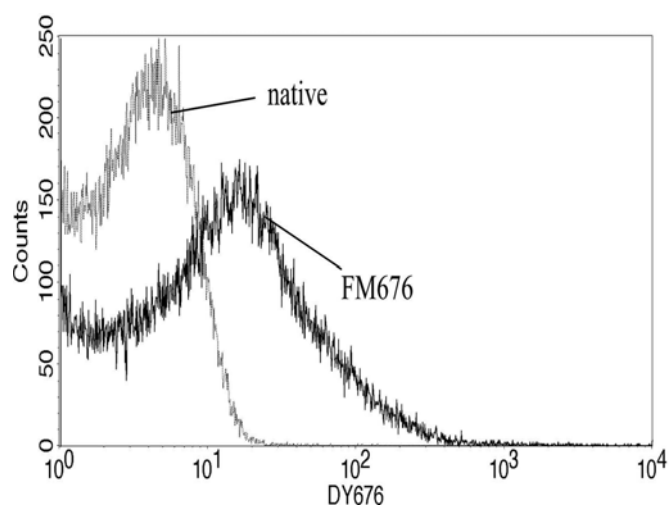
Figure 4. Fluoro-optical properties of native and fluorescent magnetosomes (FM676) as obtained by FACS analysis. Fluorochrome coupled magnetosomes FM676 showed distinctly higher fluorescence intensities >670 nm in comparison with native magnetosomes.
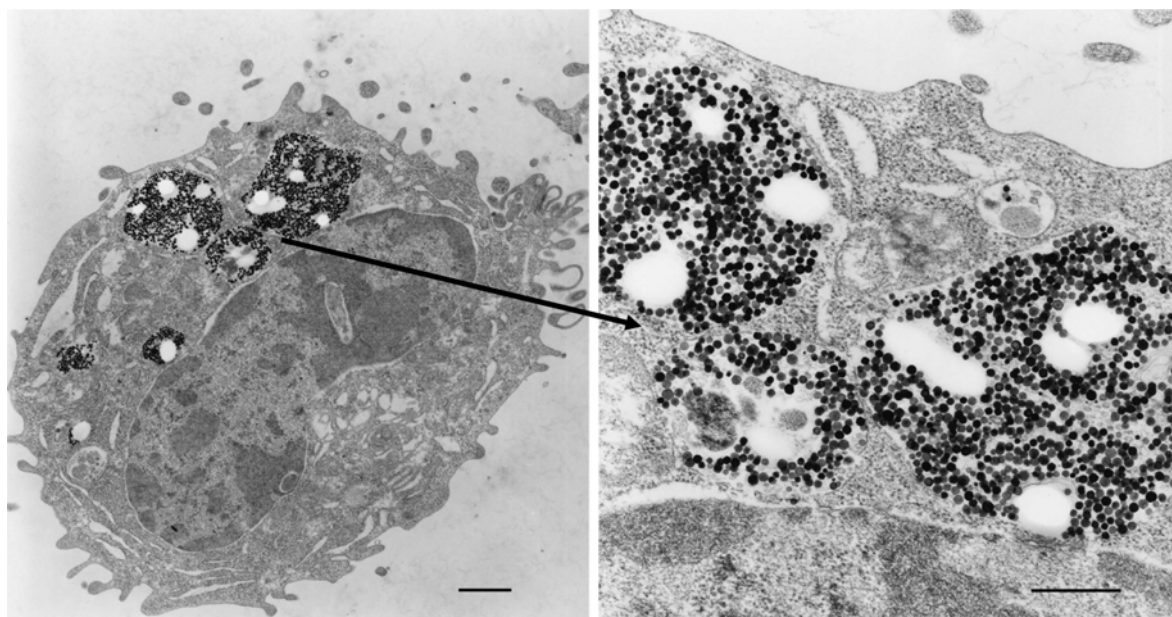

Figure 5. Ultrathin section transmission electron microscopy micrograph of *J774* macrophages incubated with fluorescent magnetosomes (FM676). Electron dense vesicle-like structures (endosomes) inside the cytoplasmic region contain phagocyted magnetosomes. The bar represents 1 μm (left) and 0.5 μm (right).
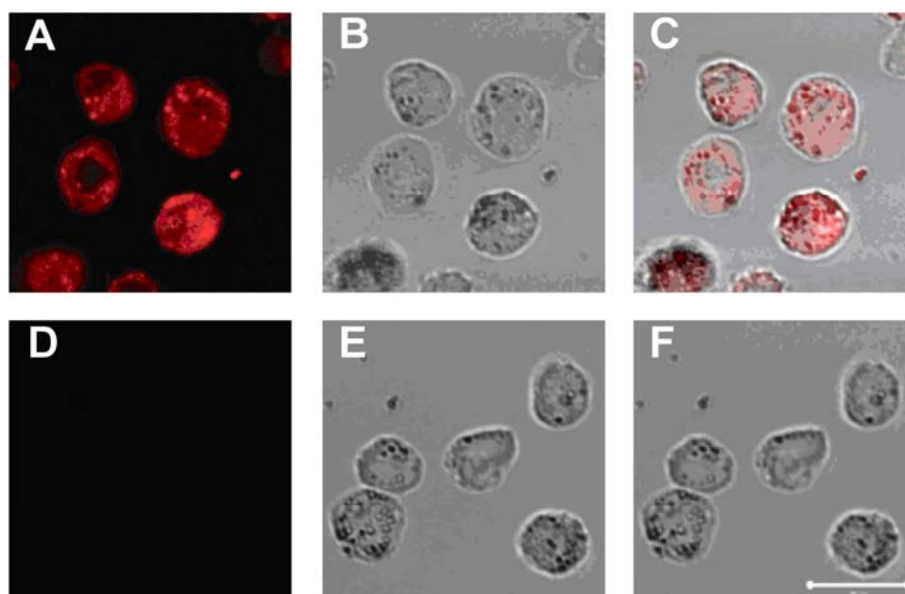
Figure 6. Fluorescence CLSM images of the macrophages *J774* incubated either with fluorescent (FM676) (A) or unlabeled magnetosomes (D). Fluorescence emission at >700 nm is pseudocolored in red. Phase contrast and merged images are depicted in B and C and D and E, respectively (scale bar = 20 μm). Both fluorescence and phase contrast images show intracellular accumulation of FM676 in labeled macrophages whereas native magnetosomes are visible only with phase contrast.

Cells incubated with	Fluorescence intensities (aU)
Medium	136±11
FM676	1768±54
magnetosomes	128±5
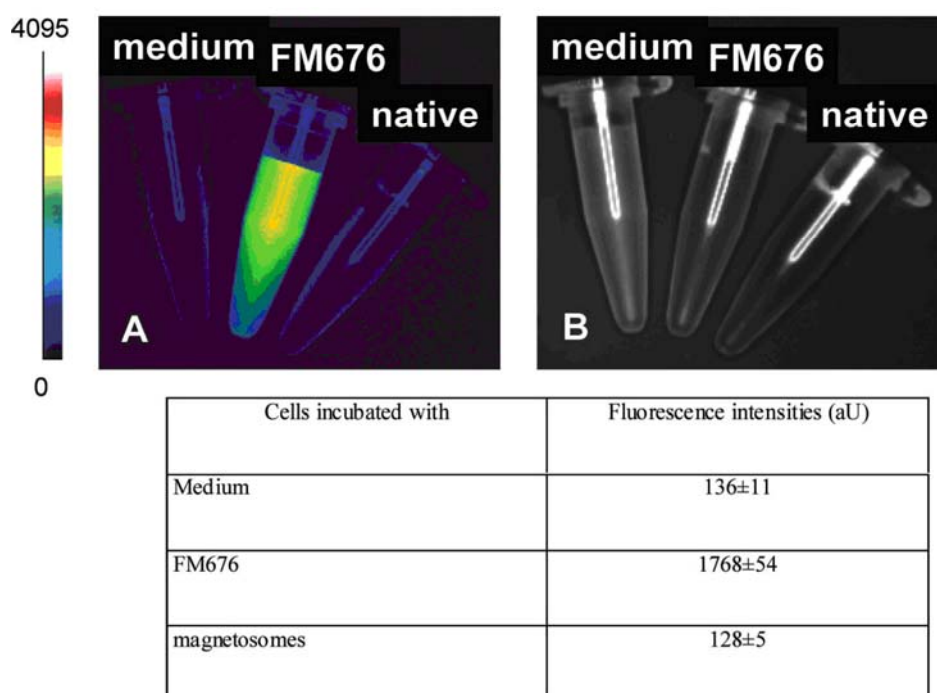
Figure 7. White light and near infrared fluorescence images of *J774* macrophages incubated with either native, fluorescent magnetosomes (FM676) or with medium only as obtained with a preclinical bio-optical NIRF small animal imager. Corresponding ROI-based and semiquantitatively estimated fluorescence intensities are listed below. The cells which were incubated with FM676 showed over 10-fold increased fluorescence intensities as compared with controls.

Sample	4	3	2	1
Relaxation time	10^7 cells/ ml	$5*10^6$ cells/ml	$2*10^6$ cells/ml	0 cells/ ml
T1 (ms)	1258±196	1594±146	1915±109	2400±32
T2 (ms)	7.7±0.9	12±1.0	19.3±0.2	70.0±1.0
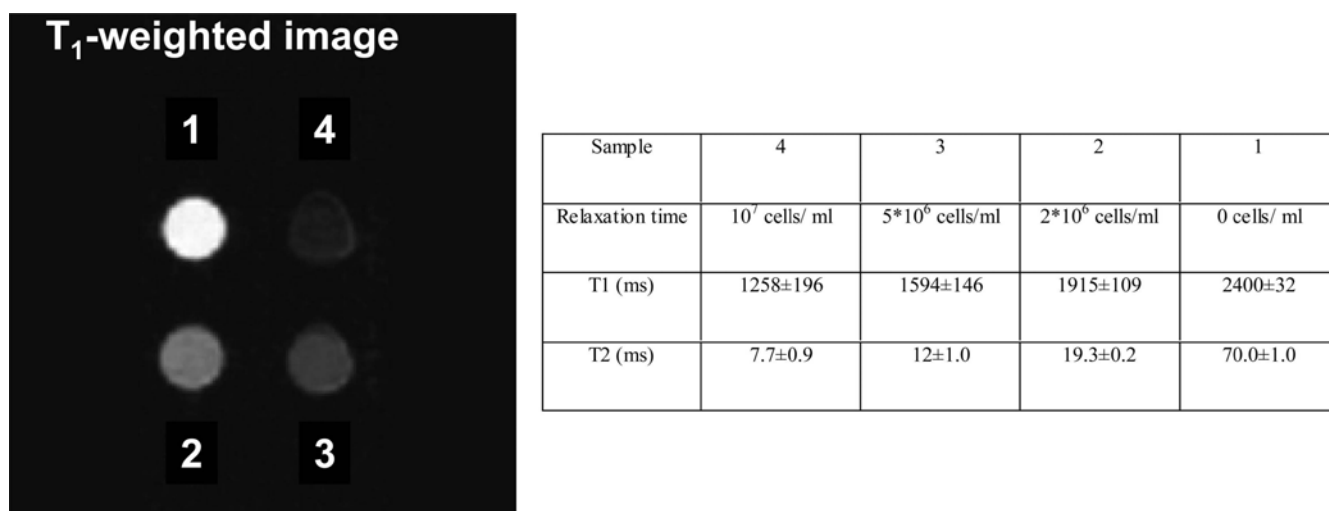
Figure 8. Left, T_1-weighted image of different concentrations of macrophages in water with 2% agarose which were incubated with fluorescent magnetosomes (FM676). Right, Corresponding relaxation times T_1 and T_2 of labeled macrophages. Labelling of macrophages with FM676 leads to a substantial decrease both of T_1 and T_2.

Discussion

The calculated relaxivities of the magnetosomes were nearly in the same range as compared with the values determined for the clinically approved MRI contrast agent Resovist (R_1 = 25.4, R_2 = 151 mM^{-1}s^{-1}, Schering, Berlin Germany). Interestingly, the transversal relaxivity of R_2 = 526 ± 56 mM^{-1}s^{-1} is substantially higher than the relaxivity of Resovist. Considering the relaxivities of synthetic nanoparticles (R_1 = 10.2 mM^{-1}s^{-1}, R_2 = 357.3 mM^{-1}s^{-1}) used by other groups,[18] the determined values are nearly comparable between each other. Even though the underlying mechanisms for the aforementioned findings are not clear, our results strongly support the applicability of magnetosomes for molecular and cellular MR imaging. The data of the FACS analysis could show that magnetosomes from *M. gryphiswaldense* were successfully labeled with DY-676 by incubation with the reactive NHS-ester. We suggest that amino groups in the magnetosomes biomembrane react with the activated ester of the fluorochrome forming a covalent amid bound (Figure 2). This leads to a contrast agent FM676 which can be detected both with MRI and fluoro-optical devices.

With the ultrathin section electron microscopic analysis, electron dense granules inside the cytoplasmic region of cultured mouse macrophages incubated with FM676 were observed. The granules are to be identified as endosomes containing large amounts of fluorochrome coupled magnetosomes. The phase contrast and fluorescence recordings labeled with FM676 showed a colocalization of NIR-fluorescence and particle-filled dense structures, respectively, within cells, supporting the results obtained by electron microscopy. These

results indicate that macrophages have been efficiently labeled and that the bimodal contrast agent is stable during cellular uptake.

Using the bio-optical planar near infrared fluorescence small animal imager bonSAI, the macroscopic images of reaction tubes containing macrophages which had internalized FM676 clearly showed more than 10-fold increased fluorescence intensities as compared with controls. In analogy to this, an up to 10-fold decreased relaxation time of labeled macrophages as compared with the unlabeled controls was observed by MRI, and these findings are based on the internalized magnetosomes resulting in weakened signal intensities. This massive signal loss even in T_1-weighted images is promising for an application of FM676 in the *in vivo* situation.

According to our results, the designed bimodal contrast agent could comprise a useful tool in future molecular imaging approaches. The simultaneous development of both innovative imaging devices as well as highly potential and specific contrast agents is significant for implementation of this technique in the clinical practice in the long-term. Some of the new probes and techniques have entered the clinical routine already or are very close to it, such as single-photon emission computed tomography,[19,20] positron emission tomography (PET)-CT,[21] and PET-MR[22] in association with appropriate contrast agents like, [18]FDG.[23,24] Recent investigations also are considering optical methods alone or in combination with MR because of its high sensitivity.[9,11] Furthermore, optical methods like intravital microscopy or fluorescence-mediated tomography[25] or the planar fluorescence imaging system used in this study are characterized by a more convenient handling as compared with the single-photon emission computed tomography and PET techniques.[26] To combine optical imaging with MRI, we used bacterial magnetic nanoparticles with a high R_2 relaxivity allowing the detection of very low concentrations of contrast agent even in T_1-weighted images. Many endeavors have been made to improve the structural properties as well as the biocompatibility of nanoparticles that are manufactured synthetically.[27,28] Moreover, a recent study considered the impact of particle size and coating of iron oxide nanoparticles on the rate of liver clearance in an animal model.[29] The magnetosomes used in this study with a narrow size distribution and equipped with a biomembrane can provide a biocompatible contrast agent for optical and MR imaging. Nevertheless, the risk of allergic reactions particularly caused by the magnetosome biomembrane as well as the aspects of the nanoparticle biodistribution have to be investigated in further *in vivo* studies to evaluate the suitability as contrast agent in patients.

Ultrathin section transmission electron microscopy and CLSM data showed that

cultured macrophages could be successfully labeled using the bimodal contrast agent. Moreover, labeled macrophages have been effectively detected both with a preclinical planar bio-optical near infrared small animal imager as well as a clinical 1.5 T MR-scanner.

Conclusion

In conclusion, we demonstrated the isolation of bacterial magnetic nanoparticles from *M. gryphiswaldense* and their covalent labeling with the near infrared fluorescent dye DY-676. The suitability of this bimodal contrast agent named FM676 for experimental optical and MR imaging purposes has been proven using both a bio-optical planar near infrared fluorescence small animal imager and a clinical 1.5 T MR scanner. Furthermore, fluorescent magnetic nanoparticles FM676 might probably be a suitable contrast agent for diagnosis of inflammatory processes by the concomitant utilization of 2 diagnostic modalities, but more investigation, particularly related to the *in vivo* situation, is necessary.

Acknowledgements

References

1. Weissleder R, Mahmood U. Molecular imaging. *Radiology*. 2001;219:316 –333.

2. Reimer P, Balzer T. Ferucarbotran (Resovist): a new clinically approved RES-specific contrast agent for contrast-enhanced MRI of the liver: properties, clinical development, and applications. *Eur Radiol*. 2003;13:1266 –1276.

3. Arbab AS, Yocum GT, Wilson LB, et al. Comparison of transfection agents in forming complexes with ferumoxides, cell labeling efficiency, and cellular viability. *Mol Imaging*. 2004;3:24 –32.

4. Matuszewski L, Persigehl T, Wall A, et al. Cell tagging with clinically approved iron oxides: feasibility and effect of lipofection, particle size, and surface coating on labeling efficiency. *Radiology*. 2005;235:155–161.

5. Giesel FL, Stroick M, Griebe M, et al. Gadofluorine M uptake in stem cells as a new

magnetic resonance imaging tracking method: an *in vitro* and *in vivo* study. *Invest Radiol*. 2006;41:868 – 873.

6. Anderson SA, Lee KK, Frank JA. Gadolinium-fullerenol as a paramagnetic contrast agent for cellular imaging. *Invest Radiol*. 2006;41:332–338.

7. Massoud TF, Gambhir SS. Molecular imaging in living subjects: seeing fundamental biological processes in a new light. *Genes Dev*. 2003;17:545–580.

8. Hilger I, Leistner Y, Berndt A, et al. Near-infrared fluorescence imaging of HER-2 protein over-expression in tumour cells. *Eur Radiol*. 2004;14:1124 –1129.

9. Schellenberger EA, Bogdanov A Jr, Hogemann D, et al. Annexin V-CLIO: a nanoparticle for detecting apoptosis by MRI. *Mol Imaging*.2002;1:102–107.

10. Kircher MF, Mahmood U, King RS, et al. A multimodal nanoparticle for preoperative magnetic resonance imaging and intraoperative optical brain tumor delineation. *Cancer Res*. 2003;63:8122– 8125.

11. Mulder WJ, Koole R, Brandwijk RJ, et al. Quantum dots with a paramagnetic coating as a bimodal molecular imaging probe. *Nano Lett*. 2006;6:1– 6.

12. Scheffel A, Gruska M, Faivre D, et al. An acidic protein aligns magnetosomes along a filamentous structure in magnetotactic bacteria. *Nature*. 2006;440:110 –114.

13. Herborn CU, Papanikolaou N, Reszka R, et al. Magnetosomes as biological model for iron binding: relaxivity determination with MRI. *Rofo*. 2003;175:830 – 834.

14. Bremer C, Ntziachristos V, Mahmood U, et al. Progress in optical imaging. *Radiologe*. 2001;41:131–137.

15. Metz S, Bonaterra G, Rudelius M, et al. Capacity of human monocytes to phagocytose approved iron oxide MR contrast agents *in vitro*. *Eur Radiol*. 2004;14:1851–1858.

16. Heyen U, Schüler D. Growth and magnetosome formation by microaerophilic Magnetospirillum strains in an oxygen-controlled fermentor. *Appl Microbiol Biotechnol*. 2003;61:536 –544.

17. Grünberg K, Müller EC, Otto A, et al. Biochemical and proteomic analysis of the magnetosome membrane in *Magnetospirillum gryphiswaldense*. *Appl Environ Microbiol*. 2004;70:1040 –1050.

18. Billotey C, Wilhelm C, Devaud M, et al. Cell internalization of anionic maghemite nanoparticles: quantitative effect on magnetic resonance imaging. *Magn Reson Med*. 2003;49:646 – 654.

19. Coleman RE, Blinder RA, Jaszczak RJ. Single photon emission computed tomography (SPECT). Part II: clinical applications. *Invest Radiol*. 1986;21:1–11.

20. Hildebrandt IJ, Gambhir SS. Molecular imaging applications for immunology. *Clin Immunol*. 2004;111:210 –224.

21. Townsend DW, Carney JP, Yap JT, et al. PET/CT today and tomorrow. *J Nucl Med*. 2004;45:4S–14S.

22. Marsden PK, Strul D, Keevil SF, et al. Simultaneous PET and NMR. *Br J Radiol*. 2002;75:53–59.

23. Willkomm P, Bender H, Bangard M, et al. FDG PET and immunoscintigraphy with 99mTc-labeled antibody fragments for detection of the recurrence of colorectal carcinoma. *J Nucl Med*. 2000;41:1657–1663.

24. Bar-Shalom R, Valdivia AY, Blaufox MD. PET imaging in oncology. *Semin Nucl Med*. 2000;30:150 –185.

25. Ntziachristos V, Ripoll J, Wang LV, et al. Looking and listening to light: the evolution of whole-body photonic imaging. *Nat Biotechnol*. 2005;23:313–320.

26. Picano E. Economic and biological costs of cardiac imaging. *Cardiovasc Ultrasound*. 2005;3:13.

27. Gupta AK, Gupta M. Synthesis and surface engineering of iron oxide nanoparticles for biomedical applications. *Biomaterials*. 2005;26:3995–4021.

28. Lee CS Lee H, Westervelt RM. Microelectromagnets for the control of magnetic nanoparticles. *Appl Phys Lett*. 2001;79:3308 –3310.

29. Briley-Saebo KC, Johansson LO, Hustvedt SO, et al. Clearance of iron oxide particles in rat liver: effect of hydrated particle size and coating material on liver metabolism. *Invest Radiol*. 2006;41:560 –571.

Manuscript 7

Synthetic and biogenic magnetite nanoparticles for tracking of stem cells and dendritic cells

Sebastian Schwarz[a, b], Fabiana Fernandes[a, c], Laura Sanroman[a, b], Michael Hodenius[b, d], Claus Lang[e], Uwe Himmelreich[f, g], Miguel Gama[c], Thomas Schmitz-Rode[b, d], Dirk Schüler[e], Mathias Hoehn[f], Martin Zenke*[a, b] and Thomas Hieronymus*[a, b]

a) Institute for Biomedical Engineering, Department of Cell Biology, RWTH Aachen University Medical School, Pauwelsstrasse 30, 52074 Aachen, Germany;

b) Helmholtz Institute for Biomedical Engineering, RWTH Aachen, Pauwelsstrasse 20, 52074 Aachen, Germany;

c) Department of Biological Engineering, University of Minho, Campus de Gualtar, 4710-057 Braga, Portugal

d) Institute for Biomedical Engineering, Department of Applied Medical Engineering, RWTH Aachen University Medical School, Pauwelsstrasse 20, 52074 Aachen, Germany;

e) Department of Microbiology, Ludwig-Maximillians-University of Munich, Maria-Ward-Str. 1a, 80638 Munich, Germany;

f) In-vivo-NMR-Laboratory, Max-Planck-Institute for Neurological Research, Gleueler Str. 50, 50931 Cologne, Germany;

g) Biomedical NMR Unit, MoSAIC, Faculty of Medicine, KU Leuven, Onderwijs en Navorsing 1, bus 505, 3000 Leuven, Belgium

*corresponding author: thomas.hieronymus@rwth-aachen.de; martin.zenke@rwth-aachen.de

Abstract

Accurate delivery of cells to target organs is critical for success of cell-based therapies with stem cells or immune cells such as antigen-presenting dendritic cells (DC). Labeling with contrast agents before implantation provides a powerful means for monitoring cellular migration using magnetic resonance imaging (MRI). In this study, we investigated the uptake of fully synthesized or bacterial magnetic nanoparticles (MNPs) into hematopoietic $Flt3^{+}$ stem cells and DC from mouse bone marrow. We show that (i) uptake of both synthetic and biogenic nanoparticles into cells endow magnetic activity and (ii) low numbers of MNP-loaded cells are readily detected by MRI.

Keywords

Iron oxide nanoparticles, Magnetosomes, Stem cells, Dendritic cells, Nanoparticle uptake, Magnetic resonance imaging, Cell tracking

Manuscript

Engineered magnetic nanoparticles (MNPs) are currently emerging as promising tools in numerous applications for medical diagnosis and therapy, such as drug delivery systems or contrast agents for magnetic resonance imaging (MRI). Cellular therapies using stem cells and immune cells, such as dendritic cells (DC), are increasingly applied in clinical trials. DC are professional antigen-presenting cells that play a key role in the induction of primary immune responses and have been implicated in determining the balance between immunity and tolerance induction [1, 2]. This makes DC a particularly attractive target for the development of therapeutics in pathological situations, such as autoimmune diseases, cancer and cardiovascular diseases, and thus DC are readily used as cellular vaccines in clinical trials [3]. Accurate delivery of DC to target organs and migration of the cells for effective antigen presentation and activation of an immune response is essential for the success of such therapies [4]. However, the ability to non-invasively monitor cell trafficking or a specific cellular function at the target site after application is rather limited. MRI is well suited for obtaining three-dimensional (3D) high-resolution images and is now widely used in clinical practice [5]. Stable labeling of cells with contrast agents has proven successful for MRI-based detection of cell deposits and their migration [6-9]. Most applications provide information about the location but not about a cellular functional status. First attempts have been made to develop functionalized MNPs that combine labeling of stem cells and DC for monitoring cellular localization and additional activities (e. g. adjuvant function of DC and measuring of

DC function *in vivo*) in one MNP formulation [10, 11]. For this purpose two strategies are currently being considered. First, fully synthetic iron oxid-based MNPs are used that allow functionalization by chemical modifications. Second, magnetosomes from magnetotactic bacteria are taken into consideration. Magnetosomes are organelles that comprise nanometersized crystals of magnetite enveloped by a biological membrane composed of phospholipids and specific proteins. The magnetosome membrane is critical for magnetosome stability, the control of magnetite crystal size and morphology, and additionally provides a matrix for functionalization of magnetosomes. This can be achieved by chemical modifications but moreover, and potentially superior to chemical approaches, by genetic engineering of the magnetosome membrane proteins.

We have recently described the synthesis and physicochemical properties of synthetic oleate stabilized magnetite MNPs [12], where the lipid-shell contributes to improved biocompatibility (in the following referred to as lipid-shell MNPs). Additionally, it has allowed further functionalization, such as biotin-conjugation and binding of the fluorescence tag streptavidin-fluorescein isothiocyanate (FITC) [10].

In this study we investigated the uptake of fully synthetic lipid-shell MNPs and of magnetosome MNPs into hematopoietic Flt3^{+} stem cells and DC from mouse bone marrow [13-15]. We show (i) that uptake of both synthetic and biogenic nanoparticles into cells endow magnetic activity on Flt3^{+} stem cells and DC (ii) that low numbers of MNP-loaded cells are readily detected by MRI.

Superparamagnetic magnetite lipid-shell MNPs were obtained by coprecipitation of Fe^{2+} and Fe^{3+} ions with NH_3 and stabilized with *cis*-9-octadecenoic acid sodium salt (oleate) as described [12]. Magnetosomes, also referred to as biogenic MNPs, were isolated and purified from the magnetotactic bacterium *Magnetospirillum gryphiswaldense* strain MSR-1 (DSM 6361) as described earlier [16]. Sterile solutions of MNPs containing 1 mg Fe/ml were used in 1:50 dilution for cell labeling.

DC were differentiated from hematopoietic Flt3^{+} stem cells (referred to as Flt3^{+} stem cells) of bone marrow suspensions from C57BL/6 mice (Charles River, Sulzfeld, Germany) as described [14]. DC were seeded at $2x10^6$ cells/ml in RPMI 1640 medium supplemented with 10% FCS, 2 mM L-glutamine, 100 U/ml penicillin/streptomycin (all from Gibco-BRL) and 50 μM β-mercaptoethanol (Sigma-Aldrich, Taufkirchen, Germany) containing 200 U/ml of recombinant mouse GM-CSF and were incubated with sterile filtered and buffered aqueous solutions of magnetosomes or lipid-shell MNPs 24 h before analyses. Cell numbers were determined with an electronic cell counter device (CASY1, Schärfe System, Reutlingen,

Germany).

MR images of agarose phantoms were acquired using a Bruker Biospin 7.0 T scanner (Ettlingen, Germany). MNP-labeled cells were suspended in 10 µl agarose (Sigma-Aldrich) and filled in 3.5 mm diameter drill holes of a 3.5 cm agarose phantom as described before [17]. Dissected lymphnodes (LN) from animal experiments were embedded into 1.6% agarose phantoms. MR images were acquired as described [17]. Phantoms were analyzed with T_2*weighted 3D gradient echo FLASH sequences (TE = 12ms, TR = 200ms and TE = 14ms, TR = 500ms, respectively; flip angle 30°) with an isotropic resolution of 78 μm^3 (for cell phantoms) and 55 μm^3 (for LN).

The interaction of MNPs with cells was first investigated by transmission electron microscopy (TEM) to determine uptake of MNPs into cells, intracellular localization and particle morphology before and after uptake. In aqueous solution, lipid-shell MNPs possess a mean iron core size of 8-10 nm whereas magnetosomes have a mean iron core size of 40-45 nm (Figs. 1a and 1b). In initial studies, uptake of MNP into DC was determined since DC are particularly potent in incorporating particles by endocytosis. After co-culture with MNPs for 24 h, DC were extensively washed with phosphate buffered saline (PBS) and fixed with 3% (w/v) glutaraldehyde. Cells were stained with OsO_4 and viewed and recorded with a Philips EM 400 T electron microscope equipped with a CCD camera. Figs. 1c to 1f reveal that both lipid-shell MNPs and magnetosome MNPs are localized intracellularly in numerous vesicles confined to the cytosol. MNPs are not found at the cell surface or in the nucleus. These results demonstrate effective uptake of both synthetic and biogenic MNPs into DC and suggest an endocytotic uptake mechanism. However, particle size and iron core morphology remained unaltered 24 h after uptake into DC (Figure 1a, b, d and f).
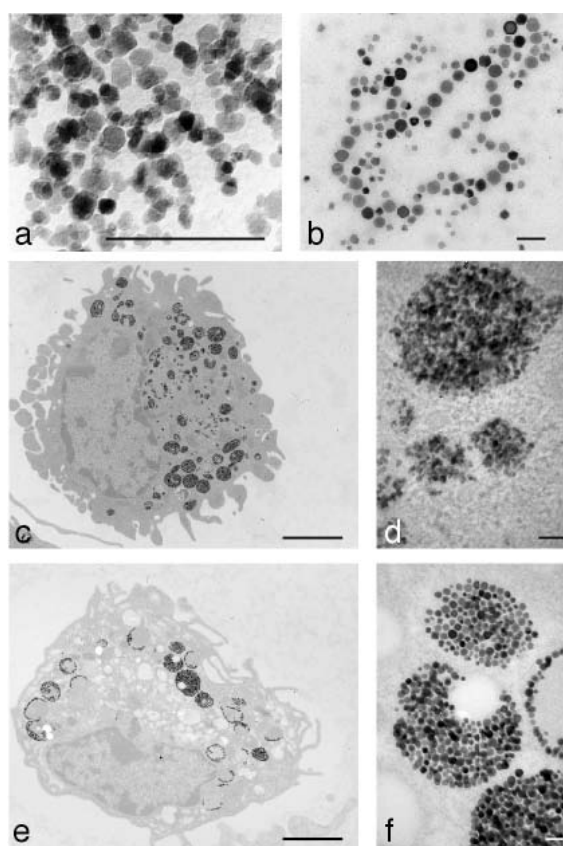
Figure 1. Electron micrographs of synthetic and biogenic MNPs before and after uptake into DC. Lipid-shell MNPs (a) and magnetosome MNPs (b) before uptake into cells. Scale bars in (a) and (b), 100 nm. DC incubated with synthetic MNPs (c and d) or magnetosome MNPs (e and f) for 24 h. Scale bars in (c) and (e), 2 μm. Micrographs (d) and (f) show higher magnifications of MNP clusters found in (c) and (e), respectively. Scale bars in (d) and (f), 100 nm.

We then proceeded to determine whether MNP-loaded Flt3$^+$ stem cells and DC acquired magnetic activity and were retained in a magnetic field. Flt3$^+$ stem cells and DC were treated with increasing concentrations of MNPs or left untreated for 24 h. MNPs exhibited no cytotoxicity on both Flt3$^+$ stem cells and DC (data not shown). Cells were recovered and extensively washed with PBS to remove unbound MNPs and then applied to a magnetic field in Miltenyi MS columns placed in a MiniMACS separator (Miltenyi Biotec, Bergisch Gladbach, Germany). In this assay, only MNP-labeled cells are retained in the magnetic field of the column. Columns were washed with PBS and not-retained cells collected. Retained cells were eluted with elution buffer (PBS containing bovine serum albumin (BSA) and EDTA; Sigma-Aldrich) after withdrawal of magnet. The numbers of both retained and notretained cells were determined; untreated cells served as control. Unlike control cells, we only observed MNP-loaded Flt3$^+$ stem cells and DC being retained in the magnetic field (Figure 2a). This was confirmed by Prussian-blue staining for iron in not-

169

retained and retained DC populations after magnetic separation showing complete absence of MNPs in not-retained cells (Figure 2b). Retention of MNP-labeled cells was dose-dependent (data not shown) and Figure 2 shows results obtained with optimal conditions for DC labeling with both lipid-shell MNPs and magnetosomes. Under these conditions, the labeling efficiency of MNPs for Flt3^{+} stem cells yielded lower rates than for DC. Interestingly, magnetosomes and lipid-shell MNPs revealed different labeling potentials for Flt3^{+} stem cells with a 2-fold higher labeling of Flt3^{+} stem cells by magnetosomes (Figure 2a). These results suggest different uptake mechanisms for Flt3^{+} stem cells and DC, which probably critically depends on MNP shell composition.
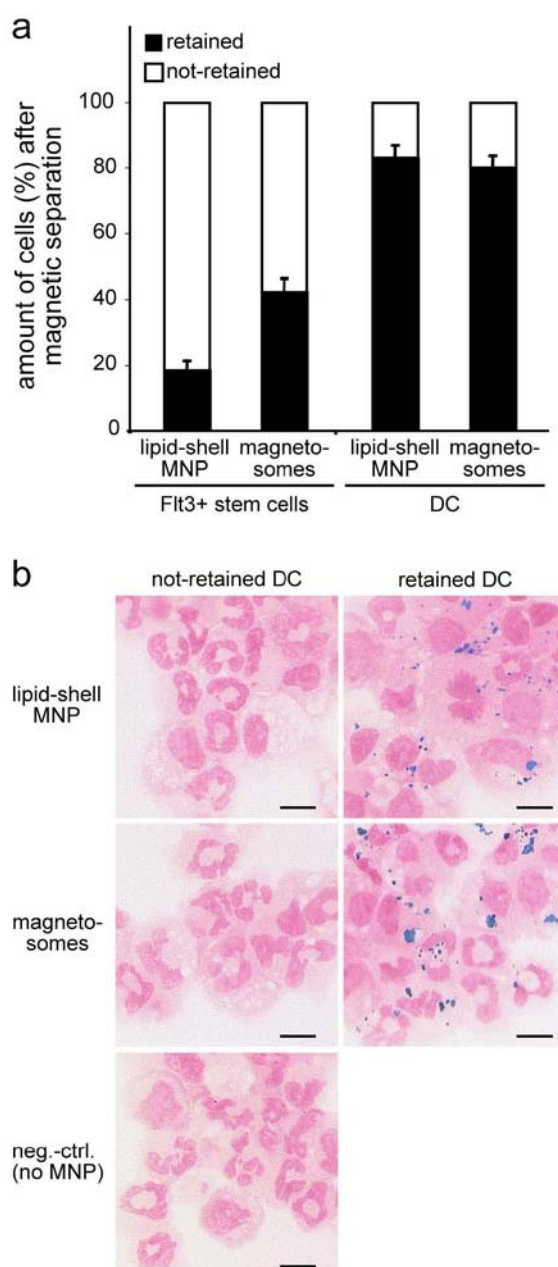
Figure 2. Differential uptake of MNPs and retention of cells in a magnetic field. (a) Flt3^{+} stem cells and DC were incubated with MNPs for 24 h and applied to a magnetic field. Number of cells after magnetic separation

were determined. Results are shown as mean ± SD (n=3). (b)Retained and not-retained cells were subjected to cytocentrifugation onto glass slides (1500rpm for 4 min) and stained with Prussian-blue for iron detection. Neutral red was used forcounterstaining. Scale bars, 5 µm.

Next, we determined the intracellular iron concentration after MNP uptake into cells by employing a ferrozine-based colorimetric assay as a direct measure for MNP quantity [18]. Flt3$^+$ stem cells and DC were cultured in the presence of lipid-shell MNPs or magnetosome MNPs comprising a total of 20 µg/ml iron (f. v.) or were left untreated. After 24 h cells were intensively washed and subjected to magnetic separation with Miltenyi MS columns. MNPlabeled cells were eluted from the columns and then lysed for iron release. Untreated cells were examined accordingly. Ascorbic acid was used to reduce Fe^{3+} to Fe^{2+} ions that form a chelate complex with ferrozine. Absorbance of Fe^{2+}-ferrozine was measured at 550 nm and compared to the absorbance of $FeCl_3$ standards. The minimum detection limit for Fe^{2+} ions in this assay set-up was 250 µMol/l, corresponding to 5 pg of iron per cell. Iron concentrations in untreated Flt3$^+$ stem cells and DC were below the detection limit. The results obtained show a higher uptake capacity of DC for MNPs than Flt3$^+$ stem cells (Figure 3). The intracellular iron concentration after labeling with lipid-shell MNPs was 77.9 ± 5.8 pg/cell in DC and 13.6 ± 1.6 pg/cell in Flt3$^+$ stem cells, respectively. Interestingly, labeling with magnetosomes resulted in lower iron concentration in DC (31.3 ± 5.4 pg/cell) but led to slightly increased uptake in Flt3$^+$ stem cells (16.8 ± 1.7 pg/cell) concomitant with the higher labeling efficiency of Flt3$^+$ stem cells by magnetosomes (Figs. 2a and 3). These findings further support the notion of different uptake mechanisms for MNPs in Flt3$^+$ stem cells and DC.
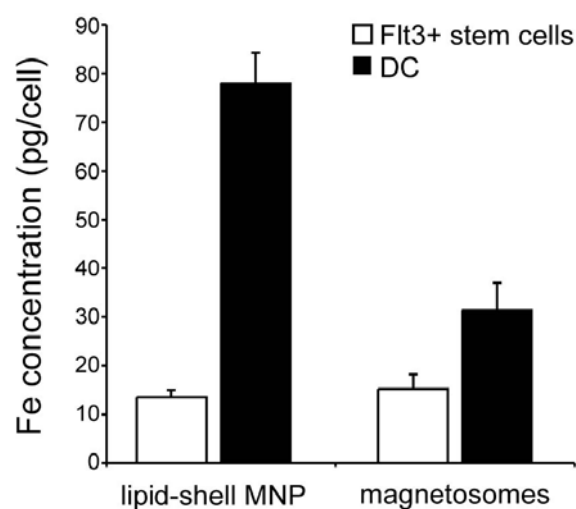

Figure 3. Intracellular iron concentration before and after uptake of MNPs by Flt3$^+$ stem cells and DC determined by ferrozine assay. Results are shown as mean ± SD (n=3).

Iron oxide nanoparticles are well known to possess longitudinal (T_1) and transversal (T_2 and T_2*) relaxation time shortening effects in magnetic resonance (MR) that make them particularly attractive as potential contrast agents for MR imaging (MRI) [5]. MR relaxometry experiments with the lipid-shell MNPs and bacterial magnetosome MNPs used in this study have been recently performed. Low R_1 relaxivities of 4.0 and 3.2 s^{-1} mM^{-1} and high R2* relaxivities of 729 and 1198 s^{-1} mM^{-1} were reported for lipid-shell MNPs and magnetosome MNPs, respectively, classifying them as potent contrast agents for both T_1 and T_2*-weighted MR imaging [12, 19]. Therefore, we investigated whether both lipid-shell and bacterial MNPs are particularly suitable contrast agents for cell tracking by MRI after uptake. To this end DC were labeled with lipid-shell MNP and magnetosome MNPs as before, magnetically separated and seeded at different cell numbers into agarose phantoms. T_2*-weighted 3D gradient echo MR images were acquired and processed using Paravision 4.0 software (Bruker Biospin) and NIH ImageJ. Scan sequences revealed a strong hypointense contrast by MNP-labeled DC in 3D T_2*-weighted MRI. Comparable signal reduction was obtained with both lipid-shell MNPs and magnetosome MNPs (Figure 4). The minimum detection limit of labeled DC was estimated at 10^1 cells µl^{-1}.
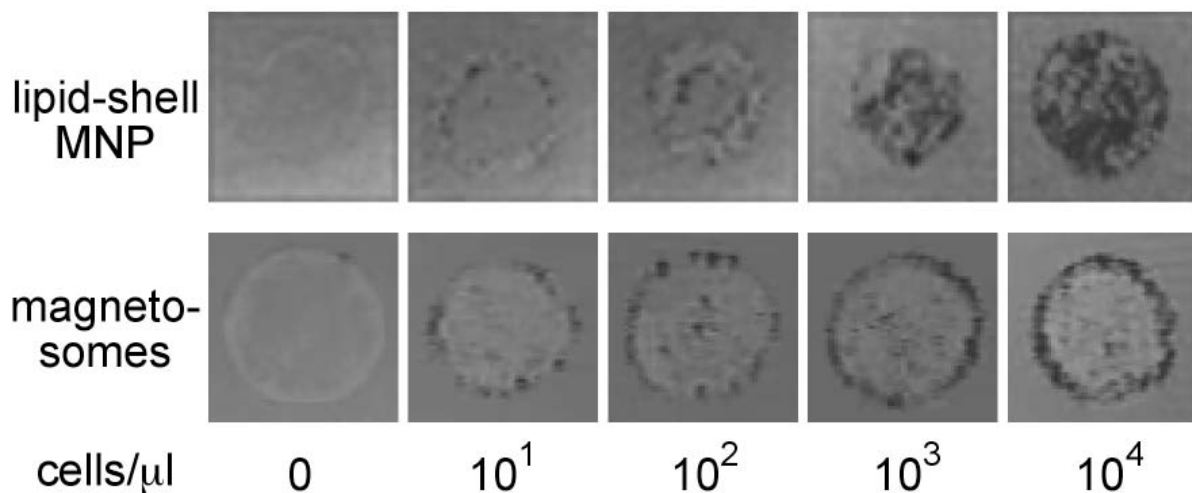

Figure 4. Sections of T_2* 3D gradient echo MR images of MNP-labeled DC in agarose phantoms. DC were labeled with MNPs for 24 h and after magnetic separation 10^2 o 10^5 cells were suspended in 10 µl agarose into 3.5 mm drill holes.

Migration from peripheral organs to regional draining LN after antigen uptake is an essential property of DC to initiate and regulate adaptive immune responses. Therefore, we investigated whether migration of MNP-labeled DC towards the draining LN after adoptive transfer into peripheral tissue is detectable by MRI. To address this question DC were labeled

with lipid-shell MNPs as before, magnetically separated and $2x10^6$ cells were intradermally transplanted into left femoral hind legs of C57Bl/6 recipient mice. As control, $2x10^6$ unlabeled DC were injected into the right femoral hind leg of the same recipient animal. A further control group of animals received $5x10^6$ MNP-labeled DC intravenously. Four mice per group were used and sacrificed 24 h after adoptive transfer of cells. Draining inguinal LN and nondraining axillary and mesenteric LN were dissected and split into halves. One half was embedded into an agarose phantom and analyzed by T_2*-weighted 3D gradient echo MR imaging. For histological comparison of MRI data, the second half was fixed, embedded into paraffin, sectioned and subjected to Prussian-blue staining for iron detection. We observed a significant intranodal signal reduction in MR images in the left inguinal draining LN 24 h after injection of MNP-labeled DC into the left hind leg (Figure 5a), whereas no signal reduction was detected in right inguinal LN where unlabeled DC were injected (data not shown). Furthermore, we found neither hypointense contrasts in non-draining LN nor after intravenous injection of MNP-labeled DC (data not shown). To corroborate whether the intranodal hypointense contrast was elicited by MNPs, Prussian-blue staining of the second halves of dissected LN were performed. No blue staining was detectable in all control LN indicating complete absence of MNP label. By contrast, a clear blue staining was localized in the T cell area of draining inguinal LN from MNP-loaded DC injection sites confirming the presence of MNPs (Figure 5b). Taken together, these results provide evidence that tracking of MNP-labeled DC towards target organs or tissues in living organisms can be achieved using MRI. Consequently, initial experiments for tracking of lipid-shell and magnetosome labeled DC *in vivo* to monitor their migration dynamics are currently under investigation.

a

b
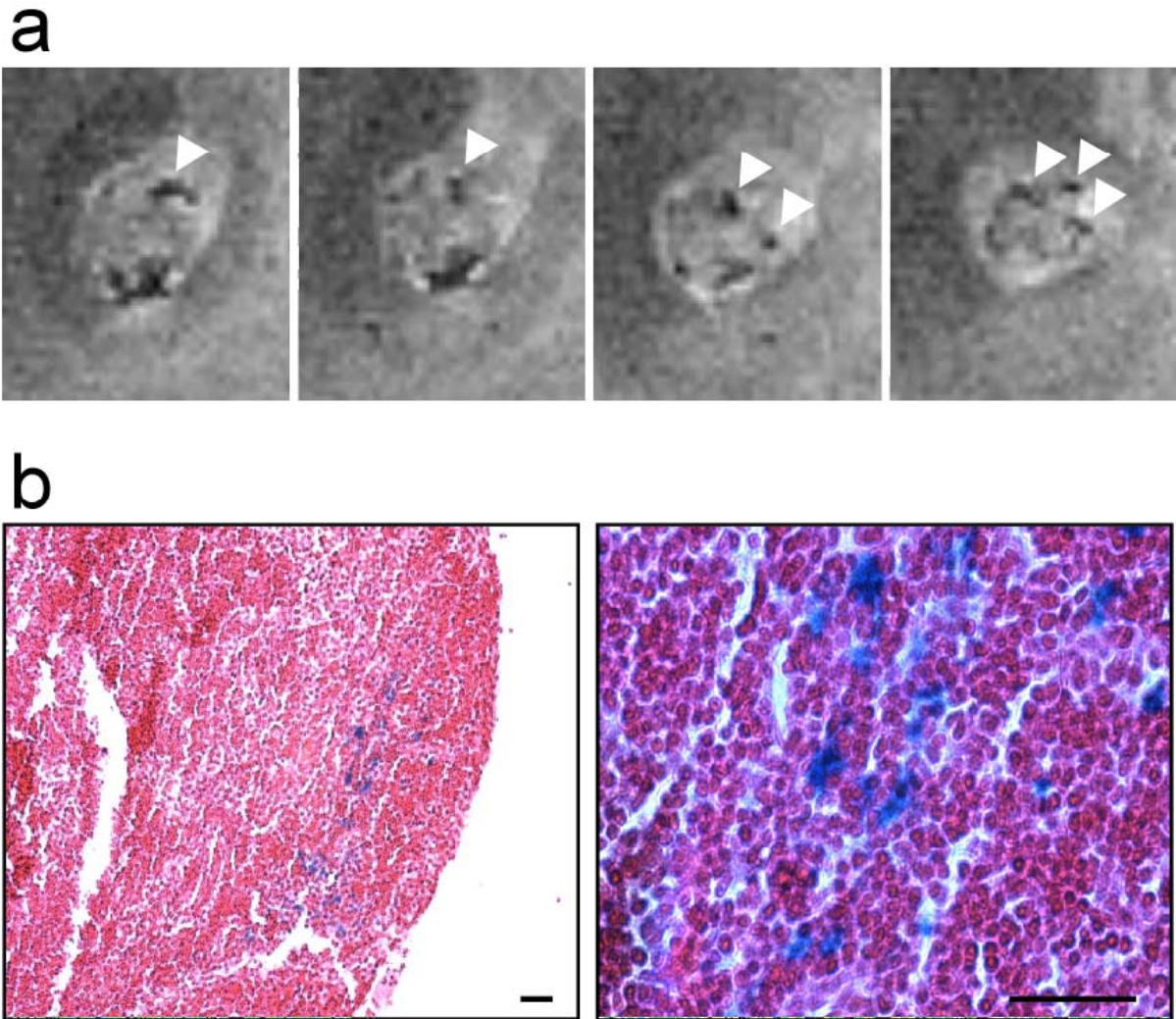
Figure 5. Detection of MNP-labeled DC after migration to draining lymphnodes. (a) T_2*weighted 3D gradient echo MR images of a single inguinal draining LN where MNP-labeled DC were injected into hind leg. Arrowheads indicate intranodal signal reduction. (b) Histochemical staining with Prussian-blue of the second half of LN as in (a). Right image shows 4 x higher magnification. Scale bars, 50 μm.

In summary, this study demonstrates effective uptake of both synthetic and biogenic MNPs into Flt3$^+$ stem cells and DC. Additionally, magnetosome MNPs were found to label hematopoietic Flt3$^+$ stem cells, albeit to a lower extent than DC. Electron microscopy analysis showed that subcellular localization of MNPs after uptake into DC was confined to intracellular vesicles. This result is in accordance to our previous study that showed colocalization of MNPs within the endosomal/lysosomal compartment, suggesting an uptake mechanism via endocytosis [10]. DC have a central role in antigen specific immune responses and detect and take up invading pathogens by specific cell surface receptors [1]. Pathogens exhibit highly conserved molecules referred to as pathogen associated molecular patterns (PAMPs; bacterial and fungal wall components, viral RNA or DNA etc). PAMPs bind to pattern recognition receptors on DC, such as Toll-like receptors (TLRs) and C-type lectins

(mannose receptor, DEC205, DC-SIGN etc.) and thus provoke antimicrobial and antiviral immune responses [20, 21].

Obviously, DC can be expected to sense MNPs through similar or identical pathways. Additionally, functional expression of PAMP recognition receptors (i.e. TLR2 and TLR4) was demonstrated on hematopoietic stem/progenitor cells [22]. Thus, depending on the molecular pattern of the particle shell, both synthetic and biogenic MNP might activate different pathways, leading to differentially regulated immune and/or cellular responses. Therefore, central questions that clearly have to be addressed are (i) to ascertain the molecular determinants on DC and stem cells that are important for the MNP/DC and MNP/stem cell interaction and (ii) how the physicochemical properties of MNP such as size, surface charge and particle shell composition determine their impact on cellular functions. Results obtained from such studies can be expected to form the foundation for further optimization and development of engineered MNPs with improved biocompatibility and labeling specificities for use in clinical therapies.

Magnetosomes represent yet another class of MNPs originating from magnetotactic bacteria as complex organelles composed of a magnetite crystal core enveloped by a biomembrane. Most fundamental, crystal mineralization and membrane composition of magnetosome MNPs are genetically determined by the bacterial strain. This opens the perspective to further enlarge MNP function by genetic engineering. Recently, this approach has been successfully used to fuse enhanced green fluorescent protein to the *mamJ* gene product from *M. gryphiswaldense* resulting in magnetosomes with bimodal imaging properties [23]. Apparently, magnetosome MNPs are emerging as a promising tool for various biotechnological and biomedical applications including MRI.

Acknowledgments

References

[1] J. Banchereau, R.M. Steinman, Nature 392 (1998) 245.

[2] M. Zenke, T. Hieronymus, Trends Immunol. 27 (2006) 140.

[3] C.G. Figdor, I.J. De Vries, W.J. Lesterhuis et al., Nat. Med. 10 (2004) 475.

[4] G.J. Adema, I.J. De Vries, C.J. Punt, et al., Current Opin. Immunol. 17 (2005) 170.

[5] U. Himmelreich, M. Hoehn, Minim. Invasive Ther. Allied Technol. 17 (2008) 132.

[6] J.W. Bulte. T. Douglas, B Witwer, et al., Nat. Biotechnol. 19 (2001) 1141.

[7] M. Hoehn, E. Kuestermann, J. Blunk, et al., PNAS 25 (2002) 16267.

[8] E.T. Ahrens, M. Feili-Hariri, H. Xu, et al., Magn. Reson. Med. 49 (2003) 1006.

[9] I.J. De Vries, W.J. Lesterhuis, J.O. Barentsz, et al., Nat. Biotechnol. 11 (2005) 1407.

[10] C. Becker, M. Hodenius, G. Blendinger, et al., J. Magn. Magn. Mater. 311 (2007) 234.

[11] U. Himmelreich, S. Aime, T. Hieronymus, et al., Neuroimage 32 (2006) 1142.

[12] M. Hodenius, T. Niendorf, G.A. Krombach, et al., J. Nanosci. Nanotechnol. 8 (2008) 2399.

[13] C. Hacker, R.D. Kirsch, X.S. Ju, et al., Nat. Immunol. 4 (2003) 380.

[14] T. Hieronymus, T.C. Gust, R.D. Kirsch, et al., J. Immunol. 174 (2005) 2552.

[15] T. Hieronymus, D. Ruau, J. Ober-Bloebaum et al., Cells Tissues Organs doi:10.1159/000112836.

[16] K. Grünberg, C. Wawer, B.M. Tebo, et al., Appl. Environ. Microbiol. 67 (2001) 4573.

[17] E. Küstermann, U. Himmelreich, K. Kandal, et al., Contrast Media Mol. Imag. 3 (2008) 27.

[18] J. Riemer, H.H. Hoepken, H. Czerwinska, et al., Analyt. Biochem. 331 (2004) 370.

[19] A. Hartung, M.R. Lisy, K.H. Herrmann et al., J. Magn. Magn. Mater. 311 (2007) 454.

[20] A. Iwasaki, R. Medzhitov, Nat. Immunol. 5 (2004) 987.

[21] M.J. Robinson, D. Sancho, E.C. Slack, et al., Nat. Immunol. 7 (2006) 1258.

[22] Y. Nagai, K.P. Garrett, S Ohta, et al., Immunity 24 (2006) 801.

[23] A. Scheffel, M. Gruska, D. Faivre, et al., Nature 440 (2006) 110.

Manuscript 8

Biomineralization of magnetosomes in bacteria: Nanoparticles with potential applications

Claus Lang, Dirk Schüler*

Microbial Bionanotechnology: Biological Self-assembly Systems and Biopolymer-based Nanostructures, Editor Bernd Rehm, Horizon Bioscience, Wymondham, 2006, Chapter 5, p. 107-124

Max Planck Institute for Marine Microbiology, Celsiusstr. 1, 28359 Bremen, Germany
*Corresponding author: dschuele@mpi-bremen.de.

Abstract

The ability of magnetotactic bacteria (MTB) to orient and migrate along magnetic field lines is caused by magnetosomes, which are membrane-enclosed intracellular crystals of a magnetic iron mineral. The biomineralization of magnetosomes is a process with genetic control over the accumulation of iron, the deposition of the magnetic crystal within a specific compartment, as well as the assembly, alignment and intracellular organization of particle chains. Magnetite crystals produced by MTB have uniform species-specific morphologies and sizes, which are mostly unknown from inorganic systems. The unique characteristics of magnetosome particles have attracted a great interdisciplinary interest and inspired numerous ideas for their biotechnological application. In this chapter, we summarize the current knowledge of the physicochemical and molecular genetic basis of magnetosome biomineralization. In addition, we give an overview over current examples and the potential for future applications of magnetic nanoparticles produced by bacteria.

Introduction

One of the most intriguing examples for the microbial synthesis of nanostructures is the biomineralization of magnetosomes. These inorganic structures are formed intracellularly in magnetotactic bacteria (MTB), in which they serve as a navigational device for spatial orientation along chemical gradients in stratified aquatic habitats, probably by interaction with the earth's magnetic field (Bazylinski and Frankel, 2004; Flies et al., 2005a). Magnetosomes comprise a magnetic mineral crystal enveloped by a biological membrane containing phospholipids and specific proteins. MTB not only exert a high degree of biological control over the design of the inorganic particles, but also the assembly, alignment and intracellular organization of magnetosomes is under genetic control, resulting in complex chain-like superstructures. Magnetosomes, which can be isolated from cells in larger quantities, also represent a new class of magnetic nanoparticles (MNP) with exceptional properties. In general, MNP provide numerous attractive possibilities in biotechnology, which is due to their unique characteristics. Their dimensions are within the order of magnitude of large biomolecules or viruses, and they can be manipulated by external magnetic field gradients and obey Coulomb's law (Tartaj et al., 2005). In addition they have a large surface, which can be used for modification. As intermediates between the molecular and solid state, nanosized magnetic particles have physical and chemical properties that are characteristic of neither the atom nor the bulk counterparts (Gupta and Gupta, 2005). In nanobiotechnology, they are ideal components for the construction of nanostructured materials and devices with adjustable

physical properties. Synthetic MNP are currently widely studied and applied in various fields of biotechnology such as magnetic drug targeting, magnetic resonance imaging (MRI), diagnostics, immunoassays, magnetic separation, and magnetic hyperthermia treatment. Using conventional inorganic synthesis, particles of magnetic iron oxide can be produced by the coprecipitation of Fe^{2+} and Fe^{3+} aqueous salt solutions (Cornell and Schwertmann, 2003). A major problem of the bulk solution synthesis is that the pH needs to be adjusted during synthesis and particle purification. Another obstacle is that the particles form aggregates during synthesis, which requires the application of nanostructured boundaries for particle formation by the use of sol-gel systems, polymer matrix-mediated synthesis or oil-in-water microemulsions. Other methods rely on aerosol-based techniques such as laser pyrolysis (for review (Gupta and Gupta, 2005; Tartaj et al., 2005). Although enormous efforts were spent during the last years to generate particles of nearly uniform size and shape, the synthesis of advanced nano-sized magnetic materials with innovative properties that can be tailored and functionalized according to the desired application has remained a challenge. As an alternative route, biomineralization processes have been suggested for the biosynthesis of MNP. One well studied example is the use of the iron-storage protein ferritin for the production of MNP. The demetallated protein shell of apoferritin assembles into a multi-subunit protein shell to form a hollow cage of about 8 nm in diameter. This represents a natural nanometer-sized bioreactor, which has been used by Mann and coworkers for the biomimetic reconstitution of the ferrimagnetic iron oxides magnetite (Fe_3O_4) and maghemite (γ-Fe_2O_3) (Meldrum et al., 1992) as well as the magnetic alloy cobalt platinum CoPt within the cores (Mayes and Mann, 2004). As a result, crystalline nanoparticles were formed with narrow size distribution and magnetic properties with promising potential for applications such as ultrahigh-density data storage. Another attractive alternative for the production of MNP by biomineralization is the use of magnetosomes produced by MTB. The current understanding of MTB biology as well the potential for future applications of magnetosomes are discussed in the following.

Magnetotactic bacteria

Magnetotactic bacteria represent a heterogeneous group of aquatic prokaryotes with a variety of morphological types, which can be assigned to various phylogenetic lineages. Commonly observed morphotypes include coccoid cells as well rods, vibrios and spirilla of various dimensions (Schüler, 1999). All known MTB are motile by means of flagella and have a cell wall resembling that of typical Gram-negative bacteria. In the environment, they

occur in highest numbers at or closely below the oxic-anoxic transition zone of marine and freshwater environments (Flies et al., 2005a). Magnetotaxis, the orientation along magnetic field lines, is thought to aid the bacteria in the navigation along the multiple and steep chemical gradients commonly found in that zone. Despite of their high abundance and ubiquitous occurrence, most MTB have proven recalcitrant to isolation and only very few species have been isolated in pure culture (Flies et al., 2005b). Difficulties in isolating and cultivating MTB arise from their lifestyle, which is adapted to complex chemical gradients that are typically encountered in stratified sediments. Accordingly, only a few species of MTB are available in pure culture. The microaerophilic alphaproteobacterium *Magnetospirillum gryphiswaldense* that has been isolated from a freshwater sample (Schleifer et al., 1991) can be grown in the lab more readily then other MTB. The cells produce a single a single chain of up to 60 magnetosome particles consisting of cubo-octahedral magnetite crystals (Figure 1). *M. gryphiswaldense* has recently emerged as a model organism both for the analysis of magnetite biomineralization and for the production of large quantitites of magnetosome particles. This has become possible by the establishment of techniques for mass cultivation and genetic manipulation as well as the availability of genome sequence data.
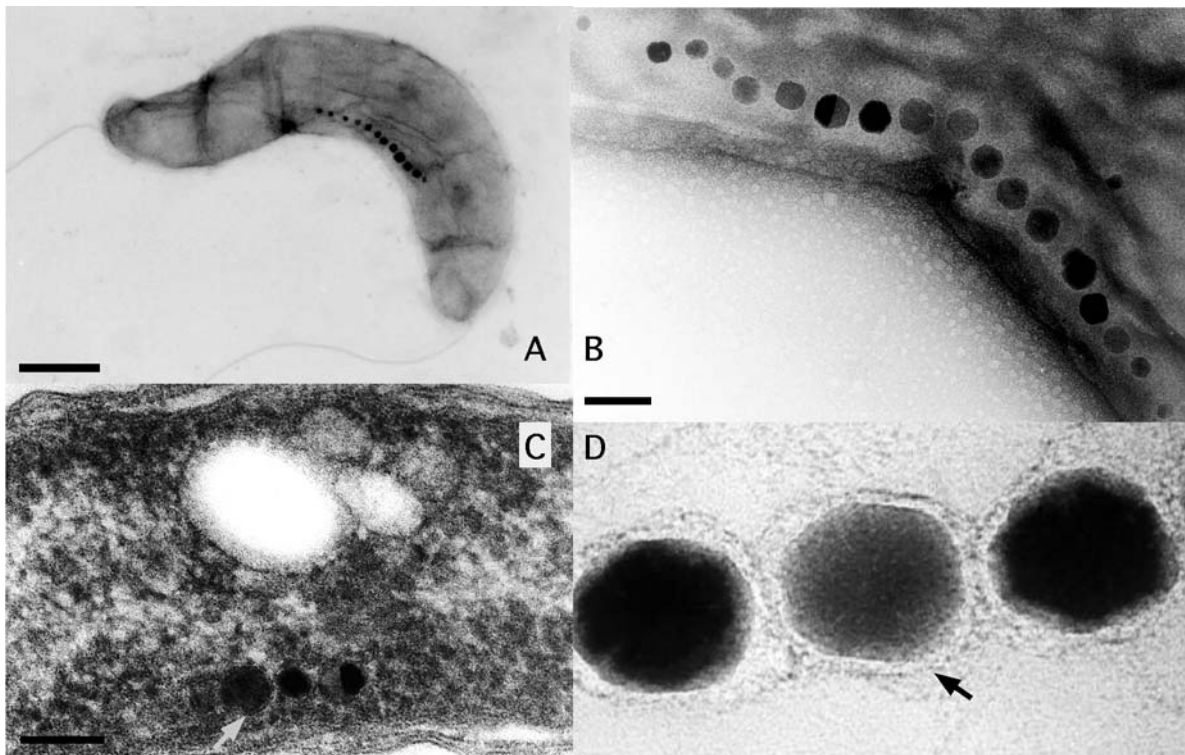

Figure 1: Magnetosomes of *Magnetospirillum gryphiswaldense*. Transmission electron micrographs displaying (A) a helically shaped cell with flagella and a single magnetosome chain, (B, C) the intracellular organization of the magnetosome chain and (D) isolated magnetosome particles with surrounding membrane. The membrane is indicated by a arrows.

Structure and biomineralization of magnetosome mineral crystals

The ability to align along magnetic field lines is based on the presence of magnetosomes, which are membrane-enclosed inorganic crystals consisting either of the magnetic mineral magnetite (Fe_3O_4) or greigite (Fe_3S_4) (Posfai et al., 1998, Schüler and Frankel, 1999). The particles are usually arranged along the cell axis in one or multiple chains, which are often located adjacent to the cytoplasmic membrane (Schüler, 1999). The particle sizes are typically 35-120 nm, which is within the single-magnetic domain-size for magnetite and greigite (Dunin-Borkowski et al., 2001; Moskowitz, 1995). The morphology, size and intracellular organization of the crystals is subject to a species-specific genetic control, and a large variety of crystal morphologies such as cubo-octahedral, elongated hexagonal-prismatic and bullet-shaped morphologies were reported (Schüler and Frankel, 1999) (Figure 2).
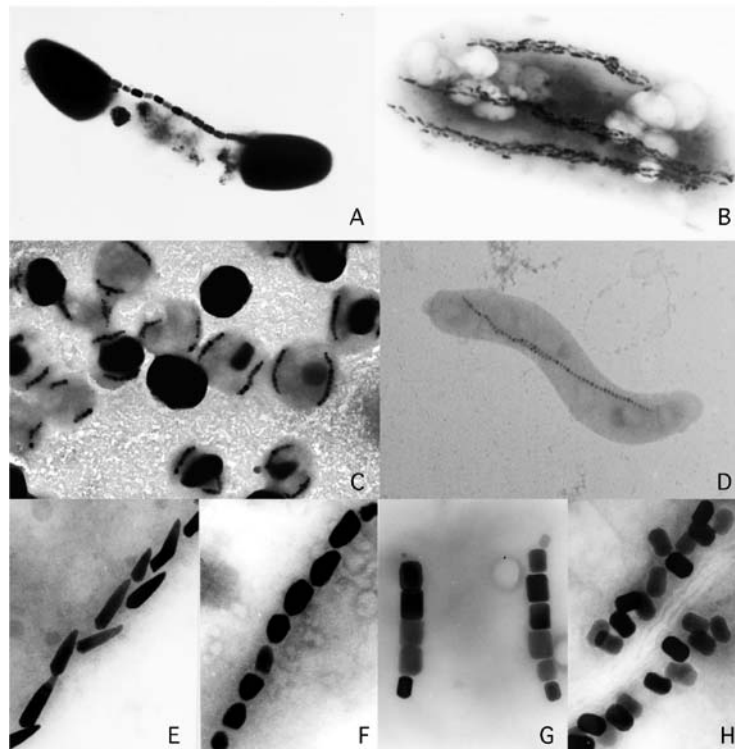

Figure 2: Diverstiy of magnetotactic bacteria and magnetosomes. A – D. Transmission electron micrographs of a variety of different morphological forms of magnetotactic bacteria, including large rod shaped bacteria with a one or several magnetosome chains (A, B), coccoid cell forms (C) and spirilla (D). E – H Electron micrographs of crystal morphologies of magnetosomes found in various magnetotactic bacteria.

It was demonstrated by high resolution transmission electron microscopy, electron diffraction and electron holography that the morphologies of magnetite crystals in magnetosomes are derived from combinations of the isometric forms {1 1 1}, {1 1 0} and {1 0 0} (Devouard et al., 1998; Moskowitz, 1995). Morphological variations such as elongated

181

and prismatic structures are due to anisotropic crystal growth, which could be explained by chemical gradients and unequally distributed ion influx into the magnetosome vesicle. Alternatively, growth of particular crystal lattice planes could be selectively favored or inhibited by the specific interaction with biomineralization-mediating proteins. For magnetite biomineralization, iron can be taken up by the cell as Fe(III) or Fe(II) from the medium. Fe(III) ions are then thought to be reduced to Fe(II) during uptake or in the cytoplasm and subsequently transported to the magnetosome vesicle (Bazylinski and Frankel, 2004). A part of the iron is then reoxidized to form a highly reactive Fe(III) oxide, probably ferrihydrite, which may react with dissolved Fe^{2+} to form magnetite by a via-solution process (Cornell and Schwertmann, 2003). Iron for magnetite synthesis is assimilated very efficiently from relatively low environmental concentrations. In *M. gryphiswaldense*, ferric iron is incorporated by a high-affinity uptake system, which is saturated at extracellular iron concentrations of 15-20 µM Fe (Schüler and Baeuerlein, 1996). Notably, the growth of a mutant, which lost the ability to form magnetosomes, was more sensitive to elevated concentrations of iron (Schübbe et al., 2003). This might be indicative of a contribution of magnetite formation to iron homeostasis and detoxification of potentially harmful high intracellular levels, similar, for instance, to the iron-storage proteins ferritin and bacterioferritin (Andrews et al., 2003). The number of magnetite particles per cell is variable depending on growth conditions. Besides the availability of micromolar amounts of iron, microaerobic conditions are required for magnetite formation.

Electron holographic studies of *M. magnetotacticum* MS-1 demonstrated that the magnetosome particles are in a single domain magnetic state in the cell and are uniformly magnetized to the saturation magnetization of magnetite (Dunin-Borkowski et al., 2001).
The magnetite particles are oriented with the [1 1 1] magnetic easy axis along the chain direction within the cell, and one or more straight chains are present parallel to the long axis of the cell (Blakemore and Frankel, 1981). In this organization, an average magnetosome chain of *M. magnetotacticum* MS-1 confers a magnetic dipole moment of 5 x 10^{-16} Am^2 to the cell (Dunin-Borkowski et al., 2001). The torque exerted by the geomagnetic field on the cellular dipole is sufficient for the passive orientation of the cell in the earth magnetic field (Frankel, 1984). Thus, mechanisms for the tight control of the mineral type of iron, the size and the shape of the magnetosomes as well as the length and orientation of the magnetosome chain developed in magnetotactic bacteria to generate a magnetic dipole which permits efficient migration along magnetic field lines.

Structure and biochemical composition of the magnetosome membrane, a unique subcellular structure in prokaryotes

Compartmentalization through the formation of membrane vesicles enables the processes of magnetite mineralization to be regulated by biochemical pathways. The MM is the crucial component in the control of crystal growth, thereby providing spatial constraints for shaping of species-specific crystal morphologies. Biomineralization of magnetite requires a precise regulation of both the redox potential and the pH. The growth of magnetite crystals is ultimately regulated by the uptake mechanisms and depends on a controlled flux of ions over the MM to provide a supersaturating iron concentration within the vesicle. Thus, the MM has to perform specific functions in the transport and accumulation of iron, nucleation of crystallization, and redox and pH control (Gorby et al., 1988; Schüler, 2002). Most of the knowledge of the MM comes from the analysis of *M. gryphiswaldense*. However, there are indications that the structure and mechanism of its formation is highly similar in related *Magnetospirilla* and other MTB (Gorby et al., 1988).

Isolated magnetosomes have a strong tendency to form chains, indicating that an inter-particle connection mediated by MM components is involved in the organization of chains. A number of common fatty acids were identified in extracts of the magnetosome membrane from *M. gryphiswaldense* (Grünberg et al., 2004). Phosphatidylethanolamin and phosphatidylglycerol were identified as the most abundant polar lipids, whereas ornithinamidlipid and an unidentified aminolipid are less abundant in the MM compared to the fraction of lipids from the outer and cytoplasmic membrane (Baeuerlein, 2000; Grünberg et al., 2004). Analysis of the extracted membrane revealed that the magnetosome is associated with a highly specific and complex subset of proteins, which are present in various quantities. The amount of MM-bound polypeptides approximately represents 0.1 % of the total cellular protein (Grünberg et al., 2001). Biochemical analysis in combination with various proteomic techniques have lead to identification of all major magnetosome membrane proteins (MMPs) (Grünberg et al., 2004; Grünberg et al., 2001; Schübbe et al., 2003). Approximately 20 major polypeptides have been identified in the magnetosome subproteom, several of them occurring in various posttranslational modifications of the same gene product. A number of minor constituents were occasionally found bound to isolated magnetosomes (Schultheiss et al., 2005). The different resistance of magnetosome proteins towards proteases and detergents indicates that some proteins (e. g., MamC, MamF) are very tightly bound to the magnetosome crystals and/or embedded within the membrane. Others, like for instance MamA, seem to be loosely attached and can be selectively solubilized by mild detergents (Grünberg et al., 2004).

Several of the proteins contain covalently bound c-type heme as revealed by peroxidase staining. No glycoproteins, which are common constituents of other biomineralizing systems, have been detected so far.

Based on sequence analysis, most MMPs can be assigned to a number of characteristic protein families, which seem to be shared by all MTB. MamA, which has been also identified in the MM of other *Magnetospirillum* species (Okuda et al., 1996), is an abundant protein of the MM and contains 4-5 copies of the TPR (tetratricopeptide repeat) motif. TPR motifs, which have been identified in a growing number of proteins with diverse functions, are known to mediate protein-protein interactions (Blatch and Lassle, 1999). It therefore has been speculated that MamA acts as a receptor in the MM interacting with cytoplasmic proteins or is involved in the assembly of multiprotein complexes within the MM (Okuda et al., 1996; Okuda and Fukumori, 2001). However, mutants of *Magnetospirillum* strain AMB-1 in which the *mamA* gene was deleted, produced magnetosome particles indistinguishable in morphology and organization from those of the wild type cells, albeit in slightly reduced numbers (Komeili et al., 2004). This clearly argues against an essential role of the MamA protein in magnetosome biomineralization.

Both MamB and MamM are members of the CDF (cation diffusion facilitator) family of metal transporters, which comprises proteins that function as efflux pumps of toxic divalent cations, such as zinc, cadmium, cobalt and other heavy metal ions. Specifically, MamB and MamM have greatest similarity to the CDF3 subfamily, which was postulated to comprise putative iron transporters (Nies, 2003). It has been speculated that MamB and MamM are involved in the magnetosome-directed uptake of iron, and preliminary evidence obtained from mutant analysis seems to support this assumption (Junge *et al*. unpublished). MamE and MamO display sequence similarity to HtrA-like serine proteases. The *mamP* gene, encoding a further deduced protein with similarity to this family, is colocated with *mamE* and *mamO* within the same operon. HtrA-like proteins share a conserved trypsin-like protease domain and one or two PDZ domains. They act as molecular chaperones and heat-shock induced proteases, which degrade misfolded proteins in the periplasm (Clausen et al., 2002). It has been suggested that MamE and MamO are involved in magnetosome formation, perhaps by the processing, maturation and targeting of MMPs during MM assembly (Grünberg et al., 2001).

The most abundant MM-associated proteins MamC, MamD, MamG, and MamF have no known homologues in organisms other than MTB, and thus represent unique, MTB-specific protein families. One noticeable feature common to several of these proteins is the

presence of repetitive motifs. Examples are MamD, Mms6 and MamG, which share conspicuous hydrophobic sequence motifs that are rich in repeated leucine and glycine residues. Similar motifs containing LG-rich repetitive sequences have been found in other proteins that have a tendency for self-aggregation or are involved in the formation of supramolecular structures (Schüler, 2004). The Mms6 protein of *Magnetospirillum* strain AMB-1 is a tightly bound constituent of the MM, which exhibits iron binding activity and has an effect on the morphology of growing magnetite crystals *in vitro* (Arakaki et al., 2003). Another conspicuous sequence pattern is found in MamJ. MamJ, which displays extensive self-similarity, is particularly rich in repeats of the acidic amino acid residues glutamate and aspartate. A number of additional conspicuous proteins with highly repetitive and/or acidic sequence motifs can be deduced from the genome assemblies of *M. gryphiswaldense* and other MTB. Clusters of polyelectrolytic groups are commonly found in proteins interacting with minerals (Baeuerlein, 2003). Thus, it can be speculated that MamJ is bound by electrostatic interactions to the surface of magnetite crystals.

Genetic organization of mam-genes and genetic manipulation of magnetite biomineralization

All identified MMPs are encoded within a single genomic region, which represents a hypervariable "magnetosome island" that could be functionally linked to magnetosome synthesis in a nonmagnetic mutant strain harboring a large chromosomal deletion (Schübbe et al., 2003). Magnetosome genes are colocated in three different operons, which are linked within less than 35 kb in the genome *of M. gryphiswaldense* (Figure 3).

As can be inferred from the available genome data of different MTB, the gene order and amino acid sequences of the predicted Mam proteins are conserved in other MTB including *M. magnetotacticum* and the remotely related magnetic coccus strain MC-1 (Grünberg et al., 2001). Remarkably, the regions within flanking these clusters are characterized by the presence of numerous genes encoding mobile DNA elements such as insertion elements and phage-associated integrases, which account for more than 22 % of the coding sequence and are involved in the extreme genetic instability of this region under conditions of stationary growth (Schübbe et al., 2003). In summary, all these features are strongly reminiscent of those described for genome islands in other bacteria. They often encode "accessory" gene functions, are genetically unstable and can transfer horizontally (Dobrindt et al., 2004). Thus, it seems that essential gene functions for magnetite synthesis are

organized within a large genomic "magnetosome island", which may have been distributed by lateral gene transfer.
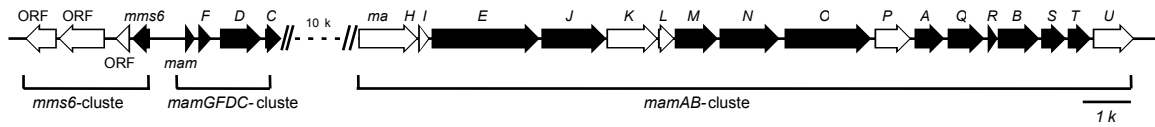

Figure 3: Molecular organization of the *M. gryphiswaldense* MSR-1 'magnetosome island'. The 35 kb genomic region comprises the *mms6*-cluster, the *mamGFDC* cluster and the *mamAB* cluster, which encode for most proteins found in the magnetosome membrane (indicated by black-filled arrows).

Cultivation of MTB and biotechnological production of magnetosomes

MTB can be enriched and collected from their natural environment sources such as mud samples by exploiting their active migration along magnetic field lines for example in 'racetrack' methods (Schüler et al., 1999; Wolfe et al., 1987). Thus, early attempts for the study and applications of the bacteria and the magnetic particles derived from them relied on magnetically collected MTB from heterogeneous natural populations without their axenic cultivation in the laboratory (Matsunaga and Kamiya, 1987; Moench and Konetzka, 1978). However, for a biochemical and molecular analysis of the magnetosome biomineralization as well as for the development of advanced applications, the isolation of appropriate strains and the establishment of for their mass cultivation was an essential requirement. Despite numerous efforts to isolate various abundant MTB from different habitats, only a limited number of isolates is available as pure cultures and most of the isolates are poorly characterized in terms of growth conditions. Problems in their cultivation are due to the fact that MTB strictly depend on complex patterns of vertical chemical and redox gradients present in their natural habitats, which are difficult to reconstruct in laboratory systems (Flies et al., 2005b; Flies et al., 2005a). Therefore, *Magnetospirillum* strains have been most widely used for the isolation of magnetosomes (Blakemore et al., 1979; Matsunaga, 1991; Matsunaga et al., 1990; Schüler and Baeuerlein, 1996; Schüler and Köhler, 1992). These strains can be grown microaerobically on simple liquid media containing short organic acids as a carbon source and ferric iron chelates as iron sources. However, although the cells have anoxygen-dependent respiratory metabolism, they do not tolerate the oxygen pressure of air. As growth and magnetosome formation depend on microaerobic conditions, the control of a low oxygen concentration in the growth medium is of critical importance and requires specific methodology. For example, cultivation on solid media is a necessary prerequisite for clonal

selection in genetic experiments, which is not easily achieved with MTB and required the establishment of a special plating technique (Schultheiss and Schüler, 2003).

Initial attempts to scale-up growth and magnetosome production were done with strain *Magnetospirillum* sp. AMB-1. Growth in a 1000 L fermenter yielded 2.6 mg l^{-1} (dry weight) magnetosomes with maximum cell densities of 1.8 x 10^8 cells per liter (Matsunaga et al., 1990). Several modifications resulted in an increase of magnetosome production to about 145 mg per liter of culture and a productivity of 1.85 mg magnetite l^{-1} day^{-1} in a 10 l fermenter (Matsunaga et al., 1996; Yang et al., 2001). Fermenter-scale fermentation of *M. gryphiswaldense* MSR-1 was first reported by Schüler and Baeuerlein (Schüler and Baeuerlein, 1997). A sophisticated technology for mass cultivation of MTB in an automated oxygen-controlled fermenter was established later, which allows the continuous maintenance of low pO$_2$ concentrations (Heyen and Schüler, 2003). This was achieved by a gas control regime that exactly maintains very low pO$_2$ tensions over a wide range of cell densities with fluctuations less then 5% of the set value. In a comparative study, a productivity of 6.3 mg magnetite l^{-1} day^{-1} was reported for *M. gryphiswaldense* compared to 3.3 and 2.0 mg magnetite l^{-1} day^{-1} for *Magnetospirillum sp.* AMB-1 and *M. magnetotacticum* MS-1, respectively (Heyen and Schüler, 2003). Among these strains, *M. gryphiswaldense* exhibited the highest oxygen tolerance, and growth was unaffected by oxygen concentration over a wide range (0.25 up to 150 mbar). However, magnetite formation occurred only below a threshold value of 10 mbar, whereas it was inhibited at higher oxygen concentrations. A clear correlation between the amount of magnetite formed and pO$_2$ exists, and most favorable conditions for magnetite biomineralization were found at 0.25 mbar (Figure 4). Interestingly, reduced particle sizes (20 nm diameter in comparison to 42 nm of particles produced under optimal conditions) and irregular particle shapes were observed when cells were grown at intermediate pO$_2$ tensions of 10 mbar. Hence, the size and morphology can be controlled by growth conditions within a certain range.

Compared to organic cell constituents, magnetosome particles are distinguished by (i) their high density (Magnetite: 5.1 g ml^{-1}) and (ii) their unique ferrimagnetic properties. This can be employed for their purification from disrupted cells using a straight-forward isolation protocol. After cell disruption the magnetosomes can be easily separated from the crude extracts by magnetic separation columns (Grünberg et al., 2004. Magnetic separation is followed by ultracentrifugation into a 55 % [w/w] sucrose cushion. This procedure results in suspensions of purified magnetosome particles with intact enveloping membrane structures (Fig 5). Isolated magnetosomes are relatively stable in the presence of mild detergents. The

MM can be easily solubilized by treatments with 1% SDS or organic solvents, which results in the agglomeration of membrane-free magnetite particles (Grünberg et al., 2004).
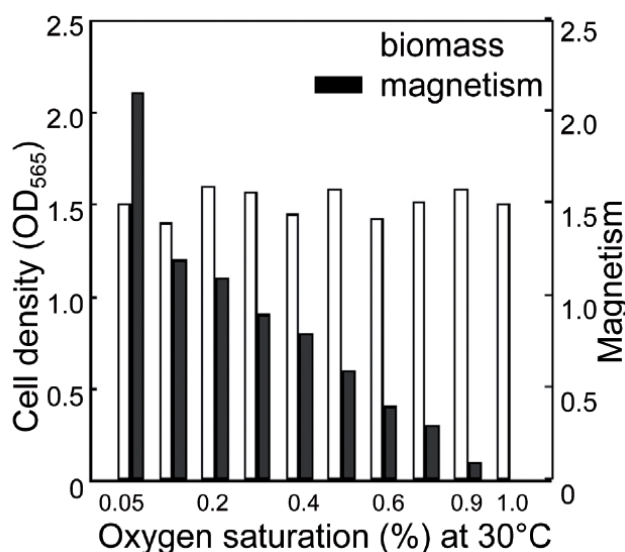

Figure 4: Oxygen dependence of cell yield and magnetosome formation in oxystat-grown *M. gryphiswaldense* **MSR-1**
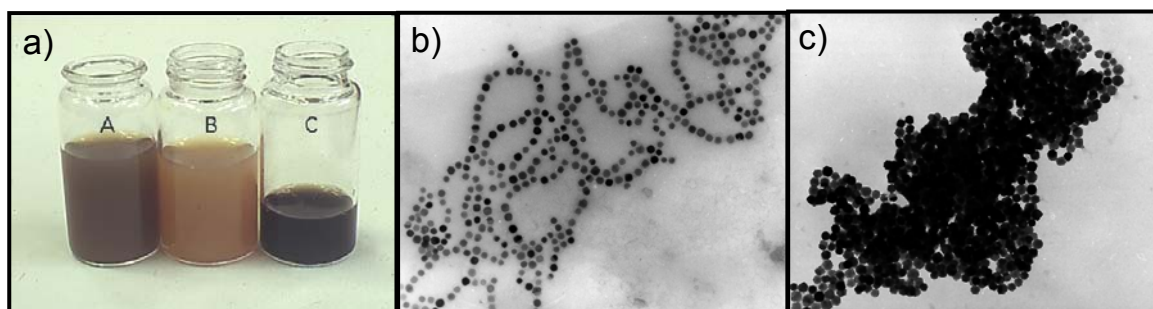

Figure 5: Magnetosome isolation from mass cultivated *M. gryphiswaldense* **MSR-1.**

A. Magnetic fractionation of total cell lysate (flask A) into non-magnetic cell-debris (flask B) and the magnetosome fraction (flask C). Isolated magnetosome particles with intact membranes display a strong tendency to chain formation (B) and form large aggregates if the membrane is removed after treatment with hot SDS (C).

Characteristics and biotechnological applications of bacterial magnetosomes

A wide range of technological and biomedical applications are based on magnetic nanoparticles (MNP). Technical applications included the use of particles in form of ferrofluids as magnetic inks, in magnetic recording media, as liquid sealings, as dampers in motors and shock absorbers, and for heat transfer in loudspeakers (Raj et al., 1995; Zahn, 2001). Another recent trend has been the development of MNP for biomedical applications (reviewed in (Berry and Curtis, 2003; Gupta and Gupta, 2005; Pankhurst et al., 2003; Safarik and Safarikova, 2002; Tartaj et al., 2003). Despite the large diversity of applications some the

following basic properties of MNP are desired in nearly all cases: Narrow size distribution, high magnetic susceptibility, uniform sizes and shapes, low toxicity, good dispersibility, tailored surface chemistry.

Since their discovery, the unique features of MTB have inspired numerous ideas for the application of MNP produced by bacteria. Magnetosome crystals display narrow size distributions and uniform morphologies. Typical sizes of the monocrystalline particles are in a range, which is not easily accessible to chemical synthesis. Moreover, the highly controlled pathway of biosynthesis has resulted in a morphological diversity and, in some bacteria, shape anisotropies, which are unknown from inorganically produced magnetite crystals. Studies on magnetosome suspensions by magnetorelaxometry, DC-magnetometry and atomic force microscopy as well magnetic force microscopy revealed that the particles have a high magnetization, and the magnetic moments of single-domain magnetosome particles are predominantly in a blocked state (Eberbeck et al., 2004; Hergt et al., 2005). Particle sizes from 5-15 nm are considered ideal for many biomedical uses of MNP (Berry and Curtis, 2003; Gupta and Gupta, 2005). Particles of this size can not only diffuse through most tissues in the human body, but also display unique magnetic properties (Berry and Curtis, 2003), as they are superparamagnetic at room temperature (Chatterjee et al., 2003). This means that the particles have high saturation magnetization values if an external magnetic field is applied, but upon removal from the magnetic field the magnetic moment fluctuates freely in response to the thermal energy (Pankhurst et al., 2003). While mature magnetosome crystals are mostly within the ferrimagnetic size range, the crystal sizes are under biological control and can be genetically modified. Mutants are already available, which display altered magnetic characteristics. As revealed by Small Angle Scattering using polarized neutrons (SANSPOL), magnetic particles from a mutant not only exhibit a narrower size distribution then those from the wild type, but with an average core diameter of 15.6 nm mutant particles predominantly fall into the superparamagnetic size range (Hoell et al., 2004). As the particles are produced by a biological process, the iron oxide cores can generally assumed to have low toxicity compared to the alloys (neodymium-iron-boron, samarium-cobalt, nickel or cobalt compounds) used for the chemical synthesis of some MNP (Tartaj et al., 2003).

On of the most interesting features of bacterial magnetosomes is the presence of a biological membrane of defined biochemical composition. The encapsulation of the magnetic crystal within the MM provides a natural "coating", which ensures superior dispersibility of the particles and provides an excellent target for modification and functionalization of the particles. Despite the enormous efforts in chemical synthesis of MNP, some unique properties

of bacterial magnetosomes are currently unmatched. These remarkable features may designate bacterial magnetic nanoparticles as an appealing alternative for numerous sophisticated applications, which rely on small amounts of highly functionalized magnetic material with extraordinary magnetic and biochemical characteristics. In the following, we summarize several studies on the application of bacterial magnetosomes, which have been reported over the last two decades.

MNP have been used in a number of *in vitro* methods, such as magnetic separation and procedures for labeling and immobilization of various biomolecules. The use of Magnetosomes has been also described for numerous purification procedures such as the extraction of mRNA and DNA from biological samples such as tissues, blood and bacterial cells. For instance, the efficiency of DNA recovery with dendrimer-modified magnetosome particles was 6-fold higher with bacterial particles than with artificial particles (Yoza et al., 2003c). The automation of a DNA extraction procedure based on dendrimer-modified particles has been reported recently (Yoza et al., 2003a; Yoza et al., 2003b). The isolation of mRNA was facilitated by oligo(dT) modified magnetosomes (Sode et al., 1993). Magnetosomes similarly modified with oligonucleotides have been employed in an automated magnetic microarray for the detection of different cyanobacterial DNA with genus specific probes (Matsunaga et al., 2001).

Another set of biotechnological applications is based on the immobilization of proteins, peptides and enzymes on magnetic particles, which allows the selective separation and reuse of immobilized enzymes from a reaction mixture. Compared to micrometric particles the use of nanosized particles is preferred due to (i) their higher specific surface area and therefore higher binding capacity and (ii) their lower mass transfer resistance. Because of their large surface-to-volume ratio bacterial magnetosomes particles could be successfully harnessed for immobilization of the enzymes glucose oxidase and uricase as early as 1987 (Matsunaga and Kamiya, 1987). Likewise, the immobilization of immunoglobulins has received great attention and inspired the development of diverse applications. One approach of immunoglobulin immobilization on magnetic particles relied on chemical crosslinking of the antibody with the magnetosome membrane (Nakamura and Matsunaga, 1993). Another approach attempted the genetic modification of magnetosome membrane proteins to generate protein fusions of a magnetosome membrane protein and an immunoglobulin binding protein such as the Z domain of protein A or protein G (Tanaka and Matsunaga, 2000; Yoshino et al., 2004). The second approach is potentially superior to chemical crosslinking, as the antibody is oriented more accurately, although it remains to be shown that the polypeptides used for the

genetic fusion are in fact native constituents of the MM. Antibody-magnetosome conjugates were employed for automated immunoassays to detect environmental pollutants, hormones and toxic substances (Tanaka and Matsunaga, 2000; Tanaka et al., 2004). In addition, antibody-modified magnetosomes have been used successfully for the specific separation of target cells from human blood (Kuhara et al., 2004). Another application is the use of streptavidin-modified magnetosomes for the automated discrimination of single nucleotide polymorphism. The streptavidin-modified particles were coupled to biotinylated oligonucleotides to facilitate magnetic separation of DNA hybrids. Single nucleotide polymorphisms were detected as decreased fluorescent intensities in a fluorescence resonance energy transfer (FRET) system with FITC (donor)-labeled DNA and a POPO-3 (acceptor), which preferentially intercalates double stranded sequence of complementary strands (Tanaka et al., 2003)

MNP have been also attracted an increasing interest for their use in a number of biomedical *in vivo* applications. One field, in which synthetic MNP have already found commercial application is magnetic resonance imaging (MRI). MRI enables the discrimination of tissues which is facilitated by the utilization of MRI contrast agents such as iron oxide particles. Tumor cells can be detected by MRI because they do not accumulate resonance enhancing particles due to the lack of an effective reticuloendothelial system (reviewed in (Pankhurst et al., 2003)). The potential of biomineralization for this purpose has been recognized a few years ago (Bulte and Brooks, 1997; Bulte et al., 1994a; Bulte et al., 1994b). The usefulness of magnetosomes for the detection of microtumors in rats by MRI has been already demonstrated and might provide the application of lower doses due to the superior magnetic properties of bacterial particles (Baeuerlein et al., 2001; Reszka, 2000).

Magnetic particles bearing pharmaceutical drugs comprise a promising tool for targeted drug delivery. In principle, drug-modified particles are injected into the blood stream and concentrated at a target tissue by strong external magnetic fields. The drug can then be released by enzymatic activity or changes of temperature, pH or osmolarity. Based on a similar principle as drug targeting is the magnetofection approach for targeted *in vivo* and *in vitro* gene delivery ("Magnetofection"). Here, magnetic fields are employed to concentrate genetic vectors immobilized on MNP in target tissues and enhance the efficiency of gene delivery (reviewed in (Plank et al., 2003). In preliminary studies it was observed that magnetosomes modified by encapsulation in liposomes can efficiently capture organic model substances such as FITC labeled DNA and chemotherapeutic drugs and release of the substances can be induced by application of a rotating magnetic field (Matsunaga et al.,

2004). Despite these promising results *in vivo* studies to demonstrate the efficient magnetic drug targeting with bacterial magnetic particles are still not available.

Another promising biomedical application for biogenic magnetic particles is the method of hyperthermia treatment, in which MNP are used for controlled tissue heating to promote cell necrosis. After MNP are applied to the target tissue, an alternating external magnetic field is applied. Due to loss processes resulting from the reorientation of the magnetic moments of the particles, heat is generated, which results in cell necrosis in tumor cells (Hilger et al., 2000). The method relies on the development of magnetic nanoparticles with high specific loss powers (Hergt et al., 2005). In comparison to artificial magnetic particles bacterial magnetosome particles display an enormous hysteresis, which corresponds to a coercive field of 6500 A m^{-1} in comparison to 20 A m^{-1} of the artificial particles (Eberbeck et al., 2004). In a recent study of magnetosomes from *M. gryphiswaldense* in biomedical applications such as hyperthermia and thermoablation, Hergt and coworkers found exceptionally high specific powers losses (960 g W^{-1} at 10 kA m^{-1} and 410 kHz), which substantially exceed the results obtained with artificial particles (Hergt et al., 2005). The broad hysteresis and high coercivity indicates that the particles are promising candidates for heating applications.

Conclusions and Outlook

Magnetotactic bacteria have solved the problem of intracellularly synthesizing magnetic nanostructures with unique characteristics that cannot yet be fully replicated by inorganic approaches. The solution involves a hierarchical structure –the magnetosome chain– and a mineralization process with control over the chemical composition, morphology, size and intracellular location of the magnetic mineral. In this chapter, we have highlighted much of the current knowledge about the physiological and genetic basis of magnetosome biomineralization as well as potential uses of magnetosome particles in a number of biotechnological applications. Research progress in this field has increased tremendously over the last few years and we can expect to see many new insights within this exciting field of research. Beside the establishment of techniques for the improved handling and cultivation of MTB in the laboratory, the establishment of methods for genetic manipulations for several MTB species as well as efforts in the determination of their genome sequence represented major breakthroughs. This has contributed much to the advancement of this field, although there are many open questions left. For instance, functions of many of the genes identified within the magnetosome island and of several MMPs have remained cryptic. However, with

the recent advent of genetic technology for transformation and site-directed mutagenesis for MTB (Schultheiss et al., 2005; Schultheiss et al., 2004; Schultheiss and Schüler, 2003), genetic analysis has become a powerful tool in the study of magnetosome formation. The capabilities of MTB to precisely control the composition and morphology of inorganic of particles has been explored only recently, and has contributed to the development of a new and largely unexplored area based on the use of MTB in biosynthesis of magnetic nanomaterials. The available genetic technology will not only allow to elucidate the pathways of magnetosome formation at molecular level, but also holds great promise for the design of biogenic magnetic nanoparticles with desired properties by genetic engineering. An *in vivo* "tailoring" can be applied both to organic and inorganic constituents of magnetosomes. It has already been demonstrated that certain mutants produce magnetite crystals that are superior to wild-type magnetosome in terms of morphology, size distribution and magnetic characteristics (Hoell et al., 2004). The site-directed mutagenesis of identified iron-transporting magnetosome proteins might be used to generate magnetosome with a modified specificity for the magnetosome-directed uptake of different metals, potentially resulting in inorganic magnetic cores with an altered chemical composition. Likewise, the biochemical composition of the magnetosome membrane may be altered *in vivo* by genetic engineering. A highly attractive and promising approach will be the design of magnetosomes with functionalized surfaces. This can be achieved for instance by the generation of chimeric proteins, which are specifically displayed on the surfaces of isolated magnetosomes. It has been already demonstrated that magnetosome proteins can be used for the construction of functional genetic fusions with the *green fluorescent protein*, which do not interfere with the formation of magnetite crystals (Komeili et al., 2004; Schultheiss et al., 2005). In an analogous manner, coupling to magnetosomes proteins, either *in vivo* by genetic technology or *in vitro* by chemical means, might be used for the introduction of functional moieties, as for instance biomolecular recognition groups such as the biotin-streptavidin system (Fig 6). This would endow improved functionality to isolated magnetosome particles, which would be extremely useful as building blocks in a variety of nanotechnological approaches, where controlled self-assembly of magnetic MNP into ordered structures are required (Lee et al., 2004; Niemeyer, 2001).

Although the *in vivo* fabrication of engineered and functionalized magnetosome holds great promise, the production and processing of bacterially synthesized particles is still relatively laborious and costly. Therefore, another attractive approach is the biomimetic synthesis of MNP with properties comparable to bacterial magnetosomes. The *in vitro*

reconstitution of bacterial magnetite precipitation will not only help to elucidate the chemical pathway of biomagnetite formation, but could also be used for the production of magnetic nanomaterials with advanced properties. In initial biocrystallization experiments, a magnetosome protein (Mms6) was shown to affect *in vitro* the morphology of magnetite crystals (Arakaki et al., 2003). Mms6 and several more candidates that potentially might provide control over nucleation and growth of magnetite crystals were identified among magnetosome-associated proteins (Schüler, 2004). The use of biomolecular-mediated synthesis may offer a variety of morphologies and sizes and could provide the design of desired magnetic and crystalline properties in the future.
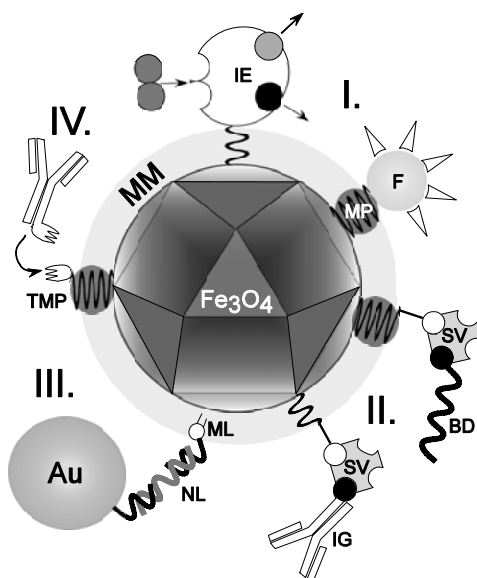

Figure 6: Schematic illustration of a notional magnetosome particle featuring a variety of functional moieties. Conceivable modifications of magnetosome particles are (I) the expression of genetically-engineered magnetosome membrane proteins fused to enzymes and fluorophores, (II) the biotinylation of membrane lipids and proteins, which facilitate the streptavidin-mediated coupling of various molecules such as nucleic acids or immunoglobulins, (III) the attachment of gold particles and quantum dots (IV) the expression of fusion tags as anchor groups for the *in vitro* modification of the particles. Au – gold particle, BD – biotinylated DNA, Fe_3O_4 – magnetite crystal, ML – magnetosome lipid, MM – magnetosome membrane, MMP – magnetosome proteine, SV – streptavidin, TMMP – tagged magnetosome proteine

Acknowledgement

References:

Andrews, S. C., Robinson, A. K., and Rodriguez-Quinones, F. (2003). Bacterial iron homeostasis. FEMS Microbiol Rev *27*, 215-237.

Arakaki, A., Webb, J., and Matsunaga, T. (2003). A novel protein tightly bound to bacterial magnetic particles in *Magnetospirillum magneticum* Strain AMB-1. J Biol Chem *278*, 8745-8750.

Baeuerlein, E. (2000). Single magnetic crystals of magnetite (Fe_3O_4) synthesized in intracytoplasmic vesicles of *Magnetospirillum gryphiswaldense*. In Biomineralization, E. Baeuerlein, ed. (Weinheim, Wiley-VCH), pp. 61-80.

Baeuerlein, E. (2003). Biomineralization of unicellular organisms: an unusual membrane biochemistry for the production of inorganic nano- and microstructures. Angew Chem Int Ed Engl *42*, 614-641.

Baeuerlein, E., Schüler, D., Reszka, R., and Päuser, S. (2001). Specific magnetosomes, method for the production and use thereof. US patent 6,251,365 B1.

Bazylinski, D. A., and Frankel, R. B. (2004). Magnetosome formation in prokaryotes. Nat Rev Microbiol *2*, 217-230.

Berry, C. C., and Curtis, A. S. G. (2003). Functionalisation of magnetic nanoparticles for applications in biomedicine. J Physics D-Appl Physics *36*, R198-R206.

Blakemore, R., Maratea, D., and Wolfe, R. S. (1979). Isolation and pure culture of a freshwater magnetic spirillum in chemically defined medium. J Bacteriol *140*, 720-729.

Blakemore, R. P., and Frankel, R. B. (1981). Magnetic navigation in bacteria. Scientific American *245*, 42-49.

Blatch, G. L., and Lassle, M. (1999). The tetratricopeptide repeat: a structural motif mediating protein-protein interactions. Bioessays *21*, 932-939.

Bulte, J. W., and Brooks, R. A. (1997). Magnetic nanoparticles as contrast agents for imaging. In Scientific and clinical applications of magnetic carriers, U. Häfeli, W. Schütt, J. Teller, and M. Zborowski, eds. (New York, London, Plenum), pp. 527-543.

Bulte, J. W., Douglas, T., Mann, S., Frankel, R. B., Moskowitz, B. M., Brooks, R. A., Baumgarner, C. D., Vymazal, J., and Frank, J. A. (1994a). Magnetoferritin. Biomineralization as a novel molecular approach in the design of iron-oxide-based magnetic resonance contrast agents. Invest Radiol *29 Suppl 2*, S214-216.

Bulte, J. W., Douglas, T., Mann, S., Frankel, R. B., Moskowitz, B. M., Brooks, R. A., Baumgarner, C. D., Vymazal, J., Strub, M. P., and Frank, J. A. (1994b). Magnetoferritin: characterization of a novel superparamagnetic MR contrast agent. J Magn Reson Imaging *4*, 497-505.

Chatterjee, J., Haik, Y., and Chen, C. J. (2003). Size dependent magnetic properties of iron oxide nanoparticles. Journal of Magnetism and Magnetic Materials *257*, 113-118.

Clausen, T., Southan, C., and Ehrmann, M. (2002). The HtrA family of proteases: implications for protein composition and cell fate. Mol Cell *10*, 443-455.

Cornell, R. M., and Schwertmann, U. (2003). The iron oxides (Structure, properties, reactions, occurrences and uses), 2nd edn (Weinheim, Wiley-VCH).

Denham, C. R., Blakemore, R. P., and Frankel, R. B. (1980). Bulk magnetic properties and magnetotactic bacteria. IEEE Transactions on Magnetics, 1006-1007.

Devouard, B., Posfai, M., Hua, X., Bazylinski, D. A., Frankel, R. B., and Buseck, P. R. (1998). Magnetite from magnetotactic bacteria: Size distributions and twinning. American Mineralogist *83*, 1387-1398.

Dobrindt, U., Hochhut, B., Hentschel, U., and Hacker, J. (2004). Genomic islands in pathogenic and environmental microorganisms. Nat Rev Microbiol *2*, 414-424.

Dunin-Borkowski, R. E., McCartney, M. R., Posfai, M., Frankel, R. B., Bazylinski, D. A., and Buseck, P. R. (2001). Off-axis electron holography of magnetotactic bacteria: magnetic microstructure of strains MV-1 and MS-1. European Journal of Mineralogy *13*, 671-684.

Eberbeck, D., Janke, V., Hartwig, S., Heyen, U., Schüler, D., Albrecht, M., and Trahms, L. (2004). Blocking of Magnetic Moments of Magnetosomes Measured by Magnetorelaxometry and Direct Observation by Magnetic Force Microscopy. J Magnetism Magnetic Materials *In press.*

Flies, C., Jonkers, H., deBeer, D., Bosselmann, K., Böttcher, M., and Schüler, D. (2005a). Diversity and vertical distribution of magnetotactic bacteria along chemical gradients in freshwater microcosms. FEMS Microbiol Ecol *In press*.

Flies, C., Peplies, J., and Schüler, D. (2005b). A polyphasic approach for the characterization of uncultivated magnetotactic bacteria from various aquatic environments. Appl Environ Microbiol *In press.*

Frankel, R. B. (1984). Magnetic guidance of organisms. Ann Rev Biophys Bioeng *13*, 85-103.

Gorby, Y. A., Beveridge, T. J., and Blakemore, R. P. (1988). Characterization of the bacterial magnetosome membrane. J Bacteriol *170*, 834-841.

Grünberg, K., Müller, E. C., Otto, A., Reszka, R., Linder, D., Kube, M., Reinhardt, R., and Schüler, D. (2004). Biochemical and proteomic analysis of the magnetosome membrane in *Magnetospirillum gryphiswaldense*. Appl Eviron Microbiol *70*, 1040-1050.

Grünberg, K., Wawer, C., Tebo, B. M., and Schüler, D. (2001). A large gene cluster encoding several magnetosome proteins is conserved in different species of magnetotactic bacteria. Appl Environ Microbiol *67*, 4573-4582.

Gupta, A. K., and Gupta, M. (2005). Synthesis and surface engineering of iron oxide nanoparticles for biomedical applications. Biomaterials *26*, 3995-4021.

Hergt, R., Hiergeist, R., Zeisberger, M., Schüler, D., Heyen, U., Hilger, I., and Kaiser, W. A. (2005). Magnetic properties of bacterial magnetosomes as diagnostic and therapeutic tools. Proc 5th International Conference on Magnetic Carriers, Lyon, Frankreich *In press*.

Heyen, U., and Schüler, D. (2003). Growth and magnetosome formation by microaerophilic *Magnetospirillum* strains in an oxygen-controlled fermentor. Appl Microbiol Biotechnol *61*, 536-544.

Hilger, I., Hergt, R., and Kaiser, W. A. (2000). Effects of magnetic thermoablation in muscle tissue using iron oxide particles - An *in vitro* study. Investigative Radiology *35*, 170-179.

Hoell, A., Wiedenmann, A., Heyen, U., and Schüler, D. (2004). Nanostructure and field-induced arrangement of magnetosomes studied by SANSPOL. Physica B *350*, 309-313.

Komeili, A., Vali, H., Beveridge, T. J., and Newman, D. K. (2004). Magnetosome vesicles are present before magnetite formation, and MamA is required for their activation. Proc Natl Acad Sci U S A *101*, 3839-3844.

Kuhara, M., Takeyama, H., Tanaka, T., and Matsunaga, T. (2004). Magnetic cell separation using antibody binding with protein a expressed on bacterial magnetic particles. Analytical Chemistry *76*, 6207-6213.

Lee, H., Purdon, A. M., Chu, V., and Westervelt, R. M. (2004). Controlled assembly of magnetic nanoparticles from magnetotactic bacteria using microelectromagnets arrays. Nano Letters *4*, 995-998.

Mann, S., NHC, S., RB, F., DA, B., and HW, J. (1990). Biomineralization of ferrimagnetic greigite (Fe_3O_4) and iron pyrite (FeS_2) in a magnetotactic bacterium. Nature *343*, 258-260.

Matsunaga, T. (1991). Applications of bacterial magnets. TIBTECH *9*, 91-95.

Matsunaga, T., and Kamiya, S. (1987). Use of Magnetic Particles Isolated From Magnetotactic Bacteria For Enzyme Immobilization. Applied Microbiology & Biotechnology *26*, 328-332.

Matsunaga, T., Nakayama, H., Okochi, M., and Takeyama, H. (2001). Fluorescent detection of cyanobacterial DNA using bacterial magnetic particles on a MAG-microarray. Biotechnol Bioeng *73*, 400-405.

Matsunaga, T., Okamura, Y., and Tanaka, T. (2004). Biotechnological application of nano-scale engineered bacterial magnetic particles. Journal of Materials Chemistry *14*, 2099-2105.

Matsunaga, T., Tadokoro, F., and Nakamura, N. (1990). Mass culture of magnetic bacteria and their application to flow type immunoassays. IEEE Transactions on Magnetics *26*, 1557-1559.

Matsunaga, T., Tsujimura, N., and Kamiya, S. (1996). Enhancement of magnetic particle-production by nitrate and succinate fed-batch culture of magnetospirillum sp amb-1. Biotechnology Techniques *10*, 495-500.

Mayes, E. L., and Mann, S. (2004). Mineralization in Nanostructured Biocompartments: Biomimetic Ferritins for High Density data Storage. In Nanobiotechnology, C. M. Niemeyer, and C. A. Mirkin, eds. (Wiley-VCH), pp. 278-287.

Meldrum, F. C., Heywood, B. R., and Mann, S. (1992). Magnetoferritin: *In vitro* Synthesis of a Novel Magnetic Protein. Science *257*, 522-523.

Moench, T., and Konetzka, W. (1978). A novel method for the isolation and study of a magnetotactic bacterium. Arch Microbiol *119*, 203-212.

Moskowitz, B. M. (1995). Biomineralization of Magnetic Minerals. Reviews of Geophysics *33*, 123-128.

Nakamura, N., and Matsunaga, T. (1993). Highly sensitive detection of allergen using bacterial magnetic particles. Analyt Chim Acta *281*, 585-589.

Niemeyer, C. M. (2001). Nanoparticles, Proteins, and Nucleic Acids: Biotechnology Meets Materials Science. Angewandte Chem Int Ed *40*, 4128-4158.

Nies, D. H. (2003). Efflux-mediated heavy metal resistance in prokaryotes. FEMS Microbiol Rev *27*, 313-339.

Okuda, Y., Denda, K., and Fukumori, Y. (1996). Cloning and sequencing of a gene encoding a new member of the tetratricopeptide protein family from magnetosomes of *Magnetospirillum magnetotacticum*. Gene *171*, 99-102.

Okuda, Y., and Fukumori, Y. (2001). Expression and characterization of a magnetosome-associated protein, TPR-containing MAM22, in *Escherichia col*i. FEBS Lett *491*, 169-173.

Pankhurst, Q. A., Connolly, J., Jones, S. K., and Dobson, J. (2003). Applications of magnetic nanoparticles in biomedicine. Journal of Physics D-Applied Physics *36*, R167-R181.

Plank, C., Schillinger, U., Scherer, F., Bergemann, C., Remy, J. S., Krotz, F., Anton, M., Lausier, J., and Rosenecker, J. (2003). The magnetofection method: Using magnetic force to enhance gene delivery. Biological Chemistry *384*, 737-747.

Posfai, M., Buseck, P. R., Bazylinski, D. A., and Frankel, R. B. (1998). Iron sulfides from magnetotactic bacteria: Structure, composition, and phase transitions. American Mineralogist *83*, 1469-1481.

Raj, K., Moskowitz, B., and Casciari, R. (1995). Advances in Ferrofluid Technology. Journal of Magnetism and Magnetic Materials *149*, 174-180.

Reimers, G. W., and Khalafalla, S. E. (1972). Preparing magnetic fluids by a peptizing method. US Bureau Mines Tech Rep *59*.

Reszka, R. (2000). Applications for magnetosomes in medical research. In Biomineralization, E. Baeuerlein, ed. (Weinheim, Wiley-VCH), pp. 81-92.

Safarik, I., and Safarikova, M. (2002). Magnetic nanoparticles and biosciences. Monatsheft Chemie *133*, 737-759.

Schleifer, K., Schüler, D., Spring, S., Weizenegger, M., Amann, R., Ludwig, W., and Köhler, M. (1991). The genus *Magnetospirillum* gen. nov., description of *Magnetospirillum*

gryphiswaldense sp. nov. and transfer of *Aquaspirillum magnetotacticum* to *Magnetospirillum magnetotacticum* comb. nov. System Appl Microbiol *14*, 379-385.

Schübbe, S., Kube, M., Scheffel, A., Wawer, C., Heyen, U., Meyerdierks, A., Madkour, M., Mayer, F., Reinhardt, R., and Schüler, D. (2003). Characterization of a spontaneous nonmagnetic mutant of *Magnetospirillum gryphiswaldense* reveals a large deletion comprising a putative magnetosome island. J Bacteriol *185*, 5779-5790.

Schüler, D. (1999). Formation of magnetosomes in magnetotactic bacteria. J Mol Microbiol Biotechnol *1*, 79-86.

Schüler, D. (2002). The biomineralization of magnetosomes in *Magnetospirillum gryphiswaldense*. Int Microbiol *5*, 209-214.

Schüler, D. (2004). Molecular analysis of a subcellular compartment: The magnetosome membrane in *Magnetospirillum gryphiswaldense*. Arch Microbiol *181*, 1-7.

Schüler, D., and Baeuerlein, E. (1996). Iron-limited growth and kinetics of iron uptake in *Magnetospirillum gryphiswaldense*. Arch Microbiol *166*, 301-307.

Schüler, D., and Baeuerlein, E. (1997). Iron transport and magnetite crystal formation of the magnetic bacterium *Magnetospirillum gryphiswaldense*. J Phys IV *7*, 647-650.

Schüler, D., and Frankel, R. B. (1999). Bacterial magnetosomes: Microbiology, biomineralization and biotechnological applications. Appl Microbiol Biotechnol *52*, 464-473.

Schüler, D., and Köhler, M. (1992). The isolation of a new magnetic spirillum. Zentralbl Mikrobiol *147*, 150-151.

Schüler, D., Spring, S., and Bazylinski, D. A. (1999). Improved technique for the isolation of magnetotactic spirilla from a freshwater sediment and their phylogenetic characterization. System Appl Microbiol *22*, 466-471.

Schultheiss, D., Handrick, R., Jendrossek, D., Hanzlik, M., and Schüler, D. (2005). The presumptive magnetosome protein Mms16 is a PHB-granule bound protein (phasin) in *Magnetospirillum gryphiswaldense*. J Bacteriol *In press*.

Schultheiss, D., Kube, M., and Schüler, D. (2004). Inactivation of the flagellin gene *flaA* in *Magnetospirillum gryphiswaldense* results in non-magnetotactic mutants lacking flagellar filaments. Appl Environ Microbiol *70*, 3624-3631.

Schultheiss, D., and Schüler, D. (2003). Development of a genetic system for *Magnetospirillum gryphiswaldense*. Archives Microbiol *179*, 89-94.

Sode, K., Kudo, S., Sakaguchi, T., Nakamura, N., and Matsunaga, T. (1993). Application of bacterial magnetic particles for highly selective messenger-RNA recovery system. Biotechnol Tech *7*, 688-694.

Tanaka, T., Maruyama, K., Yoda, K., Nemoto, E., Udagawa, Y., Nakayama, H., Takeyama, H., and Matsunaga, T. (2003). Development and evaluation of an automated workstation for single nucleotide polymorphism discrimination using bacterial magnetic particles. Biosensors & Bioelectronics *19*, 325-330.

Tanaka, T., and Matsunaga, T. (2000). Fully automated chemiluminescence immunoassay of insulin using antibody-protein A-bacterial magnetic particle complexes. Anal Chem *72*, 3518-3522.

Tanaka, T., Takeda, H., Ueki, F., Obata, K., Tajima, H., Takeyama, H., Goda, Y., Fujimoto, S., and Matsunaga, T. (2004). Rapid and sensitive detection of 17 beta-estradiol in environmental water using automated immunoassay system with bacterial magnetic particles. Journal of Biotechnology *108*, 153-159.

Tartaj, P., Morales, M. D., Veintemillas-Verdaguer, S., Gonzalez-Carreno, T., and Serna, C. J. (2003). The preparation of magnetic nanoparticles for applications in biomedicine. Journal of Physics D-Applied Physics *36*, R182-R197.

Tartaj, P., Morales, M. D., Veintemillas-Verdaguer, S., Gonzalez-Carreno, T., and Serna, C. J. (2005). Advances in magnetic nanoparticless for biotechnology applications. J Magnetism Magnetic Materials *290-291*, 28-34.

Wolfe, R. S., Thauer, R. K., and Pfennig, N. (1987). A Capillary Racetrack Method For Isolation of Magnetotactic Bacteria. FEMS Microbiology Lett *45*, 31-36.

Yang, C. D., Takeyama, H., Tanaka, T., and Matsunaga, T. (2001). Effects of growth medium composition, iron sources and atmospheric oxygen concentrations on production of luciferase-bacterial magnetic particle complex by a recombinant Magnetospirillum magneticum AMB-1. Enzyme & Microbial Technology *29*, 13-19.

Yoshino, T., Takahashi, M., Takeyama, H., Okamura, Y., Kato, F., and Matsunaga, T. (2004). Assembly of G protein-coupled receptors onto nanosized bacterial magnetic particles using Mms16 as an anchor molecule. Applied and Environmental Microbiology *70*, 2880-2885.

Yoza, B., Arakaki, A., Maruyama, K., Takeyama, H., and Matsunaga, T. (2003a). Fully automated DNA extraction from blood using magnetic particles modified with a hyperbranched polyamidoamine dendrimer. Journal of Bioscience and Bioengineering *95*, 21-26.

Yoza, B., Arakaki, A., and Matsunaga, T. (2003b). DNA extraction using bacterial magnetic particles modified with hyperbranched polyamidoamine dendrimer. J Biotechnol *101*, 219-228.

Yoza, B., Arakaki, A., and Matsunaga, T. (2003c). DNA extraction using bacterial magnetic particles modified with hyperbranched polyamidoamine dendrimer. Journal of Biotechnology *101*, 219-228.

Zahn, M. (2001). Magnetic fluid and nanoparticle applications to nanotechnology. Journal of Nanoparticle Research *3*, 73-78.

Manuscript 9

Biogenic nanoparticles: Production, characterization, and application of bacterial magnetosomes

Claus Lang and Dirk Schüler*

Max Planck Institute for Marine Microbiology, Celsiusstrasse 1, 28359 Bremen, Germany
*corresponding author: dschuele@mpi-bremen.de

Abstract

The ability of magnetotactic bacteria (MTB) to navigate along magnetic field lines is based on unique nano-sized organelles (magnetosomes), which are membrane-enclosed intracellular crystals of a magnetic iron mineral that assemble into highly ordered chain-like structures. The biomineralization of magnetosomes is a process with genetic control over the accumulation of iron, the deposition of the magnetic crystal within a specific compartment, as well as the assembly, alignment and intracellular organization of particle chains. Magnetite crystals produced by MTB have uniform species-specific morphologies and sizes, which are mostly unknown from inorganic systems. The unusual characteristics of magnetosome particles have attracted a great interdisciplinary interest and inspired numerous ideas for their biotechnological application. In this article, we summarize the current knowledge of magnetosome biomineralization in bacteria. In addition, we will present results on the mass production, as well as the biochemical and physico-chemical analysis and functionalization of bacterial magnetosomes, with emphasis on their charcterization as a novel class of magnetic nanoparticles. Finally, we describe the potential of magnetosomes in various biomedical and technological applications.

1. Introduction

An intriguing example for the biological synthesis of nanoparticles is the biomineralization of magnetosomes. These structures are formed intracellularly in magnetotactic bacteria (MTB) (Figure 1(a)), in which they serve as a navigational device for spatial orientation in marine and freshwater habitats by interaction with the earth's magnetic field [1]. Only recently, techniques have become available for the production and isolation of magnetosomes. The particles represent a new class of magnetic nanoparticles with exceptional properties. Magnetosomes provide numerous attractive possibilities in various applications, due to their unique magnetic and biochemical characteristics.

1.1. Biomineralization and structure of magnetosomes

Magnetosomes are membrane-enclosed inorganic crystals consisting either of the magnetic minerals magnetite (Fe_3O_4) or greigite (Fe_3S_4) [1-3]. The particles are usually arranged along the cell axis in one or multiple chains (Figure 1) that are oriented with the [1 1 1] magnetic easy axis along the chain direction [4], and are organized along a cytoskeletal filamentous structure [5, 6]. Particle sizes are typically 35-120 nm, which is within the single-magnetic-domain size for magnetite and greigite [7, 8]. A large variety of crystal

morphologies such as cubo-octahedral, elongated hexagonal-prismatic, and bullet-shaped morphologies were reported [9]. It was shown by high resolution transmission electron microscopy, electron diffraction and electron holography that the morphologies of magnetite crystals in magnetosomes are derived from combinations of the isometric forms {1 1 1}, {1 1 0} and {1 0 0}. Morphological variations such as elongated and prismatic structures are due to anisotropic crystal growth [10]. The morphology, size and intracellular organization of magnetosome crystals is subject to a species-specific biological control, which is genetically regulated by a complex and specific set of genes that have been identified within the "magnetosome island" within the genome of MTB [11, 12]. For magnetite biomineralization, iron is taken up as Fe(III) or Fe(II) from the medium and subsequently transported to the magnetosome vesicle [1]. Presumably, a part of the iron is then reoxidized to form a highly reactive Fe(III) oxide, probably ferrihydrite, which may react with dissolved Fe(II) to form magnetite by a via-solution process [13]. Compartmentalization through the formation of membrane vesicles enables the processes of magnetite mineralization to be regulated by biochemical pathways. The magnetosome membrane (MM) is crucial in the control of crystal growth by providing spatial constraints for shaping of species-specific crystal morphologies. Biomineralization of magnetite requires a precise regulation of the redox potential, pH, and the prevalence of a supersaturating iron concentration within the vesicle. Thus, the MM performs specific functions in the transport and accumulation of iron, nucleation of crystallization, and redox- and pH-control [14, 15].

1.2 Applications of magnetosomes

Bacterial magnetic nanoparticles have been suggested for a number of *in vitro* applications, such as magnetic separation and procedures for labeling and immobilization of various biomolecules. The use of magnetosomes has been described for numerous purification procedures such as the extraction of mRNA and DNA from biological samples such as tissues, blood and bacterial cells. For instance, the efficiency of DNA recovery with dendrimer-modified magnetosome particles was 6-fold higher with bacterial particles than with artificial magnetic particles [16]. The automation of a DNA extraction procedure based on dendrimer-modified particles has been reported recently [16, 17]. The isolation of mRNA was facilitated by oligo(dT) modified magnetosomes [18]. Magnetosomes similarly modified with oligonucleotides have been employed in an automated magnetic microarray for the detection of different cyanobacterial DNA with genus specific probes [19].

Another set of biotechnological applications is based on the immobilization of proteins, peptides and enzymes on magnetic particles, which allows the selective separation and reuse of immobilized enzymes from a reaction mixture. Compared to micrometric particles, the use of nanosized particles is preferred due to (i) their higher specific surface area and therefore higher binding capacity and (ii) their lower mass transfer resistance. Because of their large surface-to-volume ratio, bacterial magnetosomes particles were successfully harnessed for immobilization of the enzymes glucose oxidase and uricase in early experiments [20]. Likewise, the immobilization of immunoglobulins has received great attention and inspired the development of diverse applications. One approach of immunoglobulin immobilization on magnetic particles relied on chemical crosslinking of the antibody with the MM [21]. Another approach attempted the genetic modification of magnetosome membrane proteins (MMP) to generate protein fusions of a MMP and an immunoglobulin binding protein such as the staphylococcal protein A or streptococcal protein G [22, 23]. The second approach is potentially superior to chemical crosslinking, as the antibody is oriented more accurately, although it remains to be shown that the polypeptides used for the genetic fusion are in fact native constituents of the MM. Antibody-magnetosome conjugates were employed for automated immunoassays to detect environmental pollutants, hormones and toxic substances [22, 24]. In addition, antibody-modified magnetosomes have been used successfully for the specific separation of target cells from human blood [25]. Another application is the use of streptavidin-modified magnetosomes for the automated discrimination of single nucleotide polymorphism. The streptavidin-modified particles were coupled to biotinylated oligonucleotides to facilitate magnetic separation of DNA hybrids. Single nucleotide polymorphisms were detected as decreased fluorescent intensities in a fluorescence resonance energy transfer (FRET) system with FITC (donor)-labeled DNA and a POPO-3 (acceptor), which preferentially intercalates double stranded sequence of complementary strands [26]. The magnetic properties of the particles cannot only be used for the purification and immobilization of biomolecules but also for their detection. Magnetic force microscopy was used for the highly sensitive detection and quantification of streptavidin immobilized on glass slides with biotin conjugated magnetosomes [27]. The magnetosome chain is one of the most complex and highly ordered structures found in a bacterium, and it has been suggested that biomimetic approaches could be used for the fabrication of self-assembling magnetic nanostructures inspired by magnetosome chains, such as magnetic nanowires and nanotubes as building blocks in magnetic devices. In fact, it has been recently

shown by Banerjee and coworkers that magnetic nanotubes can be assembled by the incorporation of isolated bacterial magnetosomes into peptide nanotubes [28].

In summary, these examples impressively demonstrate the tremendous bio- and nanotechnological potential of bacterial magnetic nanoparticles. However, numerous fundamental questions, that have remained unsolved thus far, have prevented an application of magnetosomes at technical scale. Thus, our project aimed to produce and thoroughly characterize bacterial magnetosome particles for their use in a number of applications. This was done in a combined and collaborative approach, which is described in the following.
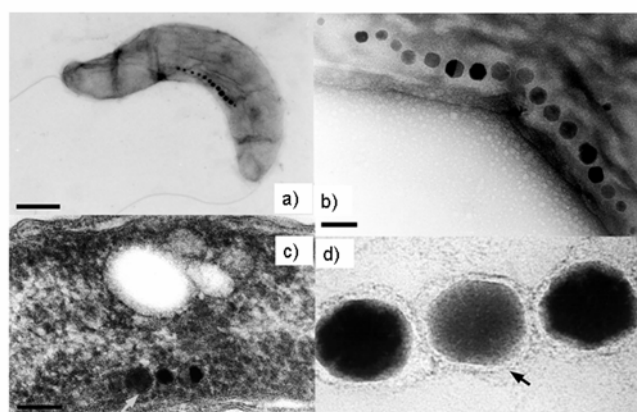

Figure 1: Transmission electron micrographs of negatively-stained cells of *M. gryphiswaldense* displaying the magnetosome chain and isolated magnetosomes. (a) single *M. gryphiswaldense* cell with the magnetosome chain localized at midcell, (b) enlarged view of the magnetosome chain, (c) ultrathin-section of a *M. gryphiswaldense* cell with magnetosomes, (d) isolated magnetosome particles with intact magnetosome membranes. The magnetosome membrane is indicated by arrows. The bars are 0.5 µm (a) and 0.1µm (b & c).

2. Production of magnetosome particles

Previous attempts to characterize and apply magnetosome particles were hampered by their limited availability. In addition, the particles were poorly characterized in terms of their biochemical and physico-chemical properties. The efforts of our group to establish protocols for the large scale production of magnetic bacteria and magnetosomes which facilitated the detailed biochemical and physical characterization of magnetosomes are summarized in the following. We also outline novel routes for the generation of functionalized magnetosomes with high technological significance.

2.1. Development of methods for mass cultivation of MTB

High yields of magnetosomes from large quantities of cells cultivated under defined growth conditions are required for both the biochemical and biophysical characterization of

magnetosomes. MTB are fastidious organisms and the few strains that are available in pure culture are difficult to grow. *M. gryphiswaldense* (Figure 1(a)) was selected as a magnetotactic model organism because it can be grown in simple liquid media containing short organic acids as a carbon source. In addition, this organism is amenable to genetic analysis, and the determination of its genome sequence has been nearly completed [12, 29]. Therefore we seeked to establish optimum conditions for the mass cultivation of the microaerophilic *M. gryphiswaldense* in flasks and in a fermenter. The first step was the optimization of the medium to increase cell yield, magnetism, resulting in a defined medium in which high yields of cells and magnetosomes can be obtained at moderate costs.

The magnetotactic strains *M. magnetotacticum*, *M. magneticum* and *M. gryphiswaldense* produce magnetite only under microaerobic conditions, whereas higher (e.g. atmospheric) oxygen concentrations inhibit growth and repress magnetite formation. Among the strains tested in our study, *M. gryphiswaldense* exhibited the highest oxygen tolerance, and growth was unaffected by oxygen concentration over a wide range (0.25 up to 150 mbar). However, we observed an increased mutability within the magnetosome island if cells were grown at higher oxygen levels, leading to the irreversible loss of the capability to form magnetosomes [12]. In initial growth experiments, cells were cultivated in flasks under a microaerobic gas mixture containing 1% oxygen in 99% nitrogen [30]. These conditions are only of limited use for growth experiments and large-scale cell production, because the oxygen supply cannot be kept constant during the incubation period. In fact, the oxygen partial pressure decreases due to cellular respiration, resulting in a metabolic shift from microaerobic to anaerobic growth and a decreased growth rate. Hence, the control of a microoxic environment is a crucial parameter for growth and magnetosome formation, which however, cannot be maintained during cultivation in conventional flasks. Therefore, a protocol for mass cultivation of MTB in an automated oxygen-controlled fermenter (Figure 2) was established, which allows the continuous maintenance of low pO_2 concentrations [30]. A Biostat A Twin (B. Braun Biotech International, Melsungen Germany) Bioreactor was specifically adapted for the microaerobic cultivation of microaerophilic bacteria under oxystat conditions. This was achieved by the installation of a highly susceptible oxygen amplifier and accessory equipment for the gas supply. Defined low oxygen partial pressures were regulated by a cascade control via separate and independent gassing with nitrogen and air. Nitrogen supply was controlled by means of a flowmeter (DK 46N; Krohne, Duisburg, Germany) installed in line with a pulsed solenoid gas valve (Bürker, Ingelfingen, Germany). The air supply was regulated by a thermal massflow controller (BRA-001F; Bronkhorst, Ruurlo,

Netherlands), and an additional pulsed solenoid control valve. The switch between nitrogen and oxygen gassing depends on the actual oxygen partial pressure in the medium. At oxygen partial pressures of 0.5% above the set value nitrogen was sparged into the fermenter at a constant rate and at oxygen partial pressures below 99.5% of the set value the aeration rate was regulated via the massflow controller and the pulsed solenoid valve. The system allows the precise maintenance of pO_2 tensions ranging from 0.25-212 mbar over a wide range of cell densities with fluctuations less then 5% of the set value. This oxystat fermenter has been used to determine optimal oxygen partial pressures for magnetite production and cultivation of *M. gryphiswaldense*. Magnetite formation occurred only below a threshold value of 10 mbar, whereas it was inhibited at higher oxygen concentrations. We found a clear correlation between the amount of magnetite formed and pO_2 exists, and most favorable conditions for magnetite biomineralization at 0.25 mbar (Figure 3) [29]. Interestingly, particles grown at 10 mbar displayed smaller sizes (c. 20 nm) compared to 42 nm of particles produced under optimal conditions (0.25 mbar), indicating that morphology and size of particles can be controlled by growth conditions. Likewise, reduced particle sizes were obtained under conditions of iron limitation, or if magnetite formation was synchronized by the addition of iron to iron-starved cells shortly before cell harvest.

In a comparative study, a productivity of 6.3 mg magnetite l^{-1} day^{-1} was found for *M. gryphiswaldense* compared to 3.3 and 2.0 mg magnetite l^{-1} day^{-1} for *Magnetospirillum magneticum* AMB-1 and *M. magnetotacticum* MS-1, respectively [30]. Cultivation of *M. gryphiswaldense* in the oxystat with the improved medium increased the maximum cell yield to 0.40 g dry weight l^{-1} compared to 0.33 g dry weight l^{-1}, which were reported earlier [31]. Thus, the protocol established for *M. gryphiswaldense* allows mass production of magnetosomes in amounts sufficient for their characterization and applications, which are described in the following.

**Figure 2: Dual -vessel (2x10l) laboratory fermenter system for mass culture of *M. gryphiswaldense***
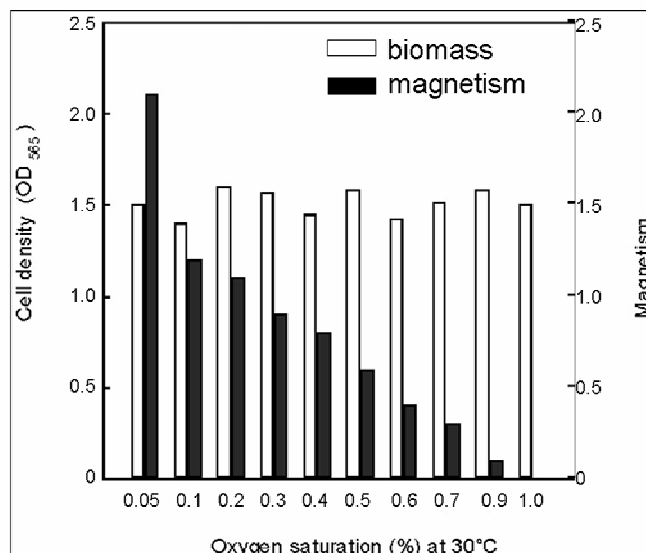
Figure 3: Biomass production (OD) and cell magnetism of oxystat grown *M. gryphiswaldens*e at different constant oxygen concentrations.

2.2. Isolation and purification of magnetosomes

We have developed a protocol for the purification of magnetosomes from *M. gryphiswaldense*. Magnetosome particles are distinguished from organic cell constituents by their high density and their magnetism. These properties can be harnessed for their purification from cells by a straight-forward isolation protocol. After cell disruption by french press and removal of cell debris by centrifugation the magnetosomes can be easily separated from the crude extracts by magnetic separation columns [32]. Magnetic separation is followed by ultracentrifugation into a 55 % [w/w] sucrose cushion. This procedure results in suspensions of purified magnetosome particles with intact enveloping membrane structures (Figure 1(d)). The isolated magnetosomes are relatively stable in the presence of mild detergents. However, treatment with strong detergents (1% SDS at 95°C) or organic solvents solubilizes the MM, which results in the agglomeration of membrane-free magnetite particles (Figure 4) [32, 33].
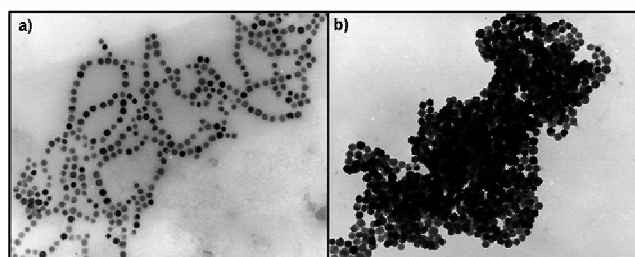
Figure 4: (a) Isolated magnetosome particles with intact MM display a strong tendency for chain formation, whereas removal of the MM by SDS treatment results in the agglomeration of membrane-free particles (b).

3. Characterization of magnetosomes

3.1. Biochemical characterization of magnetosomes

For any functionalization and subsequent application, a detailed knowledge of the biochemical composition and protein content of the isolated magnetosomes is an essential requirement. Therefore, the biochemical characteristics were thoroughly analyzed. A number of common fatty acids are present in the MM from *M. gryphiswaldense* [32, 33]. The most abundant polar lipids in the MM are phosphatidylethanolamine and phosphatidylglycerol which are also the most abundant polar lipids in whole-cell extracts. The fatty acid composition of the MM is very similar to the fatty acid composition of the whole cell in that the most abundant fatty acids are identical. However certain fatty acids, that are found in whole cells e.g. 3-hydroxyhexadecanoic acid (3 OH 16:0), 3-hydroxyoctadecanoic acid (3OH 18:0) and 2-hydroxydecenoic acid (2OH 18:1), are absent from the MM. These amide-linked fatty acids are typically present in the outer membrane of gram-negative bacteria. These results indicate that the MM originates from the cytoplasmic membrane. This has recently been confirmed directly by cryo-electron tomography, which demonstrated that magnetosomes are membrane invaginations originating from the cytoplasmic membrane [5].

For the identification of magnetosome-asssociated proteins, the MM of isolated magnetosomes was analyzed as described in detail in reference [31]. Briefly, the MM was solubilized by boiling in a buffer containing 2% w/w (SDS) and 5% (w/v) 2-mercaptoethanol. The samples were subsequently subjected to one dimensional SDS-polyacrylamide gel electrophoresis (SDS-PAGE) according to the procedure of Lämmli (Figure 5A) [34] or to Tricine-SDS-PAGE according to Schägger and Jagow (Figure 5B,C) [35]. In order to obtain improved protein separation, two-dimensional gel electrophoresis was carried out additionally (Figure 5D) [32]. After electrophoresis the proteins were blotted onto a membrane and the N-termini of separated proteins were sequenced by Edman degradation. Additionally, magnetosome-associated proteins were identified by mass spectroscopy, either after size separation from single spots or bands, or from total tryptic digests of entire magnetosome preparations. For the latter purpose, magnetosomes were reduced with dithiotreitol, alkylated with iodacetamid and digested with trypsin to completion. Afterwards the magnetic moiety was removed, and the supernatant was chromatographically separated using a capillary liquid

chromatography system. The eluted peptides were analyzed by a Q-TOF hybrid mass spectrometer.

The peptide profiles were correlated with the preliminary *M. gryphiswaldense* genome sequence [32]. Analysis of the extracted membrane revealed that the magnetosome is associated with a highly specific and complex subset of proteins, which are present in various quantities. The amount of MM-bound polypeptides approximately represents 0.1 % of the total cellular protein [33]. The combination of these proteomic techniques resulted in the identification of 18 major polypeptides in the magnetosome subproteom (Figure 5) [11, 12, 32, 33]. The different resistance of magnetosome proteins towards proteases and detergents indicates that some proteins are very tightly bound to the magnetosome crystals and/or embedded within the membrane. The highly abundant proteins MamC, MamF and Mms16 which have electrophoretic mobilities corresponding to sizes of 15 to 19 kDa are the most stable MMP. Others, as for instance MamA, are loosely attached and can be selectively solubilized by mild detergents. Based on sequence analysis, MMP can be assigned to a number of characteristic protein families, which are presumed to perform specific functions in MM vesicle formation and assembly, iron transport, and control of nucleation and growth of magnetite crystals. Several of the proteins contain covalently bound c-type heme as revealed by peroxidase staining. No glycoproteins, which are common constituents of other biomineralizing systems, have been detected so far. Both MamB and MamM are members of the CDF (cation diffusion facilitator) family of metal transporters, which comprises proteins that function as efflux pumps of toxic divalent cations, such as zinc, cadmium, cobalt and other heavy metal ions. Specifically, MamB and MamM have greatest similarity to the CDF3 subfamily, which was postulated to comprise putative iron transporters [36]. It has been speculated that MamB and MamM are involved in the magnetosome-directed uptake of iron, and preliminary evidence obtained from mutant analysis seems to support this assumption (Junge et al. unpublished). MamE and MamO display sequence similarity to HtrA-like serine proteases. The mamP gene, encoding a further deduced protein with similarity to this family, is colocated with mamE and mamO within the same operon. HtrA-like proteins share a conserved trypsin-like protease domain and one or two PDZ domains. They act as molecular chaperones and heat-shock induced proteases, which degrade misfolded proteins in the periplasm [37]. It has been suggested that MamE and MamO are involved in magnetosome formation, perhaps by the processing, maturation and targeting of MMP during MM assembly [33].

The most abundant MM-associated proteins MamC, MamD, MamG, and MamF have no known homologues in organisms other than MTB, and thus represent unique, MTB-specific protein families. One noticeable feature common to several of these proteins is the presence of repetitive motifs. Examples are MamD, Mms6 and MamG, which share conspicuous hydrophobic sequence motifs that are rich in repeated leucine and glycine residues. Similar motifs containing LG-rich repetitive sequences have been found in other proteins that have a tendency for self-aggregation or are involved in the formation of supramolecular structures [38]. The Mms6 protein of *Magnetospirillum magneticum* AMB-1 is a tightly bound constituent of the MM, which exhibits iron binding activity and has an effect on the morphology of growing magnetite crystals *in vitro* [39]. Another conspicuous sequence pattern is found in MamJ. This protein displays extensive self-similarity and is particularly rich in repeats of the acidic amino acid residues glutamate and aspartate. These features are typical for other proteins involved in biomineralization processes and originally lead to the speculation that MamJ might mediate nucleation and growth of magnetite crystals. However, the targeted deletion of the *mamJ* gene revealed its involvement in the alignment of the magnetosome chain in the cell, probably by interaction with a filamentous structure [6].
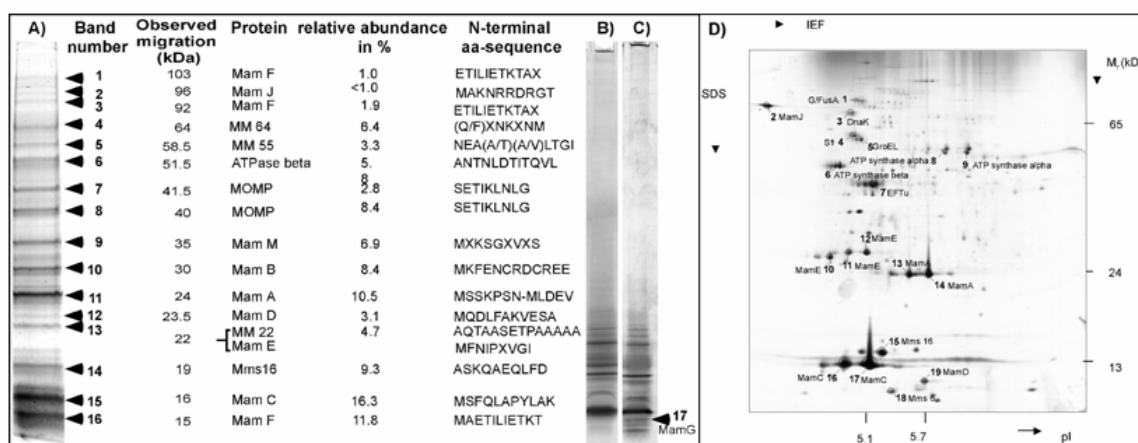
Figure 5: MM-associated proteins separated by one- and two-dimensional PAGE (redrawn after Grünberg et al., 2004). (A) Summary of MM-proteins detected by Coomassie stain in 1D SDS-PAGE (16%). Proteins from indicated bands were identified by N-terminal amino acid analysis (Edman degradation). (B) Coomassie and C) silver stained SDS-Tricine gels (16.5 %) of MM proteins. (D) Silver-stained 2D-PAGE of MM proteins from M. gryphiswaldense. Proteins from marked spots were identified by mass spectrometric sequencing (2D PAGE analysis was performed by R. Reszka, MDC Berlin).

3.2. Physico-chemical characterization of magnetosome particles

The analysis of the physico-chemical and magnetic properties of magnetosomes is of great relevance for technological application, because biogenic magnetosomes can be expected to have unique magnetic characteristics as they have evolved as a navigational device in magnetic bacteria that is sensitive to the geomagnetic field and provides a magnetic moment sufficient to align bacterial cells [40]. The magnetic characteristics of the particles were subject to several studies. The hysteresis of isolated magnetosome particles was measured in different magnetometers by Eberbeck et al. and Hergt et al. [41, 42]. In the first study a hysteresis corresponding to a coercive field of 6500 A/m was measured at room temperature. In the study carried out by Hergt et al. coercivities of 2600 A/m were obtained for gelatine immobilized magnetosomes. Hysteresis loops for immobilized magnetosomes further were measured at frequencies between 100Hz and 1MHz in a vibrating sample magnetometer. The coercivity of magnetosomes is extremely high compared to commercially available magnetic nanoparticles (Resovist®, trademark of Schering AG, Germany) with 20 A/m [42].

Another magnetic characteristic of magnetosomes, which is of potential relevance for various applications is their relaxation time. In a fluid state a relaxation time of 80 ms was measured, which is attributed to Brownian relaxation. Néel relaxation was largely beyond the measurement time window of the instrument which suggests that the particles can be considered blocked [42].

Atomic force microscopy and magnetic force microscopy were used to determine if the blocking behaviour is attributable to the formation of aggregates or if single magnetosomes possess remanent magnetic moments. Particles with a size of about 27 nm still bear a remanent magnetic moment [42, 43]. The presence of single magnetosomes was verified with the same methods by Albrecht *et al* [41].

While mature magnetosome crystals are mostly within the ferrimagnetic size range, the crystal sizes are under biological control and can be genetically modified. For instance, magnetic particles from a mutant exhibit a narrower size distribution and smaller diameters (figure 6) that predominantly fall into the superparamagnetic size range, as revealed by Small Angle Scattering using polarized neutrons (SANSPOL) [44].

So far the analysis of the magnetic properties of the particles has shown that magnetosomes are single magnetic domain particles with unique magnetic characteristics, which are hardly matched by synthetic magnetic particles. These properties designate them

for medical applications such as hyperthermia and magnetic resonance imaging. An outline of the recent developments in this field will be given in the next section.
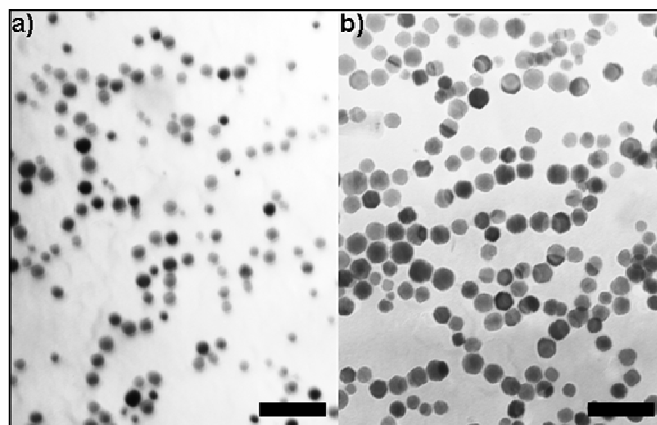

Figure 6: TEM picture of magnetosomes isolated from a *M. gryphiswaldense* mutant strain (MSR1K (a)) with reduced particle size and from the wild type strain (MSR-1 (b)). The bar size is 150 nm.

4. Evaluation of magnetosomes for medical applications

Superparamagnetic nanoparticles are used as magneto-pharmaceuticals for diagnostic purposes. They serve as contrast agents in magnetic resonance imaging to enhance the contrast between normal and diseased tissue or to indicate the status of an organ. Magnetosome-based ferrofluids are promising candidates for Magnetic Resonance Tomography contrast agents, which can be detected at very low concentrations in clinically employed MR tomographs. That magnetosomes are an expedient alternative to synthetic ferrofluids was shown in *in vitro* experiments by Herborn et al. [45]. The longitudinal and the transversal relaxivity (R_1 = 7.688 mmol^{-1} s^{-1}; R_2 145.67 mmol^{-1} s^{-1}) were calculated after studying different magnetosome dilutions in a clinical 1.5 T MR tomography (63 Mhz, 21°C). The low detection limit of magnetosomes in MRI systems can be harnessed for MR molecular imaging. An approach for the twofold labeling of macrophages with fluorescence labeled magnetosomes by MRI and near infrared fluorescence was presented recently. The modified macrophages may find application in the simultaneous detection of inflammations by NIRF and MRI [46].

Another promising application for magnetosomes might be the method of hyperthermia treatment, in which magnetic nanoparticles are used for controlled tissue heating to promote cell necrosis in tumors. After magnetic nanoparticles are applied to the target tissue, an alternating external magnetic field is applied. Due to loss processes resulting from the reorientation of the magnetic moments of the particles, heat is generated, which results in cell necrosis in tumor cells [47]. The method relies on the development of magnetic

nanoparticles with high specific loss powers [41]. In a recent study of magnetosomes from *M. gryphiswaldense* in biomedical applications such as hyperthermia and thermoablation, Hergt and coworkers found exceptionally high specific powers losses (960 g W^{-1} at 10 kA m^{-1} and 410 kHz), which substantially exceed the results obtained with artificial particles [41].

5. Functionalization of magnetosomes

The encapsulation of the magnetic crystal within the MM provides a natural "coating", which ensures superior dispersibility of the particles and provides an excellent target for modification and functionalization of the particles. Besides in vivo "tailoring" of magnetite crystals, also the biochemical composition of the MM can be altered by genetic engineering. A highly promising approach is the design of magnetosomes with functionalized surfaces (Figure 7). This can be achieved by the generation of chimeric proteins, which are specifically displayed on the surfaces of isolated magnetosomes. It has been demonstrated that magnetosome proteins can be used for the construction of functional genetic fusions [48, 49]. In initial experiments we were able to specifically label magnetosomes with a fusion of a green fluorescent protein and a MMP (Figure 8). Replacement of the GFP-function with other relevant polypeptide sequences could be used for the introduction of functional moieties, as for instance biomolecular recognition groups such as the biotin-streptavidin system [50]
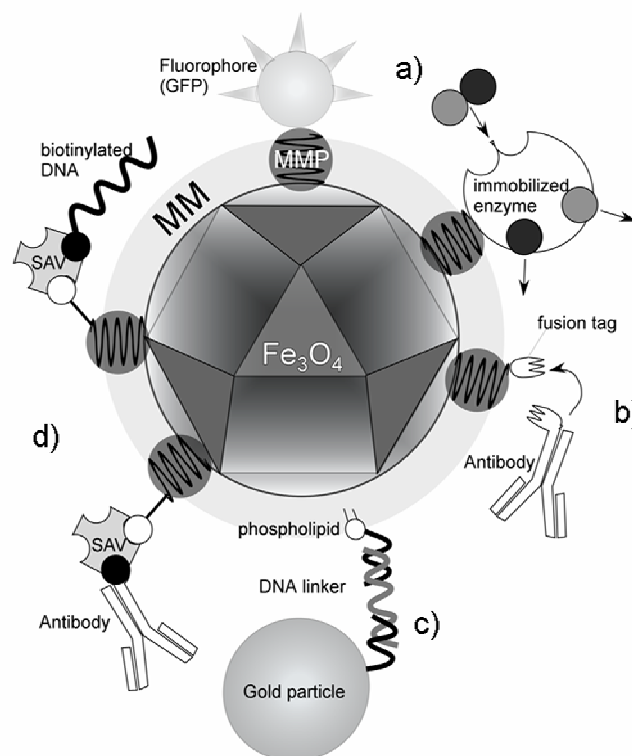

Figure 7: P**otential modifications of magnetosome particles by the introduction of different functional moieties resulting in hybrid bacterial magnetic nanoparticles** (modified after Lang and Schüler, 2006).

Magnetosomes could be modified by (a) magnetosome-specific expression of enzyme and fluorophore proteins (e. g. GFP) by genetic fusion to MMP, (b) expression of fusion tags such as intein- or strep-tags as anchor groups for subsequent conjugate formation with various biomolecules, (c) formation of conjugates with gold particles or quantum dots via a DNA linker, (d) biotinylation of membrane lipids and proteins, which would facilitate the subsequent streptavidin-mediated conjugation to various molecules such as nucleic acids or antibodies. MM – magnetosome membrane, MMP – magnetosome protein, SAV – streptavidin
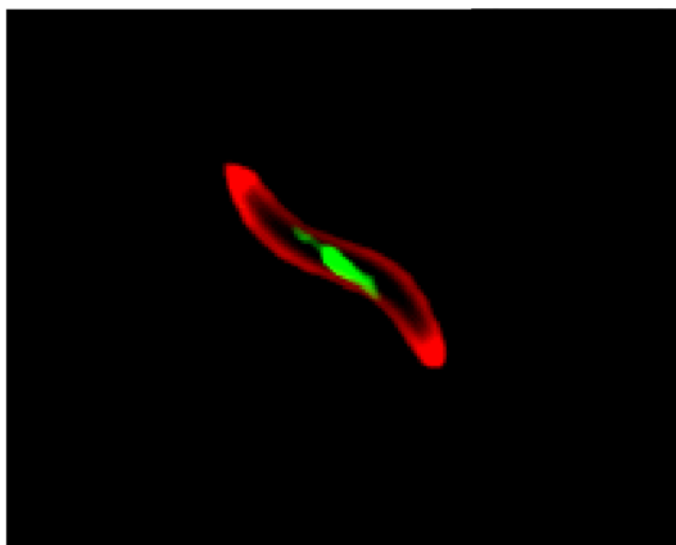

Figure 8: Fluorescent micrograph of *M. gryphiswaldense* expressing enhanced green fluorescent protein (EGFP) fused to a MMP. The green fluorescence signal originates from the magnetosome chain displaying EGFP at midcell. Cell membranes (red) were stained with the fluorescent dye FM4-64 (Invitrogen). This demonstrates that heterologous proteins can be fused to functional MMP for magnetosome-specific display. In future this approach could be extended to the immobilization of enzyme proteins or the introduction of protein tags that facilitate secondary *in vitro* functionalization of magnetosome particles by coupling to a variety of biomolecules.

6. Conclusions

Magnetosome formation in MTB provides a novel magnetic nanomaterial that is generated by a mineralization process with control over the chemical composition, morphology, size and intracellular location of the magnetic mineral. In summary, our work supported by the DFG priority program "Colloidal Magnetic Fluids" has contributed to a greatly improved knowledge about the production and characterization of these particles, which will facilitate their future application. In this article, we have highlighted much of the current knowledge about the physiological and genetic basis of magnetosome biomineralization as well as potential uses of magnetosome particles in a number of biotechnological applications. Beside the establishment of techniques for the improved handling and cultivation of MTB in the laboratory, the establishment of methods for genetic

manipulations for several MTB species as well as efforts in the determination of their genome sequence represented major breakthroughs. With the recent advent of genetic technology for transformation and site-directed mutagenesis for MTB [29, 49, 51], genetic analysis has become a powerful tool in the study of magnetosome formation. The capabilities of MTB to precisely control the composition and morphology of inorganic of particles have been explored only recently, and have contributed to the development of a new and largely unexplored area based on the use of MTB in biosynthesis of magnetic nanomaterials. The available genetic technology will not only elucidate the pathways of magnetosome formation at molecular level, but also holds great promise for the design of biogenic magnetic nanoparticles with desired properties by genetic engineering. An *in vivo* "tailoring" can be applied both to organic and inorganic constituents of magnetosomes. The site-directed mutagenesis of identified iron-transporting magnetosome proteins might be used to generate magnetosome with a modified specificity for the magnetosome-directed uptake of different metals, potentially resulting in inorganic magnetic cores with an altered chemical composition. Likewise, the biochemical composition of the MM may be altered *in vivo* by genetic engineering. A highly attractive and promising approach will be the design of magnetosomes with functionalized surfaces. This can be achieved for instance by the generation of chimeric proteins, which are specifically displayed on the surfaces of isolated magnetosomes, or by the chemical conjugation of magnetosomes and biomolecules.

Acknowlededgments

References

[1]   Bazylinski DA and Frankel RB. 2004 Nature Rev. Microbiol. 2 217

[2]   Flies C, Peplies J and Schüler D. 2005 Appl. Environ. Microbiol. 71 2723

[3]   Schüler D and Frankel RB. 1999 Appl. Microbiol. Biotechnol. 52 464

[4]   Blakemore RP and Frankel RB. 1981 Scientific American 245 42

[5]   Komeili A, Li Z, Newman DK and Jensen GJ. 2006 Science 311 242

[6]   Scheffel A, Gruska M, Faivre D, Linaroudis A, Graumann PL, Plitzko JM and Schüler D. 2006 Nature 440 110

[7]   Moskowitz BM. 1995 Reviews of Geophysics. 33 123

[8]   Dunin-Borkowski RE, McCartney MR, Posfai M, Frankel RB, Bazylinski DA and Buseck PR. 2001 Eur. J. Mineral. 13 671

[9]   Schüler D. 1999 J. Mol. Microbiol. Biotechnol. 1 79

[10]   Devouard B, Posfai M, Hua X, Bazylinski DA, Frankel RB and Buseck PR. 1998 Am. Mineral. 83 1387

[11]   Schübbe S, Kube M, Scheffel A, Wawer C, Heyen U, Meyerdierks A, Madkour M, Mayer F, Reinhardt R and Schüler D. 2003 J. Bacteriol. 185 5779

[12]   Ullrich S, Kube M, Schübbe S, Reinhardt R and Schüler D. 2005 J. Bacteriol. 187 7176

[13]   Cornell RM and Schwertmann U. 2003 The iron oxides - Structure, properties, reactions, occurrences and uses Weinheim, Germany 2nd ed. Wiley-VCH

[14]   Gorby YA, Beveridge TJ and Blakemore RP. 1988 J. Bacteriol. 170 834

[15]   Schüler D. 2002 Int Microbiol 5 209

[16]   Yoza B, Arakaki A and Matsunaga T. 2003 J Biotechnol 101 219

[17]   Yoza B, Arakaki A, Maruyama K, Takeyama H and Matsunaga T. 2003 Journal of Bioscience and Bioengineering 95 21

[18]   Sode K, Kudo S, Sakaguchi T, Nakamura N and Matsunaga T. 1993 Biotechnol. Tech. 7 688

[19]   Matsunaga T, Nakayama H, Okochi M and Takeyama H. 2001 Biotechnol Bioeng 73 400

[20]   Matsunaga T and Kamiya S. 1987 Applied Microbiology & Biotechnology 26 328

[21]   Nakamura N and Matsunaga T. 1993 Analyt. Chim. Acta 281 585

[22]   Tanaka T and Matsunaga T. 2000 Anal. Chem. 72 3518

[23]   Yoshino T, Takahashi M, Takeyama H, Okamura Y, Kato F and Matsunaga T. 2004 Applied and Environmental Microbiology 70 2880

[24]   Tanaka T, Takeda H, Ueki F, Obata K, Tajima H, Takeyama H, Goda Y, Fujimoto S and Matsunaga T. 2004 Journal of Biotechnology 108 153

[25]   Kuhara M, Takeyama H, Tanaka T and Matsunaga T. 2004 Analytical Chemistry 76 6207

[26]   Tanaka T, Maruyama K, Yoda K, Nemoto E, Udagawa Y, Nakayama H, Takeyama H and Matsunaga T. 2003 Biosensors & Bioelectronics 19 325

[27]   Amemiya Y, Tanaka T, Yoza B and Matsunaga T. 2005 J Biotechnol 120 308

[28]   Banerjee IA, Yu L, Shima M, Yoshino T, Takeyama H, Matsunaga T and Matsui H. 2005 Adv. Mater. 17 1128

[29]   Schultheiss D, Kube M and Schüler D. 2004 Appl. Environ. Microbiol. 70 3624

[30]   Heyen U and Schüler D. 2003 Appl. Microbiol. Biotechnol. 61 536

[31]   Schüler D and Baeuerlein E. 1997 J. Phys. IV 7 647

[32]   Grünberg K, Müller EC, Otto A, Reszka R, Linder D, Kube M, Reinhardt R and Schüler D. 2004 Appl. Eviron. Microbiol. 70 1040

[33]   Grünberg K, Wawer C, Tebo BM and Schüler D. 2001 Appl. Environ. Microbiol. 67 4573

[34]   Laemmli UK. 1970 Nature 227 680

[35]   Schägger H and von Jagow G. 1987 Anal Biochem 166 368

[36]   Nies DH. 2003 FEMS Microbiol. Rev. 27 313

[37]   Clausen T, Southan C and Ehrmann M. 2002 Mol Cell 10 443

[38]   Schüler D. 2004 Arch. Microbiol. 181 1

[39]   Arakaki A, Webb J and Matsunaga T. 2003 J. Biol. Chem. 278 8745

[40]   Dunin-Borkowski RE, McCartney MR, Frankel RB, Bazylinski DA, Posfai M and Buseck PR. 1998 Science 282 1868

[41]   Hergt R, Hiergeist R, Zeisberger M, Schüler D, Heyen U, Hilger I and Kaiser WA. 2005 J. Magnetism Magnetic Materials 293 80

[42]   Eberbeck D, Janke V, Hartwig S, Heyen U, Schüler D, Albrecht M and Trahms L. 2005 J. Magnetism Magnetic Materials 289 70

[43]   Albrecht M, Janke V, Sievers S, Siegner U, Schüler D and Heyen U. 2005 J. Magnetism Magnetic Materials 290-291 269

[44]   Hoell A, Wiedenmann A, Heyen U and Schüler D. 2004 Physica B 350 309

[45]   Herborn CU, Papanikolaou N, Reszka R, Grünberg K, Schüler D and Debatin JF. 2003 Rofo Fortschr. Geb. Rontgenstr Neuen Bildgeb. Verfahr. 175 830

[46]   Hartung A, Trost R, Lisy R, Hilger I, Kaiser WA and Reichenbach JR. 2006 Scientific and Clinical Application of Magnetic Carriers Krems, Austria 2006

[47]   Hilger I, Hergt R and Kaiser WA. 2000 Investigative Radiology 35 170

[48]   Komeili A, Vali H, Beveridge TJ and Newman DK. 2004 Proc. Natl. Acad. Sci. U S A 101 3839

[49]   Schultheiss D, Handrick R, Jendrossek D, Hanzlik M and Schüler D. 2005 J. Bacteriol. 187 2416

[50]   Lang C and Schüler D. 2006 Microbial Bionanotechnology: Biological self-assembly systems and biopolymer-based nanostructures Rehm B editor Wymondham, Norfolk UK Horizon Scientific Press 107

[51]   Schultheiss D and Schüler D. 2003 Arch. Microbiol. 179 89

Manuscript 10

Synthesis of magnetite nanoparticles for bio- and nanotechnology: Genetic engineering and biomimetics of bacterial magnetosomes

Claus Lang, Dirk Schüler, Damien Faivre[*]

C. Lang, D. Schüler, D. Faivre

Department of Microbiology, Max Planck Institute for Marine Microbiology, Celsiusstrasse

C. Lang, D. Schüler

Present address: Department Biologie I Bereich Mikrobiologie, Ludwig-Maximillians-Universität München, Maria-Ward-Str. 1a, 80638 München, Germany

* corresponding author: dfaivre@mpi-bremen.de

Summary

Magnetotactic bacteria (MTB) have the ability to navigate along the Earth's magnetic field. This so-called magnetotaxis is a result of the presence of magnetosomes, organelles which comprise nanometer-sized intracellular crystals of magnetite (Fe_3O_4) enveloped by a membrane. Because of their unique characteristics, magnetosomes have a high potential for nano- and biotechnological applications, which require a specifically designed particle surface. The functionalization of magnetosomes is possible either by chemical modification of purified particles or by genetic engineering of magnetosome membrane proteins. The second approach is potentially superior to chemical approaches as a large variety of biological functions such as protein tags, fluorophores, and enzymes may be directly incorporated in a site-specific manner during magnetosome biomineralization. An alternative to the bacterial production of magnetosomes are biomimetic approaches, which aim to mimic the bacterial biomineralization pathway *in vitro*. In MTB a number of magnetosome proteins with putative functions in the biomineralization of the nanoparticles have been identified by genetic and biochemical approaches. First initial results obtained by several groups indicate that some of these proteins have an impact on nanomagnetite properties *in vitro*. In this article the key features of magnetosomes are discussed, an overview of their potential applications are given, and different strategies are proposed for the functionalization of magnetosome particles and for the biomimetism of their biomineralization pathway.
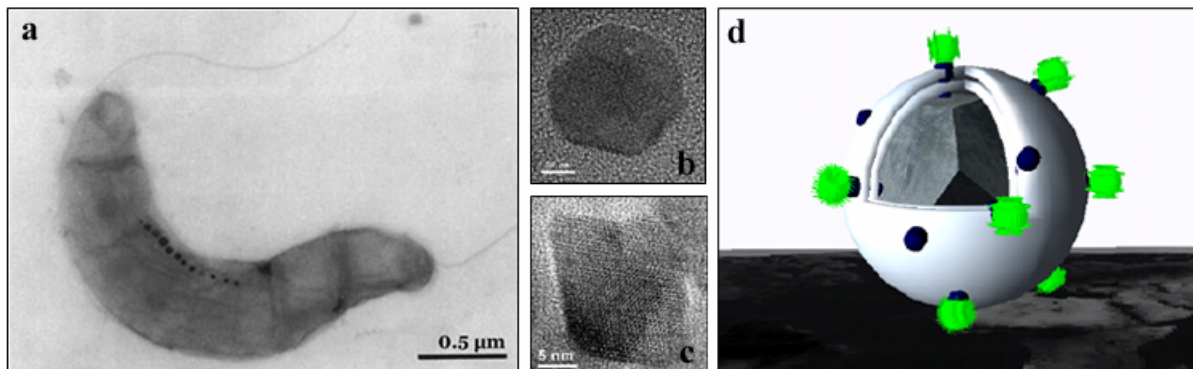
Summary figure: Transmission electron micrograph of *Magnetospirillum gryphiswaldense* (a). High Resolution image of an isolated magnetosome (b) and high resolution image of an abiogenic magnetite crystal (c). Note that purely inorganic crystals are smaller. Isolated magnetosomes can be functionalized, for example with fluorophore proteins as shown by this model (d).

Keyword: biomimetic; biotechnology; magnetite; magnetosomes; nanoparticles; nanotechnology

Biographical Sketch

Claus Lang has studied Biology at the University of Bonn, Germany and the University of New South Wales, Australia with an emphasis on Molecular Microbiology. After his graduation in 2004 he took up a position as a Research Assistant to study mRNA stability control in bacteria in the laboratory of Dr. Kathy Takayama at the University of New South Wales (Australia). Since January 2005 Claus Lang has been a doctoral student at the Max Planck Institute for Marine Microbiology in Bremen, Germany. Under the supervision of Prof. Dirk Schüler he currently explores possibilities for the biotechnological utilization of magnetosomes and primarily focuses on the genetic modification of the magnetosome membrane to design functionalized magnetic nanoparticles.

Dirk Schüler is a Professor of microbiology at the Ludwig Maximilians University of Munich (Germany). He performed his undergraduate studies at the Ernst Moritz Arndt University of Greifswald (Germany) where he started working on the isolation of magnetotactic bacteria in the group of Prof. M. Köhler (1989). In 1990, he joined the group of Prof. E. Bäuerlein at the Max Planck Institute of Biochemistry in Martinsried to study biomineralization in *Magnetospirillum gryphiswaldense*. In 1995, he left Germany with a Ph.D. to join the group of Prof. D. Bazylinski at Iowa State University (USA). His second post-doctoral position was at the Scripps Institute of Oceanography (UCSD, USA), in the laboratory of Prof. B. Tebo. In 1999, he returned to Germany to join the Max Planck Institute for marine Microbiology, where he became a research group leader on magnetotactic bacteria. In October 2006, he was made a full Professor at the University of Munich. His research focus is on the genetics and physiology of magnetosome formation by magnetotactic bacteria.

Damien Faivre is a research scientist at the Max Planck Institute for Marine Microbiology (Bremen, Germany). As an undergraduate, he studied physical chemistry at the University Claude Bernard (Lyon, France), before joining Prof. G. Peshlerbe's group in 1999 at Concordia University (Montreal, Canada) to study theoretical nanochemistry. His interests in magnetite started during his doctoral studies (2000 – 2004) at the University Denis Diderot (Paris, France). Throughout his Ph.D. under the supervision of Prof. P. Zuddas, he studied the geochemical properties of abiogenic magnetite, and their implication on the definition of biogenicity criteria. He obtained a doctoral award to spend a research semester at the California Institute of Technology (Pasadena, USA) working in Prof. D. Newman's group with Dr. A. Komeili, where for the first time he came into contact with the fascinating bacteria. Since 2005 he has worked as a Marie Curie post-doctoral fellow in Dr. D. Schüler's group, where he is involved in various projects in unraveling the biomineralization pathway of magnetosome formation and developing routes for the biomimetic formation of magnetite nanoparticles.

Introduction

Magnetite nanoparticles (MNPs) are key components to the development of many novel bio- and nanotechnological applications. Research in nanosciences and nanotechnology has aimed at using magnetic nanoparticles as nanomotors, nanogenerators, nanopumps, and other similar nanometer-scale devices.[1] Technical applications include the use of nanomagnetite in films,[2] in form of ferrofluids as magnetic inks, in magnetic recording media, in liquid sealing, as dampers in motors and shock absorbers, and for heat transfer in loudspeakers.[3] MNPs are of biotechnological and biomedical relevance in fields such as magnetic separation of biomolecules, magnetic resonance imaging (MRI), tissue repair, drug delivery, hyperthermia treatment of tumor cells, or magnetofection.[4-6] In many cases particles with a specifically tailored and functionalized surface are required. Especially in biotechnological applications, functionalized bacterial magnetosomes represent an attractive alternative to chemically synthesized iron oxide particles. Magnetosome particles have been employed in numerous applications that range from extraction of DNA and RNA to the highly sensitive detection and concentration of toxic substances and the development of immunoassays.[7-11] Magnetosomes, which can be isolated now from cells in larger quantities, consist of a magnetic mineral crystal, magnetite or greigite,[12] enveloped by a biological membrane that contains phospholipids and specific proteins.[13] The magnetosome membrane (MM) is not only critical for the control of crystal size and morphology, but also prevents the aggregation of extracted magnetosomes and thus stabilizes magnetosome suspensions. In addition, the MM provides a matrix for the functionalization of magnetosomes.

In this article two strategies for the production of MNPs for bio- and nanotechnological purposes are discussed. The first strategy is the development of functionalized magnetosomes either by chemical modification of isolated particles or genetic engineering of magnetosome membrane proteins. The second strategy is based on the biomimetic synthesis of magnetic nanoparticles with tailored properties by mimicking the bacterial biomineralization pathway *in vitro* for applications that require larger amounts of magnetosome-like MNPs.

Properties of Magnetosomes

Magnetosomes are formed and aligned intracellularly in well-ordered chains that serve as a navigational device for orientation along chemical gradients in aquatic habitats by interaction with the Earth's magnetic field.[14,15] Magnetosome crystals of MTB are typically from 30 to about 140 nm in diameter,[16-18] i.e., within the single-magnetic-domain size range,

which maximizes the efficiency of the particle as permanent magnetic carrier.[19] Statistical analysis of magnetosomes show that their crystal size distributions (CSDs) are narrow, asymmetrical, and negatively skewed with sharp cut-offs towards larger size and with shape factor (or width-to-length ratio) consistent for a given strain.[16,17,20-22] The magnetosome morphology also varies between different species, but is consistent for a given bacterial strain[18,23-25] (Figure 1). The cubooctahedral magnetite crystals produced by the magnetotactic model organism *Magnetospirillum gryphiswaldense* have an average size of approximately 35 nm. Magnetorelaxometry, DC magnetometry, and atomic force microscopy as well as magnetic force microscopy demonstrated that the particles have a high magnetic coercivity (2 600 A · m^{-1}) compared to commercially available magnetic nanoparticles, and the magnetic moments of single-domain magnetosome particles are predominantly in a blocked state.[26,27]
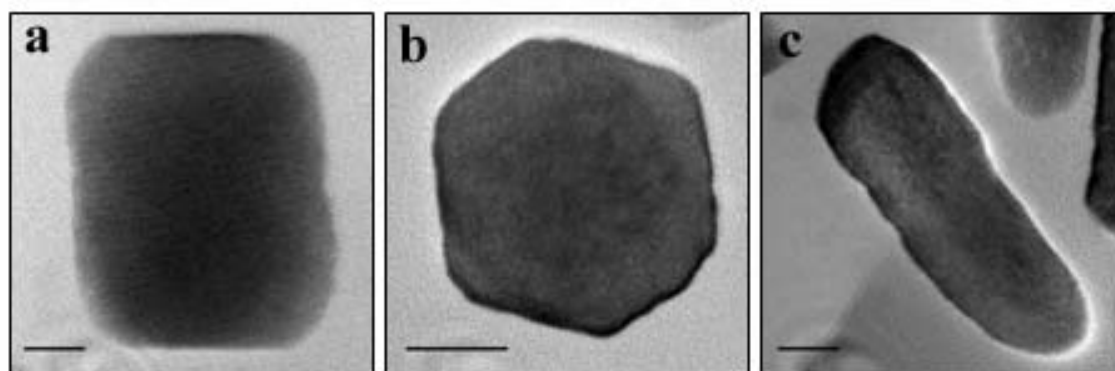

Figure 1: TEM images of magnetosomes from different bacterial strain: (a) parallelepipedal projection of a possibly pseudo-hexagonal prism, (b) hexagonal projection of a possibly cuboctahedral crystal and (c) tooth-shaped (anisotropic) magnetosomes (scale bar = 20 nm). Note that the tooth-shaped magnetosomes are usually the larger ones and the cuboctahedral the smaller ones.

However, as the crystal size is genetically determined, mutants can be isolated that display altered magnetic characteristics. As revealed by small-angle scattering using polarized neutrons (SANSPOL), magnetic particles from a mutant not only exhibit a narrower size distribution than those from the wild type, but with an average core diameter of 15.6 nm mutant particles predominantly fall into the superparamagnetic size range, which might be advantageous for certain applications as they are easily dispersible and have a higher surface-to-volume ratio.[28]

Another key feature of bacterial magnetosomes is the presence of a biological membrane with a defined biochemical composition. This natural 'coating' ensures superior

dispersibility of the particles and provides an excellent target for modification and functionalization of the particles. It was recently confirmed by cryo-electron tomographic studies that the magnetosome vesicles originate directly from the cytoplasmic membrane by invagination.[29] This explains why the lipid and fatty acid composition of the magnetosome membrane and the cytoplasmic membrane are mostly identical.[30,31] However, proteomic analysis of the membrane from isolated magnetosome particles revealed a highly specific and complex subset of proteins associated with the particles,[30-33] which amount to approximately 0.1% of the total cellular protein.[31]

Biotechnological Application and Functionalization of Magnetosomes

Because of their unique characteristics compared to synthetic particles, isolated magnetosome crystals are superior for applications that rely on small amounts of highly functionalized magnetic material with extraordinary magnetic and biochemical characteristics. For instance, magnetosomes have been used in a number of *in vitro* methods, such as procedures for labelling and immobilization of various biomolecules and magnetic separation. Bacterial magnetic particles have been employed in numerous purification procedures such as the extraction of mRNA and DNA from biological samples such as tissues, blood, and bacterial cells[8,11,34] or for the detection of different cyanobacterial DNA with genus specific probes.[35]

The immobilization of proteins, peptides, and enzymes on magnetic particles facilitates the selective separation and reuse of immobilized enzymes such as glucose oxidase and uricase[36]. Likewise, the immobilization of immunoglobulins has inspired the development of diverse applications. Antibody-magnetosome conjugates were employed for automated immunoassays to detect environmental pollutants, hormones, and toxic substances.[10,37]. In addition, antibody-modified magnetosomes have been used successfully for the specific separation of target cells from human blood.[38] Another application is the use of streptavidin-modified magnetosomes for the automated discrimination of single nucleotide polymorphism. The streptavidin-modified particles were coupled to biotinylated oligonucleotides to facilitate magnetic separation of DNA hybrids and used for the detection of single nucleotide polymorphisms.[9] Biotin-conjugated magnetosomes were used in combination with magnetic force microscopy for the highly sensitive detection and quantification of streptavidin immobilized on glass slides.[39]

The functionalization of biogenic nanoparticles is possible by both chemical and biotechnological approaches. A schematic overview over possible modifications is shown in

Figure 2. For instance, a rapid method for the immobilization of enzymes and proteins is based on glutaraldehyde-induced crosslinking.[35,36]. An alternative is the use of N-succinimidyl esters, such as the heterobifunctional reagent N-succinimidyl 3-(2-pyridyldithio) propionate, which was used for the conjugation of amine-modified oligonucleotides.[8] Myosin was immobilized on magnetic particles using sulfosuccinimidyl 6-[3'-(pyridyldithio)-propionamido]hexanoate and sulfosuccinimidyl 4-(N-maleimidomethyl) cyclohexane-1-carboxylate.[40] In addition, the biotinylation of magnetosomes was achieved with different N-hydroxy-succinimidylesters.[39,41] Biotinylation can be utilized for the modification of magnetosomes with various biotinylated biomolecules using streptavidin as a coupling reagent.
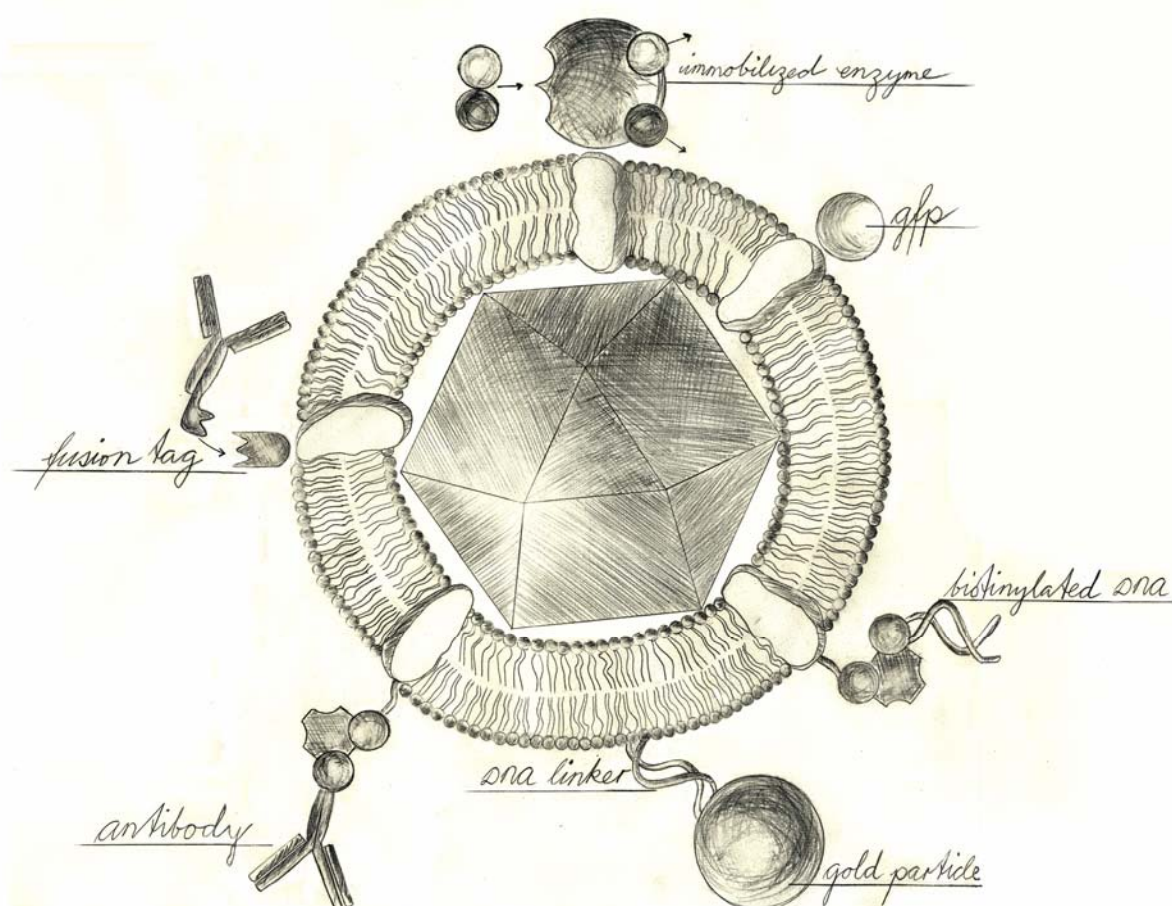
Artwork: Layla Känel, 2006

Figure 2: Potential functionalization of magnetosome particles by the introduction of different functional moieties resulting in hybrid bacterial magnetic nanoparticles. Magnetosomes could be modified by magnetosome-specific expression of enzymes and fluorophore proteins (e. g. GFP) by genetic fusion to MMP. The expression of fusion tags such as intein- or strep-tags as anchor groups could be used for the subsequent conjugate formation with various biomolecules. The biotinylation of membrane lipids facilitates the subsequent

streptavidin-mediated conjugation to various molecules, such as antibodies or nucleic acids which can also be used for the formation of conjugates with gold particles or quantum dots.

While chemical approaches allow the incorporation of a variety of functional groups, they require additional treatment upon magnetosome isolation from the cell, which can lead to denaturation and a loss of activity. Therefore, genetic approaches for the site-specific functionalization of MMP are attractive, as they are gentler with respect to the preservation of protein activity. This involves the construction of genetic fusions of magnetosome membrane anchor polypeptides with functional proteins and enzymes of choice. The chimeric proteins are expressed and incorporated into the MM within the bacterium during particle biosynthesis. Subsequently, magnetosome particles displaying functional polypeptides and enzymatic functions can be directly extracted from the bacterial cell without further chemical treatment. Another advantage of this strategy is the possibility to have control of the stoichiometry by the modification of either highly or less abundant proteins of the MM. Genetic engineering of magnetosome membrane proteins was employed to display the reporter enzymes luciferase and acetate kinase, and the antibody binding 'ZZ' protein on the magnetosome particles.[10,38,42,43] Moreover, it is possible to attach multiple functional moieties to the magnetosome surface by utilizing different magnetosome anchors, as successfully employed for expression of luciferase and an antibody binding protein on the magnetosome surface.[44] In addition, the expression of a human estrogen receptor was used for the screening of estrogenic compounds.[7] Ideal candidates for anchor polypeptides are integral membrane proteins of the MM, which are tightly attached to the crystals' surface and resist mechanical and chemical stresses. The anchor protein must not interfere with the function of the added moiety and vice versa. Moreover, it is required that functional groups are highly expressed, resistant to proteolysis, and displayed in similar quantities on the surface of all particles. In order to identify appropriate magnetosome anchor proteins we have started constructing genetic fusions of different MMPs with the enhanced green fluorescent protein (EGFP) as a reporter protein. EGFP was selected because it is a well-characterized fluorescent protein, which can be fused to many different proteins without functional interference and can be easily expressed in MTB.[29,45,46] By fluorescence microscopy we identified several fusion proteins, which are specifically targeted to the MM and exhibit high fluorescence on magnetosome chains and purified particles (Figure 3). The fluorescence of isolated magnetosome particles can be used to quantify the expression level to characterize different magnetosome anchors. Studies are in progress on the stability of the functionalized particles with respect to proteolysis and the effects of surfactants and salts. In future, the

replacement of the EGFP-function by other relevant polypeptide sequences will be used for the introduction of functional moieties as, for instance, biomolecular recognition groups such as the biotin-streptavidin system.[47] This will allow the development of multifunctional magnetic nanoparticles as innovative biomaterials, which for example, cannot only be used for biotechnological purposes but also in nanotechnology for the construction of hierarchically ordered supramolecular structures.
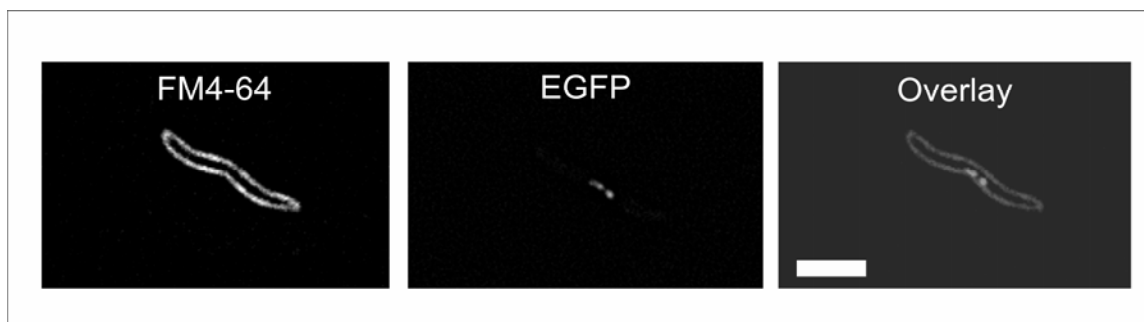

Figure 3. Fluorescent micrographs of M. gryphiswaldense expressing enhanced green fluorescent protein (EGFP) fused to an MMP. The fluorescence signal at midcell originates from the magnetosome chain displaying EGFP. Cell membranes were stained with the fluorescent dye FM4-64 (Invitrogen). EGFP fluorescence is confined to the intracellular position of magnetosomes at midcell, indicating that the fusion proteins are specifically inserted in the MM. This demonstrates that heterologous proteins can be fused to functional MMP for a magnetosome-specific display. The length of the scale bar is 2 μm.

Biomimetics

Inorganic synthesis of magnetite crystals with 'magnetosome-like' characteristics is attractive for some biomedical and nanotechnological applications. For instance, magnetosome crystals are promising candidates for applications such as magnetic resonance imaging (MRI),[48,49] targeted *in vivo* and *in vitro* gene and drug delivery ('magnetofection'),[50,51] and the hyperthermal treatment of tumours.[26,27] In these cases and in nanotechnological applications, which often require the fabrication of hybrid organic-inorganic nanocomposites, the biomimetic *in vitro* synthesis of MNPs may be advantageous.

In biomineralizing systems, organisms exert a high level of control over nucleation and growth of inorganic materials such as carbonate, silicate, or iron oxides. For example, evidence for biomineral phase control by addition of proteins have been reported for calcium carbonate, silica, and hydroxylapatite.[52,53] There are several interconnected approaches related to biomimetics. First, biological concepts can be tested in inorganic approaches to produce materials with unique properties that are exclusively known from biogenic minerals. In the case of MNPs, biomimetic approaches can be purely inorganic. The first step

encompasses magnetite precipitation, which can be performed by pyrolysis, gas deposition, sol-gel, microemulsion, or bulk solution.[4] Most developed are bulk solution syntheses since large quantities of products can be formed. Coprecipitation of ferric and ferrous iron in alkaline environments leads to the formation of magnetite crystals[54] (Figure 4). These can also be performed under bio-inspired, i.e., controlled conditions, for example, in the presence of defined salt and pH conditions that result, for example, in narrower size distributions, approximating those found for biogenic particles.[55] For most applications, functionalization of particles is required. Thus, the next step is often the coating of surfaces to prevent nanoparticles agglomeration. Organic solvent such as oleic acid or alkyl phosphate or phosphonate,[56] folic acid or poly(ethylene glycol)[57,58] were shown to be powerful surfactants (Figure 4).
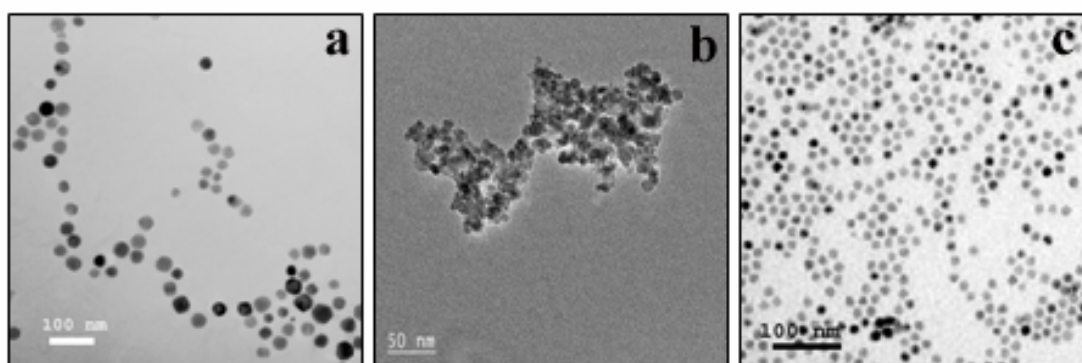

Figure 4: TEM images of isolated magnetosomes particles (a), purely inorganic nanocrystals (b), and inorganic crystals in oleic acid (c). The biogenic magnetites do not agglomerate due to their membrane, whereas inorganic particles need further treatment to prevent them from agglomeration.

Another approach of biomimetics depends on biological compounds, which are directly added to inorganic assays. For example, preformed magnetite nanoparticles can be incorporated into macroscopic threads of *Bacillus subtilis* by reversible swelling of the superstructure in colloidal sols. In this case, the organized bacterial superstructures are used as three-dimensional templates for the fabrication of ordered inorganic-organic fibrous composites.[59,60] Ultimately, the most promising approach uses isolated biological compounds such as specific proteins with defined biological activity related to mineral formation. Proteins can be extracted from the biomineralizing organism, or produced by recombinant technology and used in an *in vitro* bio-inorganic assay. This approach has already shown great potential, for example, by controlling phase switching between calcite and aragonite,[52] or in the case of silicate biomineralization.[53,61] One successful example of the bioinorganic formation of magnetite nanoparticles was reported with the use of the iron-

storage protein ferritin: The demetallated protein shell of apoferritin assembles into a multisubunit protein shell to form a hollow cage of about 8 nm in diameter. This natural nanometer-sized bioreactor has been used for the biomimetic reconstitution of the ferromagnetic iron oxides magnetite and maghemite (γ-Fe$_2$O$_3$).[62,63] Promising examples have been reported for *in vitro* magnetite formation inspired by magnetotactic bacteria.[64,65] In these studies, several low-molecular mass proteins bound to bacterial magnetite were identified. If the acidic protein Mms6 was added to a reactor concomitantly with the iron ions, nanometer-sized magnetic particles somehow reminiscent to those in magnetic bacteria were obtained, which is not the case when using another type of protein.[64, 65] This suggested that Mms6 is directly involved in biological magnetite crystal formation in MTB. However, presented morphological analyses were not fully conclusive, and further studies are required to obtain ultimate proof for the suggested activity *in vivo*.

Biomimetic approaches will be most promising when our understanding of biomineralization pathways are improved down to the molecular level. This would enable the exact reproduction of magnetosome-like nanoparticles in a test tube by means of biomimetics. So where to start? For biomimetic synthesis of magnetite crystals, the assay has to be at micrometer-scale, as the amount of proteins from purification or recombinant production is usually limited. A distinctive feature of magnetite biomineralization in magnetosomes at the physical level is the limited diffusion of ions. Biological conditions could be mimicked, for example, by the use of a gel instead of a liquid phase. Another physical limitation of bulk phase synthesis is the lack of spatial control, which *in vivo* is provided by the magnetosome membrane. This could be overcome, for instance, by the use of synthetic membranous vesicles, such as liposomes.[66] As formation of crystals occurs through nucleation and growth, a given chemical supersaturation needs to be achieved to form magnetite nanocrystals by addition of iron ions in basic conditions. The use of artificial vesicles might, therefore, also facilitate to locally maintain supersaturating concentrations, which permit magnetite nucleation, and also provide spatial constraints to restrict the maximum growth size of the particles. Eighteen specific bona fide proteins have so far been identified in the magnetosome membrane of *M. gryphiswaldense*.[67] Their functions with respect to biomineralization largely remain unknown, which requires extensive empirical approaches to test their *in vitro* activity. In some cases, putative functions of proteins could be inferred from sequence similarities to other proteins. For example MamB and MamM were identified as members of the cation diffusion facilitator (CDF) family of metal transporters and preliminary experimental evidence has suggested a key function in magnetosome-directed uptake of

supersaturating amounts of iron. If reconstituted within vesicles, transport of iron into the liposome could be controlled, with slow diffusive rates close to those occurring *in vivo*. In addition, effective buffering is required for the process, as protons are released into the solution during the formation of Fe_3O_4, which have to be removed as magnetite precipitation only occurs at basic pH[54,55] Finally, the function of Mms6 and other magnetosome proteins that contain related sequence motifs (i.e. MamD, MamG, MamS and others) should be further investigated, as initial *in vitro* results have indicated a potential role in crystals growth. This approach, for instance, will also allow identification of the proteins and their interactions between proteins required to precipitate magnetite and those responsible for the defined morphology.

Finally, coupling *in vivo* functional studies, such as the targeted mutagenesis of the gene that produces the protein of interest with bio-inorganic *in vitro* assay using the same proteins extracted from magnetotactic bacteria, will be the 'ultimate' approach to unravel the role played by a given protein, to understand biomineralization at a mechanistic level, and to develop biomimetics to obtain innovative material with rationally designed characteristics.

References

[1]   F. Gazeau, C. Baravian, J.-C. Bacri, R. Perzynski, M. I. Shliomis, *Phys. Rev. E* **1997**, *56*, 614 LP.

[2]   L. An, Z. Li, W. Li, Y. Nie, Z. Chen, Y. Wang, B. Yang, *J. Magn. Magn. Mater.* **2006**, *303*, 127.

[3]   M. Zahn, *J. Nanoparticle Res.* **2001**, *3*, 73.

[4]   A. K. Gupta, M. Gupta, *Biomater.* **2005**, *26*, 3995.

[5]   M. Sarikaya, C. Tamerler, A. K.-Y. Jen, K. Schulten, F. Baneyx, *Nature Mater.* **2003**, *2*, 577.

[6]   P. Tartaj, M. D. Morales, S. Veintemillas-Verdaguer, T. Gonzalez-Carreno, C. J. Serna, *J. Phys. D: Appl. Phys.* **2003**, *36*, R182.

[7]   T. Yoshino, F. Kato, H. Takeyama, K. Nakai, Y. Yakabe, T. Matsunaga, *Anal. Chim. Acta* **2005**, *532*, 105.

[8]   K. Sode, S. Kudo, H. Sakaguchi, N. Nakamura, T. Matsunaga, *Biotechnol. Technol.* **1993**, *7*, 688.

[9]   T. Tanaka, K. Maruyama, K. Yoda, E. Nemoto, Y. Udagawa, H. Nakayama, H. Takeyama, T. Matsunaga, *Biosens. Bioelectron.* **2003**, *19*, 325.

[10]   T. Tanaka, T. Matsunaga, *Anal. Chem.* **2000**, *72*, 3518.

[11]   B. Yoza, A. Arakaki, T. Matsunaga, *J. Biotechnol.* **2003**, *101*, 219.

[12]   R. B. Frankel, R. Blakemore, *Science* **1979**, *203*, 1355.

[13]   D. Schüler, *Arch. Microbiol.* **2004**, *181*, 1.

[14]   D. A. Bazylinski, R. B. Frankel, *Nature Rev. Microbiol.* **2004**, *2*, 217.

[15]   C. B. Flies, H. M. Jonkers, D. de Beer, K. Bosselmann, M. E. Böttcher, D. Schüler, *FEMS Microbiol. Ecol.* **2005**, *52*, 185.

[16]   B. Arató, Z. Szanyi, C. B. Flies, D. Schüler, R. B. Frankel, P. R. Buseck, M. Pósfai, *Am. Mineral.* **2005**, *90*, 1233.

[17]   B. Devouard, M. Posfai, X. Hua, D. A. Bazylinski, R. B. Frankel, P. B. Buseck, *Am. Mineral.* **1998**, *83*, 1387.

[18]   D. Faivre, N. Menguy, M. Pósfai, D. Schüler, **2006**, unpublished results.

[19]   R. F. Butler, S. Banerjee, *J. Geophys. Res.* **1975**, *80*, 4049.

[20]   D. Faivre, L. Boettger, B. Matzanke, D. Schüler, **2006**, unpublished results.

[21]   D. Faivre, P. Zuddas, *Earth Planet. Sci. Lett.* **2006**, *243*, 53.

[22]   D. Faivre, N. Menguy, F. Guyot, O. Lopez, P. Zuddas, *Am. Mineral.* **2005**, *90,* 1793.

[23]   E. Baeuerlein, *Angew. Chem. Int. Ed.* **2003**, *42*, 614.

[24] S. Mann, R. B. Frankel, R. P. Blakemore, *Nature* **1984**, *310*, 405.

[25] K. L. Thomas-Keprta, D. A. Bazlinski, J. L. Kirschvink, S. J. Clemett, D. S. McKay, S. J. Wentworth, H. Vali, E. K. Gibson Jr., C. S. Romanek, *Geochim. Cosmochim. Acta* **2000**, *64*, 4049.

[26] D. Eberbeck, V. Janke, S. Hartwig, U. Heyen, D. Schüler, M. Albrecht, L. Trahms, *J. Magn. Magn. Mater.* **2005**, *289*, 70.

[27] R. Hergt, R. Hiergeist, M. Zeisberger, D. Schüler, U. Heyen, I. Hilger, W. A. Kaiser, *J. Magn. Magn. Mater.* **2005**, *293*, 80.

[28] A. Hoell, A. Wiedenmann, U. Heyen, D. Schüler, *Phys. B* **2004**, *350*, e309.

[29] A. Komeili, Z. Li, D. K. Newman, G. J. Jensen, *Science* **2006**, *311*, 242.

[30] K. Grünberg, E. C. Müller, A. Otto, R. Reszka, D. Linder, M. Kube, R. Reinhardt, D. Schüler, *Appl. Eviron. Microbiol.* **2004**, *70*, 1040.

[31] K. Grünberg, C. Wawer, Tebo B. M., D. Schüler, *Appl. Environ. Microbiol.* **2001**, *67*, 4573.

[32] S. Schübbe, M. Kube, A. Scheffel, C. Wawer, U. Heyen, A. Meyerdierks, M. Madkour, F. Mayer, R. Reinhardt, D. Schüler, *J. Bacteriol.* **2003**, *185*, 5779.

[33] S. Ullrich, M. Kube, S. Schübbe, R. Reinhardt, D. Schüler, *J. Bacteriol.* **2005**, *187*, 7176.

[34] B. Yoza, A. Arakaki, K. Maruyama, H. Takeyama, T. Matsunaga, *J. Biosci. Bioeng.* **2003**, *95*, 21.

[35] T. Matsunaga, H. Nakayama, M. Okochi, H. Takeyama, *Biotechnol. Bioeng.* **2001**, *73*, 400

[36] T. Matsunaga, S. Kamiya, *Appl. Microbiol. Biotechnol.* **1987**, *26*, 328.

[37] T. Tanaka, H. Takeda, F. Ueki, K. Obata, H. Tajima, H. Takeyama, Y. Goda, S. Fujimoto, T. Matsunaga, *J. Biotechnol.* **2004**, *108*, 153.

[38] M. Kuhara, H. Takeyama, T. Tanaka, T. Matsunaga, *Anal. Chem.* **2004**, *76*, 6207.

[39] Y. Amemiya, T. Tanaka, B. Yoza, T. Matsunaga, *J. Biotech.* **2005**, *120*, 308.

[40] T. Tanaka, H. Yamasaki, N. Tsujimura, N. Nakamura, T. Matsunaga, *Mater. Sci. Eng. , C* **1997**, *5*, 121.

[41] B. Ceyhan, P. Alhorn, C. Lang, D. Schüler, C. M. Niemeyer, *Small* **2006**, *2,* 1251.

[42] T. Matsunaga, H. Togo, T. Kikuchi, T. Tanaka, Biotechnol. Bioeng. **2000**, 70, 704

[43] T. Matsunaga, M. Takahashi, T. Yoshino, M. Kuhara, H. Takeyama, Biochem. Biophys. Res. Comm. **2006**, 350, 1019.

[44] T. Yoshino, T. Matsunaga, *Appl. Environ. Microbiol.* **2006**, *72*, 465.

[45] A. Komeili, H. Vali, T. J. Beveridge, D. Newman, *Proc. Natl. Acad. Sci. U. S. A.* **2004**, *101*, 3839.

[46] A. Scheffel, M. Gruska, D. Faivre, A. Linaroudis, J. M. Plitzko, D. Schüler, *Nature* **2006**, *440*, 110.

[47] C. Lang, D. Schüler, in *Microbial Bionanotechnology: Biological Self-assembly Systems and Biopolymer-based Nanostructures* (Ed.: B. Rehm), Horizon bioscience, Wymondham, **2006**, pp. 107.

[48] *US patent 6,251,365 B1*(**2001**). Invs.: E. Bäuerlein, D. Schüler, R. Reszka, S. Päuser,

[49] R. Reszka, in *Biomineralization* (Ed.: E. Baeuerlein), Wiley-VCH, Weinheim, **2000**, pp. 81.

[50] C. Plank, U. Schillinger, F. Scherer, C. Bergemann, J. S. Remy, F. Krotz, M. Anton, J. Lausier, J. Rosenecker, *Biol. Chem.* **2003**, *384*, 737.

[51] T. Matsunaga, N. Tsujimura, *Appl. Microbiol. Biotechnol.* **1993**, *39*, 368.

[52] A. M. Belcher, X. H. Wu, R. J. Christensen, P. K. Hansma, G. D. Stucky, D. E. Morse, *Nature* **1996**, *381*, 56.

[53] N. Kröger, R. Deutzmann, M. Sumper, *Science* **1999**, *286*, 1129.

[54] R. M. Cornell, U. Schwertmann, *The iron oxides (Structure, properties, reactions, occurrences and uses)*. Wiley-VCH, Weinheim, **2003**.

[56] D. Faivre, P. Agrinier, N. Menguy, P. Zuddas, K. Pachana, A. Gloter, J.-Y. Laval, F. Guyot, *Geochim. Cosmochim. Acta* **2004**, *68*, 4395.

[57] Y. Sahoo, H. Pizern, T. Fried, D. Golodnitsky, L. Burstein, C. N. Sukenik, G. Markovich, *Langmuir* **2001**, *17*, 7907.

[58] Y. Zhang, J. Zhang, *J. Col. Interf. Sci.* **2005**, *283*, 352.

[59] Y. Zhang, N. Kohler, M. Zhang, *Biomater.* **2002**, *23*, 1553.

[60] S. A. Davis, H. M. Patel, E. L. Mayes, N. H. Mendelson, G. Franco, S. Mann, *Chem. Mater.* **1998**, *10*, 2516.

[61] N. H. Mendelson, *Science* **1992**, *258*, 1633.

[62] H. Menzel, S. Horstmann, P. Behrens, P. Bärnreuter, I. Krueger, M. Jahns, *Chem. Commun.* **2003**, *2003*, 2994.

[63] F. C. Meldrum, B. R. Heywood, S. Mann, *Science* **1992**, *257*, 522.

[64] S.-T. Yau, P. G. Vekilov, *Nature* **2000**, *406*, 494.

[65] T. Prozorov, S. K. Mallapragada, B. Narasimhan, L. Wang, P. Palo, M. Nilsen-Hamilton, T. J. Williams, D. A. Bazlinski, R. Prozorov, D. E. Canfield, *Adv. Funct. Mater.* **2006**, *in press*.

[66]   A. Arakaki, J. Webbs, T. Matsunaga, *J. Biol. Chem.* **2003**, *278*, 8745.

[67]   S. Mann, J. P. Hannington, *J.Col. Interf. Sci.* **1987**, *122*, 326.

[68]   C. Jogler, D. Schüler, in *Magnetoreception and magnetosomes in bacteria* (Ed.: D. Schüler), Springer, Heidelberg, **2006**.

Cation site occupancy of biogenic magnetite compared to polygenic ferrite spinels determined by X-ray magnetic circular dichroism

Victoria S. Coker[1][*], Carolyn I. Pearce[1], Claus Lang[3], Gerrit van der Laan[2,1],
Richard A. D. Pattrick[1], Neil D. Telling[2], Dirk Schüler[3], E. Arenholz[4],
Jonathan R. Lloyd[1]

[1]School of Earth, Atmospheric & Environmental Sciences & Williamson Research Centre for Molecular Environmental Science, University of Manchester, Manchester, M13 9PL, United Kingdom

[2]Magnetic Spectroscopy Group, Daresbury Laboratory, Warrington WA4 4AD, United Kingdom

[3]Max-Planck Institute for Marine Microbiology, Celsiusstr. 1, D-28359 Bremen, Germany

[4]Advanced Light Source, Lawrence Berkeley National Laboratory, Berkeley, CA 94720, USA

*corresponding author: vicky.coker@manchester.ac.uk

Abstract

Ferrite spinels, especially magnetite (Fe_3O_4), can be formed either by geological, biological or chemical processes leading to chemically similar phases that show different physical characteristics. We compare, for the first time, magnetite produced by these three different methods using X-ray magnetic circular dichroism (XMCD), a synchrotron radiation based technique able to determine the site occupancy of Fe cations in the ferrite spinels. Extracellular nanoscale magnetite produced by different Fe(III)-reducing bacteria was shown to have different degrees of stoichiometry depending on the bacteria and the method of formation, but all were oxygen deficient due to formation under anoxic conditions. Intracellular nano-magnetite synthesized in the magnetosomes of magnetotactic bacteria was found to have a Fe cation site occupancy ratio most similar to stoichiometric magnetite, possibly due to the tight physiological controls exerted by the magnetosome membrane. Chemically-synthesised nano-magnetite and bulk magnetite produced as a result of geological processes were both found to be cation deficient with a composition between magnetite and maghemite (oxidised magnetite).

Introduction

Magnetite is formed by a range of geological, chemical and biological processes leading to chemically and structurally similar phases but with very different crystallite sizes, stoichiometries and physical properties. Ferrite spinels, especially magnetite (Fe_3O_4), are of special interest as they are among the most important magnetic materials for industrial applications. This is the first study to apply the synchrotron radiation based technique of X-ray magnetic circular dichroism (XMCD) to nano-magnetite samples produced by both extracellular and intracellular biogenic processes, in order to compare and discriminate between these and non-biogenic geological bulk magnetite and chemically produced nano-magnetite. XMCD provides unique information on magnetic minerals as it is element specific and can quantify the amount and the valence state of Fe on each of the two lattice sites within the structure of ferrite spinels such as magnetite (Pattrick *et al.*, 2002; Coker *et al.*, 2006; Pearce *et al.*, 2006). XMCD has previously been extensively used to characterise the magnetic properties of used technological application such as data storage devices (van der Laan and Welbourne, 1996).

Magnetite is present throughout the Earth's crust and uppermost mantle and is the main contributor to rock magnetism. Formed by magmatic and hydrothermal processes, crystal sizes vary from the sub-micron scale to polycrystalline layers several meters thick, such as in the ultramafic Bushveld intrusion in South Africa. Nano-magnetite synthesised as a chemical precipitate requires a narrow particle size distribution in order to be used in technological or medical applications such as magnetic recording media, ferrofluids and magnetic resonance imaging (MRI) (Lee *et al.*, 2005).

Biogenic magnetite nanoparticles are considered to be potential bio-signatures of life and further interest has been stimulated by the recognition that they have potential uses in nanotechnology, which has led to research into their characterisation (Thomas-Keprta *et al.*, 2000; Safarik & Safarikova, 2002; Coker *et al.*, 2004; Faivre & Zuddas, 2006). Magnetite can be precipitated by a diverse range of bacteria through redox transformations of ferric iron and can form as either an extracellular precipitate through Fe(III) reduction (Lovley *et al.*, 1987) or Fe(II) oxidation (Chaudhuri *et al.*, 2001), or intracellularly within the magnetosomes of magnetotactic bacteria (Schüler, 1999). Magnetite formed by extracellular processes has been reported to have a broad size distribution and varied morphology, whereas magnetite formed by magnetotactic bacteria is formed within the magnetosomal membrane, and therefore the size and shape of the nanoparticles is constrained, leading to a narrow particle size distribution (Bazylinski & Moskowitz, 1997).

High-resolution electron microscopy (EM) techniques have been the most widely used to characterise the morphology and size of biogenic and chemical nanoparticles of magnetite (Thomas-Keprta *et al.*, 2000; Glasauer *et al.*, 2003; Taylor & Barry, 2004) and have also been used to differentiate between biogenic intracellular magnetite and geological magnetite (Arato *et al.*, 2005). Other techniques commonly used are iron and oxygen isotopic studies and crystal size distribution analyses (Mandernack *et al.*, 1999; Faivre & Zuddas, 2006). The magnetic methods that have been developed to identify biogenic minerals are low-temperature SQUID magnetometry (Moskowitz *et al.*, 1993), ferromagnetic resonance (Weiss *et al*., 2004) and coercivity deconvolution (Egli, 2004).

Fe(III)-reducing bacteria

Dissimilatory Fe(III)-reducing bacteria capable of magnetite production from respiration using poorly soluble Fe(III) oxides as a terminal electron acceptor include *Geobacter sulfurreducens* (*Gb. sulfurreducens*) (Caccavo Jr *et al.*, 1994), *Shewanella oneidensis* (*S. oneidensis*) (Lovley *et al.*, 1989) and *Geothrix fermentans* (*Gt. fermentans*) (Coates *et al.*, 1999). This study examines biogenic magnetite produced by these organisms as each uses a different mechanism to reduce Fe(III). A full understanding of the mechanisms involved in Fe(III)-reduction and magnetite formation is yet to be determined for these and other species. Current evidence suggests that *Geobacter* species require direct contact between the cell and the Fe(III)-containing mineral, with electron transfer mediated by outer membrane cytochromes (Lovley *et al.*, 2004). Additionally, *Gb. sulfurreducens* produces pili acting as electron transferring 'nanowires' when grown on insoluble ferric iron (Reguera *et al.*, 2005). *S. oneidensis*, a facultative anaerobe, (Lovley *et al.*, 1989) is also capable of Fe(III) reduction to form the mineral magnetite via outer membrane cytochromes (Myers & Myers, 1992) and nanowire-like assemblages (Gorby *et al.*, 2006). However, this organism can also produce a soluble extracellular electron shuttle to alleviate the need for direct contact between the cell surface and Fe(III) mineral substrate (Newman & Banfield, 2002). The identity of this compound has remained elusive, although other naturally occurring electron shuttles have been identified that promote microbial Fe(III) reduction, including humics and other extracellular quinone containing molecules (Lovley *et al.*, 1996). Finally, *Gt. fermentans,* initially isolated from a hydrocarbon-contaminated aquifer sediments, is also capable of producing magnetite through the reduction of Fe(III) (Coates *et al.*, 1999). Evidence suggests that this organism is able to produce both an extracellular electron shuttle and chelating agent,

the latter to solubilise the highly insoluble Fe(III) oxides, making it more bioavailable for respiration..

Magnetotactic Bacteria

Magnetotactic bacteria use a completely different mechanism to reduce Fe(III) and form intracellular magnetite. The first stage in magnetite biomineralization by magnetotactic bacteria is the uptake of ferrous or ferric iron (Schüler and Baeuerlein 1996). Subsequently, the formation of magnetite probably proceeds via a ferrihydrite-like mineral (Ofer *et al.*, 1984). Individual magnetite crystals form chains within the bacterial cell enveloped by a trilaminate structure, called the magnetosome membrane (Balkwill *et al.*, 1980). Magnetite formation requires the presence of mixed-valence iron complexes in solution. Therefore, biomineralization of this material depends on precise regulation of iron supersaturation and both redox potential and pH (Schüler, 2004).

Magnetite

The mineral magnetite has an inverse spinel structure with one quarter of the tetrahedral (T_d) and one half of the octahedral [O_h] sites filled by iron. The formula for magnetite is $(Fe^{3+})[Fe^{2+}Fe^{3+}]O_4^{2-}$, where the parentheses and square brackets indicate T_d and O_h sites, respectively. While the Fe(III) is equally split between T_d and O_h sites, the Fe(II) occupies only O_h sites. Hence in stoichiometric magnetite the Fe occupancy of the d^6 O_h : d^5 T_d : d^5 O_h sites is 1:1:1. The O_h and T_d sublattices contain cations with anti-parallel aligned magnetic moments, which results in a net magnetisation in the O_h sub-lattice that does not cancel out, giving rise to ferrimagnetism. Non-stoichiometry of magnetite is manifest by the presence of vacant cation sites in the structure. These are caused by oxidation of Fe(II) in the O_h sites to Fe(III), leading to a charge imbalance so that additional Fe(II) is removed from the structure giving a formula $(Fe^{3+})[Fe^{2+}_{1-3\delta}Fe^{3+}_{1+2\delta}\Delta_\delta]O_4^{2-} = Fe_{3-\delta}O_4$, where δ quantifies the deviation from stoichiometry due to cation vacancies Δ (Pearce *et al.*, 2006).

Materials and Methods

Fe(III) reduction

Gb. sulfurreducens and *Gt. fermentans* were obtained from our laboratory culture collection and grown under strictly anaerobic conditions at 30 °C in modified fresh water medium as described previously (Lloyd *et al.*, 2003). Sodium acetate (20 mM) and fumarate

(40 mM) were provided as the electron donor and acceptor, respectively. All manipulations were done under an atmosphere of N_2–CO_2 (80:20). *S. oneidensis* was obtained from laboratory cultures and grown under aerobic conditions from frozen stock at 30 ^{o}C in tryptone soy broth (TSB) media. After 24 hours a 10% inoculum of late log-phase aerobic cultures was used to inoculate anaerobic ferric citrate media (Lovley & Phillips, 1988). Sodium lactate (20 mM) and ferric citrate (56 mM) were provided as the electron donor and acceptor, respectively.

Late log-phase cultures of *Gb. sulfurreducens, Gt. fermentans* and *S. oneidensis* were harvested by centrifugation at 4920 g for 20 minutes and washed twice in carbonate buffer ($NaHCO_3$; 30 mM, pH 7.1) under N_2–CO_2 (80:20) gas prior to use. Aliquots of the washed cell suspension (1.5 ml) were added to sealed anaerobic bottles containing 28.5 ml bicarbonate buffer. The final concentration of bacteria corresponded to 0.2 mg protein per mL. The following additions were made from anaerobic stocks as required; poorly crystalline Fe(III) oxide (10 mM), sodium acetate (10 mM), sodium lactate (10 mM) and the humic analogue/electron shuttle anthraquinone-*2,6*-disulphonate (10 µM). Bottles were incubated in the dark at 20 °C. 100 µl of slurry was removed from each serum bottle periodically, after gentle shaking, using aseptic and anaerobic technique and analyzed for 0.5 M HCl-extractable Fe(II) using the ferrozine method (Lovley & Phillips, 1986). All experiments, including abiotic controls, were done in triplicate and representative data shown throughout. Standard errors were within ± 10% of the mean.

Production of Magnetosomes

The magnetotactic bacterium *Magnetospirillum gryphiswaldense* MSR1 (Schleifer, *et al.* 1991) was grown under microaerobic conditions in a 20L oxystat fermenter as described previously (Heyen and Schüler 2003). Cells were grown to stationary phase and harvested by centrifugation. Magnetosomes were purified as described by Grünberg *et al.* (2004). Upon isolation magnetosomes were resuspended in storage buffer (10 mM HEPES pH 7.4, 1 mM EDTA pH 8.0, 0.1 mM PMSF, 0.04% NaN_3) and stored in a nitrogen atmosphere to prevent oxidation.

Chemical magnetite

The chemical magnetite analyzed in this study as a comparison to biogenic and geogenic magnetite was Fe_3O_4 20–30 nm APS Powder, with a surface area > 60 m^2/g (Alfa Aesar Cas. no. 1317-61-9).

Transmission electron microscopy

Imaging of the samples produced by the various bacteria was performed on a Philips CM200 microscope operating at 120 kV. Samples were washed using degassed distilled water several times before being re-suspended in ethanol and dropped onto a carbon-coated copper grid and left to dry just prior to insertion into the TEM.

X-ray Magnetic Circular Dichroism

X-ray absorption spectra were collected on stations 1.1 and 5U.1 using the Flipper electromagnet endstation (Dudzik *et al.*, 2000) at the Synchrotron Radiation Source (SRS), Daresbury Laboratory, UK and station 4.0.2 using the octopole magnet endstation (Arenholz & Prestemon, 2005) at the Advanced Light Source (ALS), Berkeley, CA. Samples *Gb. sulfurreducens*, *Gb. sulfurreducens* + AQDS, *S. oneidensis*, *S. oneidensis* + AQDS and chemical magnetite were measured on ALS station 4.0.2, *Gt. fermentans*, *Gt. fermentans* + AQDS, both oxidised *Gt. sulfurreducens* samples and the natural magnetite sample on SRS station 1.1 and the magnetosomes were measured on SRS station 5U.1. Samples were prepared by washing aliquots of the suspension in deionised water before drying under anaerobic conditions. Approximately 0.01 g of each powder was then mounted in an anaerobic cabinet on carbon tape attached to the sample manipulator. Samples were kept anaerobic during sampling loading by saturating the manipulator in a stream of N_2 gas during insertion into the vacuum chamber. The specimen was positioned central to the magnetic pole pieces, with the X-ray beam entering through a small centred hole in one of the pole pieces, parallel to the magnetic field and perpendicular to the sample surface. The XAS were monitored in total-electron yield mode, which gives an effective probing depth of ~4.5 nm. At each energy point the XAS were measured for the two opposite magnetisation directions by reversing the applied field of 0.6 Tesla. The XAS spectra of the two magnetisation directions were normalised to the incident beam intensity and subtracted from each other to give the XMCD spectrum (Pattrick *et al.*, 2002).

The measured Fe $L_{2,3}$ XMCD was used to obtain the site occupancies of the Fe cations in the spinel structure of the magnetite. At the Fe $L_{2,3}$-edge, $2p$ core electrons are excited by electric-dipole transitions into (partially) localised unoccupied $3d$ states, so that XMCD provides information about the local electronic and magnetic structure of the absorbing atom (van der Laan & Thole, 1991). The spectrum is split by the $2p$ spin-orbit interaction into two main structures: the L_3- and L_2-edge. For magnetite, the intensities of the three main peaks in

the L_3-edge XMCD with negative, positive, negative intensity are related to the amounts of Fe d^6 O$_h$, d^5 T$_d$ and d^5 O$_h$, respectively, present in the sample (Pattrick *et al.*, 2002).

To obtain the relative amounts of the three Fe sites, the experimental spectra were fitted by means of a non-linear least-squares analysis, using calculated spectra for each of the Fe sites (Figure 1). In the calculations, as described in (van der Laan & Thole, 1991), the Hartree-Fock Slater integrals for the $3d$-$3d$ and $2p$-$3d$ Coulomb and exchange interactions were scaled to 70% and 80%, respectively, and the crystal fields for the O$_h$ and T$_d$ sites were taken as $10Dq = 1.2$ eV and 0.6 eV, respectively. The calculated spectra were convoluted by a Lorentzian of $\Gamma = 0.3(0.5)$ eV for the L_3- (L_2-) edge to account for the intrinsic core-hole lifetime broadening and by a Gaussian of $\sigma = 0.35$ for the SRS 1.1 data, $\sigma = 0.5$ eV for the SRS 5U.1 data and $\sigma = 0.2$ eV for the ALS 4.0.2 data to account for instrumental broadening. The experimental spectra were fitted over the L_3 main peaks only, which has previously been shown to give meaningful results, although fitting over the L_2 peak does give good qualitative agreement (Pattrick *et al.*, 2002; Pearce *et al.*, 2006).

To calculate the errors in the fitting of the XMCD spectra the same sample of bio-magnetite was measured on three different beamlines and then the spectra were fitted using the methods above. By taking the standard deviation of the site occupancies according to the three different spectra the error in each of the individual sites was found to be 1.10 ± 0.02, 0.99 ± 0.01, 0.98 ± 0.02 for the d^6 O$_h$, d^5 T$_d$, and d^5 O$_h$, respectively. The error in the vacancies, which indicate the degree of departure from stoichiometric magnetite, was found to be ± 0.01.
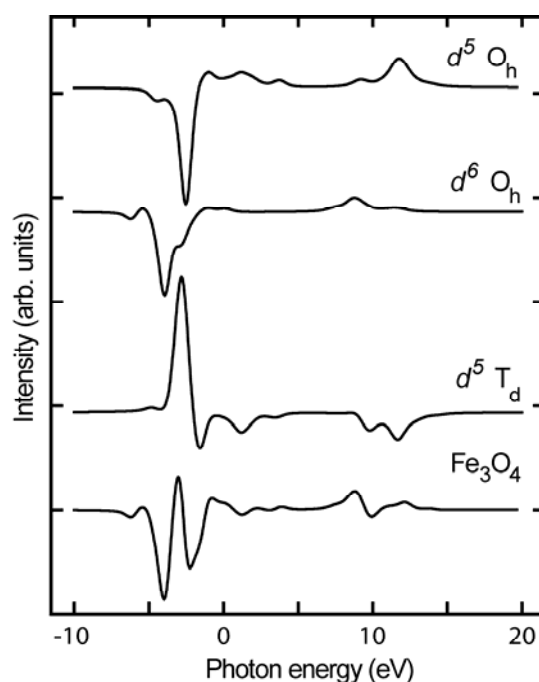
Figure 1: The calculated Fe $L_{2,3}$ XMCD spectra for the three different Fe sites in magnetite together with the total spectrum.

Results

Fe(III) reduction

During anaerobic incubation and transformation to magnetite, cultures containing Fe(III)-reducing bacteria were analyzed for Fe(II) concentration using the Ferrozine technique (Lovley & Phillips, 1986). Analyses of HCl extractable Fe(II) showed an increase in ferrous iron with time and cultures supplemented with the electron shuttle AQDS had a higher rate of Fe(III) reduction than those without AQDS (Figure 2). The final amount of Fe(II) in the AQDS-supplemented cultures was between 2.5 and 3.0 mM, whereas cultures without the electron shuttle showed that only between 1.0 and 1.5 mM of Fe(II) was detectable. However, all cultures formed a magnetic precipitate, which was confirmed by holding a bar magnet next to the microcosm. The solid also changed colour from orange-brown to black during the course of the transformation.

The size of the biogenic nano-particles was found to range depending on the method of formation. *M. gryphiswaldense* produced cubo-octahedral particles between 42–45 nm in size (see Figure 3 and (Schüler, 1999)), these are single-domain nanoparticles (Dunin-Borkowski *et al.*, 1998). Extracellular biogenic magnetite produced by the dissimilatory Fe(III)-reducers all had a less well-defined shape and the particle size range

was more varied between 20–30 nm, consistent with previous work by (Fredrickson *et al.*, 1998; Sparks *et al.*, 1990)
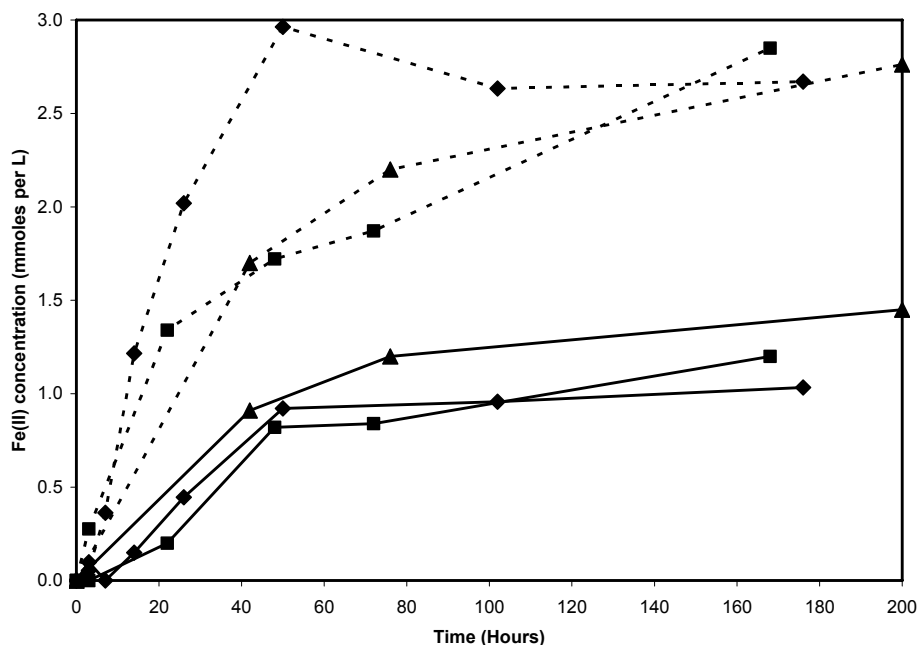

Figure 2: Fe(II) concentration variation with time for reduction of ferrihydrite to form magnetite by the Fe(III)-reducing bacteria, Gb. sulfurreducens (diamonds), S. oneidensis (squares) and Gt. fermentans (triangles), with (dotted lines) and without (solid lines) supplementation of the cultures with the electron shuttle AQDS.
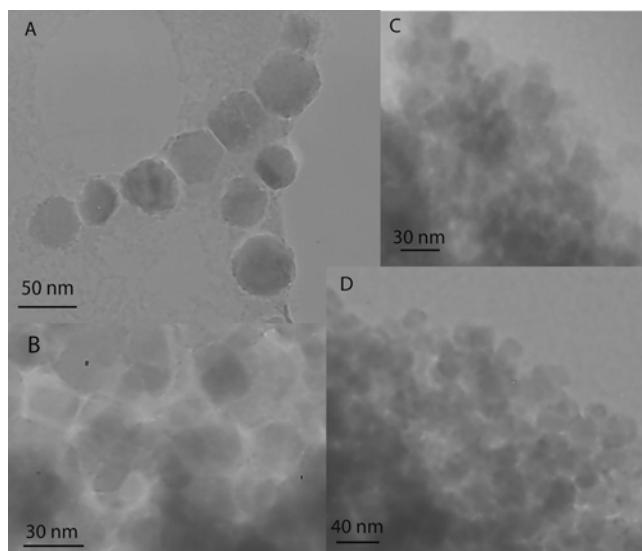

Figure 3. Transmission electron microscope (TEM) images of biogenic magnetite samples, A, *Magnetospirillum gryphiswaldense*, B , *Geobacter sulfurreducens*, C , *Shewanella oneidensis*, D , *Geothrix fermentans*.

XMCD data

The Fe $L_{2,3}$ edge XAS spectra for each biogenic magnetite sample were collected in opposite magnetic fields, and subtracted from each other to give the XMCD spectrum; an example using spectra obtained by analysing the magnetosome magnetite is shown in Figure 4. These spectra show similar characteristics to those previously recorded for magnetic ferrite-spinel structure minerals (Pattrick *et al.*, 2002; Pearce *et al.*, 2006). Figure 5 shows the XMCD spectra and fits derived from the calculated spectra for each reduced magnetite sample (all biogenic) and Figure 6 shows the spectra and fits for each oxidised magnetite sample (biogenic, chemical and geological). The curve fitting of each spectrum provides the Fe ion oxidation state and site occupancies presented in Table 1. These data were used to determine the stoichiometry of the magnetite samples and to calculate the number of vacancies in the spinel structure using the method described in (Pearce *et al.*, 2006). The data are compared to the theoretical stoichiometric magnetite spectra (see XMCD methods section, Figure 1 & Table 1).

XAS at the *L*-edge has a probing depth of 4.5 nm. Hence it does not fully reach to the core of our nanoparticles, but the fact that smaller particles have an increased surface area compared to the core volume works strongly in favour of a representative probing of the particles. For the smallest and largest sizes of nanoparticles probed in this study, 20 and 45 nm in diameter, respectively, the probing depth of XMCD results in information being gathered from 83% and 49% of the particle's material, respectively. In this calculation we assumed for simplicity that the particles are spherical. If they are not spherical then the surface contribution is even larger, so that the above given percentages can be regarded as lower values. Thus the results indicate that a large proportion of the particle is probed by XMCD, even for the largest diameter nanoparticles, and therefore it can be considered to be a bulk technique in the case of our samples. Furthermore, the results are expected be unaffected by the influence of surface effects, such as surface relaxation, which would only affect a depth up to ~ 0.35 nm (Kachkachi *et al.*, 2000).
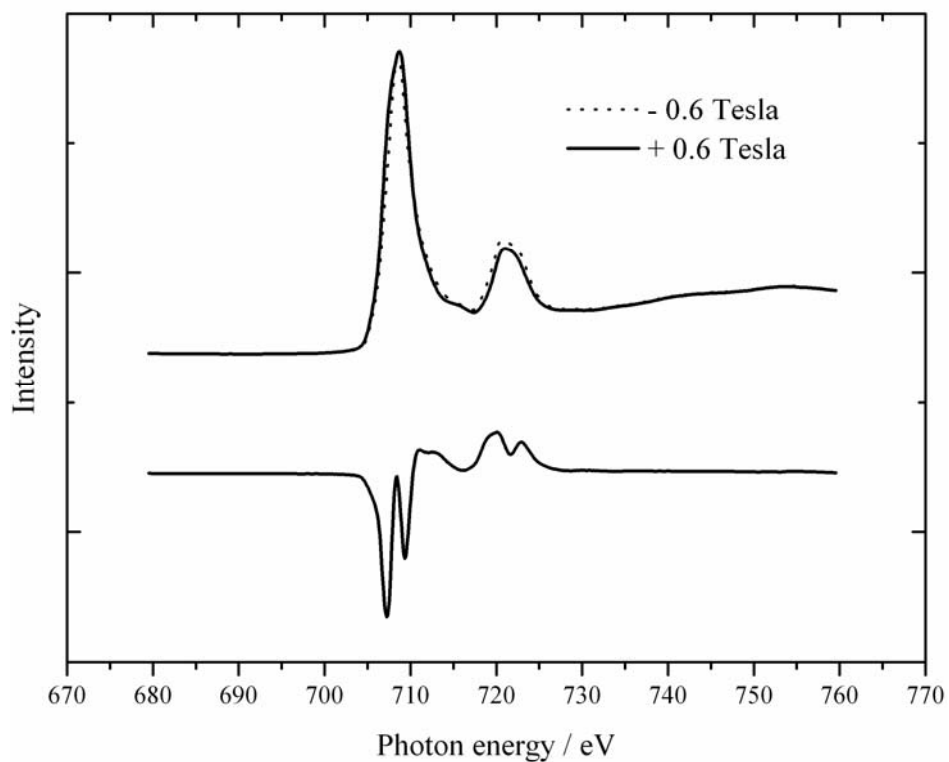
Figure 4: The Fe $L_{2,3}$ absorption spectra of magnetosomes produced by *M. gryphiswaldense*. The $L_{2,3}$ edge spectra were measured in a reversible 0.6 Tesla magnetic field (dashed and solid lines) and the resulting difference spectrum, the XMCD, is shown below (intensity multiplied by three).
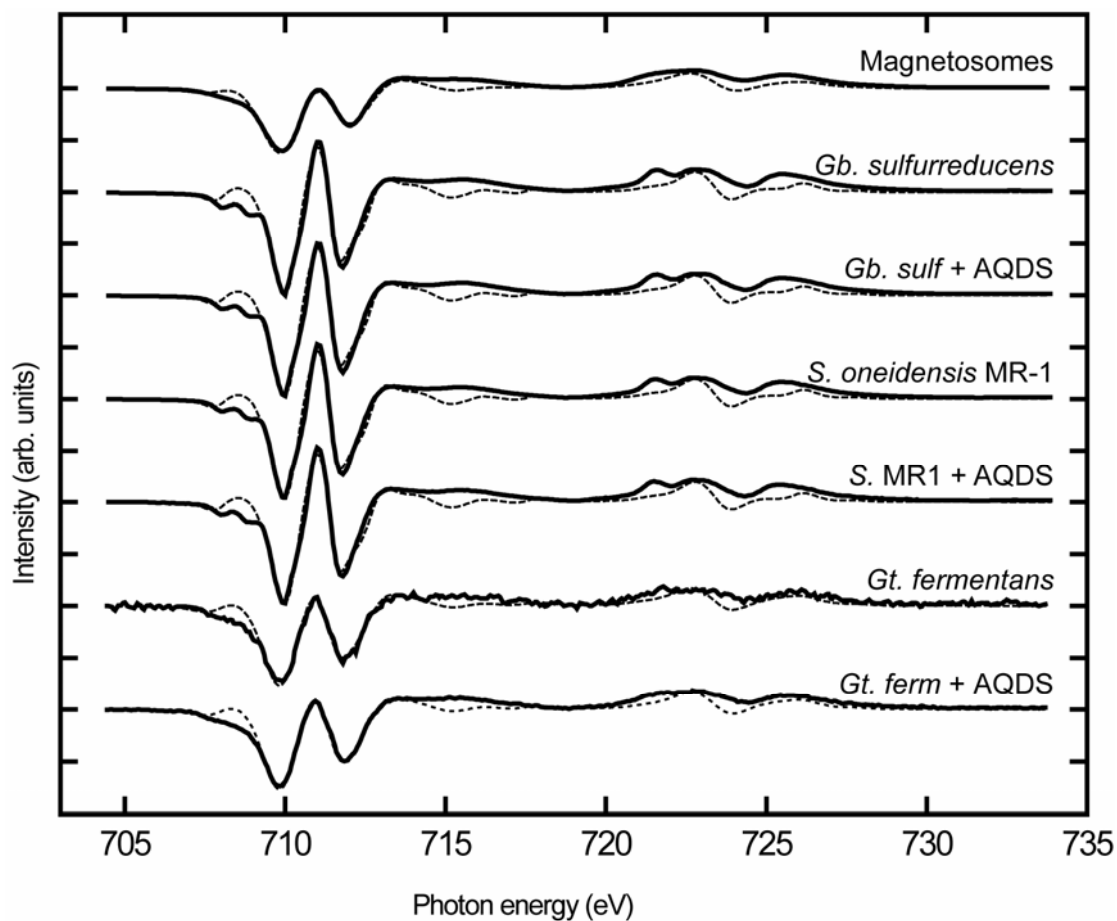
Figure 5 The Fe $L_{2,3}$ XMCD experimental (solid line) spectrum and best fit (dashed line) calculated spectrum based on the three theoretical site components listed in Table 1 for each reduced magnetite sample (biogenic). The difference in energy resolution between the spectra is mainly due to the difference in instrumental resolution of the beamlines.
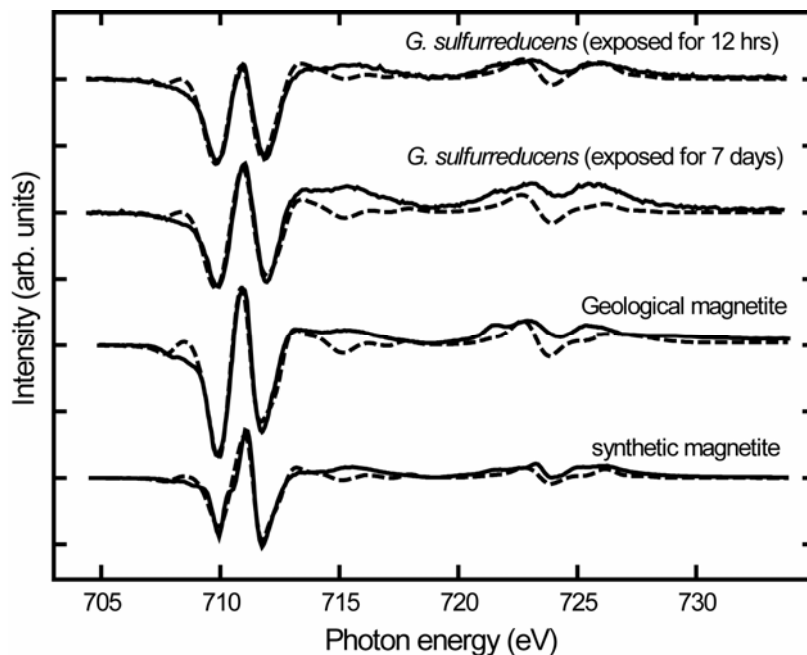
**Figure 6:** The Fe $L_{2,3}$ XMCD experimental (solid line) spectrum and best fit (dashed line) calculated spectrum based on the three theoretical site components listed in Table 1 for each reduced magnetite sample (chemical, biogenic and geological). The difference in energy resolution between the spectra is mainly due to the difference in instrumental resolution of the beamlines.

Reduced magnetite

From Table 1 it can be seen that magnetite produced by the three dissimilatory Fe(III)-reducing bacteria and measured under anaerobic conditions to preserve the characteristics of the magnetite at the time of formation, give a different value for the distribution of Fe(II) and Fe(III) across the tetrahedral and octahedral sites. These data give a different number of vacancies, δ within the spinel structure for each set of samples depending on the bacterium, varying from δ = 0 for *Gt. fermentans* to δ = - 0.03 for *Gb. sulfurreducens*. For each Fe(III)-reducing bacterium the samples produced with the electron shuttling compound, AQDS, had a value within the error bar of the samples produced without AQDS. Each magnetite sample made by *Gb. sulfurreducens* and *S. oneidensis* had an Fe(II)/Fe(III) ratio higher, but a T_d/O_h ratio lower, than that of stoichiometric magnetite. *Gt. fermentans* had an Fe(II)/Fe(III) ratio within error of that of stoichiometric magnetite but a T_d/O_h ratio similar to the other bacterial samples. Magnetosomal magnetite had a similar distribution of Fe cations to the magnetite made by *S. oneidensis* and *Gb. sulfurreducens* as the data showed an Fe(II)/Fe(III) ratio of 0.52, revealing an excess of Fe d^6 O_h compared to stoichiometric magnetite. Magnetosomal magnetite also had a T_d/O_h ratio lower than that of stoichiometric magnetite, similar to the extracellular magnetite where there is a slight deficit of d^5 cations on the T_d sites.

Table 1. Fe site occupancies and cation vacancies for magnetites, calculated from XMCD. The spectra were fitted to the three main spectral features in the Fe L_3 peaks only and the ratios were calculated to the number of Fe atoms per unit spinel formula on a 4 oxygen basis. *From Pearce et al. (2006).

Sample	d^6 O_h	d^5 T_d	d^5 O_h	Cation total	Vacancy	T_d/O_h	Fe^{2+}/Fe^{3+}
Calculated	1.00	1.00	1.00	3.00	0.00	0.50	0.50
Reduced samples (biogenic)							
Gb. sulfurreducens	1.08	0.98	0.97	3.03	-0.03	0.48	0.55
Gb. sulfurreducens + **AQDS**	1.04	0.99	0.98	3.01	-0.01	0.49	0.53
S. oneidensis	1.04	0.99	0.98	3.01	-0.01	0.49	0.53
S. oneidensis + **AQDS**	1.05	0.99	0.97	3.01	-0.01	0.49	0.54
Gt. fermentans	0.99	0.93	1.08	3.00	0.00	0.45	0.49
Gt. fermentans + **AQDS**	0.99	0.94	1.07	3.00	0.00	0.46	0.49
M. gryphiswaldense	1.03	0.97	1.00	3.00	0.00	0.48	0.52
Oxidised samples (biogenic, natural and synthetic)							
Gb. sulfurreducens (exposed to air for 24 hrs)	0.76	0.94	1.22	2.92	0.08	0.47	0.35
Gb. sulfurreducens (exposed to air for 7 days)	0.69	1.10	1.11	2.90	0.10	0.61	0.31
Natural magnetite*	0.88	1.00	1.08	2.96	0.04	0.51	0.42
Chemical magnetite	0.70	1.03	1.17	2.90	0.10	0.55	0.32

Oxidised magnetite

When any single sample of biogenic magnetite data was compared to a sample of natural magnetite analyzed using XMCD (Pearce *et al.*, 2006) the contrast was striking. The natural 'geogenic' magnetite, containing negligible trace elements, had a cation total of 2.96 and included 0.04 vacancies per formula unit (Table 1). The Fe d^6 O_h of geogenic magnetite is seen to be lower than for biogenic samples measured anoxically resulting in the Fe(II)/Fe(III)

ratio also being lower and the amount of d^5 O_h being higher (1.08) to compensate. Chemical nano-magnetite (Alfa-Aesar CAS no. 1317-61-9) also showed a site occupancy pattern different to the biogenic samples. The same changes were observed as for the sample of natural magnetite, but with a greater number of vacancies in the structure; $\delta = 0.10$, as Fe d^6 O_h was only 0.70 (Table 1).

Samples of biogenic magnetite exposed to air prior to the XMCD measurements were also measured and showed similar trends in site occupancy and vacant sites as the natural and chemically formed samples above (Table 1 and Figure 6). The amount of Fe d^6 O_h in a sample of magnetite produced by *Gb. sulfurreducens* decreased with 12 hours exposure to air with a corresponding increase in Fe d^5 O_h from 0.97 to 1.22. After further exposure to air for 7 days the sample showed a further decrease in Fe d^6 O_h from 0.76 to 0.69 with a subsequent increase in d^5 T_d from 0.94 to 1.10 and slight decrease of d^5 O_h. The T_d/O_h ratio did not change with initial exposure to an oxidising atmosphere but after 7 days had increased significantly from 0.47 to 0.61. The Fe(II)/Fe(III) ratio gradually decreased from 0.55 for reduced bio-magnetite to 0.31 for the sample exposed to air for 7 days reflecting the changing site occupancies.

Discussion

The slower ferrihydrite reduction rates in cultures without AQDS (Figure 2), which led to a slower rate of magnetite formation due to a lower concentration of Fe(II) in the system, which is thought to catalyse the formation of magnetite from ferrihydrite by Fe(III)-reducing bacteria (Hansel *et al.*, 2005; Coker *et al.*, submitted), had no effect on the XMCD spectra of the magnetite formed. However, the differences in the magnetite produced by different bacteria indicates that the mode of iron metabolism does affect the structure/chemistry of the magnetite produced.

Reduced biogenic magnetites.

Both *Gb. sulfurreducens* and *S. oneidensis* magnetite samples had Fe(II)/Fe(III) ratios larger than 0.50 indicating a more reduced form of magnetite than calculated stoichiometric magnetite (Table 1). The increase in Fe d^6 O_h compared to stoichiometric magnetite explains the excess of total Fe reflected in the 'negative' vacancies for these samples. Previous studies suggest that factors leading to cation-excess magnetite include environmental parameters such as temperature and H_2-gas flow rate (Togawa *et al.*, 1996). However, since biogenic magnetite is made within a closed system at room temperature, a different mechanism must be involved. It has previously been speculated that the anoxic environment that the bacteria

require for growth results in an oxygen-deficient spinel (Coker *et al.*, 2006). Magnetite made by *Gt. fermentans* has three Fe cations per formula unit; the same as stoichiometric magnetite. However, the XMCD results in Table 1 show that the d^5 cations are actually unevenly distributed between the T_d and O_h sites giving a T_d/O_h ratio of 0.45 and 0.46 for samples with and without AQDS, respectively. This is lower than the ratio of 0.50 for stoichiometric magnetite, showing a statistical preference for the octahedral site by the Fe cations.

If the subtle differences in the magnetites produced by the bacteria reflect different formational mechanisms, the different pathways to produce reduced Fe(II) may provide an explanation. In addition to a potentially distinct complement of enzymes in each organism that are involved in Fe(III) reduction (reviewed in Lloyd, (2003)), other factors could also be important. *Gt. fermentans* is thought to produce both a chelating agent and an electron shuttling compound in order to promote access to reducible Fe(III) (see above). Thus, at least some of the ferrihydrite could first be solubilised to form chelated Fe(III) prior to being reduced to Fe(II) in the aqueous phase, by the electron shuttle or directly by a terminal reductase on the cell, leading to magnetite production. In this situation the supply of chelated Fe(III) could play an important role in controlling the rate of Fe(III) availability as reduction proceeds to magnetite in an ordered manner. Under these conditions, the predominance of octahedral sites in chelated Fe species may explain the inheritance of a high O_h/T_d ratio in the magnetite. In contrast, chelating agents have not been detected in cultures of *Gb. sulfurreducens* and *S. oneidensis* and, interestingly, during reduction of ferrihydrite and formation of magnetite an intermediate phase of a more crystalline Fe(III)-mineral, goethite (FeO.OH), is formed (Hansel *et al.*, 2003; Coker *et al.*, 2007). The presence of such a phase in *Geothrix* cultures has yet to be assessed, but it is feasible that the diverse mechanisms at work may result in *Gt. fermentans* forming magnetite with a slightly different spinel structure to *Gb. sulfurreducens* and *S. oneidensis*. This requires further investigation, as there is an obvious need for a more detailed picture of the quantitative impact of each distinct mechanism on the rate and end point of Fe(III) reduction in the three model organisms. Nevertheless, the mineralogical form of Fe(II) and Fe(III), and therefore indirectly the mechanism of Fe(III) reduction by different bacterial species, are clearly important factors defining the stoichiometry of the mineral that forms from these processes. The rate of reduction, affected by the presence of an electron shuttle, is probably not such an important factor controlling end product formation due to the lack of difference between those cultures supplemented by AQDS compared to those that were not but contained the same bacteria.

Magnetosomal magnetite has a site occupancy ratio constistent with stoichiometric

magnetite. Magnetite produced by magnetotactic bacteria is well ordered as the magnetosomal membrane constrains the formation of the magnetite particles resulting in the formation of near-stoichiometric nanoparticles (Balkwill *et al.*, 1980; Vali & Kirschvink, 1990; Taylor & Barry, 2004)

Oxidised magnetites

Samples of magnetite produced by *Gb. sulfurreducens* exposed to air for 12 hours, and subsequently for a further 7 days, show how sensitive samples of nano-magnetite are to oxidation. The end-member of oxidised magnetite is maghemite, $Fe_{3-\delta}O_4$ where $\delta = 0.33$ for the number of vacancies. Vacancies are found on the octahedral site as represented by the formula $\left(Fe^{3+}\right)\left[Fe^{2+}_{1-3\delta}Fe^{3+}_{1+2\delta}\Delta_\delta\right]O_4$. However, this formula does not give a good description of the vacancy distribution in either of the oxidised biogenic magnetite samples since it does not account for a change in tetrahedral site occupancy. Schedin *et al.* (2004) devised a slightly different formula however, that takes into account the change in T_d site occupancy; $\left(Fe^{3+}_{1-y}\right)\left[Fe^{2+}_{1-3x}Fe^{3+}_{1+2x+y}\Delta_x\right]O_4$ where x is the number of vacant sites Δ, and y is the net transfer of Fe(III) from T_d to O_h coordination. This formula describes the partially oxidised magnetite exposed to air for only 12 h, giving values of $x = 0.08$ and $y = 0.06$, respectively. The same sample exposed for 7 days gives $x = 0.10$ and $y = 0.10$, showing a net transfer of Fe(III) ions from O_h to T_d coordination, the opposite to that reported in Schedin *et al.* (2004), as well as a continued decrease of the amount of Fe(II) in the structure, expected during an oxidation process. These two results show that the oxidation of nano-magnetite occurs in two stages. Firstly, Fe(II) O_h is oxidised to Fe(III) but remains on the octahedral sites, with an additional transfer of Fe(III) from the tetrahedral sites to maintain charge neutrality. After further oxidation, shown by a decrease in the Fe(II)/Fe(III) ratio from 0.35 to 0.31, there is a net gain of Fe(III) on the T_d sites shown by the T_d/O_h ratio increasing from 0.47 to 0.61 and the amount of vacancies increasing, again due to a requirement to keep the charge of the Fe cations balanced within the mineral. This rapid oxidation of the nano-magnetite surface is a result of a large surface to bulk ratio.

Since XMCD is a surface sensitive technique, the measurements are indicative of surface oxidation due to exposure to air. The strongly defective surface of the particle could be considered a superstructure, or a second magnetic phase, as it results in nano-particles with different magnetic properties (Nekov *et al.*, 2006), which will affect the use of these particles in technological applications. If samples of biogenic magnetite are not oxidised then XMCD

can differentiate between geogenic (for instance detrital) and biogenic magnetite in sediments and soils. However, exposure to air for short periods removes this difference.

Nanoparticulate chemical magnetite and natural magnetite were also both found to be oxidised and contained vacancies due to an iron cation deficiency on the octahedral sites (Table 1). Neither show a significant increase or decrease in T_d iron, unlike the biogenic samples, but instead the Fe cation site occupancy is described well by the simple formula for oxidised magnetite of $\left(Fe^{3+}\right)\left[Fe^{2+}_{1-3\delta}Fe^{3+}_{1+2\delta}\Delta_\delta\right]O_4$ (Schedin *et al.*, 2004), in line with maghemite. This differs from the samples of biogenic magnetite that have become oxidised with time rather than formed as oxidised precipitates.

Different Fe(III)-reducing bacteria produce magnetite with subtly different characteristics and differences to geogenic and chemically precipitated magnetites. XMCD is a very sensitive technique that reveals these differences. Magnetotactic bacteria produce magnetite similar to geogenic and chemical magnetite. Small differences in stoichiometry and structure can produce major differences in the magnetic and electrical properties that define the performance of ferrite spinels in technological devices. Thus these small differences reveal the potential of biogenic magnetites to produce materials with unique properties. By screening more extracellular magnetite producers, more variations will be revealed. By understanding the processes that control the nature of the magnetite produced (including genomic investigations) the potential to customise biogenic magnetite for technological uses can be exposed. For instance non-oxidised extracellular magnetite can be used as a catalyst for the reduction of azo dyes and other hazard waste compounds and has been found to be more efficient than chemical nano-magnetite (Pearce et al., unpublished data). The oxidation of biogenic magnetite changes its stoichiometry and its properties, thus it has the potential uses in magnetic recording media and drug delivery systems which currently use oxidised magnetite (Borrelli *et al.*, 1972; Norio *et al.*, 2005).

References

Arato, B., Szanyi, Z., Flies, C., Schüler, D., Frankel, R. B., Buseck, P. R. and Posfai, M. (2005): Crystal-size and shape distributions of magnetite from uncultured magnetotactic bacteria as a potential biomarker. *Am Mineral,* **90**(8-9), 1233-1241.

Arenholz, E. and Prestemon, S. O. (2005): Design and performance of an eight-pole resistive magnet for soft X-ray magnetic dichroism measurements. *Rev Sci Instrum,* **76**(8), 083908/1-083908/8.

Balkwill, D., Maratea, D. and Blakemore, R. (1980): Ultrastructure of a magnetotactic spirillum. *J Bacteriol,* **141**, 1399-1408.

Bazylinski, D. A. and Moskowitz, B. M. (1997): Microbial biomineralisation of magnetic iron minerals. *in* "Geomicrobiology: interactions between microbes and minerals", Mineralogical Society of America, **35,** 181-223.

Borrelli, N. F., Chen, S. L. and Murphy, J. A. (1972): Magnetic and optical properties of thin films in the system1-x Fe_3O_4.x $Fe_{8/3}O_4$. *IEEE T Magn,* **8**(3), 648-651.

Caccavo Jr, F., Lonergan, D. J., Lovley, D. R., Davis, M., Stolz, J. F. and McInerney, M. J. (1994): *Geobacter sulfurreducens* sp. nov., a hydrogen and acetate-oxidising dissimilatory matal reducing. *Appl Environ Microbiol,* **60**, 3752-3759.

Chaudhuri, S. K., Lack, J. G. and Coates, J. D. (2001): Biogenic magnetite formation through anaerobic biooxidation of Fe(II). *Appl Environ Microbiol,* **67**(6), 2844-2848.

Coates, J. D., Ellis, D. J., Gaw, C. V. and Lovley, D. R. (1999): *Geothrix fermentans* gen. nov., sp. nov., a novel Fe(III)-reducing bacterium from a hydrocarbon-contaminated aquifer. *Int J Syst Bacteriol,* **49**, 1615–1622.

Coker, V. S., Pattrick, R. A. D., van der Laan, G. and Lloyd, J. R. (2004). Use of bacteria to produce spinel nanoparticles. UK Patent**:** 0424636.9.

Coker, V. S., Gault, A. G., Pearce, C. I., van der Laan, G., Telling, N. D., Charnock, J. M., Polya, D. A. and Lloyd, J. R. (2006): XAS and XMCD evidence for species-dependent partitioning of arsenic during microbial reduction of ferrihydrite to magnetite. *Environ Sci Technol,* **40,** 7745-7750.

Coker, V. S., Bell, A. M. T., Pearce, C. I., Pattrick, R. A. D., van der Laan, G. and Lloyd, J. R. (2007): Time resolved synchrotron X-ray poxder diffraction study of the formation of magnetite by the Fe(III) reducing bacterium *Geobacter sulfurreducens. Am Mineral,* in press.

Dudzik, E., van der Laan, G. and Thompson, S. M. (2000): Flipper: a new instrument for XMCD at the SRS. *Synchrotron Radiation News,* **13**, 18-22.

Dunin-Borkowski, R. E., McCartney, M. R. Fankel, R. B. Bazylinski D. A., Posfai, M., Buseck, P. R. (1998): Magnetic microstructure of magnetotactic bacteria by electron holography. Science, 282, 1868-1870

Egli, R. (2004) Characterization of individual rock magnetic components by analysis of remanence curves, 1. Unmixing natural sediments. *Studia Geophysica et Geodaetica*, **48**(2), 391-446

Faivre, D. and Zuddas, P. (2006): An integrated approach for determining the origin of magnetic nanoparticles. *Earth Planet Sc Lett,* **243**, 53-60.

Fredrickson, J.K., Zachara, J.M., Kennedy, D.W., Dong, H., Onstott, T.C., Hinman, N.W., Li, S. (1998): Biogenic iron mineralization accompanying the dissimilatory reduction of hydrous ferric oxide by groundwater bacterium. *Geochim. Cosmochim. Acta*, **62**, 3239-3257.

Glasauer, S., Weidler, P. G., Langley, S. and Beveridge, T. J. (2003): Controls on Fe reduction and mineral formation by a subsurface bacterium. *Geochim Cosmochim Ac,* **67**(7), 1277-1288.

Gorby, Y. A., Yanina, S., McLean, J. S., Rosso, K. M., Moyles, D., Dohnalkova, A., Beveridge, T. J., Chang, I., Kim, B. H., Kim, K. S., Culley, D. E., Reed, S. B., Romine,

M. F., Saffarini, D. A., Hill, E. A., Shi, L., Elias, D. A., Kennedy, D. W., Pinchuk, G., Watanabe, K., Ishii, S., Logan, B., Nealson, K. H. and Fredrickson, J. K. (2006): Electrically conductive nanowires produced by *Shewanella oneidensis* strain MR-1 and other microorganisms. *PNAS,* **103**(30), 11358-11363.

Grünberg, K., Müller, E.C., Otto, A., Reszka, R., Linder, D.,Kube, M., Reinhardt, R., Schüler, D. (2004): Biochemical and proteomic analysis of the magnetosome membrane in *Magnetospirillum gryphiswaldense. Appl. Environ. Microbiol.,***70**(2), 1040-1050.

Hansel, C. M., Benner, S. G. and Fendorf, S. (2005): Competing Fe(II)-induced mineralization pathways of ferrihydrite. *Environ Sci Technol,* **39**, 7147-7153.

Hansel, C. M., Benner, S. G., Neiss, J., Dohnalkova, A., Kukkadapu, R. and Fendorf, S. (2003): Secondary mineralization pathways induced by dissimilatory iron reduction of ferrihydrite under advective flow. *Geochim Cosmochim Ac,* **67**(16), 2977-2992.

Heyen, U. & Schüler, D. (2003): Growth and magnetosome formation by microaerophilic *Magnetospirillum* strains in an oxygen-controlled fermentor. *Appl. Microbiol. Biotechnol.,* **61**, 536-544

Kachkachi, H., Ezzir, A., Nogues, M., Tronc, E. (2000): Surface effects in nanoparticles: applications to maghemite γ-Fe$_2$O$_3$. *Eur.Phys. J . B.,* **14**, 681-689

Lee, Y., Lee, J., Bae, C. J., Park, J.-G., Noh, H.-J., Park, J.-H., Hyeon, T. (2005): Large-scale synthesis of uniform and crystalline magnetite nanoparticles using reverse micelles as nanoreactors under reflux conditons. *Adv Funct Mater,* **15**(3), 503-509.

Lloyd, J.R. (2003): Microbial reduction of metals and radionuclides. *FEMS Microbiol. Rev.,* **27**, 411-425.

Lloyd, J. R., Leang, C., Hodges Myerson, A. L., Ciufo, S., Sandler, S. J., Methe, B. and Lovley, D. R. (2003): Biochemical and genetic characterization of PpcA, a periplasmic *c*-type cytochrome in *Geobacter sulfurreducens. Biochem J,* **369**, 153-161.

Lovley, D. R., Coates, J. D., Blunt-Harris, E. L., Phillips, E. J. P. and Woodward, J. C. (1996): Humic substances as electron acceptors for microbial respiration. *Nature,* **382**, 445-448.

Lovley, D. R., Holmes, D. E. and Nevin, K. P. (2004): Dissimilatory Fe(III) and Mn(IV) reduction. *Adv Microb Physiol,* **49**, 219-286.

Lovley, D. R. and Phillips, E. J. P. (1986): Availability of ferric iron for microbial reduction in bottom sediments of the freshwater tidal potomac river. *Appl Environ Microbiol,* **52**(4), 751-757.

Lovley, D. R. and Phillips, E. J. P. (1988): Novel mode of microbial energy metabolism: organic carbon oxidation coupled to dissimilatory reduction of iron or manganese. *Appl Environ Microbiol,* **54**(6), 1472-1480.

Lovley, D. R., Phillips, E. J. P. and Lonergan, D. J. (1989): Hydrogen and formate oxidisation coupled to dissimilatory reduction of iron or manganese by *Alteromonas putrefaciens*. *Appl Environ Microbiol,* **55**, 700-706.

Lovley, D. R., Stoltz, J. F., Nord Jr, G. L. and Phillips, E. J. P. (1987): Anaerobic production of magnetite by a dissimilatory iron-reducing microorganism. *Nature,* **330**, 252-254.

Mandernack, K. W., Bazylinski, D. A., Shanks, W. C. and Bullen, T. D. (1999): Oxygen and iron isotope studies of magnetite produced by magnetotactic bacteria. *Science,* **285**, 1892-1896.

Moskowitz, B.M., Frankel, R.B., Bazylinski, D.A. (1993): Rockmagnetic criteria for the detection of biogenic magnetite. *EarthPlanet. Sci. Lett.*, **120**(3–4), 283-300

Myers, C. R. and Myers, J. M. (1992): Localisation of cytochromes to the outer membrane of anaerobically grown *Shewanella putrefaciens* MR-1. *Journal of Bacteriology,* **174**, 3429-3438.

Nekov, I., Merodiiska, T., Slavov, L., Vanderberghe, R. E., Kusano, Y. and Takada, J. (2006): Surface oxidation, size and shape of nano-sized magnetite obtained by co-precipitation. *J Magn Magn Mater,* **300**, 358-367.

Newman, D. K. and Banfield, J. F. (2002): Geomicrobiology: How molecular-scale interactions underpin biogeochemical systems. *Science,* **296**, 1071-1077.

Norio, M., Hironori, N., Ryuichi, M., Shin-ichi, T., Fumihito, M., Bungo, T., Shigehiro, N., Yasufumi, K. and Noriaki, T. (2005): Magnetic nanoparticles with surface modification enhanced gene delivery of HVJ-E vector. *Biomed Biophys Res Comms,* **334**(4), 1121-1126.

Ofer, S., Nowik, I., Bauminger, E. R., Papaefthymiou, G. C., Frankel, R. B. and Blakemore, R. P. (1984): Magnetosome dynamics in magnetotactic bacteria. *Biophys J,* **46**, 57.

Pattrick, R. A. D., van der Laan, G., Henderson, M. B., Kuiper, P., Dudzik, E. and Vaughan, D. J. (2002): Cation site occupancy in spinel ferrites studied by X-ray magnetic circular dichroism: developing a method for mineralogists. *Eur J Mineral,* **14**, 1095-1102.

Pearce, C. I., Henderson, M. B., Pattick, R. A. D., van der Laan, G. and Vaughan, D. J. (2006): Direct determination of cation site occupancies in natural ferrite spinels by $L_{2,3}$ x-ray absorption spectroscopy and x-ray magnetic circular dichroism. *Am Mineral,* **91**, 880-893.

Reguera, G., McCarthy, K. D., Mehta, T., Nicoll, J. S., Tuominen, M. T. and Lovley, D. R. (2005): Extracellular electron transfer via microbial nanowires. *Nature,* **435**, 1098-1101.

Safarik, I. and Safarikova, M. (2002): Magnetic nanoparticles and biosciences. *Monatsh Chem,* **133**(6), 737-759.

Schedin, F., Hill, E. W., van der Laan, G. and Thornton, G. (2004): Magnetic properties of stoichiometric and nonstoichiometric ultrathin Fe_3O_4(111) films on Al_2O_3(0001). *J Appl Phys,* **96**(2), 1165-1169.

Schleifer, K.H., Schüler, D., Spring, S., Weizenegger, M.,Amann, R., Ludwig,

W., Köhler, M. (1991): The genus *Magnetospirillum* gen. nov., description of *Magnetospirillum gryphiswaldense* sp. nov. and transfer of *Aquaspirillum magnetotacticum* to *Magnetospirillum magnetotacticum* comb. nov. *Syst. Appl. Microbiol.*, **14**(4), 379-385.

Schüler, D. (1999): Formation of magnetosomes in magnetotactic bacteria. *J. Mol. Microbiol. Biotechnol.*, **1**(1), 79-86 (2004): Molecular analysis of a subcellular compartment: the magentosome membrane in *Magnetospirillum gryphiswaldense*. *Archiv Microbiol,* **181**, 1-7.

Schüler, D. (1999): Formation of magnetosomes in magnetotactic bacteria. *J. Mol. Microbiol. Biotechnol.*, **1**(1), 79-86.

Sparks, N.H.C., Mann, S., Bazylinski, D.A., Lovley, D.R., Jannasch, H.W., Frankel, R.B. (1990): Structure and morphology of magnetite anaerobically-produced by a marine magnetotactic bacterium and a dissimilatory iron-reducing bacterium. *Earth Planet. Sci. Lett.*, **98**, 14-22

Taylor, A. P. and Barry, J. C. (2004): Magnetosomal matrix: ultrafine structure may template biomineralisation of magnetosomes. *J Microsc,* **213**, 180-197.

Thomas-Keprta, K., Bazylinski, D. A., Kirschvink, J. L., Clemett, S. J., McKay, D. S., Wentworth, S. J., Vali, H., Gibson Jr, E. K. and Romanek, C. S. (2000): Elongated prismatic magnetite crystals in ALH84001 carbonate globules: Potential Martian magnetofossils. *Geochim Cosmochim Ac,* **64**(23), 4049-4081.

Togawa, T., Sano, T., Wada, Y., Yamamoto, T., Tsuji, M. and Tamaura, Y. (1996): The effect of the crystal orientation on the rate of formation of cation-excess magnetite. *Solid State Ionics,* **89**, 279-286.

Vali, H. and Kirschvink, J. L. (1990): Observation of magnetosome organisation, surface structure, and iron biomineralization of undescribed magnetotactic bacteria: evolutionary speculations. *in* "Iron Biominerals". R. B. Frankel and R. Blakemore, eds. New York, Plenum**,** 97-115.

van der Laan, G. and Thole, B. T. (1991): Strong magnetic X-ray dichroism in 2p absorption spectra of 3d transition metal ions. *Phys Rev B,* **43**, 13401-13411.

van der Laan, G. & Welbourne, L.A. (1996): Magnetism comes to light. *Endeavour,* **20**, 37-41.

Weiss, B.P., Kim, S.S., Kirschvink, J.L., Kopp, R.E., Sankaran, M., Kobayashi, A., Komeili, A. (2004): Ferromagnetic resonance and low-temperature magnetic tests for biogenic magnetite. *Earth Planet. Sci. Lett.,* **224**, 73-89

Curriculum Vitae

Name:	Claus Lang
Date of birth:	09.12.1977
Place of birth:	Bergisch Gladbach

01/2005-02/2009	Dissertation; Title: „Bacterial magnetosomes: Genetic tools, cell biology and applications" Supervision: Prof. Dr. Dirk Schüler
10/2006-02/2009	Ludwig-Maximillians-Universität, München; Department Biologie I, Bereich Mikrobiologie
01/2005-09/2006	Max-Planck Institut für Marine Mikrobiologie, Bremen Abteilung Mikrobiologie
02-12/2002	Adjunct Research Associate, University of New South Wales, Sydney Topic: Regulation of RNA stability in response to carbon starvation in *Vibrio angustum* S14
10/1998-12/2003	Biology Studies (Diplom); Rheinische Friedrich-Wilhelms-Universität Bonn
01/12/2003	Graduation (Diplom, Grade: 1.0) Major: Microbiology Minors: Zoology (Immunology), Chemistry
11/2002-12/2003	"Diplom"-thesis at the University of New South Wales, Sydney, Australia, Title: 'Identification and characterization of the gene encoding poly(A) polymerase from *Vibrio angustum* S14' Supervision: Dr. Kathy Takayama (University of New South Wales), Prof. E. A. Galinski (Universität Bonn)
02 - 12/2001	Exchange Student at the University of New South Wales,

	Sydney, Australia; funding by German Academic Exchange Service (DAAD)
08/1997 - 09/1998	Alternative civilian service as an ambulance man, German Red Cross, Rettungswache Kürten, Rheinisch-Bergischer Kreis
1988 - 1997	Gymnasium Herkenrath, Bergisch-Gladbach
06/1997	Abitur: (Grade: 1,9)
1984 - 1988	Grundschule Biesfeld

Acknowledgements

First of all, I wish to express my sincere gratitude to my supervisor, Prof. Dr. D. Schüler, for giving me the opportunity to study magnetotactic bacteria in his laboratory and for his continuous guidance and support throughout this thesis.

I am also very grateful to Prof. Dr. K. Jung for her interest in my work and for preparation of the evaluation.

I would like to thank Prof. Dr. C.M. Niemeyer, Dr. B. Ceyhan, Dr. J. Irrgang (Universtät Dortmund), Dr. R. Wacker (Chimera Biotec), Dr. T. Hieronymus, S. Schwarz (RWTH Aachen), Dr. R.M. Lisy (Universität Jena), Prof. Dr. J. Lloyd and Dr. V. Coker (University of Manchester) for the close and fruitful collaborations.

I feel highly indebted to many current and former members of the "Magnetolab" and the AG Mikrobiologie at the MPI. In particular, I want to thank Dr. Katja Junge, Dr. Sabrina Schübbe, Dr. Damien Faivre and Emanuel Katzmann for many scientific and non-scientific discussions and excellent comments on this thesis. Moreover, I thank René Sonntag for his invaluable help and advice on magnetosome production, Conny Stumpf and Manuela Löhr for most helpful technical assistance. Also, many thanks to my fellow colleagues René Uebe, Susanne Ullrich, Insa Werner and Dr. André Scheffel for many inspiring discussions and for the friendly atmosphere in the lab. Many thanks to "my" practicum students Anna Pollithy, Maria Wiese, Ivaylo Kostadinov and Maxim Messerer - it has been a lot of fun to work with you.

I sincerely thank my parents and my siblings for their continuous support, trust and patience.

Finally, my deepest gratitude goes towards Layla, my wonderful partner, for her love, support and inspiration.

269

Assertation/Erklärung

Hiermit versichere ich, dass ich die vorliegende Dissertation selbständig und nur mit den angegebenen Quellen und Hilfsmitteln angefertigt habe. Alle Ausführungen, die wörtlich oder sinngemäß übernommen wurden, sind als solche gekennzeichnet. Des Weiteren erkläre ich, dass ich nicht anderweitig ohne Erfolg versucht habe, eine Dissertation einzureichen oder mich der Doktorprüfung zu unterziehen. Die vorliegende Dissertation liegt weder ganz, noch in wesentlichen Teilen einer anderen Prüfungskommission vor.